Integrability in AdS/CFT: Exact Results for Correlation Functions

by

Jorge Escobedo

A thesis
presented to the University of Waterloo
in fulfillment of the
thesis requirement for the degree of
Doctor of Philosophy
in
Physics

Waterloo, Ontario, Canada, 2012

Declaration

I hereby declare that I am the sole author of this thesis. This is a true copy of the thesis, including any required final revisions, as accepted by my examiners.

I understand that my thesis may be made electronically available to the public.

Abstract

We report on the first systematic study of correlation functions in $\mathcal{N} = 4$ super Yang-Mills theory using integrability techniques. In particular, we show how to compute three- and four-point functions of single-trace gauge-invariant operators at tree level in the $SU(2)$ sector of the theory. Using the AdS/CFT correspondence, the correlation functions that we compute can be thought of as the joining or splitting of strings moving in $AdS_5 \times S^5$. We show that when one (two) of the operators in the three-(four-)point function are taken to be small BPS operators, our weak coupling results match perfectly with the strong coupling results in the Frolov-Tseytlin limit. We conclude by presenting some results that will be needed to extend the methods presented in this thesis beyond the $SU(2)$ sector of $\mathcal{N} = 4$ super Yang-Mills.

Acknowledgments

I feel very fortunate to have met great people during the three years of my PhD at the Perimeter Institute (PI). All of them deserve to be mentioned here and I'll do my best to do so. However, I probably won't succeed. Sorry in advance if I forgot to mention your name!

First, I'd like to thank Pedro Vieira for taking me as his student and always having his door open. It has been very stimulating, at times challenging (in a good way), and overall a pleasure to work with him. Pedro has greatly influenced the way I think about physics and problem solving in general. Moreover, most of what appears in this thesis I learned directly from interacting with him. I hope I've made him justice. Second, I'd like to thank Rob Myers for initially taking me as his student when I first arrived at PI. I worked with him for the first nine months of my PhD and it was Rob who patiently showed me the ropes of doing research. In all honesty, I cannot imagine better advisors than Pedro and Rob.

I'd also like to thank my collaborators: João Caetano, Kolya Gromov and Amit Sever, and Alex Buchel, Miguel Paulos, Aninda Sinha and Misha Smolkin. I've learned a great deal from them. Then come my friends and fellow students: João Caetano, Francesco Caravelli, Sean Gryb, Yuxiang Gu, Jonathan Hackett, Jeff Hnybida, Filippo Passerini, João Penedones, Isabeau Prémont-Schwarz, Sayeh Rajabi, Ajay Singh, Jon Toledo, Cozmin Ududec, Anton van Niekerk and Tianheng Wang. They helped me keep my mental sanity by playing football (the global one) or pool, or by talking about anything from music to the Canadian winter. I look forward to keeping in touch with all of them. Special thanks to Anton, João C., Jon, Sayeh and Tianheng for proofreading parts of this thesis.

I must also thank the administrative staff at PI. In particular, Debbie Guenther, LeeAnne Kane and Sheri Keffer made my life easier in different ways while at PI. Also, big thanks to Judy McDonnell at the Department of Physics at Waterloo for all the help with bureacratic procedures. I cannot forget to thank my friends at the Black Hole Bistro for providing great food, coffee and snacks. In particular, thanks to its manager, Dan Lynch for being a good friend and for organizing scotch, beer and wine tasting events (certainly some of the highlights of my time as a PhD student).

Lastly, and more importantly, thanks to my family. To my wife Denisse, for all her love and support, and for being so patient while I was writing this thesis. She is my love and best friend, and I remind myself everyday how lucky I am to have her in my life. This thesis is dedicated to her. To my parents, Lucy and Jorge, for always supporting my decisions and for being the best role models I could have. To my brother Tito and my grandma Mina for always being present despite the thousands of kilometers between us. I miss you all dearly.

Coco Escobedo
Waterloo, April 2012

To Denisse

Contents

List of Figures

List of Tables

Part I

Introduction and General Setup

Chapter 1

Introduction

The goal of this chapter is to introduce the physical observables that we will be studying in $\mathcal{N} = 4$ super Yang-Mills theory. As a short motivational review, we will explain how to compute the spectrum of anomalous dimensions of the theory at weak coupling using integrability techniques, and at strong coupling using the AdS/CFT correspondence. We will then move on to reviewing what is known for correlation functions in the theory at weak and strong coupling.

1.1 Correlation functions in $\mathcal{N} = 4$ SYM

Four-dimensional $\mathcal{N} = 4$ super Yang-Mills theory (or $\mathcal{N} = 4$ SYM for short) with gauge group $U(N_c)$ is a theory of scalar fields Φ_i, gluons A_μ and sixteen-component Majorana spinors Ψ. The corresponding Lagrangian is [1]

$$\mathcal{L} = \frac{1}{g_{YM}^2}\mathrm{Tr}\left[\frac{1}{2}F_{\mu\nu}F^{\mu\nu} + (D_\mu\Phi_i)^2 - \frac{1}{2}\left[\Phi_i,\Phi_j\right]^2 + \bar{\Psi}\left(\Gamma^\mu D_\mu\Psi - i\,\Gamma^i\left[\Phi_i,\Psi\right]\right)\right], \tag{1.1}$$

where greek indices run over $1,2,3,4$; latin indices run over $1,\ldots,6$; Γ are 16×16 Dirac gamma matrices and the covariant derivative is defined in the usual way:

$$D_\mu \cdot = \partial_\mu \cdot - i\left[A_\mu, \cdot\right].$$

All the fields in the theory are matrices of size $N_c \times N_c$ in the adjoint representation of $U(N_c)$:

$$\Phi_i = \Phi_i^a\, T^a\,, \qquad A_\mu = A_\mu^a\, T^a\,, \qquad \Psi = \Psi^a\, T^a\,,$$

where T^a are the generators of the group, normalized as $\mathrm{Tr}(T^aT^b) = \delta^{ab}/2$. We can group the six scalars in pairs to form three complex scalars, defined as

$$X \equiv \Phi_1 + i\Phi_2\,, \qquad Y \equiv \Phi_3 + i\Phi_4\,, \qquad Z \equiv \Phi_5 + i\Phi_6 \tag{1.2}$$

plus their respective complex conjugates $\bar{X}, \bar{Y}, \bar{Z}$.

A particularly interesting regime of the theory is the famous *'t Hooft limit*, which is given by taking

$$N_c \to \infty\,, \qquad \lambda \equiv g_{YM}^2 N_c \;\text{ fixed}\,,$$

where λ is the 't Hooft coupling. By doing the standard large N_c counting, one can see that in this limit the dominant contribution to correlation functions comes from studying planar $\mathcal{N}=4$ SYM. This means that, in double-line notation, we only have to consider those interaction diagrams that can be drawn on a sphere. Those that can only be drawn in higher-genus surfaces are supressed by factors of $1/N_c$.

For the most part of this work, we will focus on single-trace gauge-invariant operators in the $SU(2)$ subsector of the theory, which are those operators made out of two complex scalars:

$$\mathcal{O}(x) = \mathrm{Tr}\,(ZXXZZ\ldots XZXZ)\,(x)\,. \tag{1.3}$$

Our ultimate goal is to compute correlation functions of such operators in the planar limit using integrability techniques. Thus, let us review what we know in advance about these objects, which are the most natural local observables in this theory. First, it is well-known that in the 't Hooft limit, the correlation function of n gauge-invariant operators goes as

$$G_n(x_1,\ldots,x_n) \equiv \langle \mathcal{O}_1(x_1)\ldots\mathcal{O}_n(x_n)\rangle \propto \frac{1}{N_c^{n-2}}\,. \tag{1.4}$$

Second, and quite remarkably, $\mathcal{N}=4$ SYM is a conformal theory even at the quantum level. This fact alone restricts enormously the form of correlation functions in the theory, see [2, 3]. In particular, let us consider correlation functions of renormalized operators. Conformal symmetry completely fixes the form of the two-point function to be

$$G_2(x_1,x_2) \equiv \langle \mathcal{O}_i(x_1)\bar{\mathcal{O}}_j(x_2)\rangle = \mathcal{N}_i \frac{\delta_{ij}}{|x_{12}|^{2\Delta_i}}\,, \tag{1.5}$$

where $x_{ij} \equiv x_i - x_j$, $\mathcal{N}_i$ are normalization constants that may be set to one and Δ_i is the *conformal dimension* of operator $\mathcal{O}_i$. This form is valid to any loop order, as long as the operators are appropriately renormalized. With the two-point function defined as above, the three-point function is also fixed by conformal symmetry to take the form

$$G_3(x_1,x_2,x_3) \equiv \langle \mathcal{O}_1(x_1)\mathcal{O}_2(x_2)\mathcal{O}_3(x_3)\rangle = \frac{1}{N_c}\frac{\sqrt{\mathcal{N}_1\mathcal{N}_2\mathcal{N}_3}\,C_{123}}{|x_{12}|^{\Delta_1+\Delta_2-\Delta_3}|x_{23}|^{\Delta_2+\Delta_3-\Delta_1}|x_{31}|^{\Delta_3+\Delta_1-\Delta_2}}\,, \tag{1.6}$$

where the different C_{123} are known as *structure constants*.[1] The square root factor on the

[1] An alternative way of writing the structure constants in a scheme independent way is as

$$C_{123} \equiv \langle \mathcal{O}_1(x_1)\mathcal{O}_2(x_2)\mathcal{O}_3(x_3)\rangle \sqrt{\prod_{i=1}^{3}\frac{\langle \mathcal{O}_i(x_{i+1})\bar{\mathcal{O}}_i(x_{i+2})\rangle}{\langle \mathcal{O}_i(x_i)\bar{\mathcal{O}}_i(x_{i+1})\rangle\,\langle \mathcal{O}_i(x_i)\bar{\mathcal{O}}_i(x_{i+2})\rangle}}$$

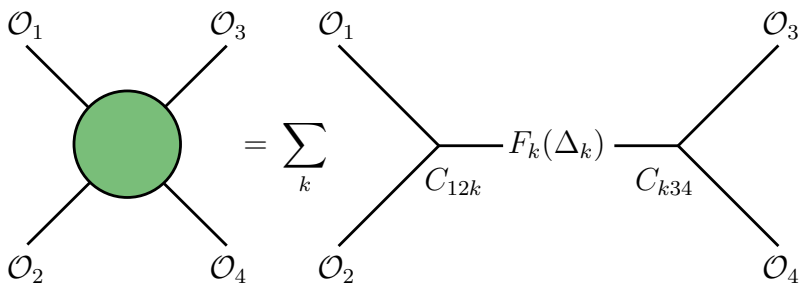

Figure 1.1: Reconstructing four-point functions. The functions $F_k(\Delta_k)$ are known as *conformal blocks* and are completely fixed by conformal symmetry: they only depend on the conformal dimensions $\Delta_1, \Delta_2, \Delta_3, \Delta_4, \Delta_k$ (and also on the positions x_1, x_2, x_3, x_4). It is clear that to reconstruct four-point functions, we need to know all conformal dimensions Δ_i and structure constants C_{ijk}. See [4, 5] for more details.

r.h.s. of this formula is necessary to take into account the normalization of the two-point functions. Without it, the three-point function would not be well-defined. Moreover, the structure constants are not completely unambiguous because we can still multiply $\mathcal{O}_i$ by a phase. That would not affect the normalization of the two-point function, but it would change C_{123} by that phase. Thus, one should consider the absolute value $|C_{123}|$ as the unambiguously defined object. Note that in these formulas we have assumed that the operators $\mathcal{O}_i$ are only made out of scalar fields. However, they are also valid for operators with spin: in that case we would have an extra index structure on the r.h.s. of the formulas above, but the space-time dependence would be the same.

As opposed to the two- and three-point functions, the form of four-point functions is not uniquely determined in $\mathcal{N} = 4$ SYM. Indeed, conformal symmetry tells us that the four-point function will depend on the cross-ratios

$$u \equiv \frac{x_{12}^2 x_{34}^2}{x_{13}^2 x_{24}^2}\,, \qquad v \equiv \frac{x_{12}^2 x_{34}^2}{x_{14}^2 x_{23}^2}$$

that we can form with the positions of the operators. For example, the four-point function takes the following form:

$$G_4(x_1, x_2, x_3, x_4) \equiv \langle \mathcal{O}_1(x_1)\mathcal{O}_2(x_2)\mathcal{O}_3(x_3)\mathcal{O}_4(x_4)\rangle = \frac{1}{N^2} f\,(u, v) \prod_{i<j}^{4} |x_{ij}|^{\Delta/3-\Delta_i-\Delta_j}\,, \qquad (1.7)$$

where $\Delta = \sum_{i=1}^{4} \Delta_i$. Then, the problem of computing four-point functions boils down to determining the function of the cross-ratios $f(u, v)$.

An important fact about conformal field theories such as $\mathcal{N} = 4$ SYM is that, in principle,

where the indices are identified modulo 3. The right hand side is indeed an x_i independent quantity which coincides with C_{123} once we use (1.5) and (1.6).

we only need to know two- and three-point functions to reconstruct higher-point functions. Let us see how this comes about. Recall that in a conformal field theory, the operator product expansion (OPE) of two local operators can be written as a sum over all primary operators $\mathcal{O}_k$ and their descendants as

$$\mathcal{O}_i(x_i)\mathcal{O}_j(x_j) = \sum_k \sum_{n=0}^{\infty} c_k^{\mu_1\dots\mu_n}(x_{ij})\partial_{\mu_1}\dots\partial_{\mu_n}\mathcal{O}_k(x_i)\,. \tag{1.8}$$

The coefficients $c_k^{\mu_1\dots\mu_n}(x_{ij})$ are related to the structure constants C_{ijk} that appear in (1.6). To see this, we need to write the three-point function $\langle\mathcal{O}_1(x_1)\mathcal{O}_2(x_2)\mathcal{O}_p(x_p)\rangle$ by using the OPE of the first two operators. By doing so, we can check that

$$c_k^{\mu_1\dots\mu_n}(x_{12}) = C_{12k}\, b_k^{\mu_1\dots\mu_n}(x_{12})\,, \tag{1.9}$$

where the functions $b_k^{\mu_1\dots\mu_n}(x_{12})$ are completely fixed by conformal symmetry.[2] Now, let us consider the four-point function $G_4(x_1,x_2,x_3,x_4)$ that we introduced in (1.7). First, let us use the OPE of the first two operators, making use of the result (1.9). We get

$$G_4(x_1,x_2,x_3,x_4) = \frac{1}{N_c^2}\sum_k C_{12k}\sum_{n=0}^{\infty} b_k^{\mu_1\dots\mu_n}(x_{12})\partial_{\mu_1}\dots\partial_{\mu_n}\langle\mathcal{O}_k(x_1)\mathcal{O}_3(x_3)\mathcal{O}_4(x_4)\rangle\,.$$

But we know the form of the three-point function appearing on the r.h.s., see (1.6). Thus, we finally arrive at the following expression for the four-point function

$$G_4(x_1,x_2,x_3,x_4) = \frac{1}{N_c^2}\sum_k C_{12k}\, F_k(\Delta_k)\, C_{k34}\,. \tag{1.10}$$

The functions $F_k(\Delta_k)$ are known as *conformal blocks* and are completely fixed by conformal symmetry: they only depend on the conformal dimensions $\Delta_1,\Delta_2,\Delta_3,\Delta_4,\Delta_k$ (and also on the positions x_1,x_2,x_3,x_4 and the spin of $\mathcal{O}_k$). Note that we could perform a similar exercise with higher-point functions. The conclusion would be the same: higher-point functions can be reconstructed using the anomalous dimensions and structure constants as building blocks.

Thus, it is clear that to compute any higher-point correlation function in $\mathcal{N}=4$ SYM, we need to know all anomalous dimensions and structure constants in the theory. We will refer to these as "the spectrum problem" and "the structure constant problem", respectively. Once this is accomplished, we could claim to have in principle solved an interacting four-dimensional gauge theory for the very first time.[3] We say in principle because to date the

[2] For example, for scalar operators $\mathcal{O}_1,\mathcal{O}_2,\mathcal{O}_k$:

$$b_k(x_{12}) = \frac{1}{|x_{12}|^{\Delta_1+\Delta_2-\Delta_k}}\,, \qquad b_k^{\mu_1}(x_{12}) = \frac{(\Delta_1+\Delta_2-\Delta_k)\,x_{12}^{\mu_1}}{2\Delta_k|x_{12}|^{\Delta_1+\Delta_2-\Delta_k}}\,,$$

etc.

[3] Of course, one would also like to compute non-local observables such as Wilson loops and scattering

conformal blocks entering (1.10) (or higher-point functions) are not known in full generality. Thus, it remains to be seen if the conformal blocks approach is more efficient than directly computing higher-point functions without recurring to the structures constants. In any event, it is useful to attack the problem from both directions. In this spirit, one of the goals of this thesis is to show how to efficiently compute four-point functions without using conformal blocks.

Let us now explain how to compute anomalous dimensions and structure constants at weak and strong coupling.

1.2 The spectrum problem

1.2.1 At weak coupling: Solving $\mathcal{N} = 4$ SYM using integrability

When $\lambda \ll 1$, we can use pertubation theory to compute physical quantities. Thus, in this regime, the conformal dimensions depend on the 't Hooft coupling as

$$\Delta(\lambda) = \Delta^{(0)} + \gamma^{(1)}\,\lambda + \gamma^{(2)}\,\lambda^2 + \dots\,, \tag{1.11}$$

where $\Delta^{(0)}$ is the classical dimension of the operator, which is given by the number of fields in the trace, while $\gamma^{(n)}$ is the n-loop anomalous dimension of the operator. For notational convenience, we will often use $\Delta^{(n)} \equiv \gamma^{(n)}\lambda^n$, where $n \geq 1$.

How do we go about computing the different terms in the expansion (1.11)? We could of course start computing hundreds of thousands of Feynman diagrams to determine a single anomalous dimension to certain loop order. Needless to say, this would be a very tedious endeavour. Fortunately, over the last decade a very large body of work has shown that in the planar limit $\mathcal{N} = 4$ SYM is an *integrable* theory, see [13] for a comprehensive review on the subject. From a physicist's perspective, this means that the theory is *exactly solvable*, i.e. one can actually compute analytically all relevant physical observables. Given this remarkable property, it is natural to expect that integrability is the right tool to address the computation of anomalous dimensions in the theory. This is indeed the case and we will now review how to exploit the underlying integrability of the theory to compute anomalous dimensions of $SU(2)$ operators (see (1.3)).

At tree level ($\lambda = 0$), there are many single-trace operators that have the same classical dimension $\Delta^{(0)}$: it is simply the number of fundamental fields in the trace, which we will denote by L. For example, both $\mathrm{Tr}(ZXZX)$ and $\mathrm{Tr}(ZZZZ)$ have the same classical dimension $L = 4$. This large degeneracy is lifted at one loop, where we can identify linear combinations of single-trace operators that have definite one-loop anomalous dimension. In order to find these linear combinations, we need to diagonalize the corresponding one-loop dilatation

amplitudes in the theory. Remarkable progress has been made in these fronts, both at weak [6, 7, 8] and strong coupling [9, 10]. Moreover, correlation functions, Wilson loops and scattering amplitudes in $\mathcal{N} = 4$ SYM are all related to each other, forming a triality of observables, see e.g. [11, 12].

operator: its eigenstates are the linear combinations we are after, while its eigenvalues are their definite anomalous dimensions $\Delta^{(1)}$. In their seminal work [14] (see [15] for a modern review), Minahan and Zarembo found by explicitly computing Feynman diagrams that the one-loop dilatation operator in the $SU(2)$ sector of $\mathcal{N}=4$ SYM is given by

$$\hat{H} = \frac{\lambda}{8\pi^2} \sum_{n=1}^{L} (\mathbb{I}_{n,n+1} - \mathbb{P}_{n,n+1}) \,, \tag{1.12}$$

where $\mathbb{I}$ and $\mathbb{P}$ are the identity and permutation operators, which act on two consecutive fields inside a trace as

$$\begin{aligned} \mathbb{I}_{n,n+1} \operatorname{Tr}(\dots \underset{n}{Z} \underset{n+1}{X} \dots) &= \operatorname{Tr}(\dots \underset{n}{Z} \underset{n+1}{X} \dots) \,, \\ \mathbb{P}_{n,n+1} \operatorname{Tr}(\dots \underset{n}{Z} \underset{n+1}{X} \dots) &= \operatorname{Tr}(\dots \underset{n}{X} \underset{n+1}{Z} \dots) \,. \end{aligned}$$

It makes perfect sense that the one-loop dilatation operator only involves nearest-neighbor interactions: at this loop order and in the planar limit, only nearest-neighbor fields can interact.

The operator appearing in (1.12) is nothing but the famous Heisenberg spin chain Hamiltonian. Thus, it is useful to think of operators of the form (1.3) as states on a closed $SU(2)$ spin chain, where at each site we have a vacuum field Z or an excitation X.[4] Moreover, we will denote the number of X fields by N, so that the number of Z fields is of course $L-N$.

Quite remarkably, it turns out that the Hamiltonian (1.12) is integrable! This means that we may use all the machinery from integrability and exactly solvable models to diagonalize it. In fact, this particular problem was solved long ago by Bethe [16] by means of the famous *Bethe Ansatz*. We will review it in great detail in chapter 3, but let us state here its main features.

The eigenvectors of $\hat{H}$ are precisely the linear combinations of operators that have definite one-loop anomalous dimension . If we consider operators of length L with N excitations, these eigenvectors are explicitly given by

$$\mathcal{O}(x) = \sum_{1 \le n_1 < n_2 < \dots < n_N \le L} \psi(n_1, \dots, n_N) \operatorname{Tr}(\dots \underset{n_1}{Z} X Z \dots \underset{n_2}{Z} X Z \dots \underset{n_N}{Z} X Z \dots)(x) \,, \tag{1.13}$$

where the wave function is

$$\psi(n_1, \dots, n_N) = \sum_{P} A(P) \prod_{j=1}^{N} e^{i p_{P_j} n_j} \,. \tag{1.14}$$

The sum in the wave function runs over all $N!$ permutations P of $(1, 2, \dots, N)$ and p_j are the momenta with which the excitations X move around the chain/trace. The plane wave

[4] The corresponding spin chain is closed because of cyclicity of the trace. Also, the choice of vacuum is our convention: we could have chosen to think of X as vacuum fields and Z as excitations.

coefficients are such that they obey the following relation

$$\frac{A(\dots,k,j,\dots)}{A(\dots,j,k,\dots)} = \frac{\frac{1}{2}\cot\frac{p_k}{2} - \frac{1}{2}\cot\frac{p_j}{2} + i}{\frac{1}{2}\cot\frac{p_k}{2} - \frac{1}{2}\cot\frac{p_j}{2} - i}\,. \tag{1.15}$$

Thus, by fixing one of the plane wave coefficients, e.g. $A(1,2,\dots,N)=1$, all the other ones are determined using (1.15). These coefficients tell us the phase acquired when two momenta are interchanged (i.e. when the corresponding excitations scatter). What should be surprising to the reader is that *any* of the plane wave coefficients is in fact a sequence of two-momenta exchanges.[5] This very non-trivial fact is a consequence of integrability. Moreover, the set of momenta $\{p_j\}$ is determined once we impose periodicity of the wave function (1.14). Doing this, one obtains the *Bethe equations*

$$e^{ip_jL}\prod_{k\neq j}^{N}\frac{\frac{1}{2}\cot\frac{p_j}{2} - \frac{1}{2}\cot\frac{p_k}{2} - i}{\frac{1}{2}\cot\frac{p_j}{2} - \frac{1}{2}\cot\frac{p_k}{2} + i} = 1\,. \tag{1.16}$$

The physical interpretation of this equation is very clear: the exponential term corresponds to the free propagation of an excitation with momentum p_j around the chain/trace, while the product of terms takes into account the scattering of this excitation with all other excitations. Of course, the total phase acquired by the excitation with momentum p_j once it comes back to its original position must be one.

The eigenvalues of $\hat{H}$ that correspond to the eigenvectors (1.13) are

$$E = \frac{\lambda}{2\pi^2}\sum_{j=1}^{N}\sin^2\frac{p_j}{2}\,. \tag{1.17}$$

These are the anomalous dimensions $\Delta^{(1)}$ of the operators (1.13), see (1.11). This is very nice: without computing a single Feynman diagram, we are able to determine the one-loop anomalous dimension of $SU(2)$ operators. All we need to know is the length L of the operator and the number of excitations N that we want to consider. With these two numbers, we find the set of momenta $\{p_j\}$ by solving the set of equations (1.16) and plug the result into (1.17) to obtain the one-loop anomalous dimension. For example, the member of the Konishi multiplet made out of two complex scalars Z and X is

$$K \propto \mathrm{Tr}(ZZXX) - \mathrm{Tr}(ZXZX)\,. \tag{1.18}$$

In this case $L=4$ and $N=2$, such that $p_1=-p_2=2\pi/3$. Hence, the one-loop anomalous

[5] That is, if we set $A(1,2,3,\dots)=1$, then $A(2,1,3,\dots)=\frac{\frac{1}{2}\cot\frac{p_2}{2}-\frac{1}{2}\cot\frac{p_1}{2}+i}{\frac{1}{2}\cot\frac{p_2}{2}-\frac{1}{2}\cot\frac{p_1}{2}-i}$, $A(2,3,1,\dots)=\frac{\frac{1}{2}\cot\frac{p_2}{2}-\frac{1}{2}\cot\frac{p_1}{2}+i}{\frac{1}{2}\cot\frac{p_2}{2}-\frac{1}{2}\cot\frac{p_1}{2}-i}\times\frac{\frac{1}{2}\cot\frac{p_3}{2}-\frac{1}{2}\cot\frac{p_1}{2}+i}{\frac{1}{2}\cot\frac{p_3}{2}-\frac{1}{2}\cot\frac{p_1}{2}-i}$, etc.

dimension of the Konishi operator is

$$\Delta_K^{(1)} = \frac{3\lambda}{4\pi^2}\,.$$

This was an oversimplified version of the story for the spectrum problem, but it is all we need for this thesis.[6] We point the interested reader who wants to learn more about it to the relevant chapters of [13]. Let us just emphasize that the general idea of computing anomalous dimensions by finding the energy spectrum of a given Hamiltonian and solving the corresponding Bethe equations persists at higher loops and all sectors of $\mathcal{N} = 4$ SYM.

Let us conclude this section by listing the two key points that the reader must remember from this section:

- Single-trace operators are mapped into spin chain states.
- Finding the spectrum of anomalous dimensions amounts to computing the energy eigenvalues of a spin chain Hamiltonian.

1.2.2 At strong coupling: Classical strings in $AdS_5 \times S^5$

When $\lambda \gg 1$, we cannot use usual pertubative methods. So, how do we go about computing anomalous dimensions in this regime? This is where the AdS/CFT correspondence comes into play. In its original formulation [21, 22, 23], the correspondence states that type IIB string theory in $AdS_5 \times S^5$ is dual to $\mathcal{N} = 4$ SYM.[7] Given that this duality relates a theory with gravity to a gauge theory defined on a lower-dimensional space, the AdS/CFT correspondence is to date the most precise realization of the holographic principle [26]. For completeness, in table 1.1 we list the map between some parameters and physical observables on each side of the correspondence as they will be relevant to this thesis (see [27, 28] for the standard reviews on the subject).

Apart from the remarkable fact that it relates two seemingly radically different theories, the AdS/CFT correspondence has another key property: it is a weak/strong duality. For example, consider the 't Hoof limit introduced in the previous section. Indeed, as can be seen from table 1.1, the weak coupling regime of $\mathcal{N} = 4$ SYM ($\lambda \ll 1$) corresponds to strongly coupled strings in $AdS_5 \times S^5$. Similarly, the strong coupling regime of the gauge theory ($\lambda \gg 1$) maps into weakly coupled strings. In this sense, the AdS/CFT correspondence is a powerful computational tool! It allows us to extract information about strongly coupled $\mathcal{N} = 4$ SYM, for which our usual perturbative techniques do not apply, by performing

[6] The state of the art regarding the spectrum problem is the Y-system of AdS/CFT [17, 18, 19]. This is a set of functional equations that one can solve numerically to obtain the anomalous dimension of any operator in the theory at any value of the 't Hooft coupling (see [20] for a plot of the anomalous dimension of the Konishi operator).

[7] Other dualities of this type have been proposed [24, 25] and, in general, one refers to them as *gravity/gauge dualities*. However, whenever we mention AdS/CFT in this thesis, we will be refering to Maldacena's original correspondence.

$\mathcal{N}=4$ $U(N)$ **super Yang-Mills**	**Type IIB strings in** $AdS_5 \times S^5$
't Hooft coupling $\lambda = g_{YM}^2 N_c$	$\lambda = \dfrac{R^4}{\alpha'^2}$
Number of colors N_c	$N_c = \dfrac{R^4}{\alpha'^2 g_s} = \dfrac{R^4}{l_s^4 g_s}$
Single-trace operators	Single-string states
Conformal dimensions Δ	Energies E of string states
Higher-point correlation functions	Splitting and joining of string states

Table 1.1: AdS/CFT dictionary relevant to this thesis. R, α', g_s and l_s are the AdS radius, the Regge slope, the string coupling and the string length, respectively.

classical computations on the AdS side. Likewise, we can learn about the highly quantum regime on the string theory side by doing usual perturbative calculations at weak coupling in $\mathcal{N}=4$ SYM.

Of particular interest to us is that we can compute conformal dimensions of single-trace operators at strong coupling by finding the energy of the dual classical single-strings moving in $AdS_5 \times S^5$. Let us then give a quick review of classical strings in this spacetime.

Five-dimensional Anti de Sitter space, which is the maximally symmetric space with constant negative curvature in five dimensions, can be embedded in $\mathbb{R}^{2,4}$ using three complex coordinates $\mathbf{W} = (W_1, W_2, W_3)$ as

$$\mathbf{W} \cdot \bar{\mathbf{W}} = W_1 \bar{W}_1 + W_2 \bar{W}_2 - W_3 \bar{W}_3 = -1 \,. \tag{1.19}$$

Similarly, a five-dimensional sphere S^5 can be embedded as a surface in $\mathbb{R}^6$ using three complex coordinates $\mathbf{U} = (U_1, U_2, U_3)$ as

$$\mathbf{U} \cdot \bar{\mathbf{U}} = U_1 \bar{U}_1 + U_2 \bar{U}_2 + U_3 \bar{U}_3 = 1 \,. \tag{1.20}$$

Note that we have set both the sphere and AdS radius to 1.

The motion of classical strings in $AdS_5 \times S^5$ is described by the Polyakov action. We are only interested in its bosonic part, which in the conformal gauge reads

$$S = -\frac{\sqrt{\lambda}}{4\pi} \int d\tau d\sigma \left[\partial_a \mathbf{W} \cdot \partial^a \bar{\mathbf{W}} + \tilde{\Lambda} \left(\mathbf{W} \cdot \bar{\mathbf{W}} + 1 \right) + \partial_a \mathbf{U} \cdot \partial^a \bar{\mathbf{U}} - \Lambda \left(\mathbf{U} \cdot \bar{\mathbf{U}} - 1 \right) \right] , \tag{1.21}$$

where τ and σ are the string worldsheet coordinates, and we are using the following signature $\partial_a \partial^a = -\partial_\tau^2 + \partial_\sigma^2$. Of course $\mathbf{W}$, $\mathbf{U}$ depend on τ, σ, but we are not writing this dependence

explicitly. The Lagrange multipliers $\tilde{\Lambda}$ and Λ impose the restrictions (1.19) and (1.20). The equations of motion for the action (1.21) are

$$\Big[\partial_a\partial^a - \big(\partial_a \mathbf{W}\cdot\partial^a\bar{\mathbf{W}}\big)\Big]W_j = 0\,, \qquad \Big[\partial_a\partial^a + \big(\partial_a \mathbf{U}\cdot\partial^a\bar{\mathbf{U}}\big)\Big]U_j = 0\,, \tag{1.22}$$

while the two Virasoro constraints can be written in the following form:

$$\partial_\tau\bar{\mathbf{U}}\cdot\partial_\tau\mathbf{U} + \partial_\sigma\bar{\mathbf{U}}\cdot\partial_\sigma\mathbf{U} + \partial_\tau\bar{\mathbf{W}}\cdot\partial_\tau\mathbf{W} + \partial_\sigma\bar{\mathbf{W}}\cdot\partial_\sigma\mathbf{W} = 0\,, \tag{1.23}$$

$$\partial_\tau\bar{\mathbf{U}}\cdot\partial_\sigma\mathbf{U} + \partial_\tau\bar{\mathbf{W}}\cdot\partial_\sigma\mathbf{W} = 0\,. \tag{1.24}$$

There are six global conserved charges associated with the bosonic string action (1.21): the energy E, two spins S_1, S_2 in AdS_5 and three angular momenta J_1, J_2, J_3 in S^5. Explicitly, they are given by

$$E = \sqrt{\lambda}\int_0^{2\pi}\frac{d\sigma}{4\pi}\, i\left(W_3\partial_\tau\bar{W}_3 - \bar{W}_3\partial_\tau W_3\right)\,, \quad S_j = \sqrt{\lambda}\int_0^{2\pi}\frac{d\sigma}{4\pi}\, i\left(W_j\partial_\tau\bar{W}_j - \bar{W}_j\partial_\tau W_j\right)\,, \tag{1.25}$$

$$J_j = \sqrt{\lambda}\int_0^{2\pi}\frac{d\sigma}{4\pi}\, i\left(U_j\partial_\tau\bar{U}_j - \bar{U}_j\partial_\tau U_j\right)\,. \tag{1.26}$$

The $SU(2)$ operators that we considered at weak coupling, see (1.13), are dual to strings that have point-like motion in the middle of AdS_5 and have two non-zero angular momenta J_1, J_3 on S^5. The map between the charges at weak and strong coupling is

$$N \leftrightarrow J_1\,, \qquad L \leftrightarrow J_1 + J_3\,.$$

Of course, the exact form of $\mathbf{W}$ and $\mathbf{U}$ as functions of the worldsheet coordinates τ, σ depends on the particular classical string solution that we want to consider and we will see an explicit example in chapter 7. The interested reader can see [29, 30, 31, 32, 33, 34, 35] and references therein for reviews and recent developments regarding the computation of string energies in $AdS_5 \times S^5$.

For now, what we should take from this section is that:

- Given a single-trace operator in $\mathcal{N} = 4$ SYM, we can find its anomalous dimension at strong coupling by computing the energy of the dual string solution using (1.25).

1.2.3 Types of operators in $\mathcal{N} = 4$ SYM

Having reviewed the spectrum problem at weak and strong coupling, we will find it useful to introduce a classification of single-trace operators in $\mathcal{N} = 4$ SYM. This depends on the strong coupling behaviour of their anomalous dimensions or the scaling of their charges at

weak coupling. Namely, the operators that we introduced in the previous sections fall into three categories:

	Weak coupling	Strong coupling
Light operators	$\Delta \sim 1$	$\Delta \sim 1$
Medium operators	$N, L \sim 1$	$\Delta \sim \lambda^{1/4}$
Heavy operators	$N, L \gg 1$	$\Delta \sim \lambda^{1/2}$

Table 1.2: Types of operators in $\mathcal{N} = 4$ SYM.

Let us explain this notation.

- Light operators are BPS operators, i.e. their anomalous dimensions are zero to all orders in perturbation theory. Thus, their conformal dimensions are simply their classical dimensions at any value of the 't Hooft coupling. At weak coupling, BPS operators correspond to any operator with $L - N$ vacuum fields Z and N excitation fields X with zero anomalous dimension. In the language of the Bethe ansatz mentioned in the previous sections, the excitations in a BPS state are frozen, i.e. they have zero momenta. At strong coupling, BPS operators are dual to supergravity modes, which are the light, massless modes of the strings.

- Operators that have non-trivial anomalous dimension correspond to massive string states. Medium operators are the lightest of these. At weak coupling, they correspond to single-trace operators with non-zero anomalous dimension and with charges L, N of order 1. For example, the Konishi operator introduced in (1.18) belongs to this class of operators. At strong coupling, medium operators are dual to short strings with angular momenta of order 1, whose energies scale as $\lambda^{1/4}$.

- Finally, heavy operators are dual to the heaviest massive string states. At weak coupling, they correspond to single-trace operators with non-zero anomalous dimension and large charges L, N. At strong coupling, they are dual to classical string states with large angular momenta, whose energies scale as $\lambda^{1/2}$.

1.3 The structure constants problem

1.3.1 At weak coupling

When $\lambda \ll 1$, the structure constants appearing in (1.6) can be expanded in the 't Hooft coupling as

$$C_{123}(\lambda) = C_{123}^{(0)} + C_{123}^{(1)}\,\lambda + C_{123}^{(2)}\,\lambda^2 + \dots\,, \tag{1.27}$$

where $C_{123}^{(n)}$ is the n-loop structure constant. As opposed to the spectrum problem, see (1.11), in this case even the leading term in this expansion is non-trivial to compute. Indeed, given three single-trace operators, $C_{123}^{(0)}$ is found by performing all possible Wick contractions between them. If the operators are very long, i.e. heavy in the sense of table 1.2, this combinatorial problem is quite involved. Since integrability played a crucial role in the spectrum problem, it is natural to expect that it will also help us in computing the different terms in (1.27), starting with the leading one. This is precisely what we will show in this thesis: $C_{123}^{(0)}$ can be computed efficiently using integrability techniques. Moreover, we will also show that the same techniques can be used to compute four-point functions at tree level. We will explain the general strategy that we will use to do so in the next chapter. However, let us anticipate a crucial difference with respect to the spectrum problem. As can be seen in figure 1.2, we will need to "break" each operator in order to perform all contractions in the three-point function (and similarly for four-point functions). Since in the integrability approach we think of each operator $\mathcal{O}_i$ to be of the form (1.13), it is clear that we will need to know the exact form of the wave functions $\psi(n_1, \dots, n_{N_i})$ of all operators. Recall that for the spectrum problem, we only needed to know the energy eigenvalues of the Hamiltonian (1.12). Thus, computing three-point functions using the integrability approach will be more involved than the spectrum problem. The notion of breaking operators/spin chains will be made precise in the next chapter. For now, let us review what is known for three-point functions in $\mathcal{N} = 4$ SYM at weak coupling.

Until recently, much less was known about correlation functions compared to the spectrum problem at weak coupling. It was shown in [36] that the three-point function of three BPS operators is protected. Earlier works had already provided evidence that integrability should play an important role in the computation of correlation functions in $\mathcal{N} = 4$ SYM. For example, [37] pointed out the importance of the algebraic Bethe ansatz in the computation of three-point functions. Also, it was found in [38, 39] that when considering one-loop three-point functions of $SO(6)$ operators, some of the corrections correspond to insertions of the integrable $SO(6)$ Hamiltonian at the points where one breaks the operators to perform the Wick contractions. An important recent development was the formulation of integrability techniques to compute three- and four-point functions of $SU(2)$ operators at tree level in $\mathcal{N} = 4$ SYM [40, 41]. Moreover, in [42] a weak/strong coupling match for three-point functions of two heavy operators and a light BPS operator in the $SU(3)$ sector of the theory was presented (see also [43] for subsequent work on $SL(2)$ operators). The results of [40, 41, 42] constitute the bulk of this thesis and will be explained in great detail in coming chapters.

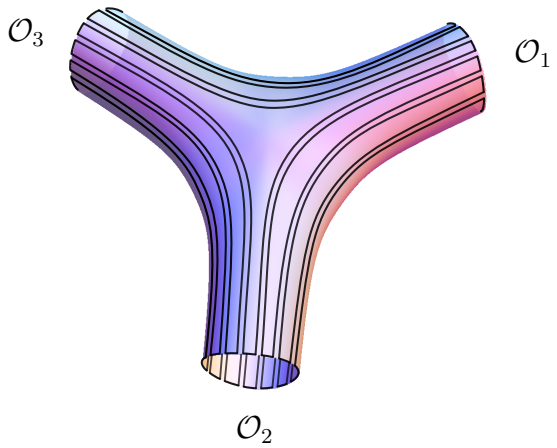

Figure 1.2: Three-point functions at tree level in the double-line notation. In order to perform all possible planar Wick contractions, we need to "break" each operator/spin chain. This requires knowing the precise form of each spin chain wave function.

Finally, more recently the classical limit of the three-point functions that we will compute in this thesis was presented in [44, 45]. Also, and quite remarkably, new integrability techniques to compute three-point functions of $SU(2)$ operators at one loop in $\mathcal{N} = 4$ SYM, i.e. $C^{(1)}_{123}$ in (1.27), were developed in [46]. We will briefly touch on these subjects in our conclusions.

What we should take from this section is that:

- In order to compute three- and higher-point functions, we need to know the exact form of the wave function of each operator, see (1.13).

1.3.2 At strong coupling

When $\lambda \gg 1$, we have to turn again to the AdS/CFT correspondence to compute correlation functions. The process that one has to consider in AdS is that of joining and splitting of strings, see table 1.1. We will refer to these processes as *holographic correlation functions*. A little more was known about them in the context of the duality, e.g. for earlier works on three- and four-point functions see [47, 48, 49, 50, 51, 52, 53, 54, 55, 56]. A common feature of most of these papers is that they were related to correlation functions of supergravity modes. In this case one can use the technology of Witten diagrams to compute correlation functions via the GKPW prescription [22, 23], see figure 1.3a (see [28] for a review).

Naturally, one would also like to compute holographic correlation functions of heavy operators. This was an open problem until Janik et al. [57] gave the correct prescription to compute the two-point function of two heavy, classical string states, see also [58]. They correctly reproduced the usual functional form of the two-point function (1.5) and the energy of the string solutions. The picture that arises is that of a worldsheet defined by the two large string states, which pinches off as it approaches the boundary of AdS at the insertion

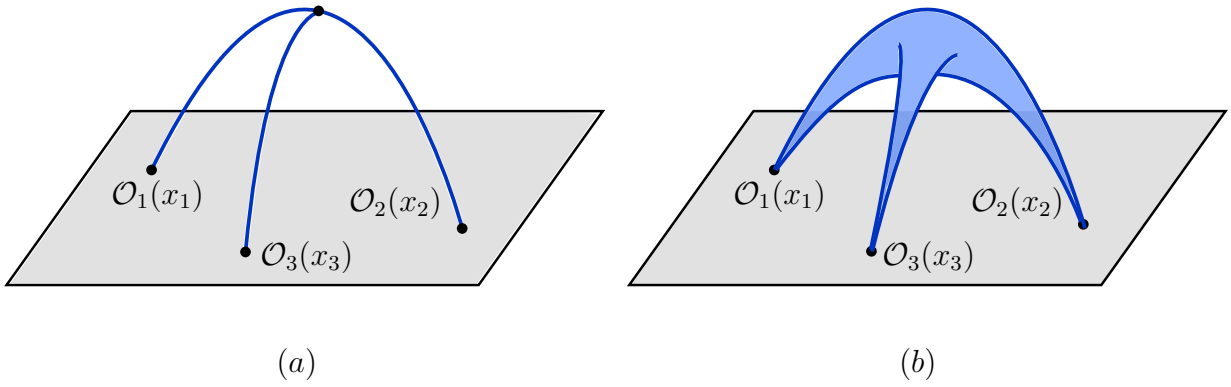

(a) (b)

Figure 1.3: Holographic correlation functions in AdS/CFT. (a) Usual Witten diagrams for supegravity modes. (b) Fattened Witten diagrams for classical strings states [57].

points x_1 and x_2 of the two-operators. An important point is that for higher-point correlation functions of heavy operators, the corresponding surface spanned by these should approach the insertion points of the operators in exactly the same way as they do in the two-point function case. For example, see figure 1.3b for a depiction of the holographic three-point function of three heavy operators. In [59] the computation of two-point functions of heavy operators was formulated in terms of vertex operators building on [60, 61].

Subsequently, these methods were extended to compute the three-point function of two heavy operators and a light BPS operator [62, 63, 64]. Various cases for this type of three-point function were worked out [65, 66, 67, 68, 69]. Moreoever, building on these results, in [70] the authors computed the four-point function of two heavy operators and two light BPS operators. They found that it factorizes into the product of two three-point functions. Very importantly, we should mention that all this progress was being made on the strong coupling side (i.e. the gravity side of the correspondence) without exploiting the underlying integrability of the string sigma model.

It is worth mentioning a couple of important recent developments on the strong coupling side using integrability techniques. In particular, in [71] the authors successfully computed part of the three-point function of three heavy operators with non-trivial motion in S^5, while [72] computed part of the case corresponding to three GKP strings [73].

In short, given that the spectrum problem is already very well understood, we expect that integrability will also play a crucial role in the computation of three- and higher-point correlation functions both at weak and strong coupling in $\mathcal{N} = 4$ SYM. The recent progress in this field suggests that this is indeed the case. With this we close our introduction and move on to explaining the general strategy that we will use to exploit the underlying integrability of the theory to compute three- and four-point functions at weak coupling.

Chapter 2

General Setup and Outline

The main goal of this thesis is to show that one can use integrability techniques to efficiently compute correlation functions of single-trace operators in $\mathcal{N} = 4$ SYM. Having introduced how spin chains arise in the theory, in this chapter we sketch our strategy to compute three- and four-point functions using spin chains. We also provide an outline of the thesis.

2.1 Three-point functions

As we saw in the previous chapter, the fundamental objects in $\mathcal{N} = 4$ SYM are the two- and three-point functions. Knowing them we can in principle construct any higher-point function by gluing these building blocks together. Given that the problem of computing two-point functions, or the anomalous dimensions of operators, has already been solved using integrability, it is natural to expect that this property should allow us to compute the structure constants appearing in the three-point functions of the theory, see (1.6). We will show in this thesis that this is indeed the case. In particular, we will compute planar three-point functions of single-trace operators at tree level in $\mathcal{N} = 4$ SYM.[8] That is, we will determine the term $C^{(0)}_{123}$ in the expansion (1.27) (from now on, we will simply refer to it as C_{123}, unless otherwise stated). The type of single-trace operators that we will consider are those in the $SU(2)$ sector of the theory, see (1.13). Let us now explain our strategy.

The setup that we will consider is the one shown in figure 2.1. We have three single-trace operators of lengths L_1, L_2 and L_3, which are contracted by free propagators. Of course, in general each operator will have vacuum and excitation fields, but we do not distinguish between them in figure 2.1. This is simply because we do not need to do so in order to explain our strategy. Since each propagator connects two fields, $L_1 + L_2 + L_3$ must be an even number. Notice that once we know the lengths of the three operators, the number of

[8] Earlier interesting and inspirational works on three-point functions in $\mathcal{N} = 4$ SYM at weak coupling are [38, 37, 39]. In particular, [38] introduced the physical picture of cutting and gluing spin chains on which we elaborate below and [37] emphasizes the usefulness of the algebraic Bethe ansatz techniques for computing scalar products of quantum spin chains, which turns out to be very relevant for this problem.

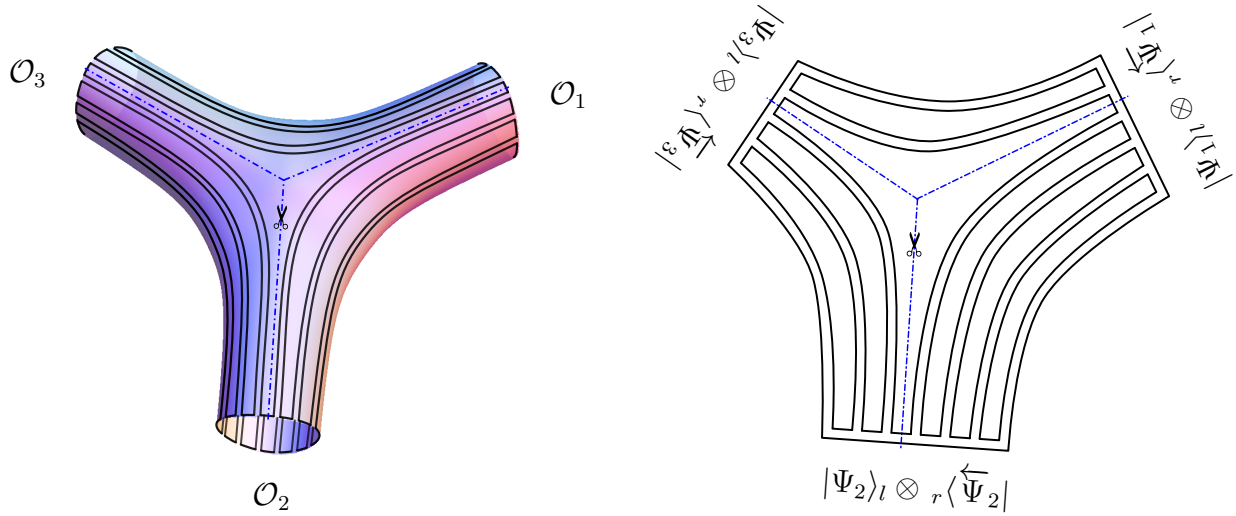

(a) (b)

Figure 2.1: (a) The planar tree-level contraction of three single-trace operators in the double-line notation. The diagram has a pair-of-pants topology (sphere with three punctures). (b) In the spin chain picture, each of the three single-trace operators corresponds to a state on a closed chain. The closed chains are cut into right and left open chains where the external states are represented. The three states are sewed together into the three-point function by overlapping the wave functions on each right chain with the wave function on the left subchain of the next operator.

free Wick contractions between $\mathcal{O}_i$ and $\mathcal{O}_j$ is

$$l_{ij} \equiv \frac{L_i + L_j - L_k}{2}\,. \tag{2.1}$$

These propagators automatically reproduce the factors $1/|x_{ij}|^{\Delta_i+\Delta_j-\Delta_k}$ in (1.6), with Δ_i being the classical dimension $\Delta_i^{(0)} = L_i$ in the case at hand. The tree-level structure constant is then given by the sum over all such Wick contractions, normalized by the two-point functions, see (1.6).

At $\lambda = 0$ many single-trace operators have the same dimension, which is simply the number of fundamental fields in the operator. That huge degeneracy is lifted at one loop. Therefore, to correctly identify the tree-level structure constants, we have to use those linear combinations of single-trace operators that have definite one-loop anomalous dimension $\Delta_i = \Delta_i^{(0)} + \gamma_i^{(1)}\lambda$.[9] As we saw in the previous chapter, these linear combinations can be thought of as states $|\Psi_i\rangle$ on a closed spin chain. In the spin chain language, the structure constant is constructed by going through the following steps (see also figure 2.1b)

1. Start with three closed chain states $|\Psi_i\rangle, |\Psi_j\rangle, |\Psi_k\rangle$ and choose a cyclic ordering (i, j, k).

[9]This is nothing but the standard textbook degenerate perturbation theory in Quantum Mechanics and needs to be taken into account. See e.g. [74, 75, 76] for discussions on the importance of this point.

2. Break the ith closed chain into *left* and *right* open subchains of lengths $(L_i+L_j-L_k)/2$, $(L_i+L_k-L_j)/2$. Do the same for the other two closed chains.

3. Express each closed chain state as an entangled state in the tensor product of the two subchains Hilbert spaces with the lengths indicated in the previous point. That is: $|\Psi_i\rangle = \sum_a |\Psi_{i_a}\rangle_l \otimes |\Psi_{i_a}\rangle_r$, where the sum runs over all possible ways of breaking the sites of the closed chain.

4. Wick contract the operator corresponding to the state $|\Psi_i\rangle_r$ with the operator corresponding to the state $|\Psi_{i+1}\rangle_l$. The Wick contraction is obtained from the spin chain contraction of a ket and bra states ${}_r\langle\overleftarrow{\Psi}_i|\Psi_{i+1}\rangle_l$ after a *flipping* operation $|\Psi_i\rangle_l \otimes |\Psi_i\rangle_r \to |\Psi_i\rangle_l \otimes {}_r\langle\overleftarrow{\Psi}_i|$, see figure 2.1b. This flipping operation maps the ket states in the right subchain into bra states with 1) reversed spin chain sites, 2) same wave function (not conjugated), 3) same charges.[10]

5. Normalize the three external states.

The resulting structure constant can then be obtained from brute force contractions of the states and is given by

$$C_{123} = \frac{L_1 L_2 L_3 \sum_{a,b,c} {}_r\langle\overleftarrow{\Psi}_{3_c}|\Psi_{1_a}\rangle_l \; {}_r\langle\overleftarrow{\Psi}_{1_a}|\Psi_{2_b}\rangle_l \; {}_r\langle\overleftarrow{\Psi}_{2_b}|\Psi_{3_c}\rangle_l}{\sqrt{L_1\langle\Psi_1|\Psi_1\rangle}\sqrt{L_2\langle\Psi_2|\Psi_2\rangle}\sqrt{L_3\langle\Psi_3|\Psi_3\rangle}} \tag{2.2}$$

Here, the factors of L_1, L_2 and L_3 arise from summing over all the ways of cutting open the closed chains, before gluing them together.

What we have said so far applies to the planar tree-level contraction of any single-trace operators, whether they have a definite one-loop anomalous dimension or not. However, operators with definite anomalous dimension are generically some linear combinations of a huge number of single-trace operators. Even at tree level the direct calculation of these contractions is a very complicated combinatorial problem, whose complexity grows rapidly as we increase the lengths of the operators in the three-point function.

Let us now focus on the $SU(2)$ operators of interest, represented by the spin chain states (1.13). One may hope, that the underlying integrability of the theory may help to simplify the problem of computing three-point functions of these types of operators. Indeed, recall that the one-loop anomalous dimension matrix is represented by the integrable spin chain Hamiltonian (1.12). We can therefore use integrability techniques to compute the external eigenstates and hence compute their normalizations. Moreover, at one loop the spin chain Hamiltonian only acts *locally* on the chain. As a result, when we decompose the external state as an entangled state in the two subchains, each of the subchain states still has the same local form as an eigenstate. Therefore, even though the subchain states are not eigenstates, we can still use integrability techniques to compute their overlaps. We will show that the

[10] This point was previously considered in [38] and it will be explained in greater detail in chapter 4.

integrability techniques applied to this problem are much more efficient than a brute force calculation and in particular allow us to make computations for asymptotically long operators, which is otherwise impossible.

From our discussion, it should be clear that, while for the spectrum problem we needed the energies of an integrable Hamiltonian, see (1.12), the central ingredient in the case of three-point functions (and higher-point functions in general) is the precise form of the eigenstates that correspond to operators with definite anomalous dimensions. This implies knowing explicitly the wave function of every operator in the three-point function, see (1.13). Therefore, at the end of the day, the structure constant (2.2) will be a function of the set of momenta of the three operators. That is

$$C_{123}\left(\{p_1\},\{p_2\},\{p_3\}\right) . \tag{2.3}$$

Explicit expressions for three-point functions in terms of the momenta of the operators will be given in chapter 5.

To summarize, the integrability tools we need in order to compute tree-level three-point functions are (they will be explained in detail in chapters 3 and 4):

- The spin chain eigenstates, including of course the precise form of the wave function.
- The decomposition of an external eigenstate into an entangled state on the direct product of the two subchains. We shall denote this decomposition procedure by *cutting*.
- Once an eigenstate state is cut in two we need to *flip* one of its halves from a ket into a bra, see figure 2.1b.
- The overlaps of subchain states and norms of spin chain eigenstates. We denote these overlapping computations by *sewing*.

2.2 Four-point functions

In principle, the techniques outlined above can be used to compute any n-point correlation function. We are now going to show how to use them to compute four-point functions of single-trace operators in the $SU(2)$ sector of $\mathcal{N}=4$ SYM. These correlation functions are interesting dynamical observables in their own right.

Let us consider the setup of figure 2.2a, where we have four operators of lengths L_1, L_2, L_3 and L_4. Again, we do not distinguish between vacuum and excitation fields in figure 2.2. As reviewed in chapter 1, four-point functions are not uniquely fixed by conformal symmetry. Rather, they may take the form (1.7). We denote the number of Wick contractions between operators $\mathcal{O}_i$ and $\mathcal{O}_j$ by l_{ij}. Recall that in the case of three-point functions, the l_{ij} were uniquely fixed by the lengths of the three operators, see (2.1). This is not the case for

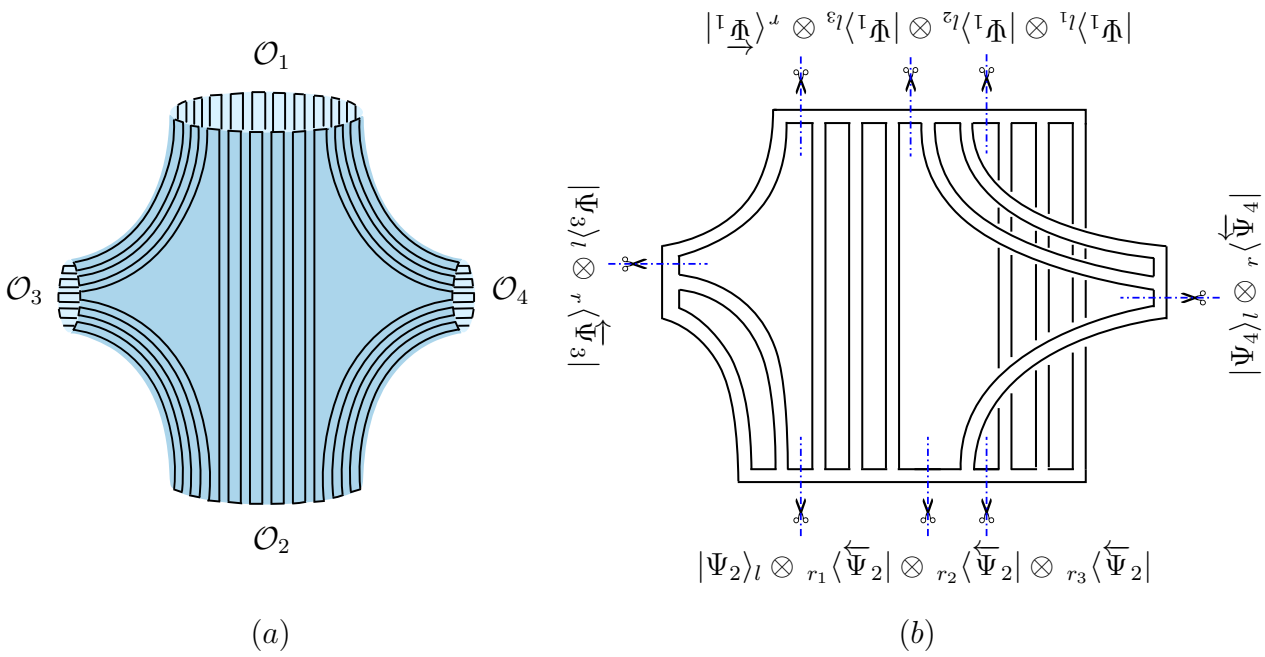

Figure 2.2: (a) The planar tree-level contraction of four single-trace operators in the double line notation. (b) In the spin chain picture, each of the four single-trace operators corresponds to a state on a closed chain. In this case we need to cut some of these closed chains more than once into open subchains. The four states are then sewed together into the four-point function by overlapping the wave functions on in the order shown in the picture. The restriction of not having Wick contractions between $\mathcal{O}_3$ and $\mathcal{O}_4$ can be trivially relaxed, see section 6.4.

four-point functions. Therefore, the tree-level four-point function can be written as[11]

$$G_4(x_1, x_2, x_3, x_4) = \frac{1}{N^2} \sum_{\text{all possible } \{l_{ij}\}} \frac{C_{1234;\{l_{ij}\}}}{\prod_{i<j} |x_{ij}|^{2l_{ij}}} \,. \tag{2.4}$$

Each $C_{1234;\{l_{ij}\}}$ can be computed using the techniques mentioned in the previous section.

As is clear from figure 2.2b, the main difference with respect to the case of three-point functions is that there is much more cutting and sewing to be done for four-point functions. Going through all the necessary steps and putting everything together, the four-point function is given by

$$C_{1234;\{l_{ij}\}} = \frac{L_1 L_2 L_3 L_4 \sum_{a,b,c,d} s(a,b,c,d)}{\sqrt{L_1 \langle \Psi_1 | \Psi_1 \rangle} \sqrt{L_2 \langle \Psi_2 | \Psi_2 \rangle} \sqrt{L_3 \langle \Psi_3 | \Psi_3 \rangle} \sqrt{L_4 \langle \Psi_4 | \Psi_4 \rangle}} \,, \tag{2.5}$$

[11] For non-planar diagrams, each $C_{1234;\{l_{ij}\}}$ will come with additional $1/N$ factors. However, in this thesis we will focus on planar diagrams, such that each $C_{1234;\{l_{ij}\}}$ is simply a number.

where

$$s(a,b,c,d) = {}_{r_3}\langle \overleftarrow{\Psi}_{2_b}|\Psi_{1_a}\rangle_{l_1}\ {}_{r}\langle \overleftarrow{\Psi}_{4_d}|\Psi_{1_a}\rangle_{l_2}\ {}_{r_1}\langle \overleftarrow{\Psi}_{2_b}|\Psi_{1_a}\rangle_{l_3}\ {}_{r}\langle \overleftarrow{\Psi}_{1_a}|\Psi_{3_c}\rangle_{l}\ {}_{r}\langle \overleftarrow{\Psi}_{3_c}|\Psi_{2_b}\rangle_{l}\ {}_{r_2}\langle \overleftarrow{\Psi}_{2_b}|\Psi_{4_d}\rangle_{l}.$$

Let us point out that the information about the number of contractions between the different operators, i.e. $\{l_{ij}\}$, is implicit in the different scalar products that appear in $s(a,b,c,d)$ (we will see this in more detail in chapters 3 and 4).

Lastly, let us point out that, since in this case we also need the precise form of the wave functions of the four operators, the four-point function will depend on the corresponding set of momenta:

$$C_{1234;\{l_{ij}\}}\left(\{p_1\},\{p_2\},\{p_3\},\{p_4\}\right)\ . \tag{2.6}$$

Explicit expressions for four-point functions in terms of the momenta of the operators will be given in chapter 6.

2.3 Outline

Let us now give an outline of how the material is organized in the rest of this thesis.

- **Part II:** In this part, we develop the necessary integrability tools to compute correlation functions at weak coupling in $\mathcal{N} = 4$ SYM. Chapter 3 reviews the coordinate and algebraic Bethe ansatz, which provide the framework to develop the tools we need. Then, in chapter 4 we explictly show how to perform the three basic operations on spin chains mentioned in the previous sections. Namely, we will show how to cut, flip and sew spin chains. These three operations will make up our *integrability toolkit*. The two chapters of this part of the thesis are based on material first published in [40].

- **Part III:** We will then use our integrability toolkit to compute correlation functions. We will explain in great detail how to go about implementing the steps outlined in sections 2.1 and 2.2. First, we start with three-point functions in chapter 5 and then move on to consider four-point functions in chapter 6. The material in these chapters is based on [40] and [41].

- **Part IV:** The subject of this part of the thesis is the weak/strong coupling match for correlation functions in the Frolov-Tseytlin limit. Chapter 7 provides the necessary strong coupling material, such as classical strings in $AdS_5 \times S^5$, the Frolov-Tseytlin limit and holographic correlation functions. In particular, to motivate the weak/strong coupling that we will present, we review the weak/strong coupling match for the spectrum in the same classical limit. In chapter 8 we use the results of Part II to provide conclusive numerical evidence to support the match, while in chapter 9 we prove it by using the language of coherent states. Finally, in chapter 10 we address the issue of back-reaction from the weak coupling point of view. The material in this part is based on [41, 42].

- **Part V:** In chapter 11 we present some results that will be needed to extend the integrability techniques for correlations functions beyond the $SU(2)$ sector of $\mathcal{N} = 4$ SYM. More specifically, in section 11.1 we present the coordinate nested Bethe ansatz for $SU(K)$ and $SU(K|J)$ spin chains, thus generalizing the discussion presented for $SU(2)$ spin chains in section 3.1. In section 11.2 we give a formula to compute the norm of Bethe eigenstates corresponding to spin chains with general Lie group. Moreover, in section 11.3 we explain how to compute the overlap of Bethe states of $SL(2)$ and $SU(1|1)$ spin chains. Part of the material in this chapter appeared in [40]. Finally, we present our conclusions and mention future directions in chapter 12.

Part II

Integrability Toolkit

Chapter 3

Bethe Ansatz

In this chapter we will review the coordinate and algebraic Bethe ansatz for $SU(2)$ spin chains. One of the goals of this chapter is to set the notation for the rest of the thesis. The expert reader is certainly familiar with the contents of this chapter and can safely skip it. However, we hope it is a useful resource for anyone trying to learn the subject.

3.1 Coordinate Bethe ansatz

As anticipated in the introduction, in this thesis we will mostly consider single-trace operators with definite one-loop anomalous dimensions made out of two complex scalars of $\mathcal{N} = 4$ SYM. An operator of this type is in fact linear combinations of single-trace operators and it can be mapped to a quantum state $|\Psi\rangle$ on a closed $SU(2)$ spin chain. We will represent an operator made of L complex scalar fields Z by a ferromagnetic vacuum state of L spins up [77]. Operators with N scalar fields X and $L - N$ fields Z are represented by flipping N of those spins up into spins down, see figure 3.1.[12] These spin flip excitations are called *magnons*. For example, in the case of the Konishi operator (1.18) we have $L = 4$ and $N = 2$.

A generic $SU(2)$ spin chain state will be of the form

$$|\Psi\rangle = \sum_{1\leq n_1<n_2<\cdots<n_N\leq L} \psi(n_1,\ldots,n_N)|n_1,\ldots,n_N\rangle\,, \tag{3.1}$$

where the ket $|n_1,\ldots,n_N\rangle$ stands for the state with spins down at positions $n_1, n_2, \ldots n_N$[13] while $\psi(n_1,\ldots,n_N)$ is the wave function, which we will fix below by requiring that the states (3.1) diagonalize the $SU(2)$ Heisenberg spin chain Hamiltonian:

$$\hat{H} = \frac{\lambda}{8\pi^2}\sum_{n=1}^{L}\left(\mathbb{I}_{n,n+1} - \mathbb{P}_{n,n+1}\right)\,. \tag{3.2}$$

[12] This is will be our convention throughout the thesis: Z fields and their conjugates $\bar{Z}$ will represent the vacuum, while X and $\bar{X}$ fields will represent excitations around this vacuum.

[13] E.g., $\mathrm{Tr}\left(Z^{n_1-1}XZ^{n_2-n_1-1}XZ^{n_3-n_2-1}XZ^{L-n_3}\right) = |\ldots\underset{n_1}{\downarrow}\ldots\underset{n_2}{\downarrow}\ldots\underset{n_3}{\downarrow}\ldots\rangle \mapsto |n_1,n_2,n_3\rangle$

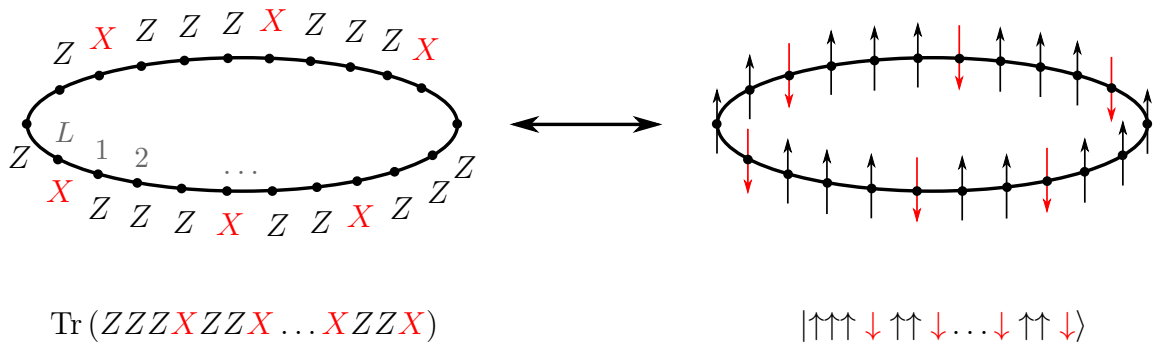

Figure 3.1: Map between single-trace operators made out of two complex scalars Z, X and $SU(2)$ spin chain states. There are $L - N$ vacuum fields Z (spins up) and N excitations X (spins down), such that the total length of the spin chain is L. The grey numbers in the left picture label the operator/spin chain sites.

In the spin chain language, the identity $\mathbb{I}_{n,n+1}$ and permutation $\mathbb{P}_{n,n+1}$ operators act on the spins at positions n and $n+1$ as follows

$$\begin{aligned} \mathbb{I}_{n,n+1}|\ldots \underset{n}{\uparrow}\ \underset{n+1}{\downarrow}\ \ldots\rangle &= |\ldots \underset{n}{\uparrow}\ \underset{n+1}{\downarrow}\ \ldots\rangle\,, \\ \mathbb{P}_{n,n+1}|\ldots \underset{n}{\uparrow}\ \underset{n+1}{\downarrow}\ \ldots\rangle &= |\ldots \underset{n}{\downarrow}\ \underset{n+1}{\uparrow}\ \ldots\rangle\,, \end{aligned}$$

where of course $L + 1 \equiv 1$. The energy spectrum of this Hamiltonian gives us the one-loop anomalous dimensions $\Delta^{(1)}$ of the operators. We will now review how to construct the wave functions $\psi(n_1, \ldots, n_N)$ which diagonalize the spin chain Hamiltonian (3.2).[14] For very pedagogical references on the coordinate Bethe ansatz, see [78, 79, 80].

Let us first consider the simplest case: a spin chain state with a single magnon, i.e. $N = 1$ in (3.1). We can diagonalize the translation-invariant Hamiltonian by going to Fourier space: $\psi(n_1) = e^{ip_1 n_1}$. With this, it is a simple exercise to show that the energy of the state $\epsilon(p_1)$, also called the *dispersion relation*, is given by

$$\epsilon(p) = \frac{\lambda}{2\pi^2} \sin^2 \frac{p}{2}\,. \tag{3.3}$$

For a two-magnon state we make the following ansatz for the wave function

$$\psi(n_1, n_2) = e^{ip_1 n_1 + ip_2 n_2} + S(p_2, p_1) e^{ip_2 n_1 + ip_1 n_2}\,. \tag{3.4}$$

The relative coefficient between the two plane waves is the amplitude for incoming momenta $\{p_1, p_2\}$ to be exchanged into $\{p_2, p_1\}$. In other words, it is the two-body S-matrix. By explicitly acting with $\hat{H}$ on this state we find that its energy is simply given by $\epsilon(p_1) + \epsilon(p_2)$

[14] In chapter 11 we explain how the coordinate Bethe ansatz works for more general spin chains.

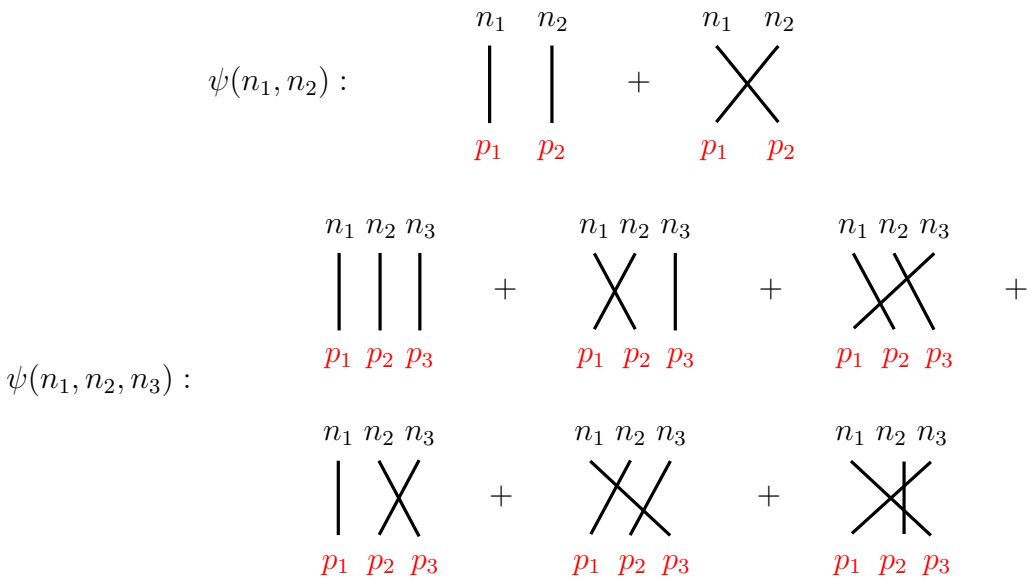

Figure 3.2: Diagramatic representation of $SU(2)$ wave functions. Note that we are only showing the plane wave terms and not their corresponding coefficients. The top diagram correspond to the two-magnon wave function (3.4), while the bottom diagram corresponds to the three-magnon wave function (3.7). The fact that in the latter case the scattering occurs in a pairwise manner is non-trivial and is a consequence of integrability. For example, the plane wave coefficient of that last term of $\psi(n_1, n_2, n_3)$ is $S(p_3, p_2)S(p_3, p_1)S(p_2, p_1)$, where $S(p_i, p_j)$ is the $SU(2)$ S-matrix shown in (3.5).

and that the S-matrix takes the following form

$$S(p_a, p_b) = \frac{\frac{1}{2}\cot\frac{p_a}{2} - \frac{1}{2}\cot\frac{p_b}{2} + i}{\frac{1}{2}\cot\frac{p_a}{2} - \frac{1}{2}\cot\frac{p_b}{2} - i}\,. \tag{3.5}$$

Given that we are in 1+1 dimensions, energy and momenta conservation imply that the individual momenta of two identical particles can at most be exchanged in an elastic scattering process between them. Thus, the two-particle wave function ansatz we made *had* to work.

For three particles the story is radically different. This is when integrability starts playing a role. Integrability means that in addition to the momentum $Q_1 = \hat{P}$ and energy $Q_2 = \hat{H}$, there exists a tower of local conserved charges Q_n which commute with the momentum and Hamiltonian. We can introduce an arbitrary complex number u and simply encode all conservation laws as follows[15]

$$\sum_{n=0}^{\infty} \Big[\hat{P}, Q_n\Big]\, u^n = \sum_{n=0}^{\infty} \Big[\hat{H}, Q_n\Big]\, u^n = 0\,. \tag{3.6}$$

[15] After some n the charges are of course not independent. For the Hamiltonian (3.2) such relation can be easily derived using the algebraic Bethe ansatz (ABA) formalism which we will review in section 3.2.

This relation has important consequences. For example, it allows us to guess the form of $\psi(n_1, n_2, n_3)$ in (3.1). The reason is that the existence of the higher conserved charges *does* imply that if we scatter three magnons with momenta $\{p_1, p_2, p_3\}$ they will scatter into some other momenta $\{p'_1, p'_2, p'_3\}$, which must be related to the original ones by a simple reshuffling. In other words, the scattering is effectively pairwise. For example, for three particles we are thus lead to

$$\psi(n_1, n_2, n_3) = e^{ip_1n_1+ip_2n_2+ip_3n_3} + A\, e^{ip_2n_1+ip_1n_2+ip_3n_3} + A'\, e^{ip_2n_1+ip_3n_2+ip_1n_3} + \dots \tag{3.7}$$

where $\dots$ stand for the remaining 3 possible plane waves. The coefficient A multiplies the plane wave which is obtained from the plane wave with unit coefficient by swapping particles with momenta p_1 and p_2. Thus

$$A = S(p_2, p_1)\,, \tag{3.8}$$

where $S(p, p')$ is the two-body S-matrix (3.5) derived above. The coefficient A' is the coefficient of the plane wave which is obtained after a sequence of two-momenta exchanges,

$$A' = S(p_2, p_1)S(p_3, p_1)\,. \tag{3.9}$$

The coefficients of the three remaining plane waves are obtained in the same way.

The generalization to $N > 3$ particles involves $N!$ plane waves whose coefficients follow again the same pattern. Therefore, the wave function of a generic N-magnon $SU(2)$ state can be nicely written as

$$\psi(n_1, \dots, n_N) = \sum_P A(P) \prod_{j=1}^{N} e^{i\, p_{P_j} n_j}\,, \tag{3.10}$$

where the sum runs over all $N!$ permutations P of $(1, 2, \dots, N)$. The plane wave coefficients are such that they obey the following relation

$$\frac{A(\dots, j, i, \dots)}{A(\dots, i, j, \dots)} = S(p_j, p_i)\,, \tag{3.11}$$

where $S(p, p')$ is the S-matrix given in (3.5). Our convention for the normalization of the wave function is that the plane wave with no momenta exchanged has unit coefficient, i.e. $A(1, \dots, N) = 1$. This choice of normalization, together with equation (3.11), fixes all plane wave coefficients. Of course, this normalization depends on the choice of an ordering of the momenta; more on this in section 3.3. The observation that the eigenstates of the Heisenberg spin chain are given by such ansatz was the key insight of the seminal work of Hans Bethe [16]. States of the form (3.1), whose wave functions are given by (3.10) are called *Bethe states*.

The energy of the multiparticle state is the sum of the energy of the individual magnons:

$$E = \sum_{j=1}^{N} \epsilon\left(p_j\right) \,. \tag{3.12}$$

Since the system is put in a finite circle of length L, the spectrum is discrete. The periodicity of the wave function imposes a set of N quantization conditions for the N momenta,

$$e^{ip_j L} \prod_{k\neq j}^{N} S(p_k, p_j) = 1 \tag{3.13}$$

which are called Bethe equations. The physical meaning of this equation is the following: if we carry a magnon with momentum p_j around the circle, the free propagation phase $p_j L$ plus the phase change due to the scattering with each of the other $N-1$ magnons must give a trivial phase. We shall denote by *Bethe eigenstates* those Bethe states whose momenta are quantized as in (3.13). Furthermore, since we are dealing with single-trace operators on the gauge theory side, we have to take into account the cyclicity of the trace by imposing the zero momentum condition on the spin chain picture:

$$\prod_{j=1}^{N} e^{ip_j} = 1.$$

Let us stress again that the fact that the simple wave functions described above diagonalize the Hamiltonian (3.2) is remarkable and very non-trivial. A generic spin chain Hamiltonian will not lead to an integrable theory, the scattering will not factorize into two-body scattering events and the set of momenta of multiparticle states will not be conserved. Hence, in general, the problem will be of exponential complexity and the best we can do is diagonalize small spin chains in a computer. The Bethe ansatz reduces this problem to a polynomial one. For example, the spectrum problem is completely solved by the simple set of algebraic equations (3.13): we first solve these equations to find the values of the momenta p_j, plug those values in (3.12) and we are done.

Before moving to the algebraic Bethe ansatz, let us introduce the rapidities u_j, which is a convenient parametrization of the momenta p_j. They are given by

$$u \equiv \frac{1}{2}\cot\frac{p}{2}\,, \qquad\qquad e^{ip} = \frac{u+i/2}{u-i/2}\,. \tag{3.14}$$

With this parametrization, the S-matrix (3.5) takes the simple form

$$S(u_a, u_b) = \frac{u_a - u_b + i}{u_a - u_b - i}\,, \tag{3.15}$$

while the Bethe equations (3.13) become simple polynomial equations

$$e^{i\phi_j} = 1 \qquad \text{where} \qquad e^{i\phi_j} \equiv \left(\frac{u_j + i/2}{u_j - i/2}\right)^L \prod_{k\neq j}^{N} \frac{u_j - u_k - i}{u_j - u_k + i}\,. \tag{3.16}$$

If the rapidities u_j satisfy the Bethe equations, they are also known as *Bethe roots*. Note that we have introduced the phases ϕ_j, which we will use in later chapters. Finally, in this parametrization, the eigenvalues of the Hamiltonian (3.2), see (3.12), read

$$E = \frac{\lambda}{8\pi^2} \sum_{j=1}^{N} \frac{1}{u_j^2 + \frac{1}{4}}\,. \tag{3.17}$$

3.2 Algebraic Bethe ansatz

While the coordinate Bethe ansatz we just reviewed gives us a nice physical picture of Bethe states and the Bethe equations, it does not really provide a rigorous explanation as to why the wave functions (3.10) diagonalize the Heisenberg Hamiltonian. The algebraic Bethe ansatz [81], which we now proceed to review, provides the explanation for this "miracle". We will show why relation (3.6) is indeed true and we will recall that the wave function (3.10) can be constructed by acting on the "ferromagnetic" state with some nonlocal "creation" operators $\mathcal{B}(u)$. For example, the state (3.1) with wave function (3.10) is simply given by

$$|\Psi\rangle = \mathcal{N}\mathcal{B}(u_1)\mathcal{B}(u_2)\dots\mathcal{B}(u_N)\,|\uparrow\dots\uparrow\rangle$$

where $\mathcal{N}$ is some simple known normalization factor which we will write down later.

The algebraic Bethe ansatz is a formalism developed by the Leningrad school for constructively producing and solving integrable theories (see [78, 81, 82] for nice introductions to the subject and for further references). Originally "solving" meant "computing the spectrum"; however, the algebraic Bethe ansatz was later used to solve more dynamical quantities, such as correlation functions [83, 84]. The great advantage over the coordinate Bethe ansatz is the constructive nature of the method and the mathematical elegance. The main drawback is that the physical picture is somehow obscured. For example, the magnon physical picture of (3.10) is somehow hidden in this formalism.

The starting point of our review is the statement that the Hamiltonian $\hat{H}$ (3.2) can be obtained from the following object:

$$\hat{H} - \frac{\lambda L}{8\pi^2} = -\frac{\lambda}{8\pi^2}\sum_{n=1}^{L}\mathbb{P}_{n,n+1} = \frac{\lambda}{8i\pi^2}\frac{d}{du}\Big(\log \mathrm{Tr}_0\Big[(u\,\mathbb{I} + i\,\mathbb{P})_{01}\dots(u\,\mathbb{I} + i\,\mathbb{P})_{0L}\Big]\Big)_{u=0}\,. \tag{3.18}$$

Before deriving this fact or explaining its relevance, let us digest the notation that we just introduced. First, u is the so-called *spectral parameter*. It is an arbitrary complex number

which we set to zero after taking the derivative.[16] Then, we introduce the *R-matrix*, defined as[17]

$$R_{0j}(u) \equiv (u\,\mathbb{I} + i\,\mathbb{P})_{0j}\ . \tag{3.19}$$

This is an operator acting on a tensor product of two vector spaces: the physical spin chain vector space at site j and an extra auxiliary vector space labeled by the index 0. Both these spaces are isomorphic to $\mathbb{C}^2$, the space where the spin 1/2 lives. Just as in (3.2), $\mathbb{I}$ is the identity operator and $\mathbb{P}$ is the permutation operator that interchanges the spins at physical position j and auxiliary position 0. We can of course write the R-matrix as a simple 4×4 matrix acting on the vector space $|\uparrow\uparrow\rangle, |\uparrow\downarrow\rangle, |\downarrow\uparrow\rangle, |\downarrow\downarrow\rangle$.

The operator inside the square brackets in (3.18) is the *monodromy matrix*, defined as

$$L_0(u) \equiv R_{01}(u)\dots R_{0L}(u)\,. \tag{3.20}$$

It acts on the tensor product of $L+1$ spaces: the L physical spaces corresponding to the L spin chain sites plus the auxiliary space 0. Since it is crucial to understand well the notation we are introducing let us be maximally pedestrian for a second. Using indices $i_i,\dots i_L$, $j_1,\dots,j_L$ for the physical spaces and a,b for the auxiliary space, the monodromy matrix is an object with indices

$$L_0(u)^{j_1\dots j_L;b}_{i_1,\dots i_L;a} \equiv \begin{pmatrix} L_0(u)^{j_1\dots j_L;1}_{i_1,\dots i_L;1} & L_0(u)^{j_1\dots j_L;2}_{i_1,\dots i_L;1} \\ L_0(u)^{j_1\dots j_L;1}_{i_1,\dots i_L;2} & L_0(u)^{j_1\dots j_L;2}_{i_1,\dots i_L;2} \end{pmatrix} \equiv \begin{pmatrix} \mathcal{A}(u+i/2)^{j_1\dots j_L}_{i_1,\dots i_L} & \mathcal{B}(u+i/2)^{j_1\dots j_L}_{i_1,\dots i_L} \\ \mathcal{C}(u+i/2)^{j_1\dots j_L}_{i_1,\dots i_L} & \mathcal{D}(u+i/2)^{j_1\dots j_L}_{i_1,\dots i_L} \end{pmatrix}^{b}_{a}\ .$$

The shifts by $i/2$ are introduced for future convenience. In other words, we can make the $\mathbb{C}^2$ auxiliary space manifest and write

$$L_0(u) = \begin{pmatrix} \mathcal{A}(u+i/2) & \mathcal{B}(u+i/2) \\ \mathcal{C}(u+i/2) & \mathcal{D}(u+i/2) \end{pmatrix} \tag{3.21}$$

where $\mathcal{A},\mathcal{B},\mathcal{C},\mathcal{D}$ are operators which only have physical indices, i.e. they act on the physical spin chain Hilbert space $\mathcal{H} = (\mathbb{C}^2)^{\otimes L}$. These operators obey an algebra, which we will derive below.

The next object we see in (3.18) is the trace of the monodromy matrix with respect to the auxiliary space. This defines the *transfer matrix*

$$\hat{T}(u) \equiv \mathrm{Tr}_0 L_0(u)\,. \tag{3.22}$$

Since we traced over the auxiliary space the transfer matrix is an operator acting on the

[16] This variable u will be soon identified with u appearing in (3.6) and (3.14) in the previous section.

[17] Since $\mathbb{I}$ and $\mathbb{P}$ are the only two invariant tensors of $SU(2)$, it is natural that we use them to construct the R-matrix. But what about the coefficients of these operators in (3.19)? If we write $R(u) = r(u)\,\mathbb{I} + s(u)\,\mathbb{P}$ and plug this into the Yang-Baxter relation, see (3.32), we find that $r(u)/s(u) = u/i$. Of course, this does not completely fix the R-matrix and as such, (3.19) is our choice of normalization for this operator.

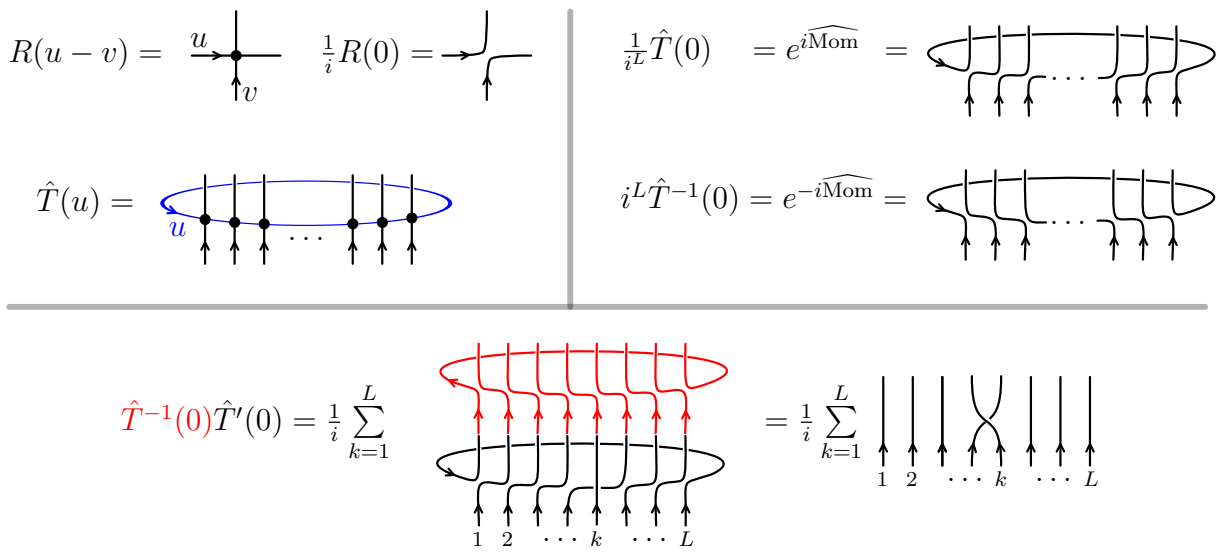

Figure 3.3: Since $i^{-1}R(0) = \mathbb{P}$, $i^{-L}\hat{T}(0)$ is the unit shift operator to the right, see the upper right corner of the figure. By definition of inverse $i^L\hat{T}^{-1}(0)$ is the unit shift operator to the left. When computing $\hat{T}'(0)$ the derivative will act on one of the R's at position k, hence the sum in the last line. Also, note that $R'(0) = \mathbb{I}$. We see that $\hat{T}'(0)$ is a sum of terms which are *almost* a total shift of one unit to the right except for a small "impurity" at site k. Therefore, when multiplying by $\hat{T}^{-1}(0)$, we *almost* get the identity operator acting on the full Hilbert space. The impurity simply leads to a permutation acting on sites k and $k-1$. Hence (3.24) leads to (3.2).

physical Hilbert space. More explicitly we can write it in terms of the operators $\mathcal{A}$ and $\mathcal{D}$ as

$$\hat{T}(u) = \mathcal{A}(u + i/2) + \mathcal{D}(u + i/2)\,. \tag{3.23}$$

Finally, in (3.18) we have the derivative of the logarithm of an operator (or big matrix). This is understood as usual as the inverse of the matrix times its derivative. With the notation introduced above, (3.18) simply reads

$$\hat{H} - \frac{\lambda L}{8\pi^2} = \frac{\lambda}{8i\pi^2}\,\hat{T}^{-1}(0)\,\hat{T}'(0) \tag{3.24}$$

where the prime stands for derivative with respect to the spectral parameter u. With all we know so far, we can readily show that the r.h.s of (3.24) does indeed give its l.h.s. This derivation is illustrated in figure 3.3.

An important feature of this construction is that, as explained in figure 3.4, transfer matrices with different spectral parameters commute,

$$\left[\hat{T}(v), \hat{T}(u)\right] = 0\,, \qquad \forall \quad u, v\,. \tag{3.25}$$

The Hamiltonian is just the log derivative of the transfer matrix and hence $[\hat{H}, \hat{T}(u)] = 0$. Also $[\hat{H}, \log \hat{T}(u)] = 0$. The latter relation is quite nice since it implies (3.6) neatly. Recall

that the existence of the higher local charges Q_n is what ensures integrability of the model. Indeed, we can Taylor expand $\log \hat{T}(u)$ around $u = 0$,

$$\log \hat{T}(u) = \sum_{n=0}^{\infty} Q_n u^n \,, \tag{3.26}$$

and generate in this way a tower of local conserved charges.[18] The first one, Q_1, is the momentum and the second, Q_2, is the energy, see figure 3.3. The higher terms are the higher charges we were looking for. Hence, indirectly, we now understand why the multi-particle ansatz (3.10) ought to work.

Relation (3.25) has another interesting consequence. Since the transfer matrices commute with each other for different values of the spectral parameter we can diagonalize $\hat{T}(u)$ with a spectral-parameter-*independent* base of 2^N states $|\Psi_i\rangle$ such that

$$\hat{T}(u)|\Psi_i\rangle = \Big(\mathcal{A}(u + i/2) + \mathcal{D}(u + i/2)\Big)|\Psi_i\rangle \equiv T(u)_i|\Psi_i\rangle \,. \tag{3.27}$$

These states diagonalize all the higher charges at the same time since they are simple derivatives of the transfer matrix. We could have picked any of the higher charges as the Hamiltonian. The algebraic Bethe ansatz approach tells us that all these Hamiltonians can be diagonalized at once with the same wave functions! We start seeing the constructive nature of this approach.

We already encountered the state $|\Psi\rangle$ in the coordinate Bethe ansatz approach: it is simply (3.1) with the wave function given by (3.10). For us it is important to construct this state in the algebraic Bethe ansatz language. It turns out that the monodromy matrix elements $\mathcal{B}(u)$ can be used as creation operators for the magnons.[19] More precisely, the claim is that

$$|\Psi\rangle = \mathcal{B}(u_1) \dots \mathcal{B}(u_N)\, |\uparrow \dots \uparrow\rangle \ , \tag{3.28}$$

yields a state proportional to (3.1) once we identify u_i and p_i according to (3.14). In other words $|\Psi\rangle$ is a *Bethe state*. If u_i are Bethe roots satisfying the Bethe equations (3.16), then $|\Psi\rangle$ satisfies (3.27) and is a *Bethe eigenstate*.

To understand why (3.27) indeed holds we need to

1) understand how to take the operators $\mathcal{A}$ and $\mathcal{D}$ through the creation operators $\mathcal{B}$,

2) derive the action of $\mathcal{A}$ and $\mathcal{D}$ on the ferromagnetic vacuum.

[18] Of course we would also get conserved charges by expanding $\hat{T}(u)$ or *any* functional of the transfer matrix around *any* point $u = u^*$. The advantage of expanding $\log \hat{T}(u)$ around $u = 0$ is that the charges generated in this way are local. This follows from the important relation $R(0) = \mathbb{P}$, see the derivation in figure 3.3 for an illustration of the importance of this property.

[19] This will be made more clear below, see discussion after (3.39).

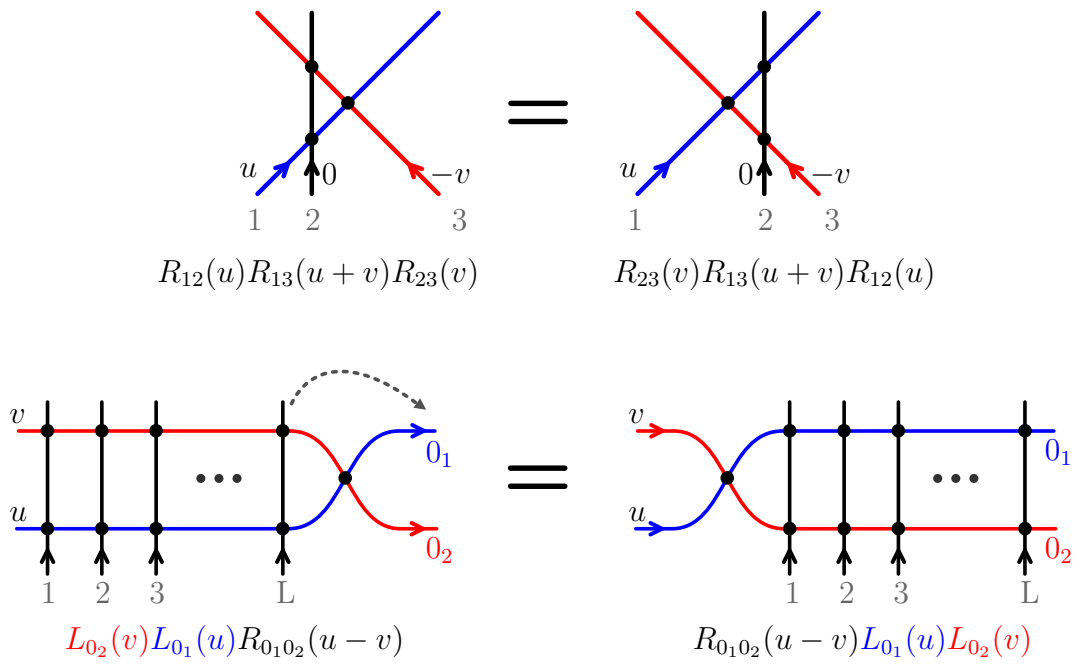

Figure 3.4: The R-matrix is a very special operator. It is designed to satisfy the Yang-Baxter equation depicted at the top. This equation is arguably the most important equation in quantum integrability. In particular it implies the $LLR = RLL$ type relation represented at the bottom. To prove this relation we simply move one of the vertical lines from the left group to the right region using Yang-Baxter and repeat this procedure until all the vertical lines are to the right of the R-matrix. From this simple equation all the algebra relations (table 3.1) of the monodromy matrix elements $\mathcal{A}, \mathcal{B}, \mathcal{C}, \mathcal{D}$ follow trivially as explained in the main text. Finally, multiplying this equation by R^{-1} and taking the trace over the tensor product of the two auxiliary spaces 0_1 and 0_2 we derive (3.25).

The latter is simple. From the definition (3.20) we easily see that

$$\mathcal{A}(u)\,|0\rangle = a(u)\,|0\rangle\,, \qquad \mathcal{D}(u)\,|0\rangle = d(u)\,|0\rangle\,, \tag{3.29}$$

$$\mathcal{C}(u)\,|0\rangle = 0\,, \qquad \mathcal{B}(u)\,|0\rangle = \text{a non-trivial single spin excitation}\,, \tag{3.30}$$

where $|0\rangle = |\uparrow \ldots \uparrow\rangle$ is the ferromagnetic vacuum state and[20]

$$a(u) \equiv \left(u + \frac{i}{2}\right)^L\,, \qquad d(u) \equiv \left(u - \frac{i}{2}\right)^L\,. \tag{3.31}$$

Next we need to understand the algebra of the elements of the monodromy matrix $\mathcal{A}, \mathcal{B}, \mathcal{C}$ and $\mathcal{D}$. In order to do so, we first note that the R-matrix is constructed in such a way that

[20]Different overall normalizations of the R-matrix (3.19) lead to different functions $a(u)$ and $d(u)$. The ration $a(u)/d(u)$ is however independent of that choice of normalization and any physical quantity will depend in a and d only through that ratio. With our choice of normalization for the R-matrix we have that $[\mathcal{B}(u)]^\dagger = -\mathcal{C}(u^*)$.

it obeys the following equation

$$R_{12}(u)R_{13}(u+v)R_{23}(v) = R_{23}(v)R_{13}(u+v)R_{12}(u)\,. \tag{3.32}$$

This is the famous Yang-Baxter relation, which is depicted at the top of figure 3.4. As explained in that figure, the fact that the R-matrix obeys this equation implies that the monodromy matrix $L(u)$ satisfies the relation

$$L_{0_2}(v)L_{0_1}(u)R_{0_1 0_2}(u-v) = R_{0_1 0_2}(u-v)L_{0_1}(u)L_{0_2}(v)\,, \tag{3.33}$$

where 0_1 and 0_2 are two auxiliary spaces isomorphic to $\mathbb{C}^2$. This relation encodes the algebra of the monodromy matrix elements. More explicitly we can choose a basis $|\uparrow\uparrow\rangle\,, |\uparrow\downarrow\rangle\,, |\downarrow\uparrow\rangle\,, |\downarrow\downarrow\rangle$ spanning the tensor product of these two spaces. In this basis the left-hand side of (3.33) simply reads

$$\begin{pmatrix} \mathcal{A}(v) & \mathcal{B}(v) & 0 & 0 \\ \mathcal{C}(v) & \mathcal{D}(v) & 0 & 0 \\ 0 & 0 & \mathcal{A}(v) & \mathcal{B}(v) \\ 0 & 0 & \mathcal{C}(v) & \mathcal{D}(v) \end{pmatrix} \begin{pmatrix} \mathcal{A}(u) & 0 & \mathcal{B}(u) & 0 \\ 0 & \mathcal{A}(u) & 0 & \mathcal{B}(u) \\ \mathcal{C}(u) & 0 & \mathcal{D}(u) & 0 \\ 0 & \mathcal{C}(u) & 0 & \mathcal{D}(u) \end{pmatrix} \begin{pmatrix} u-v+i & 0 & 0 & 0 \\ 0 & u-v & i & 0 \\ 0 & i & u-v & 0 \\ 0 & 0 & 0 & u-v+i \end{pmatrix}$$

while the right-hand side is obtained by multiplying the same matrices in the opposite order. In this way we get 16 algebra relations between the several elements, which we present in table 3.1.

To justify the identification of $\mathcal{B}$ and $\mathcal{C}$ as creation and annihilation operators, we compute the commutation relations of these nonlocal operators with the total spin generators $S^i \equiv \sum_{n=1}^{L} \sigma^i$. For that aim we consider the limit $v \to \infty$ with u held fixed. In this limit we have, from the definition (3.20), that $\mathcal{A}(v)/a(v) \simeq 1 + \frac{i}{2v}(1+S^z)$, $\mathcal{C}(v)/a(v) \simeq \frac{i}{v}S^+$, $\mathcal{D}(v)/a(v) \simeq 1 + \frac{i}{2v}(1-S^z)$ and

$$\frac{\mathcal{B}(v)}{a(v)} \simeq \frac{i}{v}\,S^- \ . \tag{3.39}$$

Now, from the sixteen algebra relations in table 3.1 we can read for example the commutation relations $[\mathcal{B}(u), S^z] = 2\,\mathcal{B}(u)$ and $[\mathcal{C}(u), S^z] = -2\,\mathcal{C}(u)$. This means that $\mathcal{B}(u)$ is a single spin creation operator while $\mathcal{C}(u)$ is a single spin annihilation operator. We also have $[\mathcal{A}(u), S^z] = [\mathcal{D}(u), S^z] = 0$. Furthermore,

$$\big[S^+, \mathcal{B}(u)\big] = \mathcal{A}(u) - \mathcal{D}(u)\ , \tag{3.40}$$

Equations (3.39) and (3.40) have further important consequences which we will discuss at the end of the next section.

Recall that our goal was to learn how to carry $\mathcal{A}$ and $\mathcal{D}$ through the $\mathcal{B}$ operators. Relations (3.34) and (3.35) tell us how to do this. Suppose we would drop the second term in the right-hand side of (3.34) and (3.35). Then it is clear that (3.28) would be an eigenstate of $\hat{T}(u-i/2)$

$$\mathcal{A}(v)\mathcal{B}(u) = f(u-v)\mathcal{B}(u)\mathcal{A}(v) + g(v-u)\mathcal{B}(v)\mathcal{A}(u) \tag{3.34}$$
$$\mathcal{B}(v)\mathcal{A}(u) = f(u-v)\mathcal{A}(u)\mathcal{B}(v) + g(v-u)\mathcal{A}(v)\mathcal{B}(u)$$
$$\mathcal{D}(v)\mathcal{B}(u) = f(v-u)\mathcal{B}(u)\mathcal{D}(v) + g(u-v)\mathcal{B}(v)\mathcal{D}(u) \tag{3.35}$$
$$\mathcal{B}(v)\mathcal{D}(u) = f(v-u)\mathcal{D}(u)\mathcal{B}(v) + g(u-v)\mathcal{D}(v)\mathcal{B}(u)$$
$$\mathcal{C}(v)\mathcal{A}(u) = f(v-u)\mathcal{A}(u)\mathcal{C}(v) + g(u-v)\mathcal{A}(v)\mathcal{C}(u)$$
$$\mathcal{A}(v)\mathcal{C}(u) = f(v-u)\mathcal{C}(u)\mathcal{A}(v) + g(u-v)\mathcal{C}(v)\mathcal{A}(u)$$
$$\mathcal{C}(v)\mathcal{D}(u) = f(u-v)\mathcal{D}(u)\mathcal{C}(v) + g(v-u)\mathcal{D}(v)\mathcal{C}(u)$$
$$\mathcal{D}(v)\mathcal{C}(u) = f(u-v)\mathcal{C}(u)\mathcal{D}(v) + g(v-u)\mathcal{C}(v)\mathcal{D}(u)$$

$$[\mathcal{C}(v),\mathcal{B}(u)] = g(u-v)\left[\mathcal{A}(v)\mathcal{D}(u) - \mathcal{A}(u)\mathcal{D}(v)\right] = g(u-v)\left[\mathcal{D}(u)\mathcal{A}(v) - \mathcal{D}(v)\mathcal{A}(u)\right] \tag{3.36}$$
$$[\mathcal{D}(v),\mathcal{A}(u)] = g(u-v)\left[\mathcal{B}(v)\mathcal{C}(u) - \mathcal{B}(u)\mathcal{C}(v)\right] = g(u-v)\left[\mathcal{C}(u)\mathcal{B}(v) - \mathcal{C}(v)\mathcal{B}(u)\right]$$

$$[\mathcal{B}(u),\mathcal{B}(v)] = [\mathcal{C}(u),\mathcal{C}(v)] = [\mathcal{A}(u),\mathcal{A}(v)] = [\mathcal{D}(u),\mathcal{D}(v)] = 0 \tag{3.37}$$

where

$$g(u) \equiv \frac{i}{u} \qquad , \qquad f(u) \equiv 1 + \frac{i}{u}\,. \tag{3.38}$$

Table 3.1: Algebra of the monodromy matrix elements which follows from the $LLR = RLL$ relations described in the text and depicted in figure 3.4.

with eigenvalue

$$T(u-i/2) = \left(u+\frac{i}{2}\right)^L \prod_{j=1}^{N} \frac{u-u_j-i}{u-u_j} + \left(u-\frac{i}{2}\right)^L \prod_{j=1}^{N} \frac{u-u_j+i}{u-u_j}\,. \tag{3.41}$$

Because of the second term in the right hand side of (3.34) and (3.35) the state $|\Psi\rangle$ is typically *not* an eigenstate of the transfer matrix. We can wonder what conditions do we need to impose so that the contribution of these extra terms vanishes. These conditions are nothing but the Bethe equations (3.16)![21]

[21] Indeed, those extra terms would lead to terms of the form $\sum_{k=1}^{N}(\alpha_k+\delta_k)\,\mathcal{B}(u)\prod_{j\neq k}\mathcal{B}(u_j)\,|\uparrow\ldots\uparrow\rangle$ where α_k is the contribution coming from $\mathcal{A}(u)$ and δ_k is the contribution coming from $\mathcal{D}(u)$ in (3.27). Suppose we want to find α_k. We start with $\mathcal{A}(u)\mathcal{B}(u_k)\prod_{j\neq k}\mathcal{B}(u_j)\,|\uparrow\ldots\uparrow\rangle$ and need to carry $\mathcal{A}(u)$ to the right until it hits the vacuum. Note that we ordered the creation operators so that $\mathcal{B}(u_k)$ comes first. We can always do it since $[\mathcal{B}(u),\mathcal{B}(v)]=0$. Now it is clear that to end up with terms contributing to α_k we must first use the second term in (3.34) to commute $\mathcal{A}(u)$ through $\mathcal{B}(u_k)$ so that $\mathcal{B}(u_k)$ becomes $\mathcal{B}(u)$ ($\mathcal{A}(u)$ becomes $\mathcal{A}(u_k)$). *But then* we must always use the first term in (3.34) to commute $\mathcal{A}(u_k)$ through all other $\mathcal{B}$'s since we are already happy with the arguments of the $\mathcal{B}$ operators. Hence we conclude that $\alpha_k = a(u_k)g(u-u_k)\prod_{j\neq k}^{N} f(u_j-u_k)$. Similarly $\delta_k = d(u_k)g(u_k-u)\prod_{j\neq k}^{N} f(u_k-u_j)$. The condition $\alpha_k+\delta_k=0$ yields the Bethe equations (3.16) once we recall (3.31) and (3.38).

3.3 A few comments and summary of notation

As explained above, the coordinate Bethe states (3.1) and the algebraic Bethe states (3.28) are proportional to each other. Let us write a precise relation between the two. First, recall that to define the coordinate Bethe state normalized according to (3.10) we pick a particular order for the momenta. Given an ordering $p_1, \dots, p_N$ for the momenta, the relation between the Bethe states normalized according to the coordinate Bethe ansatz (CBA) (3.10) and the algebraic Bethe ansatz (ABA) (3.28) is[22]

$$|\Psi\rangle^{\text{al}} = d^{\{u\}}\, g^{\{u+\frac{i}{2}\}} f_{<}^{\{u\}\{u\}}\ |\Psi\rangle^{\text{co}}\,, \tag{3.42}$$

where we have introduced the shorthand notation

$$F^{\{u\}} \equiv \prod_{u_j\in\{u\}} F(u_j)\ \ ,\ \ F_{<}^{\{u\}\{u\}} \equiv \prod_{\substack{u_i,\,u_j\,\in\,\{u\}\\ i<j}} F(u_i-u_j)\,, \tag{3.43}$$

where $F(u)$ is any given function. We will use this notation throughout the rest of this thesis. Also, from now on we should explicitly attach an upper index "al" or "co" where necessary to specify if we are referring to a given object in the algebraic or coordinate normalizations. For example, we will often denote the CBA and ABA Bethe states by $|\{u\}\rangle^{\text{co}}$ and $|\{u\}\rangle^{\text{al}}$, respectively, where $\{u\}$ denotes the set of all rapidities of the state. That is, from now on

$$|\Psi\rangle^{\text{al}} \leftrightarrow |\{u\}\rangle^{\text{al}}\ ,\qquad |\Psi\rangle^{\text{co}} \leftrightarrow |\{u\}\rangle^{\text{co}}\ . \tag{3.44}$$

Of course the normalization of the algebraic Bethe ansatz state (3.28) does not depend on the order of the momenta. After all, we see from (3.37) that the $\mathcal{B}(u_i)$ operators commute with each other. Hence we can also use (3.42) to go between two coordinate Bethe state with different ordering of the same magnons.

Let us rewrite the Konishi state (1.18) in the coordinate and algebraic normalizations. The Konishi state has $L=4$, $N=2$ and momenta $p_1=-p_2=2\pi/3$ or Bethe roots $u_1=-u_2=\sqrt{3}/6$. This leads to

$$\begin{aligned} K^{\text{co}} &= 4\, e^{-i\pi/3}\Big[\text{Tr}(ZZXX)-\text{Tr}(ZXZX)\Big]\,,\\ K^{\text{al}} &= \frac{8}{27}\Big[\text{Tr}(ZZXX)-\text{Tr}(ZXZX)\Big]\,, \end{aligned}$$

Finally let us end this section with a discussion on the completeness of the basis of states discussed so far. Using (3.40) and the same kind of reasonings of footnote 21 we can easily

[22] In the local basis of states (3.1), the wave functions are rational function of the rapidities $\{u_i\}$. The conversion factor in (3.42) can be simply derived by demanding that the two wave functions have the same zeros, poles and large u_k behavior.

prove that

$$S^+\mathcal{B}(u_1)\dots\mathcal{B}(u_N)\,|\uparrow\dots\uparrow\rangle = 0 \tag{3.45}$$

if the roots u_j obey Bethe equations. In other words, S^+ kills Bethe *eigenstates*. This means that Bethe eigenstates are *highest weight* states. Indeed, if we count the solutions to the Bethe equations (3.16) we find that there are precisely [81]

$$Z_{L,N} = \binom{L}{N} - \binom{L}{N-1}$$

solutions with N spin flips. This is exactly the number of highest weights for a chain of length L and $S^z = L/2 - N$. All other states are found by acting with S^- on these states. Indeed

$$\sum_{N=0}^{L/2}\left[2\left(\frac{L}{2}-N\right)+1\right]Z_{L,N} = 2^L\,. \tag{3.46}$$

Hence a complete basis of states is given by

$$\left(S^-\right)^n|\{u\}\rangle^{\rm al} = \left(S^-\right)^n\mathcal{B}(u_1)\dots\mathcal{B}(u_N)\,|\uparrow\dots\uparrow\rangle \tag{3.47}$$

where u_j obey Bethe equations and $n = 0,\dots,L-2N$. All these states have the same energy (or any other charge) as the highest weight state $\mathcal{B}(u_1)\dots\mathcal{B}(u_N)\,|\uparrow\dots\uparrow\rangle$ since the Hamiltonian (or the transfer matrix) commutes with S^i for $i = z,+,-$.

Note also that these states can be written using only the creation operators $\mathcal{B}(u)$ since for large rapidities this operator becomes the lowering operator, see (3.39). More precisely, this state is simply given by

$$\left(S^-\right)^n|\{u\}\rangle^{\rm al} = \lim_{\Lambda_k\to\infty}\left(\prod_{k=1}^{n}\frac{\Lambda_k^{1-L}}{i}\right)\mathcal{B}(\Lambda_1)\dots\mathcal{B}(\Lambda_n)\mathcal{B}(u_1)\dots\mathcal{B}(u_N)\,|\uparrow\dots\uparrow\rangle\,. \tag{3.48}$$

In short, we see that if we consider the Bethe equations for u_j and then add a few Bethe roots at infinity we describe the full Hilbert space. The factor $\left(\prod_{k=1}^{n}\Lambda_k^{1-L}/i\right)$ simply ensures a good limit when the roots go to infinity.

The coordinate Bethe ansatz states have a better limit when we send some of the roots u_* to infinity

$$\lim_{u_k\to\infty}|\{u\}\rangle^{\rm co} = S^-|\{u_j\}_{j\neq k}\rangle^{\rm co}\,. \tag{3.49}$$

Particularly important states are the so-called vacuum descendants

$$|\{\infty^N\}\rangle^{\rm co} = \left(S^-\right)^N|\uparrow\dots\uparrow\rangle \tag{3.50}$$

which correspond to a state with N roots at infinity only. They correspond to a ferromagnetic vacuum rotated away from the z axis. In the $\mathcal{N}=4$ language it corresponds to an operator with $L-N$ scalar fields Z and N scalar fields X without any anomalous dimension. These

are BPS states whose anomalous dimension is zero to all orders in perturbation theory as a consequence of supersymmetry. In the string theory dual language these states correspond to BMN point like strings which rotate around one of the equators of S^5 at the speed of light. Different values of N correspond to different equators of S^5 which are of course related by a global rotation.

Chapter 4

Integrability Toolkit

In this chapter we will present the necessary tools for computing correlation functions in $\mathcal{N} = 4$ SYM in the fashion explained in the introduction. That is, we will express a closed spin chain Bethe eigenstate as an entangled state in the tensor product of the two open subchain Hilbert spaces (section 4.1). Then we will explain how to map a state in one of the two subchains from ket to bra (section 4.2). Finally, we will compute the overlap of Bethe states (section 4.3). We call these three procedures *cutting*, *flipping* and *sewing*. In chapters 5 and 6 these tools will be used to put the pieces together into the three- and four-point functions as illustrated in figures 2.1 and 2.2. Two references that give a nice, pedagogical introduction to the techniques used in the cutting and sewing sections below (from the algebraic Bethe ansatz point of view) are [78, 82].

4.1 Cutting

Consider a spin chain of length L and a generic state (3.1) of that spin chain. We denote the first l spins starting from the left of that chain by *left* subchain and the last $r = L - l$ spins by *right* subchain. We can represent that state in the big chain (3.1) as an entangled state in the tensor product of the left and right subchains as

$$|\Psi\rangle = \sum_{k=0}^{\min\{N,l\}} \sum_{1\le n_1<\cdots<n_k\le l} \sum_{l<n_{k+1}<\cdots<n_N\le L} \psi(n_1,\ldots,n_N)\,|n_1,n_2,\ldots,n_k\rangle \otimes |n_{k+1}-l,\ldots,n_N-l\rangle\,. \tag{4.1}$$

The sum over k is the sum over how many magnons are in the left chain. The sum on the right-hand side of (4.1) has $\binom{L}{N}$ terms. For Bethe states there is a huge simplification. Namely, when we represent a Bethe state as an entangled state in the two subchains, each of the subchain states still has the same Bethe state form.

The reason is that – locally – these are eigenstates of a local Hamiltonian and therefore take the specific local form presented in the previous chapter. As a result, when we represent a Bethe state as an entangled state in the two subchains, each of the subchain states still has

the same local Bethe state form.

In other words, a magnon that is locally propagating along the chain does not know that at some far away point the chain was broken. To write the corresponding piece of the wave function, all we need to know is whether that magnon propagates on the left or right subchains. A Bethe state therefore breaks into two as

$$|\{u\}\rangle = \sum_{\alpha\cup\bar{\alpha}} H(\alpha,\bar{\alpha})|\alpha\rangle_l \otimes |\bar{\alpha}\rangle_r \,, \tag{4.2}$$

where the sum is over all 2^N possible way of splitting the rapidities into two groups α and $\bar{\alpha}$ such that $\alpha \cup \bar{\alpha} = \{u\}$. For example, if $N = 2$, the possible partitions $(\alpha, \bar{\alpha})$ would be $(\{\}, \{u_1, u_2\}), (\{u_1\}, \{u_2\}), (\{u_2\}, \{u_1\}), (\{u_1, u_2\}, \{\})$. As opposed to the $\binom{L}{N}$ terms in (4.1), we only have 2^N terms in (4.2). This is a very convenient simplification whenever $L \gg N$.

The function $H(\alpha, \bar{\alpha})$ takes different forms in the coordinate and algebraic bases. Below we will compute that function for each of these normalizations. Before moving on, let us introduce some further notation in the same spirit of (3.43). We shall use

$$F^{\alpha} \equiv \prod_{u_j\in\alpha} F(u_j) \,, \qquad F^{\alpha\bar{\alpha}} \equiv \prod_{\substack{u_i\,\in\,\alpha\\ v_j\,\in\,\bar{\alpha}}} F(u_i - v_j) \,, \qquad F^{\alpha\alpha}_{<} \equiv \prod_{\substack{u_i,\,u_j\,\in\,\alpha\\ i<j}} F(u_i - u_j) \,. \tag{4.3}$$

Cutting a coordinate Bethe state

The normalization of a Bethe state in the coordinate basis $|\{u\}\rangle^{\rm co}$ depends on the choice of ordering $u_1, u_2, \ldots, u_N$ of the magnons, see (3.10). For the states in the two subchains $|\alpha\rangle_l^{\rm co}$ and $|\bar{\alpha}\rangle_r^{\rm co}$ we choose the ordering induced from the ordering of $|\{u\}\rangle^{\rm co}$. With these conventions we will now derive $H^{\rm co}(\alpha, \bar{\alpha})$.

We first consider the case where all the magnons are in the left subchain: $\alpha = \{u\}$, $\bar{\alpha} = \emptyset$. In this case, by construction, the wave function of $|\alpha\rangle_l^{\rm co}$ coincides with the wave function of $|\{u\}\rangle^{\rm co}$ and therefore

$$H^{\rm co}(\{u\}, \emptyset) = 1 \,.$$

Now suppose we shift some set of magnons from α to $\bar{\alpha}$. There will be two factors contributing to $H^{\rm co}(\alpha, \bar{\alpha})$. One is the phase shift acquired by the $\bar{\alpha}$ magnons when translated trough the first l sites[23]

$$\prod_{\bar{\alpha}} \left(\frac{\bar{\alpha}_j + \frac{i}{2}}{\bar{\alpha}_j - \frac{i}{2}}\right)^l \equiv \frac{a_l^{\bar{\alpha}}}{d_l^{\bar{\alpha}}} \equiv e_l^{\bar{\alpha}} \,. \tag{4.4}$$

where a_l (a_r) and d_l (d_r) are defined as in (3.31) but using the length of the left (right) subchain instead of L. The second contribution to $H^{\rm co}(\alpha, \bar{\alpha})$ is the scattering phase between

[23] In other words, this factor arises because we shifted the label of the positions of the magnons of the right chain by l in order to start counting them from 1 as usual, see (4.1).

all pairs of magnons $u_j \in \alpha$ and $u_i \in \bar{\alpha}$ such that $i < j$

$$\prod_{\substack{i<j \\ u_j\in\alpha,\ u_i\in\bar{\alpha}}} \frac{f(u_j-u_i)}{f(u_i-u_j)}\,.$$

Multiplying the two factors and using our shorthand notation introduced in (4.3), we can write $H^{\rm co}(\alpha,\bar{\alpha})$ as

$$H^{\rm co}(\alpha,\bar{\alpha}) = e_l^{\bar{\alpha}}\,\frac{f^{\alpha\bar{\alpha}}\,f_<^{\bar{\alpha}\bar{\alpha}}\,f_<^{\alpha\alpha}}{f_<^{\{u\}\{u\}}}\ . \tag{4.5}$$

Finally, note that cutting a descendant of a coordinate state is trivially obtained from (3.49)

$$|\{u,\infty^n\}\rangle^{\rm co} = \sum_{\alpha\cup\bar{\alpha}=\{u\}} H^{\rm co}(\alpha,\bar{\alpha}) \sum_{m=0}^{n}\binom{n}{m}\,|\alpha\cup\{\infty\}^m\rangle_l^{\rm co}\otimes|\bar{\alpha}\cup\{\infty\}^{n-m}\rangle_r^{\rm co}\,. \tag{4.6}$$

Cutting an algebraic Bethe state

We can now use the relation between the coordinate and the algebraic normalizations (3.42) to conclude that

$$H^{\rm al}(\alpha,\bar{\alpha}) = f^{\alpha\bar{\alpha}}\,d_r^{\alpha}a_l^{\bar{\alpha}}\ . \tag{4.7}$$

Alternatively, we can also derive (4.7) by writing the monodromy matrix (3.20) as a product of the monodromy matrices of the left and right subchains, $L = (R_{01}\dots R_{0l})\,(R_{0l+1}\dots R_{0L}) \equiv L_lL_r$. More explicitly, the monodromy matrix elements are split as

$$\begin{pmatrix}\mathcal{A}(u) & \mathcal{B}(u)\\ \mathcal{C}(u) & \mathcal{D}(u)\end{pmatrix} = \begin{pmatrix}\mathcal{A}_l(u) & \mathcal{B}_l(u)\\ \mathcal{C}_l(u) & \mathcal{D}_l(u)\end{pmatrix}\begin{pmatrix}\mathcal{A}_r(u) & \mathcal{B}_r(u)\\ \mathcal{C}_r(u) & \mathcal{D}_r(u)\end{pmatrix}\ . \tag{4.8}$$

In particular, the Bethe state (3.28) can be written as

$$\mathcal{B}(u_1)\dots\mathcal{B}(u_N)\,|0\rangle = \prod_{j=1}^{N}\Big(\mathcal{A}_l(u_j)\mathcal{B}_r(u_j)+\mathcal{B}_l(u_j)\mathcal{D}_r(u_j)\Big)|0\rangle\,. \tag{4.9}$$

We could open the parentheses and get a sum of 2^N terms parametrized by which roots end up in the left spin chain creation operator $\mathcal{B}_l$. That set of roots is denoted by α. The set of roots ending up in the right spin chain creation operator $\mathcal{B}_r$ is denoted by $\bar{\alpha}$. Of course $\{u\} = \alpha\cup\bar{\alpha}$. This is precisely the sum over partitions in (4.2). To get rid of the $\mathcal{A}$ and $\mathcal{D}$ operator in (4.9) we use the commutation relations in table 3.1 to commute them through the $\mathcal{B}$'s plus the actions of these operators on the vacuum of the corresponding chains as given in (3.30). In this way one arrives at (4.7). This technique is known as the *generalized two-component model* [84, 83].

4.2 Flipping

After splitting the states into two (which we did in the previous section), we need to represent the Wick contraction of the elementary fields in the single-trace operators as a spin chain operation. In this language, the Wick contraction operation takes two subchain ket states on two different operators and produces a number. This can be achieved in two steps. We first flip one of the two subchain kets into a bra and then, in the next section, contract the ket and bra states. The result does not depend on which of the two kets we choose to flip. In what follows we will always flip the state in the right subchain before contracting it with the state on the left subchain of the next operator (as illustrated in figures 5.1 and 2.2). As explained in the introduction, the flipping procedure is not the usual conjugation. The latter acts on the corresponding operator by conjugation and therefore flips the order of fields and their charges. On the contrary, the flipping procedure $\mathcal{F}$ does not change the operator. As a result, the contraction of a ket state with a flipped bra state is the same as the Wick contraction of the corresponding operators.

In the introduction we added an upper arrow to distinguish ${}_r\langle\overleftarrow{\Psi}| = \mathcal{F}\,|\Psi\rangle_r$ from ${}_r\langle\Psi| = (|\Psi\rangle_r)^\dagger$. Let us give an example of how the usual conjugation and flipping operations act on a given ket state. For real ϕ, we have

$$\begin{aligned} \dagger \;:\quad & e^{i\phi}|XZXZZ\rangle \quad\mapsto\quad \langle XZXZZ|e^{-i\phi}\,, && (4.10)\\ \mathcal{F} \;:\quad & e^{i\phi}|XZXZZ\rangle \quad\mapsto\quad \langle \bar{Z}\bar{Z}\bar{X}\bar{Z}\bar{X}|e^{+i\phi}\,. && (4.11) \end{aligned}$$

Note that in our conventions $\langle Z|Z\rangle = \langle\bar{Z}|\bar{Z}\rangle = 1$, $\langle\bar{Z}|Z\rangle = 0$ and the spins (or fields) in the kets and bras are ordered from left to right, i.e. $\langle ZX|ZX\rangle = 1$, while $\langle XZ|ZX\rangle = 0$. Summarizing, the difference between the two maps is most clearly illustrated by their action on the local basis (3.1)

$$\begin{aligned} \dagger \;:\quad & \psi(n_1,\ldots,n_N)\,|n_1,\ldots,n_N\rangle \quad\mapsto\quad \psi^\dagger(n_1,\ldots,n_N)\,\langle n_1,\ldots,n_N|\,,\\ \mathcal{F} \;:\quad & \psi(n_1,\ldots,n_N)\,|n_1,\ldots,n_N\rangle \quad\mapsto\quad \psi(n_1,\ldots,n_N)\,\langle L-n_N+1,\ldots,L-n_1+1|\,\hat{C}\,, \end{aligned}$$

where $\hat{C}$ stands for charge conjugation, which exchanges $Z \leftrightarrow \bar{Z}$ and $X \leftrightarrow \bar{X}$.

We can now flip any Bethe state. Since the Hamiltonian is invariant under flipping the orientation of the chain and the charges, the operation $\mathcal{F}$ maps a ket Bethe state into a bra Bethe state. The overall factor relating these two states depends on the normalization. To determine this factor in the coordinate normalization, consider first a two-magnon state

$$|\{u_1,u_2\}\rangle^{\text{co}} = \sum_{1\le n_1<n_2\le L} \left[e^{ip_1n_1+ip_2n_2} + S(p_2,p_1)e^{ip_2n_1+ip_1n_2}\right]|n_1,n_2\rangle\,.$$

By changing variables to $m_1 \equiv L-n_2+1$ and $m_2 \equiv L-n_1+1$ it is easy to see that

$$\mathcal{F}\,|\{u_1,u_2\}\rangle^{\text{co}} = e^{i(L+1)(p_1+p_2)}S(p_2,p_1)\,{}^{\text{co}}\langle\{u_1^*,u_2^*\}|\,\hat{C}\,.$$

This construction is trivially generalized to any number of magnons. We find

$$\mathcal{F}\,|\{u\}\rangle^{\rm co} = e_{L+1}^{\{u\}}\,\frac{f_{>}^{\{u\}\{u\}}}{f_{<}^{\{u\}\{u\}}}\;{}^{\rm co}\langle\{u^*\}|\,\hat{C}\,, \tag{4.12}$$

where $e_{L+1}^{\{u\}}$ is defined as in (4.4). Recall that our goal was to flip the second ket in (4.2) which we can now do. We have

$$\mathcal{F}_{\text{second chain}}\,|\{u\}\rangle^{\rm co} = \sum_{\alpha\cup\bar{\alpha}\in\{u\}} e_{L+1}^{\bar{\alpha}}\,\frac{f^{\alpha\bar{\alpha}}\,f_{>}^{\bar{\alpha}\bar{\alpha}}\,f_{<}^{\alpha\alpha}}{f_{<}^{\{u\}\{u\}}}\;|\alpha\rangle_l^{\rm co}\otimes\,{}^{\rm co}_{r}\langle\bar{\alpha}^*|\,\hat{C}\,, \tag{4.13}$$

where $\bar{\alpha}^*$ is the set $\bar{\alpha}$ with its elements complex conjugated. Similar expressions can be written in the algebraic normalization using the conversion factor derived before.[24]

4.3 Sewing

The last building block that we need to understand to compute correlation functions is the overlap of Bethe wave functions, i.e. scalar products. The procedure of overlapping the wave functions is what we denote as *sewing*. The importance of spin chain scalar products in $\mathcal{N}=4$ SYM was first pointed out in [37].

The quantity we are interested in is

$$S_N^{\rm al}\,(\{v\},\{u\}) \equiv \langle 0|\prod_{j=1}^{N}\mathcal{C}(v_j)\prod_{j=1}^{N}\mathcal{B}(u_j)|0\rangle\,. \tag{4.16}$$

The explicit form of this quantity is actually known [85] and it is written for completeness in (A.2) in appendix A. Note that it is trivially related to the scalar product through

$$S_N^{\rm al}\,(\{v^*\},\{u\}) = (-1)^{N\;{\rm al}}\langle\{v\}|\{u\}\rangle^{\rm al}\,,$$

which in turn follows from $\mathcal{C}(u^*) = -\,[\mathcal{B}(u)]^\dagger$, see footnote 20. Luckily, when $\{u\},\{v\}$ take particular values the scalar product (4.16) simplifies dramatically. Let us look at two particular cases, which will be relevant for the computation of correlation functions in the next part of this thesis.[25]

[24] Using (3.42) we see that the algebraic Bethe states transforms as

$$\mathcal{F}\,|\{u\}\rangle^{\rm al} = (-1)^{N\;{\rm al}}\langle\{u^*\}|\hat{C}\,. \tag{4.14}$$

Furthermore

$$\mathcal{F}_{\text{second chain}}\,|\{u\}\rangle^{\rm al} = \sum_{\alpha\cup\bar{\alpha}\in\{u\}} f^{\alpha\bar{\alpha}}\,d_r^{\alpha}a_l^{\bar{\alpha}}\;\mathcal{B}^{\alpha}|0\rangle_l\otimes_r\langle 0|\mathcal{C}^{\bar{\alpha}^*}\hat{C}\;. \tag{4.15}$$

Recall that in our normalization $\mathcal{C}(u^*) = -\,[\mathcal{B}(u)]^\dagger$.

[25] There is one more case where the general formula (4.16) simplifies. This is the case when one of the

Norm of a Bethe eigenstate

For example, when we consider the norm of a Bethe eigenstate we have $\{u\} = \{v\}$ and both sets of roots obey the Bethe equations. In this case we have the remarkably simple result [86, 87]

$$S_N^{\rm al}(\{u\},\{u\}) = d^{\{u\}}\, a^{\{u\}}\, f_>^{\{u\}\{u\}}\, f_<^{\{u\}\{u\}} \det_{j,k} \partial_j \phi_k \tag{4.17}$$

where ϕ_k was introduced in (3.16), $\partial_j = \frac{\partial}{\partial u_j}$ and we are using the shorthand notation introduced in (3.43). We shall also use $\det_{j,k} \partial_j \phi_k \equiv \det \phi'_{\{u\}}$. The norm of a Bethe eigenstate in the coordinate basis reads

$$\mathcal{N}^{\rm co}(\{u\}) \equiv {}^{\rm co}\langle\{u\}|\{u\}\rangle^{\rm co} = \frac{1}{g^{\{u+\frac{i}{2}\}} g^{\{u-\frac{i}{2}\}}} \frac{f_>^{\{u\}\{u\}}}{f_>^{\{u^*\}\{u^*\}}} \det \phi'_{\{u\}} \,. \tag{4.18}$$

As explained in section 3.3, descendants of Bethe states are obtained by sending some of the roots to infinity, see (3.49). Using N to denote the total number of roots and M to denote the number of finite roots $\{u\}$, the norm of a Bethe eigenstate descendant is related to (4.18) by the square of the Clebsch-Gordan coefficients

$${}^{\rm co}\langle\{u;\infty^{N-M}\}|\{u;\infty^{N-M}\}\rangle^{\rm co} = \frac{(L-2M)!\,(N-M)!}{(L-M-N)!}\, {}^{\rm co}\langle\{u\}|\{u\}\rangle^{\rm co} \,. \tag{4.19}$$

Scalar product with a vacuum descendant

Another notable simplification occurs when we send one set of Bethe roots, e.g. $\{v\}$, to infinity. The resulting state is a vacuum descendant, see (3.50). In this case we find that the scalar product takes the form[26]

$${}^{\rm co}\langle\{\infty\}|\{u\}\rangle^{\rm co} = \frac{(-1)^N\, N!}{g^{\{u+\frac{i}{2}\}} f_<^{\{u\}\{u\}}} \sum_{\alpha\cup\bar\alpha=\{u\}} (-1)^{|\alpha|}\, e^{\alpha}\, f^{\bar\alpha\alpha} \,, \tag{4.20}$$

where the sum runs over all possible partitions of the N elements of the set $\{u\}$ into subsets $\alpha, \bar\alpha$ and $|\alpha|$ denotes the number of elements in α. Similarly, the scalar product of a Bethe state descendant with a vacuum descendant is related to (4.20) by a product of Clebsch-Gordan coefficients

$${}^{\rm co}\langle\{\infty\}|\{u,\infty^{N-M}\}\rangle^{\rm co} = \frac{(L-M)!\,N!}{M!\,(L-N)!}\, {}^{\rm co}\langle\{\infty\}|\{u\}\rangle^{\rm co} \,. \tag{4.21}$$

Again, in this formula the number of roots $\{u\}$ is M.

operators is a Bethe eigenstate while the other one is left generic. This is presented in (A.7) in appendix A.

[26] Note that in this case the algebraic Bethe states are not well normalized. Indeed, as we saw before, $\mathcal{C}(u_j) \sim i\, a(u_j)/u_j\, S^+ \to \infty$ as $u_j \to \infty$. The coordinate wave functions are better normalized and do not vanish or diverge in this limit, see (3.49).

Note that sewing Bethe states involves at most sums over partitions of the magnons. The number of terms therefore only grows as a power of the number of magnons and is independent of the chains' lengths.

4.3.1 A new recursion relation for $SU(2)$ scalar products

For completeness let us illustrate how we could compute (4.16) for arbitrary $\{u\}, \{v\}$. A possible strategy to compute this quantity is to derive a recursion relation yielding S_N in terms of S_{N-1}. Such recursion relations exist in the literature, see e.g. [85], and are presented in appendix A for completeness.

Here we derive a new recursion relation which we found quite efficient computationally. The idea is to get rid of particle creation operator $\mathcal{B}(u_1)$ by writing

$$S_N^{\text{al}}(\{v\},\{u\}) = \langle 0| \left[\prod_{j=1}^{N} \mathcal{C}(v_j), \mathcal{B}(u_1)\right] \prod_{j=2}^{N} \mathcal{B}(u_j)|0\rangle \tag{4.22}$$

which holds since the $\mathcal{B}$ operator kills the bra vacuum. Next we use the algebra relations (3.36) to compute this commutator. We have

$$\left[\prod_{j=1}^{N} \mathcal{C}(v_j), \mathcal{B}(u_1)\right] = \sum_n \left(\prod_{j=1}^{n-1} \mathcal{C}(v_j)\right) g(u_1 - v_n)\Big(\mathcal{A}(v_n)\mathcal{D}(u_1) - \mathcal{A}(u_1)\mathcal{D}(v_n)\Big) \left(\prod_{j=n+1}^{N} \mathcal{C}(v_j)\right), \tag{4.23}$$

where the sum over n runs of course from 1 to N. The term between the two products is just $[\mathcal{C}(v_n), \mathcal{B}(u_1)]$. Now we pick the operators $\mathcal{A}$ and $\mathcal{D}$ in this expression and carry them to the left through the $\mathcal{C}$'s using the algebra relations. Recall that $\mathcal{A}$ and $\mathcal{D}$ have a trivial action on the left vacuum. This procedure does not change the number of $\mathcal{C}$'s which is now equal to $N-1$. So, what are the possible final arguments of the remaining $N-1$ $\mathcal{C}$'s? When commuting an $\mathcal{A}$ through a $\mathcal{C}$ we have

$$\mathcal{C}(v)\mathcal{A}(u) = f(v-u)\mathcal{A}(u)\mathcal{C}(v) + g(u-v)\mathcal{A}(v)\mathcal{C}(u)\,, \tag{4.24}$$

which means that $\mathcal{A}$ can keep the same argument or swap arguments with $\mathcal{C}$. The same is true for a $\mathcal{D}$ operator passing through a $\mathcal{C}$. It is clear that we will get terms where the arguments of the $\mathcal{C}$'s are $N-1$ out of the N original v's. There is however one more possibility which comes from the algebra terms which swap the argument of the operators: we can also end up with $N-2$ of the original v's together with the root u_1. That is

$$\begin{aligned} S_N^{\text{al}}(\{v_1,\ldots,v_N\},\{u_1,\ldots,u_N\}) &= \sum_n b_n^{\text{al}}\, S_{N-1}^{\text{al}}(\{v_1,\ldots,\hat{v}_n,\ldots,v_N\},\{\hat{u}_1,u_2,\ldots,u_N\}) \\ &- \sum_{n<m} c_{n,m}^{\text{al}}\, S_{N-1}^{\text{al}}(\{u_1,v_1,\ldots\hat{v}_n,\ldots,\hat{v}_m,\ldots v_N\},\{\hat{u}_1,u_2,\ldots,u_N\})\,, \end{aligned} \tag{4.25}$$

where the hat means that the corresponding root is omitted. Naturally $S_0^{\rm al} = 1$. We simply need to find b_n and $c_{n,m}$! Let us derive b_n. We start by re-ordering the $\mathcal{C}$'s in a smart way and write (4.23) as[27],

$$\left[\left(\prod_{j\neq n}^{N}\mathcal{C}(v_j)\right)\mathcal{C}(v_n),\mathcal{B}(u_1)\right]. \tag{4.26}$$

We are interested in b_n. In other words we want to consider the contribution to the scalar product where $\mathcal{C}(v_n)$ and $\mathcal{C}(u_1)$ are not present. This means that we must get rid of $\mathcal{C}(v_n)$ in (4.26) and therefore the only term which will contribute is

$$\left(\prod_{j\neq n}^{N}\mathcal{C}(v_j)\right)[\mathcal{C}(v_n),\mathcal{B}(u_1)] = \left(\prod_{j\neq n}^{N}\mathcal{C}(v_j)\right)g(u_1-v_n)\Big(\mathcal{A}(v_n)\mathcal{D}(u_1)-\mathcal{A}(u_1)\mathcal{D}(v_n)\Big). \tag{4.27}$$

Now the $\mathcal{A}$'s must travel to the left using (4.24). Furthermore, when using these relations we must always pick the first term in the right-hand side. This is the term where the $\mathcal{A}$ and $\mathcal{C}$ do *not* swap their arguments. Otherwise we would end up with a $\mathcal{C}$ with an argument v_n or u_1 and therefore this would not contribute to b_n. For example,

$$\langle 0|\left(\prod_{j\neq n}^{N}\mathcal{C}(v_j)\right)\mathcal{A}(v_n) = a(v_n)\prod_{j\neq n}^{N}f(v_j-v_n)\,\langle 0|\left(\prod_{j\neq n}^{N}\mathcal{C}(v_j)\right)+\dots \tag{4.28}$$

where $\dots$ stand for terms where one of the $\mathcal{C}$'s ended up with the argument v_n. We used the fact that the action of $\mathcal{A}(v_n)$ on the bra vacuum simply yields $a(v_n)$. The other $\mathcal{A}$ and $\mathcal{D}$ operators in (4.27) are treated in the same way. It should be clear that at the end of the day we get

$$b_n^{\rm al} = g(u_1-v_n)a(v_n)d(u_1)\prod_{j\neq n}^{N}f(u_1-v_j)f(v_j-v_n)+(u_1\leftrightarrow v_n), \tag{4.29}$$

With a similar reasoning we could derive $c_{n,m}$. We would find

$$c_{n,m}^{\rm al} = g(u_1-v_n)g(u_1-v_m)a(v_m)d(v_n)f(v_n-v_m)\prod_{j\neq n,m}^{N}f(v_n-v_j)f(v_j-v_m)+(n\leftrightarrow m) \tag{4.30}$$

Since we know how to convert between the coordinate and algebraic Bethe states we can easily write a recursion relation for scalar products in the coordinate Bethe ansatz normalization. This is presented in appendix A.

The recursion relation (4.25) with (4.29) and (4.30) provides a complete solution to any scalar product in a straightforward way. For example, it is straightforward to implement this recursion in Mathematica. As mentioned above, there exists another recursion for the

[27]Note that we can order them in any way we want since they commute, $[\mathcal{C}(u),\mathcal{C}(v)]=0$, see table 3.1.

general scalar product (4.16) in the literature, which we present for completeness in (A.6).

It is interesting to compare the two recursions in the following table:

New recursion (4.25)	**Usual recursion (A.6)**
Uses scalar products with less particles as fundamental building blocks.	Uses generalized objects as building blocks. I.e., scalar products in different theories with different a and d functions appear at every step of the recursion and less particles.
Derived by reducing the number of particles in a very explicit way. Notion of particle is fundamental.	Derived from the analytic properties of the result. The scalar product is a rational function which can be therefore reconstructed from its poles and zeros. The notion of reducing the number of particles is secondary.
Contains much less terms than a brute force computation of the scalar product but still more terms than the recursion (A.6).	Contains much less terms than a brute force computation of the scalar product and less terms than the recursion (4.25).

Table 4.1: Comparison between the two recursion relations obeyed by the scalar product (4.16).

Given this comparison, it is fun to draw an analogy with two very important recursion relations in $\mathcal{N} = 4$ SYM which are used in studying scattering amplitudes: the CSW recursion relations [88] and the BCFW expansion [89]. A very similar table would be suitable for comparing these two recursions. The CSW and BCFW recursions would be the analogue of (4.25) and (A.6) respectively.

Part III

Exact Results for Correlation Functions

Chapter 5

Three-Point Functions

Having introduced the necessary integrability tools in the previous chapter, we are now ready to put them to use in order to compute the objects of interest of this paper: correlation functions in $\mathcal{N} = 4$ SYM. In this chapter, we will start by computing structure constants C_{123} of three single-trace operators in $\mathcal{N} = 4$ SYM at tree level. We will focus on a particular subset of operators as we will now describe.

5.1 Setup

The operators we will consider are linear combinations of single-trace operators made out of two complex scalars. As reviewed in the previous chapters, such operators with definite one-loop anomalous dimensions can be represented by Bethe eigenstates on a spin-$\frac{1}{2}$ chain. This fact will allow us to use the integrability technology introduced in the previous chapter for cutting, flipping and sewing the operators.

The general setup that we will use in this chapter is presented in figure 5.1a. We consider three operators $\mathcal{O}_1$, $\mathcal{O}_2$ and $\mathcal{O}_3$, with corresponding lengths L_1, L_2 and L_3. The number of propagators between operators i and j is fixed to be

$$l_{ij} = \frac{1}{2}\left(L_i + L_j - L_k\right), \tag{5.1}$$

where (i, j, k) is a permutation of $(1, 2, 3)$. We will restrict ourselves to the non-extremal case, that is where all l_{ij}'s are strictly positive. This is not only the generic case but it also has one important advantage: for non-extremal correlators the contribution of the operator mixing with double trace operators is suppressed in $1/N_c$ and need not be considered. Furthermore, there is considerable evidence in the literature that the extremal correlators can be considered as an analytic continuation of the non-extremal ones when some $l_{ij} \to 0$ [90, 91].

Each operator $\mathcal{O}_i$ is a single-trace operator made out of two complex scalars and is mapped to a spin chain state. One of the scalars we interpret as being the vacuum (or spin up) while the other scalar we interpret as excitations on that vacuum (or spin down). The total length

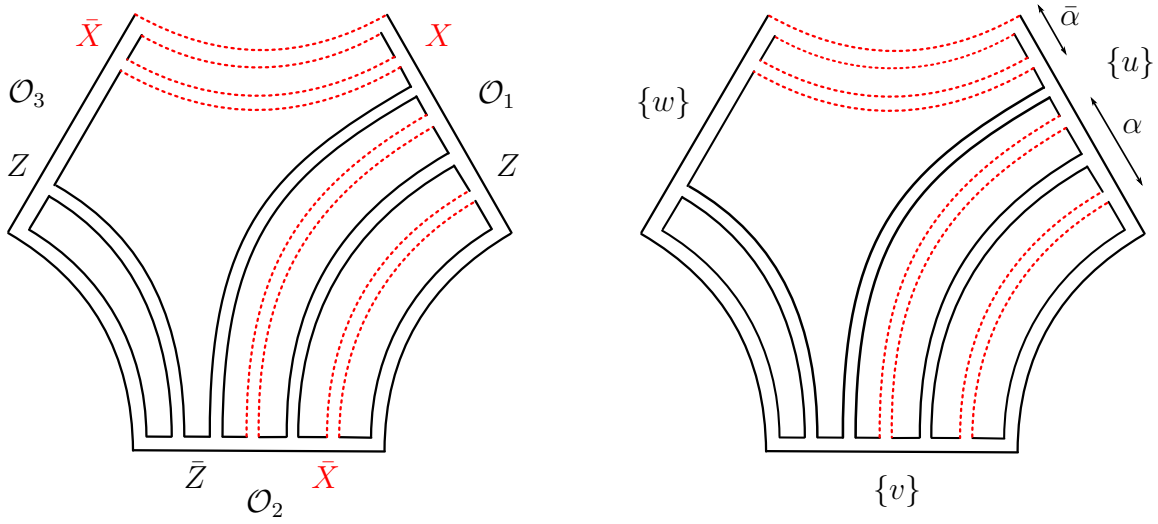

Figure 5.1: (a) Three-point function of $SU(2)$ operators at tree level. All contractions are such that R-charge is preserved. This is the simplest non-trivial configuration which is not extremal. Note that the number of excitations on each chain is subject to the condition $N_1 = N_2 + N_3$. Also, if we denote by l_{ij} the number of propagators between operators i and j, we have $l_{12} = L_1 - N_3$, $l_{13} = N_3$ and $l_{23} = L_3 - N_3$. (b) We show the partitions of the excitations in $\mathcal{O}_1$. Note that we only need to use the operation of cutting for this operator, as a part of its excitations (α) are contracted with those of $\mathcal{O}_2$ and another part ($\bar{\alpha}$) with those of $\mathcal{O}_3$.

of the operator is L_i and the number of excitations is denoted by N_i. The different scalars for the different operators are summarized in the following table:[28]

	Vacuum	Excitations	Notations
$\mathcal{O}_1$	Z	X	$\#\{Z, X\} = \{L_1 - N_1, N_1\}$
$\mathcal{O}_2$	$\bar{Z}$	$\bar{X}$	$\#\{\bar{Z}, \bar{X}\} = \{L_2 - N_2, N_2\}$
$\mathcal{O}_3$	Z	$\bar{X}$	$\#\{Z, \bar{X}\} = \{L_3 - N_3, N_3\}$

(5.2)

Note that this is the only setup that is fully contained in the $SU(2)$ sector and which involves non-extremal correlators at the same time. Due to R-charge conservation, when Wick contracting the single-trace operators with each other we can only connect a scalar with its conjugate. Therefore we see that all the vacuum constituents of $\mathcal{O}_3$ are connected to $\mathcal{O}_2$, while all excitations of $\mathcal{O}_3$ are contracted with $\mathcal{O}_1$, i.e.

$$l_{23} = L_3 - N_3 \qquad , \qquad l_{13} = N_3 \,.$$

[28]Note that there is no physical difference between $\mathcal{O}_1$ and $\mathcal{O}_2$. Indeed, our results will be invariant under the exchange of the two. The choice of vacuum (5.2) however is not symmetric. Still, we found this choice more convenient to work with than a more symmetric one.

The richest contraction is between operators $\mathcal{O}_1$ and $\mathcal{O}_2$, which has length

$$l_{12} = L_1 - N_3 \ .$$

In this case we can overlap both vacuum and excitations. Finally, note that the total number of excitations in the three operators are constrained by

$$N_1 = N_2 + N_3 \, .$$

All these statements are illustrated in figure 5.1a.

5.2 Brute force computation

Representing each operator by a spin chain state of the form (3.1) and writing the Bethe wave functions as $\psi_{n_1,\dots,n_N}$ instead of $\psi(n_1,\dots,n_N)$ for space convenience, we can always compute the three-point function of figure 5.1a by brute force as

$$C_{123} = \Omega_{123} \sum_{1\le n_1<\cdots<n_{N_2}\le L_1-N_3} \psi^{(1)}_{n_1,\dots n_{N_2},L_1-N_3+1,L_1-N_3+2,\dots,L_1} \, \psi^{(2)}_{L_2+1-n_{N_2},\dots,L_2+1-n_1} \, \psi^{(3)}_{1,2,\dots,N_3} \tag{5.3}$$

where

$$\Omega_{123} = \sqrt{\frac{L_1\, L_2\, L_3}{\mathcal{N}_1\, \mathcal{N}_2\, \mathcal{N}_3}} \tag{5.4}$$

and $\psi^{(j)}$ is the wave function of $\mathcal{O}_j$ given in (3.10). The factor Ω_{123} contains the symmetry factors mentioned in the introduction, see (2.2), and the normalization of the states $\mathcal{N}_j$ which is given by

$$\mathcal{N}_j = \sum_{1\le n_1<\cdots<n_{N_j}\le L_j} \left(\psi^{(j)}_{n_1,\dots,n_{N_j}}\right)^* \left(\psi^{(j)}_{n_1,\dots,n_{N_j}}\right) \, . \tag{5.5}$$

This way of computing the structure constant is equivalent to the direct Feynman diagram computation and involves the precise form of the N-particle wave function (3.10), which has $N!$ plane wave terms, and a sum of $O\left((L_1-N_3)^{N_2}\right)$ terms. For large number of excitations and long chains, (5.3) is very inefficient. This is when the techniques we introduced in the previous chapter will prove most powerful. Namely, we will see that using the operations of cutting, flipping and sewing, one can express the structure constant purely in terms of the rapidities and lengths of each spin chain.

Note that the *absolute value* of the structure constants is independent of the normalization of the three operators since we divide the overlap by the normalization of the wave functions. On the other hand changing the phase of these wave functions does not change their norm but it *will* modify the overlap by a phase. Therefore the *phase* of the structure constants is sensitive to the normalization of the operators. The phase is important however for bootstrapping higher-point functions and therefore we will keep track of it. To fix this

phase we choose to work with the coordinate convention for the wave functions.[29] Note that in order to make our formulas less clutered, we will deliberately omit the superscript "co" from most quantities in this chapter.

5.3 Three-point functions using integrability toolkit

To compute the three-point function using the integrability tools introduced in chapter 4, we use the notation shown in figure 5.1b and denote the rapidities of $\mathcal{O}_1, \mathcal{O}_2, \mathcal{O}_3$ by $\{u\}, \{v\}, \{w\}$ respectively. First, we need to use the cutting and flipping operations to cut the three operators and prepare them to be sewed. As mentioned in the introduction, we always choose to flip the right subchain of a given operator. Thus, in principle each operator should be decomposed and flipped as in (4.13), where the lengths of the left and right subchains of operator $\mathcal{O}_i$ in our setup are respectively $l_{i-1,i}$ and $l_{i,i+1}$ (with the indices identified modulo 3), see (5.1). However, as depicted in figure 5.1, only very particular subsets contribute when we cut the operators $\mathcal{O}_2$ and $\mathcal{O}_3$. Namely we need the left subchain of $\mathcal{O}_2$ and the right subchain of $\mathcal{O}_3$ to contain no excitations. The non-trivial cutting is that of $\mathcal{O}_1$. The lengths of the left and right subchains for this operator are $L_1 - N_3$ and N_3 respectively. Therefore, after using (4.13) to cut each operator and flip its corresponding right subchain, the three operators will have been schematically decomposed as

$$|\{u\}\rangle \to |\alpha\rangle \otimes \langle\bar{\alpha}^*|\,, \qquad |\{v\}\rangle \to |\{\}\rangle \otimes \langle\{v^*\}|\,, \qquad |\{w\}\rangle \to |\{w\}\rangle \otimes \langle\{\}|\,,$$

where we are of course leaving out the various factors appearing in (4.13).

The second step is to compute the scalar products between the different subchains, this is what we called the sewing procedure above. Note that the contractions between operators $\mathcal{O}_2$ and $\mathcal{O}_3$ are trivial, as we are simply contracting vacuum fields. On the other hand, the contractions between $\mathcal{O}_1$ and $\mathcal{O}_2$ and between $\mathcal{O}_1$ and $\mathcal{O}_3$ are nontrivial and we need to use the scalar products of Bethe states to compute them. Finally, we normalize our result dividing it by the norm $\mathcal{N}_j$ of each $\mathcal{O}_j$.

At the end of the day, the three-point function is given by

$$C_{123} = \Omega_{123}\, \frac{e_{L_2}^{\{v\}} f_{>}^{\{v\}\{v\}}}{f_{<}^{\{v\}\{v\}} f_{<}^{\{u\}\{u\}}} \sum_{\alpha\cup\bar{\alpha}=\{u\}} e_{L_1+1}^{\bar{\alpha}}\, f^{\alpha\bar{\alpha}} f_{>}^{\bar{\alpha}\bar{\alpha}} f_{<}^{\alpha\alpha} \langle\{v^*\}|\alpha\rangle\langle\bar{\alpha}^*|\{w\}\rangle\,, \tag{5.6}$$

where Ω_{123} is given in (5.4), we are using the notation introduced in (4.3) and

$$e_l^{\{u\}} \equiv \frac{a_l^{\{u\}}}{d_l^{\{u\}}} = \prod_{u_j\in\{u\}} \left(\frac{u_j + \frac{i}{2}}{u_j - \frac{i}{2}}\right)^l\,, \qquad f(u) = 1 + \frac{i}{u}\,. \tag{5.7}$$

[29] Recall that the coordinate normalization is sensitive to the order of Bethe roots. Therefore, different orders will give different structure constants. Of course, the absolute value of C_{123} is always the same but the phase does change.

Again, in these formulas all quantities are computed in the coordinate normalization, but we chose to omit the explicit "co" superscript to make the formulas less cluttered.[30] So,

$$\langle\bar{\alpha}^*|\{w\}\rangle \equiv {}^{\rm co}_{N_3}\langle\bar{\alpha}^*|\{w\}\rangle^{\rm co}_{N_3} , \qquad \langle\{v^*\}|\alpha\rangle \equiv {}_{L_1-N_3}{}^{\rm co}\langle\{v^*\}|\alpha\rangle^{\rm co}_{L_1-N_3}$$

and the norms appearing in Ω_{123} (5.4) are

$$\mathcal{N}_1 = {}^{\rm co}_{L_1}\langle\{u\}|\{u\}\rangle^{\rm co}_{L_1} , \qquad \mathcal{N}_2 = {}^{\rm co}_{L_2}\langle\{v\}|\{v\}\rangle^{\rm co}_{L_2} , \qquad \mathcal{N}_3 = {}^{\rm co}_{L_3}\langle\{w\}|\{w\}\rangle^{\rm co}_{L_3} ,$$

where we added subscripts to the bras and kets to indicate the length of the correponding (sub)chain. Our expression (5.6) is completely given in terms of scalar products between Bethe states in the coordinate normalization. These scalar products can be found using the new recursion relation (4.25) in the coordinate basis or using the general formula (A.3). Thus we solved the problem of computing C_{123} for generic states in our setup.

Furthermore, in most cases the scalar products in (5.6) are not the most generic ones and therefore the formula can be simplified considerably. For example, for the normalization factors $\mathcal{N}_j$ we can simply use (4.18) which is of course much simpler than the generic scalar product! Then, we note that $\langle\bar{\alpha}^*|\{w\}\rangle$ is also quite simple: since the states $|\{w\}\rangle$ and $|\bar{\alpha}\rangle$ are proportional the vacuum descendant with all spins down (see figure 5.1b), the product $\langle\bar{\alpha}^*|\{w\}\rangle$ factorizes into[31]

$$\langle\bar{\alpha}^*|\{w\}\rangle = \frac{\langle\bar{\alpha}^*|\{\infty\}^{N_3}\rangle\langle\{\infty\}^{N_3}|\{w\}\rangle}{\langle\{\infty\}^{N_3}|\{\infty\}^{N_3}\rangle} . \tag{5.8}$$

For the inner products in this expression we can now use (4.20) and (4.21) which are again much simpler than the general case (A.3). In sum, the only complicated scalar product in (5.6) is $\langle\{v^*\}|\alpha\rangle$. For this case we should indeed use (4.25) or (A.3) generically. Of course, there are some cases when even this general scalar product simplifies. For example, if we send the roots $\{u\}$ (and thus α) or $\{v\}$ to infinity, i.e. when either $\mathcal{O}_1$ or $\mathcal{O}_2$ is a BPS operator.

5.4 Simplest examples

Let us now use (5.6) in a couple of examples. In what follows, we will use $\circ$ to indicate a protected (BPS) operator and $\bullet$ to label a non-BPS operator. The simplest three-point function involves three BPS operators. This case is protected by supersymmetry and was studied in [36]: the tree-level result holds at any coupling. In our language this correlation function involves three operators where all excitations have zero momentum, i.e. all Bethe

[30] As explained above, different normalizations of the wave functions yield the same absolute value for C_{123} but different phase for the structure constant. In other words, we get the same absolute value for C_{123} for the coordinate wave function with any order of Bethe roots or even for states in the algebraic normalization. But the phase will differ for all these cases.

[31] Again we omit the subscript N_3 and the superscript "co" which is common to all ket's and bra's in this expression.

roots are sent to infinity. In other words, all three operators are vacuum descendants in the $SU(2)$ sense. In this case (5.6) simplifies to a simple combinatorial factor[32]

$$C_{123}^{\circ\circ\circ} = \frac{\sqrt{L_1 L_2 L_3}\binom{L_1 - N_3}{N_2}}{\sqrt{\binom{L_1}{N_1}\binom{L_2}{N_2}\binom{L_3}{N_3}}} \,. \tag{5.9}$$

This is indeed the result obtained in [36]. The fact that our general formula for three-point functions (5.6) reduces to this simple combinatorial result is a check that we did not make any mistake when deriving it.

The next-to-simplest case is when one of the operators is not protected. In this case the three-point function is no longer fixed by supersymmetry and it has a very interesting and rich structure. Consider for example the case when $\mathcal{O}_1$ and $\mathcal{O}_3$ are BPS states (i.e. vacuum descendants) while $\mathcal{O}_2$ is a generic Bethe eigenstate. In this case, the structure constant $C_{123}^{\circ\bullet\circ}$ will be a function of the N_2 Bethe roots characterizing the operator $\mathcal{O}_2$. If all these roots are finite, the operator corresponds to a highest weight spin chain state. When $N_2 - M_2$ of these roots are sent to infinity we obtain $SU(2)$ descendants; i.e. we generate the full $SU(2)$ multiplets by acting on the highest weights with $(S^-)^{N_2-M_2}$. The number of finite roots is M_2 and we use $\{v\}$ to denote the set of finite roots. The structure constant for the case when only $\mathcal{O}_2$ is non-BPS is then given from (5.6) by

$$C_{123}^{\circ\bullet\circ} = \frac{\sqrt{L_1 L_2 L_3}\binom{L_1 - N_3 - M_2}{N_2 - M_2}}{\sqrt{\binom{L_1}{N_1}\binom{L_3}{N_3}\binom{L_2 - 2M_2}{N_2 - M_2}}} \sqrt{\frac{g^{\{v+\frac{i}{2}\}} g^{\{v-\frac{i}{2}\}} f_{>}^{\{v^*\}\{v^*\}}}{f_{>}^{\{v\}\{v\}} \det \phi'_{\{v\}}}} \frac{\sum_{\beta\cup\bar{\beta}=\{v\}} (-1)^{|\beta|} f^{\beta\bar{\beta}} / e^{\beta}_{L_1 - N_3}}{g^{\{v+\frac{i}{2}\}} f_{<}^{\{v\}\{v\}}} \,. \tag{5.10}$$

There are several interesting limits which we can take in (5.10). We can consider many magnons, few magnons, the near-BMN limit, the classical limit, etc. The simplification of this result in the BMN limit is discussed in appendix B. We should note that the classical limit of (5.10) was recently studied in [44] and we will comment on it in our conclusions.

For example, the simplest possible nontrivial case is when $\mathcal{O}_2$ has only two particles with opposite momenta. In this case we have simply $M_2 = N_2 = 2$ and $v_1 = -v_2 \equiv v \equiv \frac{1}{2}\cot\frac{p}{2}$. Furthermore, from the Bethe equations (3.13) we can see that in this case $p = 2\pi n/(L_2 - 1)$, with $n \in \mathbb{Z}$. Then (5.10) simplifies to

$$C_{123}^{\circ\bullet\circ} = e^{-ip/2} \sqrt{\frac{L_1 L_2 L_3}{2\binom{L_1}{N_1}\binom{L_2}{2}\binom{L_3}{N_3}}} \frac{\sin\left(\frac{p\, l_{12}}{2}\right)\sin\left(\frac{p}{2}(l_{12}-1)\right)}{\sin^2\left(\frac{p}{2}\right)}, \tag{5.11}$$

[32]The normalization of the coordinate Bethe state when all roots are sent to infinity is given by ${}^{\rm co}\langle\{\infty\}^N|\{\infty\}^N\rangle^{\rm co} = \binom{L}{N}(N!)^2$, see (4.21).

where $l_{12} = (L_1 + L_2 - L_3)/2$, $N_3 = (L_1 + L_3 - L_2)/2$ and $N_1 = N_3 + 2$.

5.5 General cases

In this section we summarize the final results obtained from (5.6) for generic operators $\mathcal{O}_i$. As we can see from (5.10), even in a simple example the expression for the three-point function looks a little long. Thus, to present the results in a concise way we find it convenient to introduce some useful notation. As before we use L_i to denote the length of operator $\mathcal{O}_i$, N_i to denote the number of excitations of this operator and M_i to denote the number of finite Bethe roots. The sets of finite roots of the three operators are denoted by $\{u\}, \{v\}, \{w\}$.

We first introduce the following quantity

$$\mathscr{A}(l|\{u\}) \equiv \sum_{\alpha\cup\bar{\alpha}=\{u\}} (-1)^{|\alpha|} f^{\alpha\bar{\alpha}}/e_l^{\alpha}\,, \tag{5.12}$$

which is related to the scalar product with a vacuum descendant (4.20) and (4.21). Recall that e_l and f were defined in (4.4) and (5.7), respectively. The next quantity that we will use is related to the norm of Bethe states (4.18) and (4.19). It reads

$$\mathscr{B}_j \equiv \frac{g^{\{r-\frac{i}{2}\}} f_<^{\{r\}\{r\}}}{\sqrt{g^{\{r+\frac{i}{2}\}} g^{\{r-\frac{i}{2}\}}}} \sqrt{\frac{f_>^{\{r\}\{r\}}}{f_>^{\{r^*\}\{r^*\}}} \frac{\det \phi'_{\{r\}}}{L_j} \begin{pmatrix} L_j - 2M_j \\ N_j - M_j \end{pmatrix}}\,, \tag{5.13}$$

where the set of Bethe roots $\{r\}$ appearing in $\mathscr{B}_j$ is $\{u\}, \{v\}, \{w\}$ for $j = 1, 2, 3$ respectively (recall that these sets comprise only the M_j finite roots of each operator). Recall that ϕ_j was introduced in (3.16) and, as usual, we are using the shorthand notation (3.43) and (4.3).

Finally, the last object that we need is related to the general scalar product (A.3) and is given by

$$\mathscr{C}(l|\{u\},\{v\}) \;\equiv \sum_{\substack{\alpha\,\cup\,\bar{\alpha}\,=\,\{u\} \\ \beta\,\cup\,\bar{\beta}\,=\,\{v\}}} g_<^{\{u\}\{u\}} g_>^{\{v\}\{v\}} (-1)^{P_\alpha + P_\beta} e_l^{\bar{\alpha}} e_l^{\beta} h^{\alpha\beta} h^{\bar{\beta}\bar{\alpha}} h^{\alpha\bar{\alpha}} h^{\bar{\beta}\beta} \det t^{\alpha\beta} \det t^{\bar{\beta}\bar{\alpha}}\,.$$

where $(-1)^{P_\alpha}$ is defined as the sign of a permutation of the ordered set $\{u\}$ which gives $\alpha \cup \bar{\alpha}$.[33] We have also introduced

$$h(u) = 1 - iu\,, \qquad t(u) = -\frac{1}{u(u+i)}\,, \tag{5.14}$$

[33] In Mathematica we define $(-1)^{P_\alpha}$ as sign[a_List, ab_List, u_List] := Signature[Join[a, ab]]Signature[u].

$$C_{123}^{\circ\circ\circ} = \binom{l_{12}}{N_2} \frac{1}{\mathscr{B}_1\mathscr{B}_2\mathscr{B}_3} \quad , \quad C_{123}^{\circ\bullet\circ} = \binom{l_{12}-M_2}{N_2-M_2} \frac{\mathscr{A}(l_{12}|\{v\})}{\mathscr{B}_1\mathscr{B}_2\mathscr{B}_3}$$

$$C_{123}^{\circ\circ\bullet} = \binom{l_{12}}{N_2} \frac{\mathscr{A}(l_{13}|\{w\})}{\mathscr{B}_1\mathscr{B}_2\mathscr{B}_3} \quad , \quad C_{123}^{\bullet\circ\circ} = \binom{l_{12}-M_1}{N_2} \frac{\mathscr{A}(l_{13}|\{u\})}{\mathscr{B}_1\mathscr{B}_2\mathscr{B}_3}$$

$$C_{123}^{\circ\bullet\bullet} = \binom{l_{12}-M_2}{N_2-M_2} \frac{\mathscr{A}(l_{12}|\{v\})\mathscr{A}(l_{13}|\{w\})}{\mathscr{B}_1\mathscr{B}_2\mathscr{B}_3} \quad , \quad C_{123}^{\bullet\circ\bullet} = \binom{l_{12}-M_1}{N_2} \frac{\mathscr{A}(l_{13}|\{u\})\mathscr{A}(l_{13}|\{w\})}{\mathscr{B}_1\mathscr{B}_2\mathscr{B}_3}$$

$$C_{123}^{\bullet\bullet\circ} = \frac{1}{\mathscr{B}_1\mathscr{B}_2\mathscr{B}_3} \sum_{\substack{\alpha\cup\bar{\alpha}=\{u\} \\ |\bar{\alpha}|=l_{13}}} e_{L_1}^{\bar{\alpha}} f^{\alpha\bar{\alpha}} \mathscr{A}(l_{13}|\bar{\alpha})\mathscr{C}(l_{12}|\alpha,\{v\})$$

$$C_{123}^{\bullet\bullet\bullet} = \frac{\mathscr{A}(l_{13}|\{w\})}{\mathscr{B}_1\mathscr{B}_2\mathscr{B}_3} \sum_{\substack{\alpha\cup\bar{\alpha}=\{u\} \\ |\bar{\alpha}|=l_{13}}} e_{L_1}^{\bar{\alpha}} f^{\alpha\bar{\alpha}} \mathscr{A}(l_{13}|\bar{\alpha})\mathscr{C}(l_{12}|\alpha,\{v\})$$

Table 5.1: Tree-level structure constants C_{123} for three $SU(2)$ operators in the setup of figure 5.1. We use $\circ$ to indicate a BPS state and $\bullet$ to label a non-BPS state. So, for example, $C_{123}^{\circ\bullet\bullet}$ corresponds to the structure constants when $\mathcal{O}_1$ is a protected BPS operator while $\mathcal{O}_2$ and $\mathcal{O}_3$ are generic Bethe eigenstates. The most general case is of course $C_{123}^{\bullet\bullet\bullet}$. The last two cases were computed for highest weights only, i.e. for $M_j = N_j$. It is straightforward to generalize them to the case comprising descendants but the formulas become more involved. The first two cases were discussed in greater detail in the previous section.

as well as the shorthand notation

$$\det t^{\alpha\beta} \equiv \det_{\substack{u_i\in\alpha \\ v_j\in\beta}} t(u_i - v_j) \tag{5.15}$$

We can now use these useful objects to present the final results for C_{123} using (5.6). They are presented in table 5.1, which is one of the main results of this thesis. Note that $C_{123}^{\circ\bullet\circ}$ and $C_{123}^{\bullet\circ\circ}$, as well as $C_{123}^{\circ\bullet\bullet}$ and $C_{123}^{\bullet\circ\bullet}$, are not different cases. That is, $\mathcal{O}_1$ and $\mathcal{O}_2$ are exchanged if we choose to view the same operators as Z ($\bar{Z}$) excitations on a vacuum of X ($\bar{X}$) instead of X ($\bar{X}$) excitations on a vacuum the Z ($\bar{Z}$). We notice that $C_{123}^{\circ\bullet\circ}$ and $C_{123}^{\circ\bullet\bullet}$ are only nonzero when $M_2 \leq l_{12} \leq L_2 - M_2$ due to cancelations in $\mathscr{A}(l_{12}|\{v\})$.

We should stress that the integrability-based formulas presented in table 5.1 are far more efficient from a computational point of view than the brute force computation (5.3). For the reader's convenience, we present in appendix E the Mathematica codes needed to compute three-point functions in both ways, as well as some specific examples showing how to use the codes. As noted in that appendix, even when the number of excitations and lengths of the operators are not too large, the brute force formula (5.3) becomes computationally much slower than the formulas obtained from (5.6).

5.6 Three-point functions as determinants

The general formula for structure constants (5.6) is already a huge improvement compared to the brute force result, both from a conceptual and computational point of view. However, in [92], an expression for this general formula was obtained as a product of two determinants. It turns out that the matrices whose determinants one needs to compute are of size $N_1 \times N_1$ and $N_3 \times N_3$. Naturally, this is computationally more efficient than performing the sum over the 2^{N_1} terms appearing in (5.6), while also computing scalar products at each step.

The general strategy is to rewrite the two scalar products in (5.6). More specifically, recall that schematically we have

$$C_{123} \propto \sum_{\alpha \cup \bar{\alpha} = \{u\}} {}_{L_1-N_3}\langle \{v^*\}|\alpha\rangle_{L_1-N_3} \; {}_{N_3}\langle \bar{\alpha}^*|\{w\}\rangle_{N_3} \,, \tag{5.16}$$

where we included the subscripts to denote the lengths of the states for convenience, see figure 5.1. Following [92], we recast this equation in such a way that it involves the scalar product between the full state of operator $\mathcal{O}_1$, i.e. $|\{u\}\rangle$, and the two subchains in $\mathcal{O}_2$ and $\mathcal{O}_3$. Namely:

$$C_{123} \propto \Big({}_{N_3}\langle \{w\}| \otimes_{L_1-N_3} \langle \{v^*\}| \Big) |\{u\}\rangle_{L_1} \,. \tag{5.17}$$

Very importantly, in this way we have got rid of the sum over partitions of the rapidities $\{u\}$! This is a huge simplification.

To obtain an explicit expression for the r.h.s. of (5.17), we need to recast the computation of the three-point function considered in figure 5.1 in terms of the language of the six-vertex model, based on the algebraic Bethe ansatz. Here we will only sketch the idea behind the derivation of the determinant form of equation (5.6) and we refer the reader to [92] for more details.[34] However, let us simply recall that in the language of the algebraic Bethe ansatz, the states entering (5.17) are

$$\begin{aligned} |\{u\}\rangle_{L_1} &= \mathcal{B}(u_1) \dots \mathcal{B}(u_{N_1}) \, |\uparrow\rangle^{\otimes L_1} \,, \\ |\{v\}\rangle_{L_1-N_3} &= \mathcal{B}(v_1) \dots \mathcal{B}(v_{N_2}) \, |\uparrow\rangle^{\otimes L_1-N_3} \,, \\ |\{w\}\rangle_{N_3} &= \mathcal{B}(w_1) \dots \mathcal{B}(w_{N_3}) \, |\uparrow\rangle^{\otimes N_3} \,. \end{aligned} \tag{5.18}$$

5.6.1 Graphical rules

The starting point is to consider a spin chain of length L where at each site we have an impurity θ_j, with $1 \leq j \leq L$. These impurities are introduced because they will be necessary to obtain the determinant form of three-point functions. Then, we have an $SU(2)$ R-matrix

[34] We should point out that some of our conventions/normalizations are different from the ones used in [92]. Ours are such that they comply with the ones used in chapter 3 for the algebraic Bethe ansatz. Of course, the final result is independent of whatever normalization we choose to work with.

given by

$$R(u-\theta) \equiv (u-\theta)\,\mathbb{I} + i\,\mathbb{P}\,, \tag{5.19}$$

where we are using the normalization that we introduced in chapter 3, see (3.19). Of course, the latter is recovered by taking $\theta \to 0$. We can represent the R-matrix graphically as

$R(u-\theta) =$ 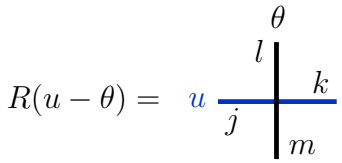

$= (u-\theta)\,\delta_{jk}\delta_{lm} + i\,\delta_{jl}\delta_{km}$

A nice way to keep track of the flow of the four indices in the R-matrix is to assign an arrow to each of its legs. In this way, one quickly realizes that the only non-zero components of the R-matrix are those shown in figure 5.2. These are the building blocks of the so-called *six-vertex model*. An important feature of this model is that the number of incoming and outgoing arrows at each vertex is conversed.

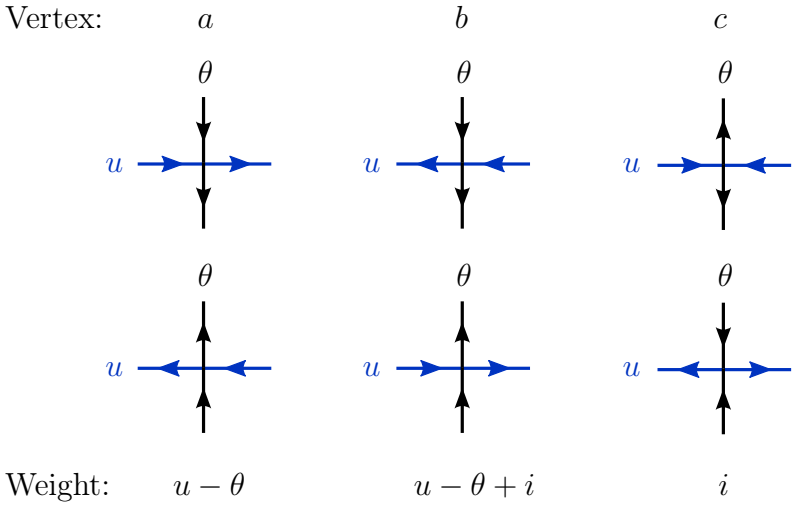

Figure 5.2: Non-vanishing components of the R-matrix (5.19) and their corresponding weights. This is known as the six-vertex model. Note that the number of incoming and outgoing arrows at each vertex is conserved. The weights are easy to read-off from the graphical representation of the R-matrix. For example, in the case of a-vertices, both the identity and permutation contribute, hence the factor $u - \theta + i$.

Recall from chapter 3 that, once we define the R-matrix, we can construct the monodromy matrix as

$$L(u) \equiv R(u-\theta_1)\dots R(u-\theta_L)\,. \tag{5.20}$$

Of course, the monodromy matrix introduced in (3.20) is recovered from the one above by taking the homogeneous limit $\theta_j \to 0$. The upper-right component of the monodromy matrix is $\mathcal{B}(u)$, which acts as a creation operator when acting on the ket vacuum, see (3.21) and

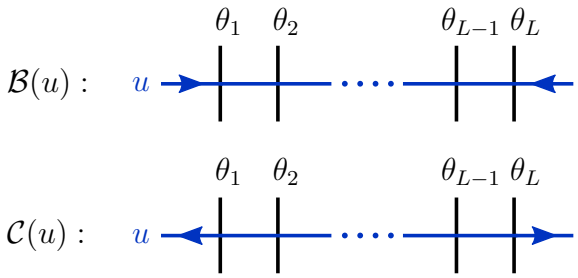

Figure 5.3: $\mathcal{B}$- and $\mathcal{C}$-lines, which are the graphical representation of the operators $\mathcal{B}(u)$ and $\mathcal{C}(u)$.

(3.30). Similarly, the lower-left component of $L(u)$ is $\mathcal{C}(u)$, which acts as an annhilation operator on the ket vacuum. Also, since in our normalization $[\mathcal{B}(u)]^\dagger \propto \mathcal{C}(u^*)$, see footnote 20, $\mathcal{C}(u)$ can be regarded as a creation operator on the bra vacuum. These two operators can be represented graphically by so-called $\mathcal{B}$- and $\mathcal{C}$-lines, see figure 5.3. At first, this graphical representation of the operators $\mathcal{B}(u)$ and $\mathcal{C}(u)$ might seem obscure, so, let us explain how they come about by introducing the *freezing trick*. Our convention is that in any graph, the top row of arrows represents a ket state, while the bottom row of arrows represents a bra state. Suppose that $\mathcal{B}(u)$ acts on the state $|\uparrow\rangle^{\otimes L}$. Then, let us pick any of the vertices and fix it to be a c-vertex from figure 5.2. This implies that the spin at that site will be flipped, while it is easy to check using conservation of arrow flow at all vertices that the other spins will be left untouched, see figure 5.4a. In short, acting with $\mathcal{B}(u)$ on the vacuum, we obtain a one-magnon ket, i.e. $\mathcal{B}(u)$ acts as a creation operator. This is precisely what we wanted. Using a similar logic, one can check that $\mathcal{C}(u)$ acting on $\langle\uparrow|^{\otimes L}$ creates a one-magnon bra, see figure 5.4b.

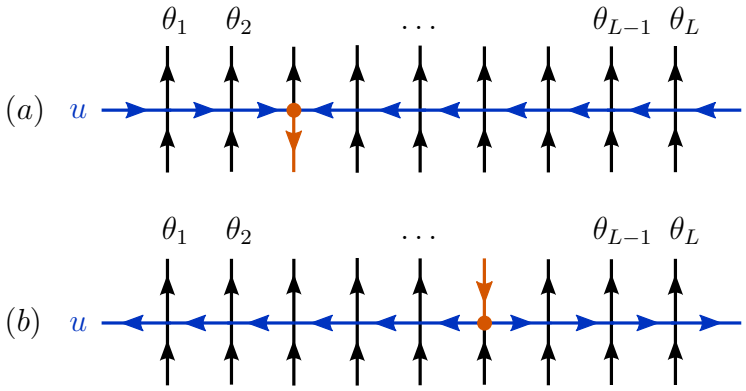

Figure 5.4: Freezing trick. (a) $\mathcal{B}(u)$ acting on the ket vacuum $|\uparrow\rangle^{\otimes L}$. Note that we can choose any of the nine vertices (e.g. the one with the orange bullet) and fix it to be a c-vertex, see figure 5.2. Using conservation of arrow flow at each vertex, it is easy to see that the resulting state will be a one-magnon ket. (b) $\mathcal{C}(u)$ acting on the bra vacuum $\langle\uparrow|^{\otimes L}$. Using a similar logic as for $\mathcal{B}(u)$, it is easy to see that the resulting state will be a one-magnon bra.

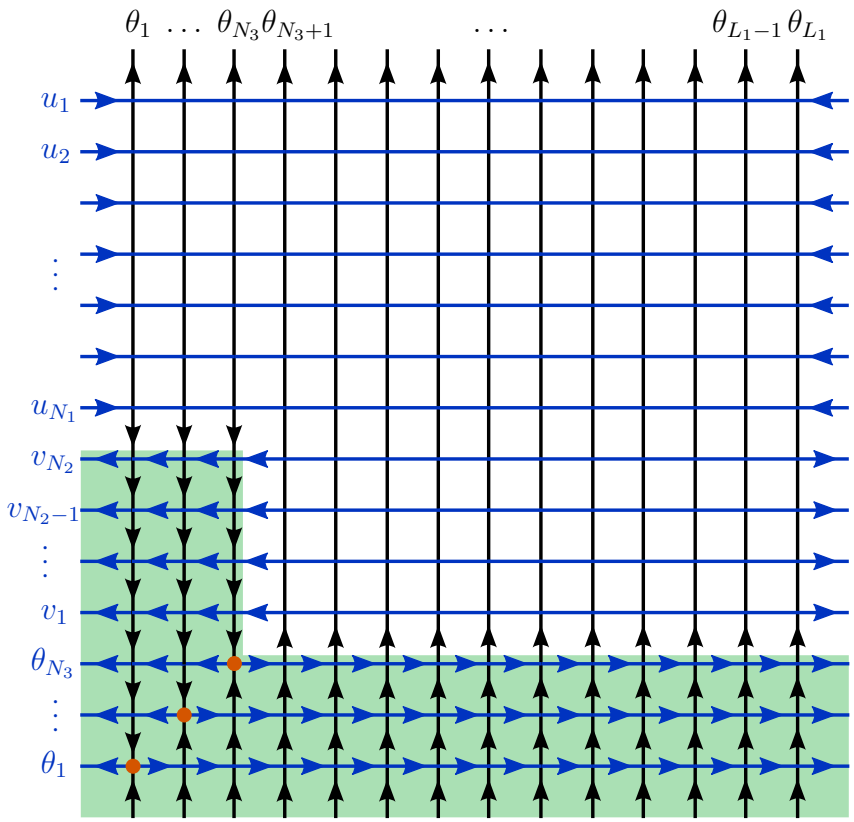

Figure 5.5: Toward three-point functions from the six-vertex model using the freezing trick.

We can repeat a similar exercise by acting on the ket vacuum with a stack of two $\mathcal{B}$-lines and freezing a single vertex in each of them (of course, on different vertical lines). The resulting state is a two-magnon ket. It should now be clear how one can represent an N-magnon state using the graphical rules given above. For example, an N-magnon ket is represented by stacking N $\mathcal{B}$-lines on top of each other, such that the arrows in the top row would be all pointing up. Since different $\mathcal{B}(u)$ operators commute, see (3.1), the order in which we label the rapidities of the magnons in the graphical representation is not relevant. Similarly, to create an N-magnon bra, we stack N $\mathcal{C}$-lines on top of each other, such that the arrows in the bottom row are all pointing up.

5.6.2 Determinant form of three-point functions

We now have the necessary tools to represent graphically the three-point function of interest. The steps we need are the following (see figures 5.5 and 5.6):

- First we draw L_1 vertical lines with rapidities $\theta_1, \ldots, \theta_{L_1}$ and N_1 $\mathcal{B}$-lines with rapidities $u_1, \ldots, u_{N_1}$. Conventionally, we choose to label the rapidities on these $\mathcal{B}$-lines from

top to bottom, see figure 5.5. Also, the rapidities $\{u\}$ satisfy the Bethe equations for an $SU(2)$ spin chain of length L_1 and with N_1 magnons. By fixing the upper row of vertical segments to have arrows pointing up, we have effectively created operator $\mathcal{O}_1 = |\{u\}\rangle_{L_1}$.

- Then, below the $\mathcal{B}$-lines that we just drew, we stack N_1 $\mathcal{C}$-lines with some arbitrary rapidities, i.e. they need not satisfy any set of Bethe equations. So, we choose to label these rapidities from bottom to top as $\theta_1, \ldots, \theta_{N_3}, v_1, \ldots, v_{N_2}$, where of course $N_1 = N_2 + N_3$. Moreover, we fix the lower row of vertical segments to have arrows pointing up, see figure 5.5. Notice that with this step, we have not created any other state appearing in (5.17) yet.

- We will now use the freezing trick on the lower N_3 vertices in the diagonal of the diagram. Let us start by picking the lower orange dot in figure 5.5 and fixing it to be a c-vertex. Doing so, once can easily check using conservation of arrow flow that all vertices on the $\mathcal{C}$-line with rapidity θ_1 and those in the vertical line with rapidity θ_1, but below the $\mathcal{B}$-line with rapidity u_{N_1}, will be frozen. Namely, they are b-vertices.

- Similarly, fixing the remaining $N_3 - 1$ orange dots in the diagonal to be c-vertices, one can check that all vertices in the green shaded area of the diagram in figure 5.5 have been frozen! Thus, the contribution from this part of the diagram is trivial: it is simply the product of weights of all b- and c-vertices contained in it (see figure 5.2).

- What are we left with by removing the shaded area of figure 5.5? Of course, we still have the state $|\{u\}\rangle_{L_1}$ at the top of the diagram. The bottom right state is an N_2-magnon bra created with $\mathcal{C}$-lines of length $L_1 - N_3$. Since the rapidities $\{v\}$ were arbitrary, we can choose them to be the Bethe roots of operator $\mathcal{O}_2$. Thus, with this we have represented graphically the state ${}_{L_1-N_3}\langle\{v\}|$ appearing in (5.17), see figure 5.6.

- Of course, we still need the state ${}_{N_3}\langle\{w\}|$ and the curious reader must have noticed by now that there are no rapidities w_j in any of the figures so far. So, where do they come from? Recall that after removing the shaded area of figure 5.5 we still have the bottom left state, which is an N_3-magnon bra of length N_3. As pointed out in [92], we must consider all possible ways in which these excitations can be created by inserting N_3 $\mathcal{C}$-lines with rapidities labeled by $w_1, \ldots, w_{N_3}$ from bottom to top. We take these to be the Bethe roots of $\mathcal{O}_3$. The red-shaded area in figure 5.6 corresponds to this contribution, which is known as a domain-wall partition function.

After following all the steps listed above, we end up with the six-vertex diagram of figure 5.6. This is the six-vertex model representation of our formula for three-point functions (5.6). The domain-wall partition function (red-shaded area) has a determinant expression, found by Izergin [93]. The rest of the diagram is a restricted version of the Slavnov scalar product [83] between a Bethe eigenstate and a generic Bethe state. In our case, both sets of rapidities

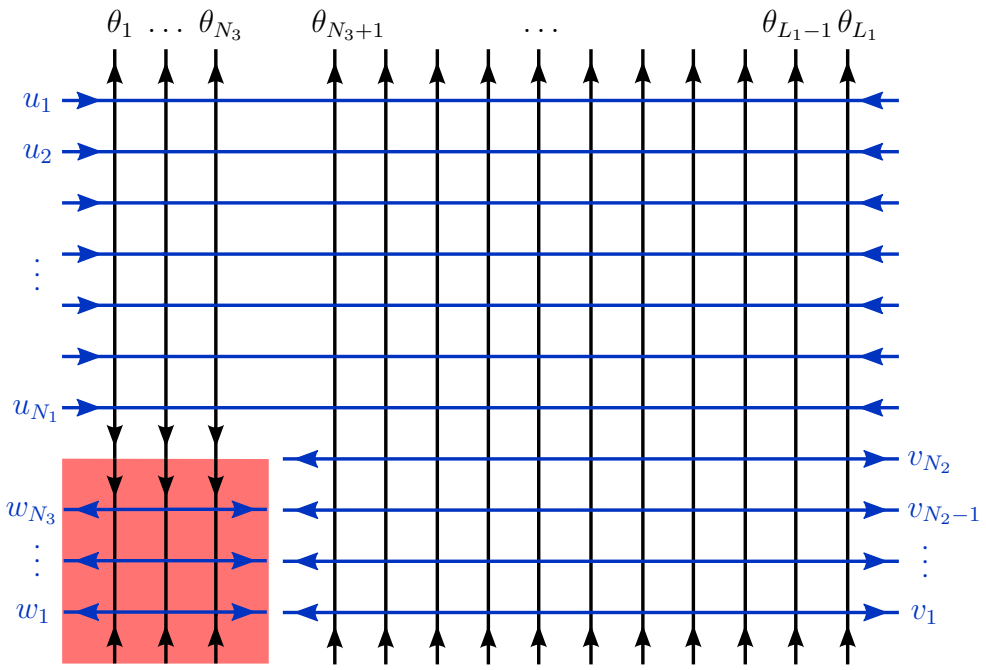

Figure 5.6: Three-point functions from the six-vertex model. The red-shaded area is the contribution from the Bethe roots of operator $\mathcal{O}_3$. This corresponds to a domain-wall partition function of size $N_3 \times N_3$, which has a determinant expression found by Izergin [93]. The rest of the diagram is a restricted version of the Slavnov scalar product [83] between a Bethe eigenstate and a generic Bethe state, which also has a determinant expression [94, 95].

$\{u\}$ and $\{v\}$ are the Bethe roots of $\mathcal{O}_1$ and $\mathcal{O}_2$. There is also a known determinant expression for this scalar product [94, 95]. Working out the details, one arrives at the following formula for three-point functions in terms of two determinants [92]:

$$C_{123} = \bar{\Omega}_{123}\, F\, \det\left(\mathcal{Z}_{jk}\right) \det\left(\mathcal{R}_{jk} \oplus \mathcal{S}_{jk}\right) , \tag{5.21}$$

where

$$F = \frac{\prod_{j=1}^{N_1}\left(u_j + \frac{i}{2}\right)^{N_3} \prod_{j=1}^{N_3}\left(w_j + \frac{i}{2}\right)^{N_3}}{\prod_{j<k}^{N_1}(u_k - u_j) \prod_{j<k}^{N_2}(v_j - v_k) \prod_{j<k}^{N_3}(w_j - w_k)} , \tag{5.22}$$

$$\mathcal{Z}_{jk} = \frac{1}{(k-1)!}\, \partial_\theta^{k-1} \left(\frac{i}{(w_j - \theta + \frac{i}{2})(w_j - \theta - \frac{i}{2})} \right) , \tag{5.23}$$

$$\mathcal{R}_{jk} = \frac{i}{u_j - v_k} \left[\left(\frac{v_k + \frac{i}{2}}{v_k - \frac{i}{2}} \right)^{L_1} \prod_{l \neq j}^{N_1} (u_l - v_k + i) - \prod_{l \neq j}^{N_1} (u_l - v_k - i) \right] , \tag{5.24}$$

$$\mathcal{S}_{jk} = \frac{1}{(k-1)!}\,\partial_\theta^{k-1}\left(\frac{i}{(u_j-\theta+\frac{i}{2})(u_j-\theta-\frac{i}{2})}\prod_{l=1}^{N_2}\frac{1}{v_l-\theta-\frac{i}{2}}\right). \tag{5.25}$$

and $\bar{\Omega}_{123}$ is defined in a similar way as (5.4), except that the norms in this case are given by

$$\bar{\mathcal{N}}_1 = \prod_{j\neq k}^{N_1}\frac{u_j-u_k+i}{u_j-u_k}\det\phi'_{\{u\}} \tag{5.26}$$

and similarly for $\bar{\mathcal{N}}_2$ and $\bar{\mathcal{N}}_3$ (compare with (4.18)). Note that in all these formulas, we must take the homogeneous limit $\theta_j \to 0$.

Chapter 6

Four-Point Functions

In this chapter, we will describe the computation at weak coupling of tree-level four-point functions of generic operators in the $SU(2)$ sector of $\mathcal{N} = 4$ SYM. That is, we will show how to compute the quantity $C_{1234;\{l_{ij}\}}$ appearing in (2.4). The discussion and notation are similar to those used in the previous chapter.

6.1 Setup

We will consider the configuration shown in figure 6.1. Unlike in the case of three-point functions, the number of contractions between operators $\mathcal{O}_i$ and $\mathcal{O}_j$ is not simply given in terms of the lengths of the operators, see (5.1). However, note that in our setup there is only one choice for the number of contractions $\{l_{ij}\}$ between the different operators, which is completely determined by their charges. For example, denoting again the length and number of excitations of operator $\mathcal{O}_i$ by L_i and N_i, we have that

$$l_{23} = L_3 - N_3\,, \qquad l_{24} = L_4 - N_4\,, \qquad l_{14} = N_4\,,$$

etc. More importantly, $l_{34} = 0$. Hence, we will simply denote the quantity $C_{1234;\{l_{ij}\}}$ appearing in (2.4) by C_{1234}, such that the four-point function shown in figure 6.1 is simply

$$G_4(x_1, x_2, x_3, x_4) = \frac{1}{N^2} \frac{C_{1234}}{\prod\limits_{i<j} |x_{ij}|^{2l_{ij}}}\,. \tag{6.1}$$

Our choice of vacuum and excitations for the operators is shown in the following table:

	Vacuum	Excitations
$\mathcal{O}_1$	Z	X
$\mathcal{O}_2$	$\bar{Z}$	$\bar{X}$
$\mathcal{O}_3$	Z	$\bar{X}$
$\mathcal{O}_4$	Z	$\bar{X}$

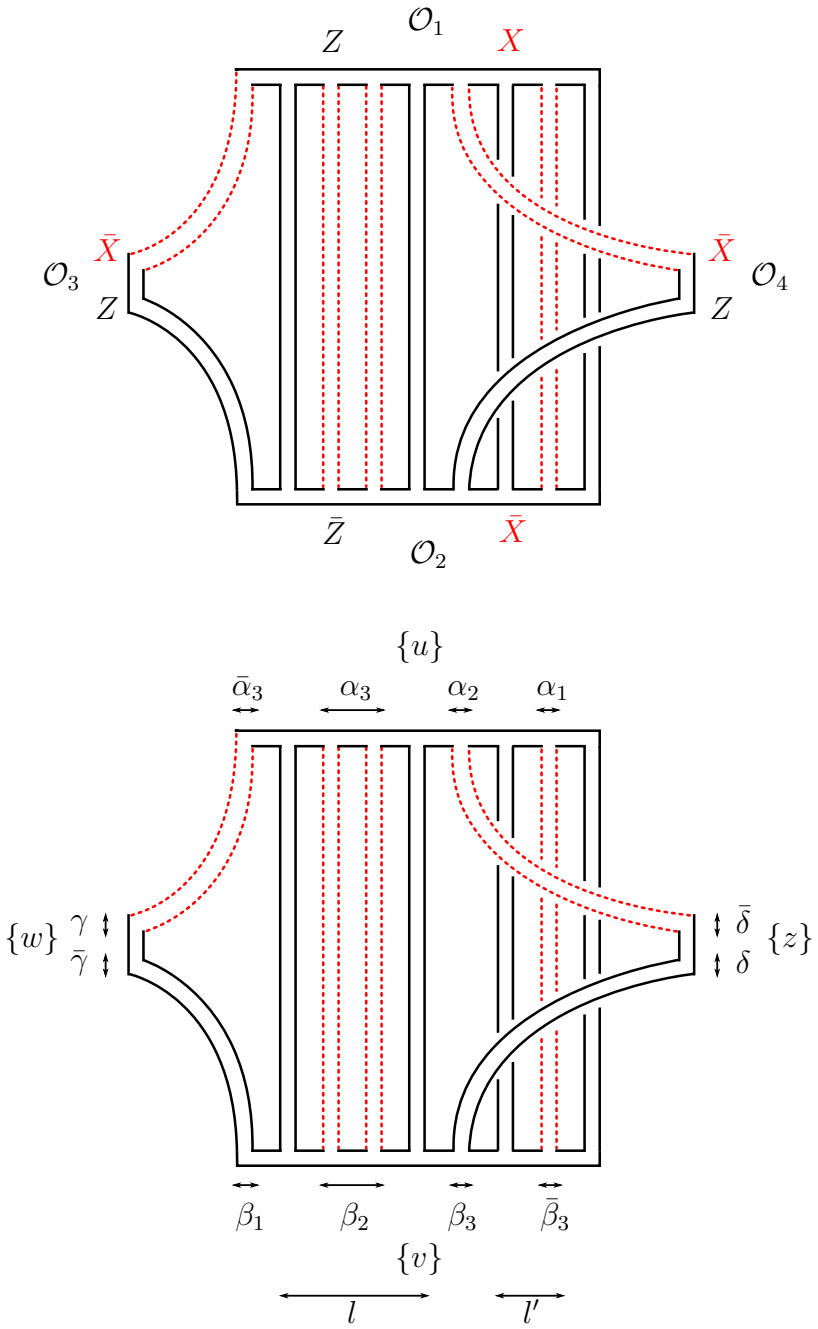

Figure 6.1: Setup for the computation of the four-point function of $SU(2)$ operators. The black (solid) lines represent vacuum fields, while the red (dashed) lines represent excitations. The top figure shows the vacuum (Z or $\bar{Z}$) and excitation choice (X or $\bar{X}$) for each operator. The figure at the bottom shows the labelling of the excitations of each operator and the different partitions needed to perform the Wick contractions. Of course, we could have used only l or l', but it turns out that some our formulas are more concisely written using one or the other.

Before showing how to compute the quantity C_{1234} appearing in (6.1), we should stress that the results from this chapter are valid for generic $SU(2)$ operators. In figure 6.1, operators $\mathcal{O}_3$ and $\mathcal{O}_4$ look small compared to the other two, but they are general $SU(2)$ operators with the charges indicated in the figure. They were simply drawn in this way for convenience: all their $\bar{X}$ or Z fields are contracted with $\mathcal{O}_1$ and $\mathcal{O}_2$ respectively. Also, as mentioned above, the configuration we are considering does not include interactions between operators $\mathcal{O}_3$ and $\mathcal{O}_4$. However, it is trivial to modify the formulas we present below to consider the more general case in which $\mathcal{O}_3$ and $\mathcal{O}_4$ interact with each other.[35] Finally, note that the four-point functions that we are considering are non-extremal.

6.2 Brute force computation

We can always do a brute force computation to determine C_{1234} using the explicit form of the Bethe states representing each of the operators, see (3.1). Then, writing the Bethe wave functions as $\psi_{n_1,\dots,n_N}$ instead of $\psi(n_1,\dots,n_N)$ and using the parameter l' instead of l in figure 6.1 for convenience, we have

$$\begin{aligned} C_{1234} = \Omega_{1234} \sum_{l'=0}^{L_1-N_3-N_4} \sum_{|\alpha_1|=0}^{\min\{l',N_1-N_3-N_4\}} \sum_{1\le n_1<\dots<n_{|\alpha_1|}\le l'} \sum_{1\le m_1<\dots<m_{N_1-N_3-N_4-|\alpha_1|}\le L_1-N_3-N_4-l'} \\ \times\ \psi^{(1)}_{n_1,\dots,n_{|\alpha_1|},l'+1,\dots,l'+N_4,N_4+l'+m_1,\dots,N_4+l'+m_{N_1-N_3-N_4-|\alpha_1|},L_1-N_3+1,\dots,L_1} \\ \times\ \psi^{(2)}_{L_2-(L_4-N_4+l'+m_{N_1-N_3-N_4-|\alpha_1|})+1,\dots,L_2-(L_4-N_4+l'+m_1)+1,L_2-n_{|\alpha_1|}+1,\dots,L_2-n_1+1} \\ \times\ \psi^{(3)}_{1,2,\dots,N_3}\,\psi^{(4)}_{L_4-N_4+1,\dots,L_4} \end{aligned} \tag{6.2}$$

where $\psi^{(i)}$ is the Bethe wave function associated to operator $\mathcal{O}_i$, $|\alpha_1|$ is the number of Bethe roots in partition α_1, see figure 6.1, and[36]

$$\Omega_{1234} = \sqrt{\frac{L_1L_2L_3L_4}{\mathcal{N}_1\mathcal{N}_2\mathcal{N}_3\mathcal{N}_4}}\,. \tag{6.4}$$

This factor takes into account the equivalent ways of breaking the spin chains (i.e. due to cyclicity we can rotate each chain before cutting it). Finally, $\mathcal{N}_i$ denotes the norm of operator $\mathcal{O}_i$, which is defined in (5.5).

[35] We consider such four-point functions in section 6.4.

[36] We can also include a symmetry factor in Ω_{1234} to take into account the case when $\mathcal{O}_3$ or $\mathcal{O}_4$ are dropped from the four-point function:

$$\Omega_{1234} = \sqrt{\frac{L_1L_2L_3^{\delta_{L_3>0}}L_4^{\delta_{L_4>0}}}{\mathcal{N}_1\mathcal{N}_2\mathcal{N}_3\mathcal{N}_4}}\,\frac{1}{(L_1-j_1-k_1)\big(\Theta(L_3)\Theta(L_4)-\delta_{L_3>0}\delta_{L_4>0}\big)+1}\,, \tag{6.3}$$

with $\Theta(x)$ being the Heaviside theta function, defined as $\Theta(x)=1$, for $x\ge 0$ and $\Theta(x)=0$, for $x<0$. In this case we recover the brute force formula for three-point functions, see (5.3).

Since each Bethe wave function $\psi^{(i)}$ has $N_i!$ terms, we see that for large N_i, L_i equation (6.2) is computationally extremely inefficient due to the huge number of terms involved. Below, we will see that using integrability techniques, we are able to simplify the computation of C_{1234} significantly.

6.3 Four-point functions using integrability toolkit

The combinatorial problem associated with the multiple Wick contractions required to compute the tree-level four-point function can be solved using the integrability tools introduced in chapter 4. Thinking of each operator a closed spin chain state and denoting the rapidities of the four operators by $\{u\}, \{v\}, \{w\}, \{z\}$ respectively, one simply needs to follow these steps:

- We cut each of the closed spin chains 1 and 2 into four open subchains. Formally this means that we write each of the states $|\Psi_1\rangle$ and $|\Psi_2\rangle$ as a linear combination of tensor products of four states in open subchains. Schematically, i.e. leaving out the sums over the different partitions and the factors arising from cutting the chains, see (4.2) and (4.5), and using the notation in figure 6.1:

$$|\{u\}\rangle \to |\alpha_1\rangle \otimes |\alpha_2\rangle \otimes |\alpha_3\rangle \otimes |\bar{\alpha}_3\rangle\,, \qquad |\{v\}\rangle \to |\beta_1\rangle \otimes |\beta_2\rangle \otimes |\beta_3\rangle \otimes |\bar{\beta}_3\rangle\,.$$

- Similarly, we cut each of the closed spin chains 3 and 4 into two open subchains, i.e. we write each of the states $|\{w\}\rangle$ and $|\{z\}\rangle$ as a linear combination of tensor products of two states in open subchains. However, in this case all excitations of $\mathcal{O}_3$ and $\mathcal{O}_4$ are in their corresponding left- and right-subchains, respectively. Thus, schematically we have:

$$|\{w\}\rangle \to |\{w\}\rangle \otimes |\{\}\rangle\,, \qquad |\{z\}\rangle \to |\{\}\rangle \otimes |\{z\}\rangle\,.$$

- In order to perform the Wick contractions among the operators in the four-point function, we first need to flip some subchain states. Again, leaving out the sum over partitions and the relevant factors coming from the flipping procedure (4.12), we schematically have

$$|\{u\}\rangle \to |\alpha_1\rangle \otimes |\alpha_2\rangle \otimes |\alpha_3\rangle \otimes \langle\bar{\alpha}_3^*|\,, \qquad |\{v\}\rangle \to |\beta_1\rangle \otimes \langle\beta_2^*| \otimes \langle\beta_3^*| \otimes \langle\bar{\beta}_3^*|\,,$$

$$|\{w\}\rangle \to |\{w\}\rangle \otimes \langle\{\}|\,, \qquad |\{z\}\rangle \to |\{\}\rangle \otimes \langle\{z^*\}|\,.$$

- We contract, or sew, the different subchain states as shown in figure 6.1. This involves the computation of scalar products of Bethe states. Note that some scalar products are trivial, as they only involve contractions of vacuum fields.

- Finally, we normalize the states and sum over the distinct ways of breaking them, see the factor defined in (6.4).

After all the dust has settled, we get[37]

$$C_{1234} = \Omega_{1234} \sum_{l=0}^{L_1-N_3-N_4} \sum_{\alpha_1\cup\bar{\alpha}_1=\{u\}} \sum_{\alpha_2\cup\bar{\alpha}_2=\bar{\alpha}_1} \sum_{\alpha_3\cup\bar{\alpha}_3=\bar{\alpha}_2} \sum_{\substack{\beta_2\cup\bar{\beta}_2=\{v\}\\ |\beta_2|=|\alpha_3|\\ |\bar{\beta}_2|=|\alpha_1|}} e^{\bar{\alpha}_1}_{L_1-N_3-N_4-l}\, e^{\bar{\alpha}_2}_{N_4}\, \frac{f^{\alpha_1\bar{\alpha}_1} f_<^{\alpha_1\alpha_1} f^{\alpha_2\bar{\alpha}_2} f_<^{\alpha_2\alpha_2}}{f_<^{\{u\}\{u\}}}$$
$$\times\ e^{\bar{\alpha}_3}_{l+N_3+1}\, f^{\alpha_3\bar{\alpha}_3} f_>^{\bar{\alpha}_3\bar{\alpha}_3} f_<^{\alpha_3\alpha_3}\, e^{\{v\}}_{L_3-N_3+l+1}\, e^{\bar{\beta}_2}_{L_2-L_3+N_3-l}\, \frac{f^{\beta_2\bar{\beta}_2} f_>^{\beta_2\beta_2} f_>^{\bar{\beta}_2\bar{\beta}_2}}{f_<^{\{v\}\{v\}}}\, e^{\{z\}}_{L_4+1}\, \frac{f_>^{\{z\}\{z\}}}{f_<^{\{z\}\{z\}}}$$
$$\times\ \langle\beta_2^*|\alpha_3\rangle\langle\bar{\beta}_3^*|\alpha_1\rangle\langle\{z^*\}|\alpha_2\rangle\langle\bar{\alpha}_3^*|\{w\}\rangle\,. \tag{6.5}$$

This is the main result of this chapter: it computes the four-point function of generic $SU(2)$ operators obeying the setup of figure 6.1.

Clearly, the integrability-based result for four-point functions (6.5) is much more complicated than the result for three-point functions (5.6). The latter involves a single sum over partitions, while the former involves four different sums over partitions plus the sum over l. Thus, there is not really much point in trying to present a table for four-point functions summarizing the results for different configurations of BPS and non-BPS operators: they would not look terribly simpler. Of course, in some particular cases, the scalar products in (6.5) can be computed using one of the simpler formulas for scalar products presented in chapter 4. For example, this is the case when $\mathcal{O}_3$ and $\mathcal{O}_4$ are BPS operators. We will come back to this particular configuration in later chapters.

Let us stress that the integrability-based formula (6.5) proves to be far more efficient than the brute force computation (6.2). For the reader's convenience, we present in appendix E the Mathematica codes needed to compute four-point functions using both formulas, as well as some specific examples showing how to use the codes. As noted in that appendix, even when the number of excitations and lengths of the operators are not too large, the brute force formula (6.2) becomes computationally much slower than formula (6.5).

6.4 More general four-point functions

In the case we studied in the previous sections, operators $\mathcal{O}_3$ and $\mathcal{O}_4$ did not Wick contract between them due to R-charge conservation, see figure 6.1. The motivation to first study such a setup was that it will be used to obtain a match with the strong coupling result in the Frolov-Tseytlin limit when $\mathcal{O}_3$ and $\mathcal{O}_4$ are taken to be light, small BPS operators. For reasons that will become clear in the strong coupling picture, the four-point function in this case is of order $O(L_1^2)$.[38]

[37] As opposed to the brute-force formula (6.2), where we used l', we now use the parameter l from figure 6.1.

[38] The curious reader can see figure 7.4, which is the holographic counterpart of the four-point functions of figure 6.1. In a nutshell, each factor of L_1 comes from integrating the insertion point of a light operator over the worldsheet defined by the heavy operators.

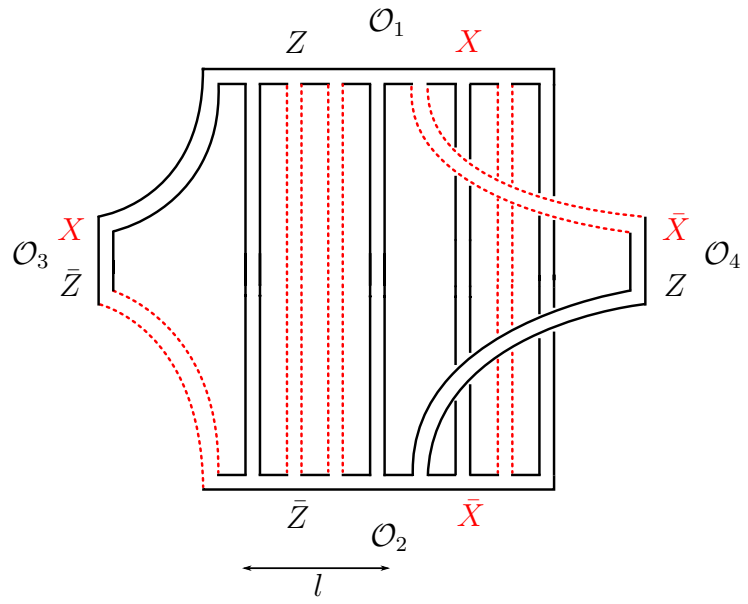

(a)

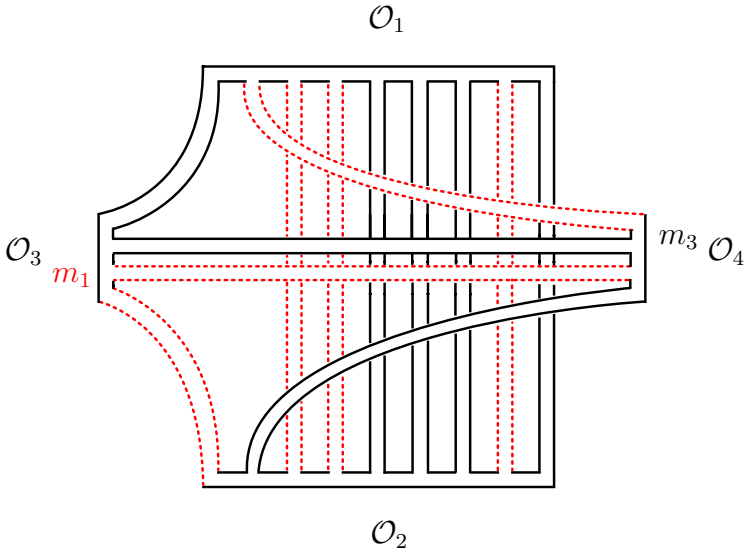

(b)

Figure 6.2: More general four-point functions in the $SU(2)$ sector. (a) It is clear that the diagrams with no contractions between $\mathcal{O}_3$ and $\mathcal{O}_4$ are planar for any $l \geq 0$. (b) If there are contractions between $\mathcal{O}_3$ and $\mathcal{O}_4$, the only planar diagrams are those in which $l = 0$. We denote by m_1 and m_3 the number of fields X and Z (and their conjugates) contracted between $\mathcal{O}_3$ and $\mathcal{O}_4$.

In this section, we consider a more general class of four-point functions of $SU(2)$ operators. In particular, our new setup is such that it allows for contractions between $\mathcal{O}_3$ and $\mathcal{O}_4$, see figure 6.2. Just like in our previous case, we should stress that $\mathcal{O}_3$ and $\mathcal{O}_4$ are general $SU(2)$ operators with the charges indicated in the figure. They were drawn small compared to the other two operators for convenience. It should be clear by looking at this setup that when there are no contractions between $\mathcal{O}_3$ and $\mathcal{O}_4$, the four-point function is planar for any value of l, see figure 6.2a. This is basically equivalent to the first setup that we considered in figure 6.1 and thus is also of order $O(L_1^2)$. However, once we consider interactions between $\mathcal{O}_3$ and $\mathcal{O}_4$, the resulting diagrams will be planar only for $l = 0$ and are of order $O(L_1)$[39], see figure 6.2b.

The choice of vacuum and excitations for the four operators in this new setup is summarized in the following table:

	Vacuum	Excitations
$\mathcal{O}_1$	Z	X
$\mathcal{O}_2$	$\bar{Z}$	$\bar{X}$
$\mathcal{O}_3$	$\bar{Z}$	X
$\mathcal{O}_4$	Z	$\bar{X}$

Note that in this case we need to specify the number of excitations (X and $\bar{X}$) and vacuum fields (Z and $\bar{Z}$) contracted between operators $\mathcal{O}_3$ and $\mathcal{O}_4$. We will denote these by m_1 and m_3, respectively. Hence, we have

$$l_{23} = N_3 - m_1\,, \qquad l_{24} = L_4 - N_4 - m_3\,, \qquad l_{14} = N_4 - m_1\,,$$

etc. Therefore, in this case the four-point function (2.4) in the planar limit reads[40]

$$G_4(x_1,x_2,x_3,x_4) \;=\; \frac{1}{N^2}\,\mathcal{G}_{\{0,0\}}(x_1,x_2,x_3,x_4) \sum_{l=0}^{L_1-L_3+N_3-N_4} C_{1234,\{0,0,l\}} \;+ \\ \frac{1}{N^2} \sum_{m_1=0}^{\min\{N_3,N_4\}} \sum_{m_3=0}^{\min\{L_3-N_3,L_4-N_4\}} \delta_{m_1+m_3\neq 0}\, C_{1234,\{m_1,m_3,0\}}\, \mathcal{G}_{\{m_1,m_3\}}(x_1,x_2,x_3,x_4)\,, \tag{6.6}$$

[39] Indeed, the holographic process dual to figure 6.2b is the tree-level diagram of figure 9.4. Since only a single integration over the worldsheet is performed, this process is suppressed by $1/L_1$ with respect to the diagram of figure 6.2a.

[40] We are excluding the disconnected diagrams that may appear when $\{N_3, L_3 - N_3\} = \{N_4, L_4 - N_4\}$.

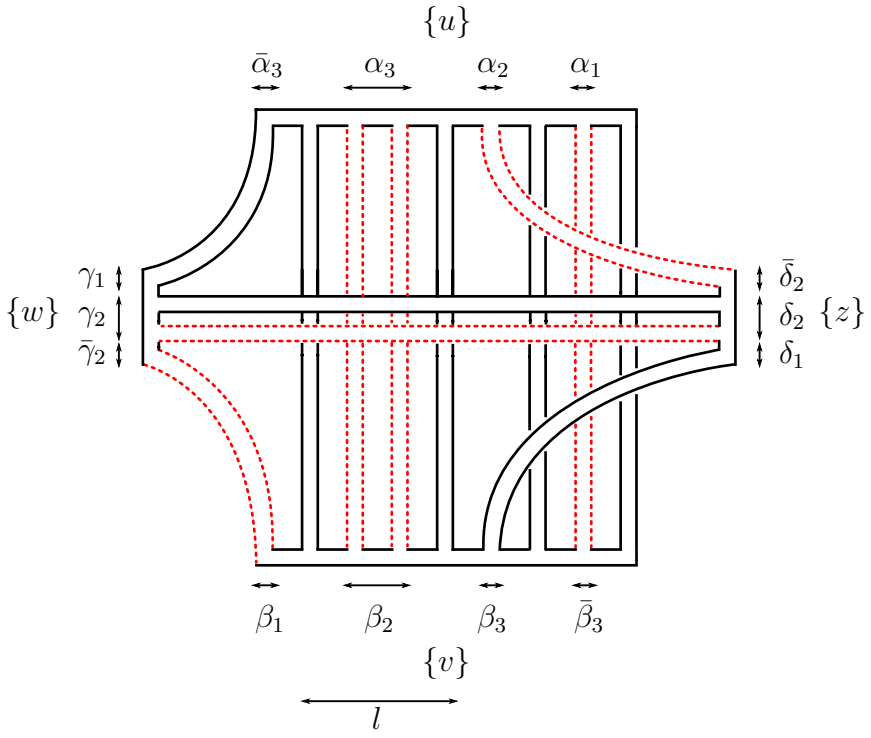

Figure 6.3: Setup for the computation of the four-point functions of section 6.4 at weak coupling. The black (solid) lines represent vacuum fields, while the red (dashed) lines represent excitations. The figure shows the labelling of the excitations of each operator and the different partitions needed to perform the Wick contractions.

where

$$\mathcal{G}_{\{m_1,m_3\}}(x_1,x_2,x_3,x_4) = \frac{1}{|x_{12}|^{2(L_1-L_3+N_3-N_4+m_1+m_3)}|x_{13}|^{2(L_3-N_3-m_3)}|x_{14}|^{2(N_4-m_1)}} \times \\ \times \frac{1}{|x_{23}|^{2(N_3-m_1)}|x_{24}|^{2(L_4-N_4-m_3)}|x_{34}|^{2(m_1+m_3)}} \,. \tag{6.7}$$

The first term in (6.6) corresponds to the contribution of diagrams for which $m_1, m_3 = 0$ and $l \geq 0$, while the second term takes into account the contribution of planar diagrams where $\mathcal{O}_3$ and $\mathcal{O}_4$ operators can contract between themselves and therefore we must have $l = 0$. We can compute $C_{1234,\{m_1,m_3,l\}}$ using the integrability tools of chapter 4, see figure 6.3. The steps we need to follow are very similar to the ones outlined for the setup of figure 6.1, except that now we also have to cut operators $\mathcal{O}_3$ and $\mathcal{O}_4$ more than once and perform some extra scalar products. The result is

$$
\begin{aligned}
C_{1234,\{m_1,m_3,l\}} = \Omega_{1234} \sum_{\alpha_1\cup\bar{\alpha}_1=\{u\}} \sum_{\alpha_2\cup\bar{\alpha}_2=\bar{\alpha}_1} \sum_{\beta_1\cup\bar{\beta}_1=\{v\}} \sum_{\substack{\beta_2\cup\bar{\beta}_2=\bar{\beta}_1 \\ |\beta_2|=|\alpha_3| \\ |\bar{\beta}_2|=|\alpha_1|}} \sum_{\gamma_2\cup\bar{\gamma}_2=\{w\} \atop |\bar{\gamma}_2|=|\beta_1|} \sum_{\delta_2\cup\bar{\delta}_2=\{z\} \atop |\bar{\delta}_2|=|\alpha_2|} \\
\times\ e^{\bar{\alpha}_1}_{L_1-L_3+N_3-N_4+m_1+m_3-l}\, e^{\bar{\alpha}_2}_{L_3-N_3-m_1}\, \frac{f^{\alpha_1\bar{\alpha}_1} f^{\alpha_1\alpha_1}_{<} f^{\alpha_2\bar{\alpha}_2} f^{\alpha_2\alpha_2}_{<} f^{\bar{\alpha}_2\bar{\alpha}_2}_{<}}{f^{\{u\}\{u\}}_{<}} \\
\times\ e^{\bar{\beta}_1}_{N_3-m_1}\, e^{\beta_2}_{l+1}\, e^{\bar{\beta}_2}_{L_2-N_3+m_1+1}\, \frac{f^{\beta_1\bar{\beta}_1} f^{\beta_1\beta_1}_{<} f^{\beta_2\bar{\beta}_2} f^{\beta_2\beta_2}_{>} f^{\bar{\beta}_2\bar{\beta}_2}_{>}}{f^{\{v\}\{v\}}_{<}}\, \frac{f^{\delta_2\bar{\delta}_2} f^{\delta_2\delta_2}_{>} f^{\bar{\delta}_2\bar{\delta}_2}_{>}}{f^{\{z\}\{z\}}_{<}} \\
\times\ e^{\{w\}}_{L_3-N_3-m_3}\, e^{\bar{\gamma}_2}_{N_3+m_3+1}\, \frac{f^{\gamma_2\bar{\gamma}_2} f^{\gamma_2\gamma_2}_{<} f^{\bar{\gamma}_2\bar{\gamma}_2}_{>}}{f^{\{w\}\{w\}}_{<}}\, e^{\{z\}}_{L_4-N_4-m_3}\, e^{\delta_2}_{m_1+m_3+1}\, e^{\bar{\delta}_2}_{N_4+m_3+1} \\
\times\ \langle\beta_2^*|\alpha_3\rangle\langle\bar{\beta}_3^*|\alpha_1\rangle\langle\bar{\gamma}_2^*|\beta_1\rangle\langle\bar{\delta}_2^*|\alpha_2\rangle\langle\delta_2^*|\gamma_2\rangle\,, \qquad (6.8)
\end{aligned}
$$

where Ω_{1234} is given in (6.4) and the labeling for the Bethe roots is indicated in figure 6.3.[41] Note that for the first term in (6.6) this expression (6.8) simplifies since the partitions δ_2 and γ_2 become empty. This is the main result of this section. Again, we emphasize that equation (6.8) is valid for *any* four operators obeying the setup presented in figure 6.2.

[41] Just like for the setup of figure 6.1, we can also include a symmetry factor in Ω_{1234} to take into account the case when $\mathcal{O}_3$ or $\mathcal{O}_4$ are dropped from figure 6.2. In this case, it reads

$$
\Omega_{m_1,m_3} = \sqrt{\frac{L_1 L_2 L_3^{\delta_{L_3>0}} L_4^{\delta_{L_4>0}}}{\mathcal{N}_1\mathcal{N}_2\mathcal{N}_3\mathcal{N}_4}}\, \frac{1}{(L_1 - L_3 + N_3 - N_4 + m_1 + m_3)\big(\Theta(L_3)\Theta(L_4) - \delta_{L_3>0}\delta_{L_4>0}\big) + 1}\,.
$$

Part IV

Weak/Strong Coupling Match

Chapter 7

The Frolov-Tseytlin limit and Holographic Correlation Functions

In this chapter we review the basics of classical strings in $AdS_5 \times S^5$ in the Frolov-Tseytlin limit. We also review the computation of holographic three- and four-point functions involving two heavy operators. Finally, we motivate the weak/strong coupling match for correlation functions that we will present in coming chapters by reviewing the weak/strong coupling match for the spectrum problem in the Frolov-Tseytlin limit.

7.1 The Frolov-Tseytlin limit

We gave a short review of classical strings in $AdS_5 \times S^5$ in the introduction. In this thesis, we will only be interested in classical strings that are dual to single-trace operators made out only of the three complex scalars X, Y, Z of $\mathcal{N} = 4$ SYM. Hence, we will only consider solutions whose motion is non-trivial in S^5 and point-like in AdS_5 with global time

$$t = \kappa\tau \,. \tag{7.1}$$

This means that for us, $W_1 = W_2 = 0$ and $W_3 = e^{i\kappa\tau}$ in (1.19), such that the energy (1.25) of the solutions that we will consider will always be

$$E = \sqrt{\lambda}\,\kappa \,. \tag{7.2}$$

The simplest classical string solutions in S^5 are point-like strings rotating around one of the equators

$$\mathbf{U}(\tau, \sigma) = e^{i\kappa\tau}\mathbf{v} \,, \tag{7.3}$$

where $\mathbf{v}$ is a constant unitary vector which can be parametrized as

$$v_a = \sqrt{\frac{J_a}{J}} \quad , \quad J = J_1 + J_2 + J_3 \,, \tag{7.4}$$

where J_a are defined in (1.26) and $J = \sqrt{\lambda}\,\kappa$ is the total angular momentum of the point-like string. The energy of this solution is of course given by (7.2). In the classical limit we should have $\kappa \gg 1$. This solution is simply the BMN point-like string [77] dual to the BPS operator

$$\mathcal{O}_{\rm BPS} \propto {\rm Tr}\left(X^{J_1} Y^{J_2} Z^{J_3}\right) + \text{all possible permutations}\,.$$

A simple generalization of the BMN solution is given by considering solutions of the form

$$\mathbf{U}(\tau,\sigma) = e^{i\kappa\tau}\mathbf{u}(\tau,\sigma)\,. \tag{7.5}$$

This is an important subclass of classical solutions, because when one considers the limit [96, 97]

$$\kappa \to \infty \;\text{ with }\; \kappa\,\partial_\tau \mathbf{u}\,,\; \partial_\sigma \mathbf{u} \;\text{ held fixed} \tag{7.6}$$

these solutions can be mapped to coherent spin chain states at weak coupling. This fact will allow us to perform the analytical weak/strong coupling match for three- and four-point functions in chapter 9. In this limit, the equation of motion and the Virasoro constraints reduce to[42]

$$2i\kappa\,\partial_\tau \mathbf{u} = \partial_\sigma^2 \mathbf{u} + 2\mathbf{u}\,(\partial_\sigma \bar{\mathbf{u}}\cdot\partial_\sigma \mathbf{u}) \tag{7.7}$$

and

$$\bar{\mathbf{u}}\cdot\partial_\sigma \mathbf{u} = 0\,, \tag{7.8}$$

while the global charges (1.26) read

$$J_a = \sqrt{\lambda}\int_0^{2\pi}\frac{d\sigma}{2\pi}\left(\kappa \bar{u}_a u_a - i\bar{u}_a\partial_\tau u_a\right)\,. \tag{7.9}$$

Using $J = J_1 + J_2 + J_3$ and the fact that the energy of these solutions is given by (7.2), this equation leads to

$$J = E - \frac{\lambda}{2E}\int_0^{2\pi}\frac{d\sigma}{2\pi}\,\partial_\sigma \bar{\mathbf{u}}\cdot\partial_\sigma \mathbf{u}\,,$$

which allows us to find the energy of the string in the limit (7.6). We obtain

$$E = J\left[1 + \frac{\lambda}{2J^2}\int_0^{2\pi}\frac{d\sigma}{2\pi}\,\partial_\sigma \bar{\mathbf{u}}\cdot\partial_\sigma \mathbf{u} + O\left(\frac{\lambda^2}{J^4}\right)\right]\,. \tag{7.10}$$

This result resembles a weak coupling expansion in the coupling λ/J^2. This is precisely the

[42] Note that when writing (7.7), we used the fact that in this limit, the Virasoro constraint (1.23) implies that $2i\kappa\bar{\mathbf{u}}\cdot\partial_\tau \mathbf{u} = \partial_\sigma \bar{\mathbf{u}}\cdot\partial_\sigma \mathbf{u}$. Equation (7.8) follows directly from the other Virasoro constraint (1.24).

result in the famous Frolov-Tseytlin limit [98, 99, 100, 101], which corresponds to

$$\lambda, J \to \infty\,, \qquad \text{with} \qquad \frac{\lambda}{J^2} \ll 1\,. \tag{7.11}$$

The fact that the limits (7.6) and (7.11) are equivalent was first pointed out in [96].

Given that the expansion in powers of λ/J^2 (7.10) resembles a weak coupling expansion in λ, the AdS/CFT correspondence tells us that in this particular limit we should be able to compare the coefficients of λ in both expansions. Indeed (7.10) turns out to coincide precisely with the weak coupling spin chain spectrum in the classical limit $L \to \infty$! (Of course, the spin chain length L is identified with the total momentum of the string solution J.) Moreover, the same result can be obtained when describing the spin chain states by coherent states, as we will show in chapter 9. The Frolov-Tseytlin limit was instrumental in establishing a first bridge between weak and strong coupling for non-protected operators in the spectrum problem [100, 102, 103, 96, 104]. We hope that the weak/strong coupling match for correlation functions that we will present in chapters 8 and 9 will also have the same consequences for three- and four-point functions.

7.2 The folded string and weak/strong coupling match for the spectrum

Having introduced the Frolov-Tseylin limit and its importance in the previous section, we will now motivate the weak/strong coupling match for three- and four-point functions by reviewing the weak/strong coupling match for the spectrum problem in a specific example.[43] As we saw in the previous section, the energy of a classical string solution in the Frolov-Tsetylin limit resembles a weak coupling expansion in λ/J^2:

$$E = J\left(1 + a_1\frac{\lambda}{J^2} + a_2\frac{\lambda^2}{J^4} + \dots\right) = J + a_1\frac{\lambda}{J} + a_2\frac{\lambda^2}{J^3} + \dots\,, \tag{7.12}$$

where J is the total angular momentum of the string. On the gauge theory side, the conformal dimension of the dual single-trace operator has the following expansion in the limit where $L \to \infty$ [101]

$$\Delta = L + b_1\frac{\lambda}{L} + b_2\frac{\lambda^2}{L^3} + \dots\,, \tag{7.13}$$

with L being the classical dimension of the operator (which is identified with J above). Given that the AdS/CFT dictionary identifies energies of strings with conformal dimensions of operators, see table 1.1, we can compare the coefficients of the two expansions above and see if they agree. In particular, we will see that the first correction to the string energy a_1

[43] Here we will show the match numerically. However, we will also provide an analytical match for the spectrum in section 9.1 by representing large, classical operators as coherent states.

agrees with the one-loop correction to the anomalous dimension b_1 [102, 100, 105, 103, 106]. We refer to this as a *weak/strong coupling match*. Let us see how this match works for a specific example.

We want to consider a folded string with unit mode number rotating in $R\times S^3 \subset AdS_5\times S^5$, with angular momenta (J_1, J_3). The explicit form of $\mathbf{U}_j(\tau,\kappa) = e^{i\kappa\tau}\mathbf{u}_j(\tau,\kappa)$ for this solution is:

$$U_1 = e^{i\kappa\tau}\sin\psi(\sigma)\, e^{iw_1\tau}\,, \qquad U_3 = e^{i\kappa\tau}\cos\psi(\sigma)\, e^{iw_3\tau}\,, \tag{7.14}$$

where the function $\psi(\sigma)$ obeys a differential equation [101], which is solved by

$$\sin\psi(\sigma) = \sqrt{q}\,\mathrm{sn}(w_{31}\sigma|q)\,, \qquad \cos\psi(\sigma) = \mathrm{dn}(w_{31}\sigma|q)\,,$$

where

$$q \equiv \frac{\kappa^2 - w_1^2}{w_3^2 - w_1^2}\,, \qquad w_{31} \equiv \sqrt{w_3^2 - w_1^2} = \frac{2}{\pi}\mathrm{K}(q) \tag{7.15}$$

and $\mathrm{K}(q)$ is the complete elliptic integral of the first kind, while $\mathrm{sn}(x|y)$ and $\mathrm{dn}(x|y)$ are Jacobi elliptic functions. For them, we use Mathematica's convention: $\mathrm{K}(q) =$ `EllipticK[q]`, $\mathrm{sn}(x|y) =$ `JacobiSN[x,y]` and $\mathrm{dn}(x|y) =$ `JacobiDN[x,y]`.

By solving the two equations in (7.15) we can find the form of the folded string solution in the Frolov-Tseytlin limit $\kappa\to\infty$. It is given by [100, 96]

$$\begin{aligned} u_1(\tau,\sigma) &= e^{\frac{2i(1-q)\mathrm{K}(q)^2}{\pi^2}\frac{\tau}{\kappa}}\sqrt{q}\,\mathrm{sn}\left(\frac{2\mathrm{K}(q)}{\pi}\sigma\Big|q\right)\,,\\ u_3(\tau,\sigma) &= e^{\frac{2iq\mathrm{K}(q)^2}{\pi^2}\frac{\tau}{\kappa}}\,\mathrm{dn}\left(\frac{2\mathrm{K}(q)}{\pi}\sigma\Big|q\right)\,. \end{aligned} \tag{7.16}$$

Also in this limit, one can use the formula for the angular momenta (7.9) to find that q is related to the *filling fraction* α by

$$\alpha \equiv \frac{J_1}{J_1+J_3} = 1 - \frac{\mathrm{E}(q)}{\mathrm{K}(q)}\,, \tag{7.17}$$

where we use Mathematica's convention for the complete elliptic integral of the second kind, such that $\mathrm{E}(q) =$ `EllipticE[q]`. Finally, the energy of this solution is given by (7.10):

$$E = J + \frac{2\mathrm{K}(q)(\mathrm{E}(q) - (1-q)\mathrm{K}(q))}{\pi^2}\frac{\lambda}{J} + O\left(\frac{\lambda^2}{J^3}\right)\,. \tag{7.18}$$

Of course, this has precisely the form of the expansion (7.12). For a given filling fraction α, we solve (7.17) to find q and use this value in (7.18) to compute a_1, the first correction to the string energy. The first column in table 7.1 and the four horizontal lines in figure 7.2 show the value of a_1 for $\alpha = 1/3, 1/4, 1/5, 1/6$.

On the weak coupling side, the corresponding single-trace operator is made out of N (or J_1) scalar fields X and $L-N$ (or J_3) scalar fields Z. This object can be mapped into an

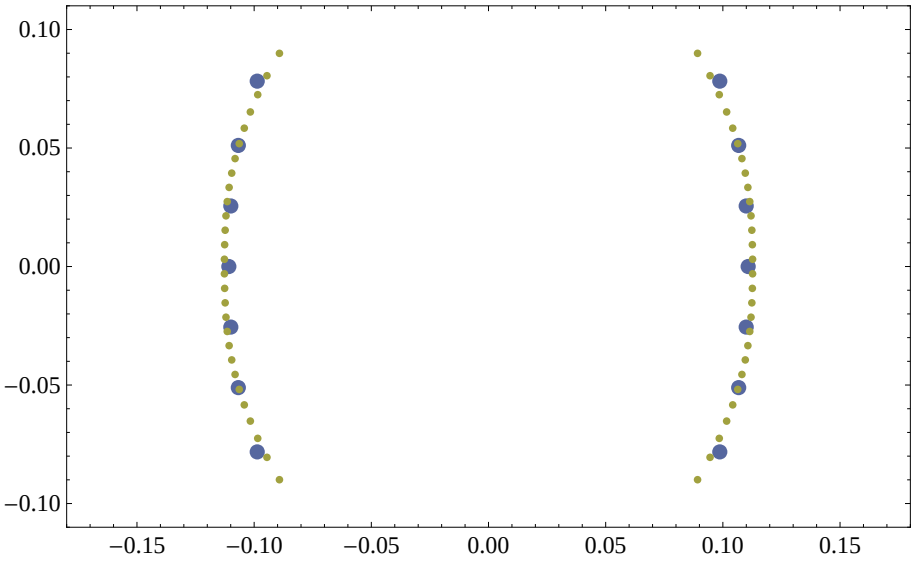

Figure 7.1: Two Bethe roots configurations for a folded string with $\alpha = 1/3$ and $L = 42, 168$, represented by the larger and smaller bullets respectively. The horizontal and vertical axes are the real and imaginary part of u/L, where u is the rapidity of an excitation, related to its momentum by $u = \frac{1}{2}\cot\frac{p}{2}$. Note that even though the number of roots for $L = 42$ is not very large, we see that they lie nicely along the cuts formed by the clearly classical configuration $L = 168$.

$SU(2)$ spin chain, whose corresponding Bethe roots lie along two symmetric cuts, see figure 7.1. The positions of these roots can be easily found by solving the one-loop Bethe equations (3.16), see [107] or appendix E for an explicit implementation in Mathematica. Once this is done, we can compute the one-loop anomalous dimension $\gamma^{(1)}$ of the operator from (3.17)

$$\gamma^{(1)} = \frac{1}{8\pi^2}\sum_{j=1}^{N}\frac{1}{u_j^2 + \frac{1}{4}}\,, \tag{7.19}$$

where u_j are the Bethe roots. Since $\Delta = L + \gamma^{(1)}\lambda + \ldots$, see (1.11), in the Frolov-Tseytlin limit we can compare this expansion with (7.13), so that $b_1 = L\gamma^{(1)}$. The bullet points in figure 7.2 correspond to the values of b_1 for a given filling fraction $\alpha = 1/3, 1/4, 1/5, 1/6$ and different lengths of the operator. Given that for each value of α we have 20 data points, we can collect this data as $\{L, b_1\}$, fit it in Mathematica as $\sum_{j=1}^{20} c_j L^{-j+1}$ and read off the leading contribution to b_1 when $L \to \infty$, i.e. c_1. Table 7.1 shows the values of b_1 in this limit, as well as the values of a_1. Clearly, we have a perfect match between the weak and strong coupling results.

From a more modern perspective, we now know that the match in the Frolov-Tseytlin limit is, to a great extent, a fortunate accident. A priori the limit $\lambda, J \to \infty$ with $\lambda/J^2 \to 0$ is not the same as $\lambda \to 0$. Indeed, the weak/strong coupling match persists at two loops [103], but breaks down at three loops [108]. However, the match in the spectrum problem was instrumental in establishing a first bridge between weak and strong coupling for non-protected

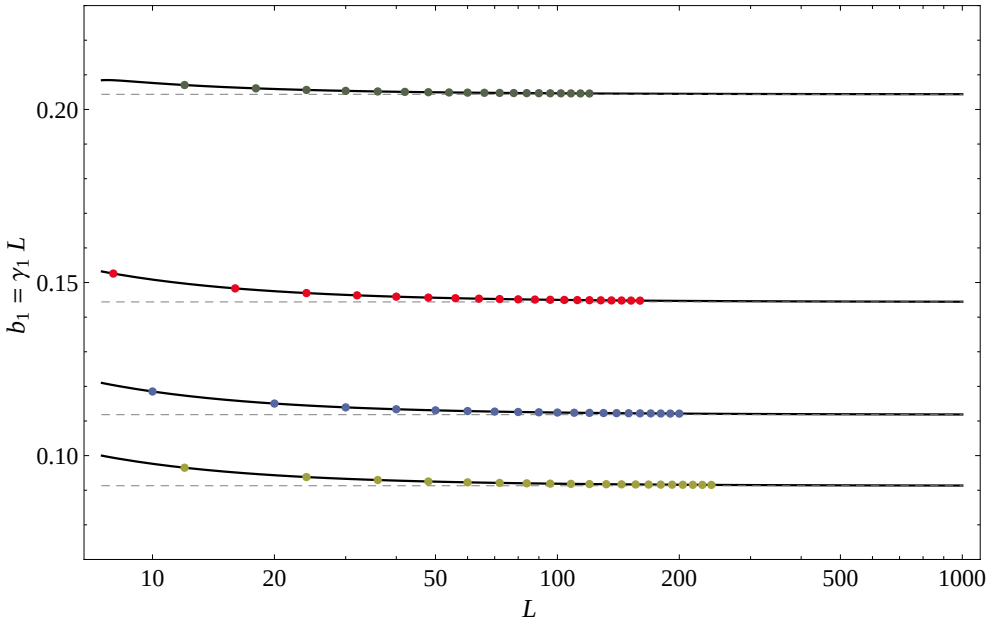

Figure 7.2: Weak/strong coupling match for the spectrum in the Frolov-Tseytlin limit for different filling fractions $\alpha = 1/3, 1/4, 1/5, 1/6$, from top to bottom. The bullet points correspond to the one-loop correction to the anomalous dimension times the length of the operator: $b_1 = L\gamma_1$, where γ_1 is computed in the spin chain picture using (7.19). The dashed horizontal lines correspond to a_1, the first correction to the energy of the string in the Frolov-Tseytlin limit, see (7.12). Clearly, we obtain a perfect match when extrapolating the weak coupling data to very large L.

α	a_1	b_1 Extrapolated	Error
1/3	**0.204374192779560**665	**0.204374192779560**645	10^{-16}
1/4	**0.144397676184627956471**3582	**0.144397676184627956471**3279	10^{-22}
1/5	**0.111824564813279108872823**31	**0.111824564813279108872823**264	10^{-24}
1/6	**0.091296367035266718581114873**869	**0.091296367035266718581114873**369	10^{-26}

Table 7.1: Numerical values of a_1, the first correction to the string energy (7.12), and $b_1 = \gamma_1 L$, where γ_1 is the one-loop anomalous dimension of the dual operator (7.13). Both results agree to *very* high numerical precision, making it clear that the match is perfect.

operators. For example, the weak/strong coupling match for the spectrum can be derived by showing that both weak and strong coupling classical limits are properly described by some algebraic curves [104, 109, 110] which become identical in the Frolov-Tseytlin limit.[44] Such algebraic curves were one of the main ingredients involved in conjecturing the form of the

[44]It was explained in [104] that any string classical motion can be mapped to a Riemann surface defined by some quasimomenta $\tilde{q}(x)$. The same is true at weak coupling: each solution to Bethe equations in the classical limit is described by some quasimomenta $q(u)$. The main difference between the weak and the strong coupling quasi-momenta is in their pole singularities: in properly chosen variables the strong coupling quasimomenta has two poles at $x = \pm\lambda/J^2$ while the weak coupling quasi-momenta has a single pole at $u = 0$. In the FT limit the strong coupling poles go to zero and the weak and strong coupling curves coincide.

strong coupling Arutyunov-Frolov-Staudacher equations [111] and even the all-loop Beisert-Staudacher equations [112] which are important input for the Y-system for AdS/CFT [17] mentioned in the introduction. Those quantum equations can be interpreted as a proper discretization of the classical algebraic curves. We hope that the match we will present for structure constants will be equally important in the study of three-point functions in $\mathcal{N} = 4$ SYM.

7.3 Holographic three-point functions

As anticipated in the introduction, we will consider the holographic three-point function of single-trace $SU(3)$ operators, which are made out of three complex scalars of $\mathcal{N} = 4$ SYM. This is a straightforward generalization of the case considered by Zarembo [62]. Our choice of vacuum and excitations is summarized in the following table[45]

	Vacuum	Excitations	Notations
$\mathcal{O}_1$	Z	X and Y	$\#\{X, Y, Z\} = \{J_1, J_2, J_3\}$
$\mathcal{O}_2$	$\bar{Z}$	$\bar{X}$ and $\bar{Y}$	$\#\{\bar{X}, \bar{Y}, \bar{Z}\} = \{J_1 - j_1, J_2 - j_2, J_3 + j_3\}$
$\mathcal{O}_3$	Z	$\bar{X}$ and $\bar{Y}$	$\#\{\bar{X}, \bar{Y}, Z\} = \{j_1, j_2, j_3\}$

(7.20)

The total length of operators $\mathcal{O}_1$ and $\mathcal{O}_3$ are, respectively,

$$J \equiv J_1 + J_2 + J_3 \qquad \text{and} \qquad j \equiv j_1 + j_2 + j_3 \,.$$

We will take $\mathcal{O}_1$ and $\mathcal{O}_2$ to be dual to heavy, classical string solutions, while $\mathcal{O}_3$ is taken to be a small BPS operator, with $j \ll J$, of the form $\mathrm{Tr}\left(\bar{X}^{j_1}\bar{Y}^{j_2}Z^{j_3}\right)$ + all possible permutations. In short, and using the notation of chapter 5, we will be computing $C_{123}^{\bullet\bullet\circ}$ at strong coupling. We will also need to compute the structure constant of three BPS operators with the charges shown in (7.20), which in the limit we are considering reads [36]:[46]

$$C_{123}^{\circ\circ\circ} = J v_1^{j_1} v_2^{j_2} \bar{v}_3^{j_3} (j_1 + j_2)! \sqrt{\frac{j\, j_3!}{j_1! j_2! j!}}\,, \tag{7.22}$$

where, as introduced in (7.4), $v_i = \sqrt{J_i/J}$.

Following Zarembo [62], the holographic three-point function of two heavy operators

[45] Note that the notation we will use at strong coupling to denote the length and number of excitations of an operator differs from that used at weak coupling, see (5.2). We do this simply to comply with the usual strong coupling notation used in previous sections and elsewhere in the literature.

[46] For general BPS operators with the charges shown in (7.20), the structure constants reads

$$C_{123}^{\circ\circ\circ} = \frac{\binom{J-j_1-j_2}{J_1+J_2-j_1-j_2}\binom{J_1+J_2-j_1-j_2}{J_1-j_1}\binom{j_1+j_2}{j_1}\sqrt{Jj(J-j_1-j_2+j_3)}}{\sqrt{\binom{J}{J-J_3}\binom{J-J_3}{J_2}\binom{j}{j_1+j_2}\binom{j_1+j_2}{j_1}\binom{J-j_1-j_2+j_3}{J_1+J_2-j_1-j_2}\binom{J_1+J_2-j_1-j_2}{J_1-j_1}}}\,. \tag{7.21}$$

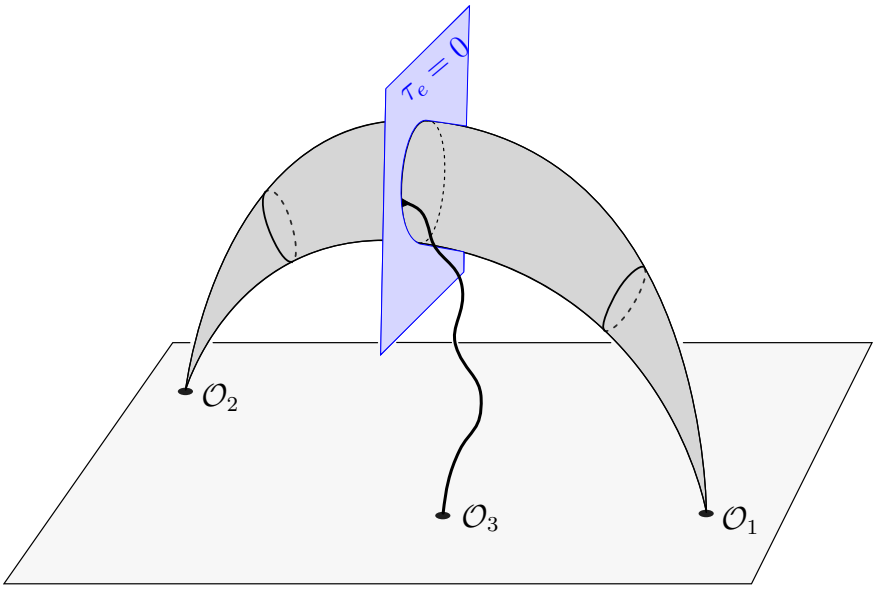

Figure 7.3: Holographic three-point function of two heavy operators and a light BPS operator. The computation involves a two-dimensional integration of a boundary-to-bulk propagator over the full string worldsheet. In the Frolov-Tseytlin limit the integration becomes localized in the slice $\tau_e = 0$ and only the integral over σ survives. Note that $\tau_e = 0$ is the only point that is shared between the Lorentzian and Euclidean solutions; the localization mechanism tell us to take a snapshot of the string at precisely this physical point.

and a light chiral primary operator can be computed by integrating the bulk-to-boundary propagator corresponding to $\mathcal{O}_3$ over the worldsheet defined by $\mathcal{O}_1$ and $\mathcal{O}_2$, see figure 7.3. The two-point function solution for two large, classical states was first worked out in [57]. After all the dust has settled, one obtains [62]

$$C_{123}^{\bullet\bullet\circ} = \mathcal{C} \int_{-\infty}^{\infty} d\tau_e \int_0^{2\pi} \frac{d\sigma}{2\pi} \frac{\sqrt{\lambda}}{J} \frac{U_1^{j_1} U_2^{j_2} \bar{U}_3^{j_3}}{\cosh^j \kappa\tau_e} \left[\frac{2\kappa^2}{\cosh^2 \kappa\tau_e} - \kappa^2 - \partial_a \bar{\mathbf{U}} \cdot \partial^a \mathbf{U} \right] , \tag{7.23}$$

where

$$\mathcal{C} = \frac{\mathcal{R}\, C_{123}^{\circ\circ\circ}}{v_1^{j_1} v_2^{j_2} \bar{v}_3^{j_3}} , \qquad \mathcal{R} = \frac{j+1}{2^{j+2}} \binom{j}{j_3} , \tag{7.24}$$

κ relates the global and worldsheet time coordinates, see (7.1), and the Euclidean time is $\tau_e = i\tau$. As mentioned above, $\mathbf{v} = \{v_1, v_2, v_3\}$ is associated with the point-like BPS string, see (7.4), while $\mathbf{U} = \{U_1, U_2, U_3\}$ are the three complex sphere embedding coordinates given in (7.5) and they depend on the particular classical string solution that one considers.

Given that we are interested in the Frolov-Tseytlin limit, where $\kappa \to \infty$ while $\kappa\, \partial_\tau \mathbf{u}$ and $\partial_\sigma \mathbf{u}$ are held fixed, the integral over τ_e in (7.23) can be easily computed because only the first term in square brackets contributes at leading order, while the remaining two are subleading.

This can be seen by using the Virasoro contraint (7.8):

$$\frac{2\kappa^2}{\cosh^2\kappa\tau_e}-\kappa^2-\partial_a\bar{\mathbf{U}}\cdot\partial^a\mathbf{U}=\frac{2\kappa^2}{\cosh^2\kappa\tau_e}-2\partial_\sigma\bar{\mathbf{u}}\cdot\partial_\sigma\mathbf{u}\overset{\kappa\to\infty}{\simeq}\frac{2\kappa^2}{\cosh^2\kappa\tau_e}\,.$$

Then, plugging $U_i(\sigma,\tau_e)=e^{\kappa\tau_e}u_i(\sigma,\tau_e)$ into (7.23), we notice that we can set $\tau_e=0$ in u_i because the factor $1/\cosh^{j+2}(\kappa\tau_e)$ localizes the integral around $\tau_e\simeq 1/\kappa$, while $\mathbf{u}$ is a slowly changing variable. Hence, we can evaluate the integral over τ_e as (here $T=\kappa\tau_e$)

$$\int_{-\infty}^{\infty}dT\,\frac{e^{(j_1+j_2-j_3)T}}{\cosh^{j+2}T}=\frac{2^{j+1}}{(j+1)\binom{j}{j_3}}=\frac{1}{2\mathcal{R}}\,.$$

Therefore, the three-point function (7.23) takes the simple form

$$C_{123}^{\bullet\bullet\circ}=J\frac{(j_1+j_2)!}{j_1!j_2!}\sqrt{j\frac{j_1!j_2!j_3!}{j!}}\int_0^{2\pi}\frac{d\sigma}{2\pi}\,u_1^{j_1}\,u_2^{j_2}\,\bar{u}_3^{j_3}\Big|_{\tau_e=0}\,. \tag{7.25}$$

In order to remove any dependence on the normalization convention, we take the ratio of the structure constant of interest to the three-point function of three BPS operators. Moreover, we also take the absolute value of this ratio to avoid the ambiguity that arises when multiplying each operator in the three-point function by a phase. Finally, if we use the equation that relates $\mathcal{R}$ and $\mathcal{C}$ (7.24), we find a simple expression for the ratio $C_{123}^{\bullet\bullet\circ}/C_{123}^{\circ\circ\circ}$:

$$r_{123}\equiv\left|\frac{C_{123}^{\bullet\bullet\circ}}{C_{123}^{\circ\circ\circ}}\right|=\left|\frac{1}{v_1^{j_1}\,v_2^{j_2}\,\bar{v}_3^{j_3}}\int_0^{2\pi}\frac{d\sigma}{2\pi}\,u_1^{j_1}\,u_2^{j_2}\,\bar{u}_3^{j_3}\right|_{\tau_e=0}\,. \tag{7.26}$$

This is the main result of this section. As we see, it is a simple and elegant result that depends only on the heavy classical solution that we wish to consider $\mathbf{u}$, its charges J_i, which define $v_i=\sqrt{J_i/J}$, and the charges j_1,j_2,j_3 of the light BPS operator. It is precisely the ratio r_{123} which we will use to perform the weak/strong coupling match in the next two chapters.

7.4 Holographic four-point functions

Let us now consider the holographic four-point function of two heavy operators $\mathcal{O}_1,\mathcal{O}_2$ and two light BPS operators $\mathcal{O}_3,\mathcal{O}_4$, see figure 7.4. Just like in the previous section, we consider $SU(3)$ operators made out of three complex of $\mathcal{N}=4$ SYM. Our choice of vacuum and

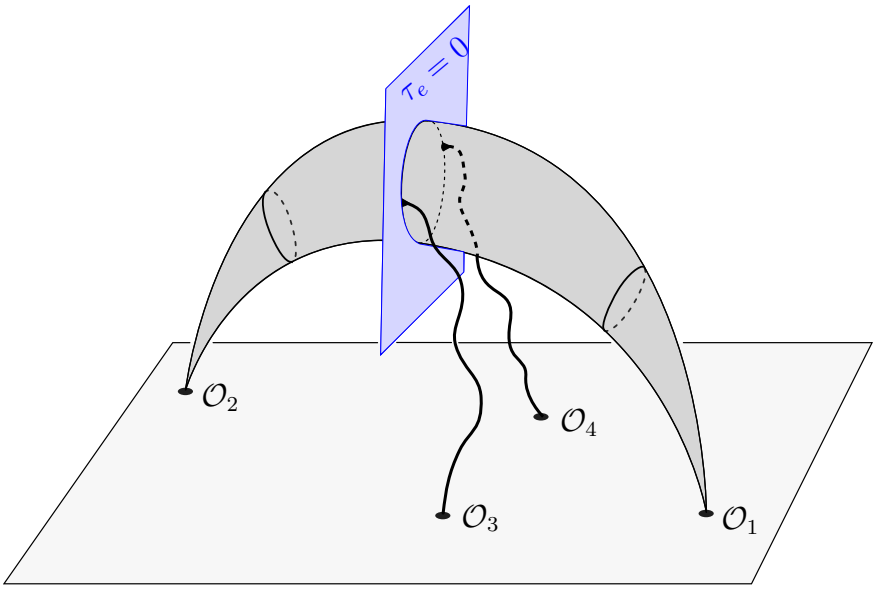

Figure 7.4: The holographic four-point function of two heavy operators and two light BPS operators factorizes into a product of two three-point functions, each of which involves a two-dimensional integration of a boundary-to-bulk propagator over the full string worldsheet.

excitations is summarized below

	Vacuum	Excitations	Notations
$\mathcal{O}_1$	Z	X and Y	$\#\{X,Y,Z\} = \{J_1, J_2, J_3\}$
$\mathcal{O}_2$	$\bar{Z}$	$\bar{X}$ and $\bar{Y}$	$\#\{\bar{X},\bar{Y},\bar{Z}\} = \{J_1 - j_1 - k_1, J_2 - j_2 - k_2, J_3 + j_3 + k_3\}$
$\mathcal{O}_3$	Z	$\bar{X}$ and $\bar{Y}$	$\#\{\bar{X},\bar{Y},Z\} = \{j_1, j_2, j_3\}$
$\mathcal{O}_4$	Z	$\bar{X}$ and $\bar{Y}$	$\#\{\bar{X},\bar{Y},Z\} = \{k_1, k_2, k_3\}$

(7.27)

where

$$J \equiv J_1 + J_2 + J_3\,, \qquad j \equiv j_1 + j_2 + j_3\,, \qquad k \equiv k_1 + k_2 + k_3\,,$$

such that $j, k \ll J$. Note that our current setup allows for a single choice of $\{l_{i,j}\}$, the number of contractions between operators $\mathcal{O}_i$ and $\mathcal{O}_j$. Moreover, if we restrict to $SU(2)$ operators (only Z and X fields and their conjugates), the object in figure 7.4 is the holographic realization of the four-point function of figure 6.1 that we considered at weak coupling. This is because the charges shown in (7.27) *do not* allow for contractions between $\mathcal{O}_3$ and $\mathcal{O}_4$, just like our weak coupling setup.

In [70], the holographic computation of four-point functions $G_4(x_1, x_2, x_3, x_4)$ of single trace gauge-invariant operators was considered. It was argued that if the charges of the operators $\mathcal{O}_1$ and $\mathcal{O}_2$ are much larger than those of the operators $\mathcal{O}_3$ and $\mathcal{O}_4$, such that

$\mathcal{O}_1 \simeq \bar{\mathcal{O}}_2$, then the four-point function factorizes into a product of two three-point functions[47]

$$G_4(x_1, x_2, x_3, x_4) = \frac{G_3(x_1, x_2, x_3)\, G_3(x_1, x_2, x_4)}{G_2(x_1, x_2)}\,, \tag{7.28}$$

where $G_4(x_1, x_2, x_3, x_4)$ is given in (2.4). Since we are considering the setup shown in (7.27), so that only one choice of $\{l_{ij}\}$ survives in (2.4) and expression (7.28) simply translates into

$$C_{1234}^{\bullet\bullet\circ\circ} = C_{123}^{\bullet\bullet\circ} C_{124}^{\bullet\bullet\circ}\,, \tag{7.29}$$

where $\bullet$ denotes a non-BPS operator, while $\circ$ denotes a BPS operator. Consequently, we just need to know how to compute the holographic three-point function of two large operators and a light BPS operator. This is precisely what we accomplished in the previous section! Thus, after dividing equation (7.29) by $C_{123}^{\circ\circ\circ} C_{124}^{\circ\circ\circ}$, we can simply borrow the result (7.26) valid in the Frolov-Tseytlin limit to compute r_{123} and

$$r_{124} \equiv \left| \frac{C_{124}^{\bullet\bullet\circ}}{C_{124}^{\circ\circ\circ}} \right| = \left| \frac{1}{v_1^{k_1} v_2^{k_2}\, \bar{v}_3^{k_3}} \int_0^{2\pi} \frac{d\sigma}{2\pi}\, u_1^{k_1} u_2^{k_2}\, \bar{u}_3^{k_3} \right|_{\tau_e = 0}\,, \tag{7.30}$$

where $C_{124}^{\circ\circ\circ}$ is of course exactly the same as $C_{123}^{\circ\circ\circ}$ with $j_i \to k_i$, see (7.22). Hence, the factorization formula (7.29) in the Frolov-Tseytlin limit reads

$$r_{1234} \equiv \left| \frac{C_{1234}^{\bullet\bullet\circ\circ}}{C_{123}^{\circ\circ\circ} C_{124}^{\circ\circ\circ}} \right| = r_{123}\, r_{124}\,. \tag{7.31}$$

This is the main formula of this section.

A few remarks are in order. The charges of the operators in the four-point function in the factorization formula (7.28), or equivalently in (7.31), are those specified in (7.27). However, the charges of the operators entering the three-point functions in (7.28) and (7.31) must be, due to charge conservation, *slightly* different. This point was already raised in [70]; however, the operators considered therein were made out of the complex scalars Z and $\bar{Z}$ only. Since in this paper we are considering operators that also have X, Y and $\bar{X}, \bar{Y}$, let us give the correct prescription for the charges of the operators in the three-point functions entering the factorization formulas above. Given the charges shown in (7.27), the charges of the operators in the three-point function C_{123} are $\{J_1, J_2, J_3\}$, $\{J_1 - j_1, J_2 - j_2, J_3 + j_3\}$ and $\{j_1, j_2, j_3\}$, respectively. Similarly, the charges of the operators in C_{124} are $\{J_1, J_2, J_3\}$, $\{J_1 - k_1, J_2 - k_2, J_3 + k_3\}$ and $\{k_1, k_2, k_3\}$.

[47] In fact, the more general claim is that the n-point function of two heavy operators and $n-2$ light BPS operators factorizes into the product of $n-2$ three-point functions of two heavy operators and a light BPS operator.

Chapter 8

Numerical Match

In this chapter we will provide conclusive numerical evidence to support the weak/strong coupling match of three- and four-point functions in the Frolov-Tseytlin limit. To generate the results of this chapter, we will use formulas from chapters 5, 6 and 7.

8.1 Three-point functions

8.1.1 $\mathcal{O}_3 = \mathrm{Tr}(Z^2\bar{X}^2)$

Let us first focus on the strong coupling computation. We want to consider the three-point function between the following operators. We take $\mathcal{O}_3$ to be the small BPS operator

$$\mathcal{O}_3 = 2\,\mathrm{Tr}(ZZ\bar{X}\bar{X}) + \mathrm{Tr}(Z\bar{X}Z\bar{X})\,, \tag{8.1}$$

meaning that we consider $j_1 = j_3 = 2$ and $j_2 = 0$ in the setup (7.20). For the classical states $\mathcal{O}_1$ and $\mathcal{O}_2$ we will take operators dual to the folded string with unit mode number and angular momenta (J_1, J_3) that we reviewed in section 7.2. That is, we will have $J_2 = 0$ in the setup (7.20). In short, we are considering the three-point function of $SU(2)$ operators. Given the we know the precise form of $\mathbf{u} = \{u_1, u_3\}$ for this solution, see (7.14) and (7.16), we can plug these expressions into (7.26) and obtain[48]

$$r_{123} = \frac{\alpha + q\,(1-2\alpha)}{3\,\alpha\,(1-\alpha)}\,, \tag{8.3}$$

[48]For a general BPS operator $\mathcal{O}_3$ in the $SU(2)$ sector, that is with $j_2 = 0$ and any j_1, j_3, we find

$$r_{123} = \frac{\sqrt{\pi}\,\Gamma\left(\frac{1+j_1}{2}\right)\,q^{j_1/2}\,(1-q)^{j_3/2}\,{}_2F_1\left(\frac{1}{2},\frac{1+j}{2};\frac{2+j_1}{2};q\right)}{\alpha^{j_1/2}\,(1-\alpha)^{j_3/2}\,j_1\,\Gamma\left(\frac{j_1}{2}\right)\,\mathrm{K}(q)}\,, \tag{8.2}$$

where j_1 is an even number so that when $\mathcal{O}_2$ is a zero-momentum state, so is $\mathcal{O}_1$.

where we used (7.17) to simplify the result. For different filling fractions α of $\mathcal{O}_1$ we find q from (7.17), plug it in this expression and get a number. For example, for $\alpha = 1/4$ we find

$$r_{123} \simeq 0.85689762237703939665\,. \tag{8.4}$$

Several such predictions are represented by the gray dashed lines in figure 8.1. The claim of this chapter is that these numbers, which were obtained in the Frolov-Tseytlin limit, can be matched with the same ratio computed at weak coupling in the classical limit.

Here we will check this claim by comparing (8.3) with the ratio $C_{123}^{\bullet\bullet\circ}/C_{123}^{\circ\circ\circ}$ obtained from the exact tree-level results of chapter 5. Since $C_{123}^{\circ\circ\circ}$ is a protected quantity and is a simple combinatorial factor, we only need to worry about computing $C_{123}^{\bullet\bullet\circ}$. The data required to compute this structure constant using the formula in table 5.1 or the determinant formula (5.21) are the positions of the Bethe roots of operators $\mathcal{O}_1$ and $\mathcal{O}_2$.

For a folded string the Bethe roots are distributed along two symmetric cuts, see figure 7.1. Consider first the operator $\mathcal{O}_2$. Using for convenience the strong coupling notation of (7.20), the total number of Bethe roots in this operators is the number of $\bar{X}$ fields which is equal to $J_1 - 2$. Hence, each of the cuts will have $(J_1 - 2)/2$ roots. For $\mathcal{O}_1$ we have J_1 scalars X. Hence, operator $\mathcal{O}_1$ is parametrized by J_1 Bethe roots, two more roots than $\mathcal{O}_2$. We want to consider an operator $\mathcal{O}_1$ which is *roughly* the complex conjugate of $\mathcal{O}_2$. So, where do we put the extra two roots of $\mathcal{O}_1$ with respect to the configuration of Bethe roots of $\mathcal{O}_2$? We will add them to the already existing classical cuts. As we are about to see, this choice corresponds to $\mathcal{O}_1 \simeq \bar{\mathcal{O}}_2$, thus allowing us to perform the weak/strong coupling match.[49]

We will now provide a numerical check of the agreement between the weak and strong coupling results in the Frolov-Tseytlin limit. We will discuss the general analytical match for general BPS states and general classical solutions later. For the numerics we need to find the solutions to Bethe equations with two symmetric cuts for both $\mathcal{O}_1$ and $\mathcal{O}_2$. This is very simple to do even for a very large number of roots (e.g. one can use the Mathematica code given in appendix E). When [40] appeared, the obstacle when computing $C_{123}^{\bullet\bullet\circ}$ using the formula of table 5.1 was that this expression involves sums over partitions of Bethe roots, computations of sub-determinants and so on. In practice this means that the computationally-doable numbers of roots using this formula is not very large. However, now that we have the determinant form of equations (5.1), see (5.21), we can do much better.

Indeed, we can now generate more data than in [40] to perform the weak/strong coupling match. For example, when $\mathcal{O}_1$ has filling fraction $\alpha = 1/4$ we can use the Mathematica function `r123` defined in appendix E to find[50]

```
data={{8,1.2741623922635346 4467},{16,0.9768680822930029 9151},
```

[49] As we will explain in detail in chapter 10, there are two more options when adding extra roots to a classical configuration of Bethe roots: they can be put at infinity or they can be placed at finite, symmetric values outside the classical cuts. These options have important implications.

[50] In practice, we collected this data with 50 digits of numerical precision. However, here we simply show 20 digits for presentation purposes.

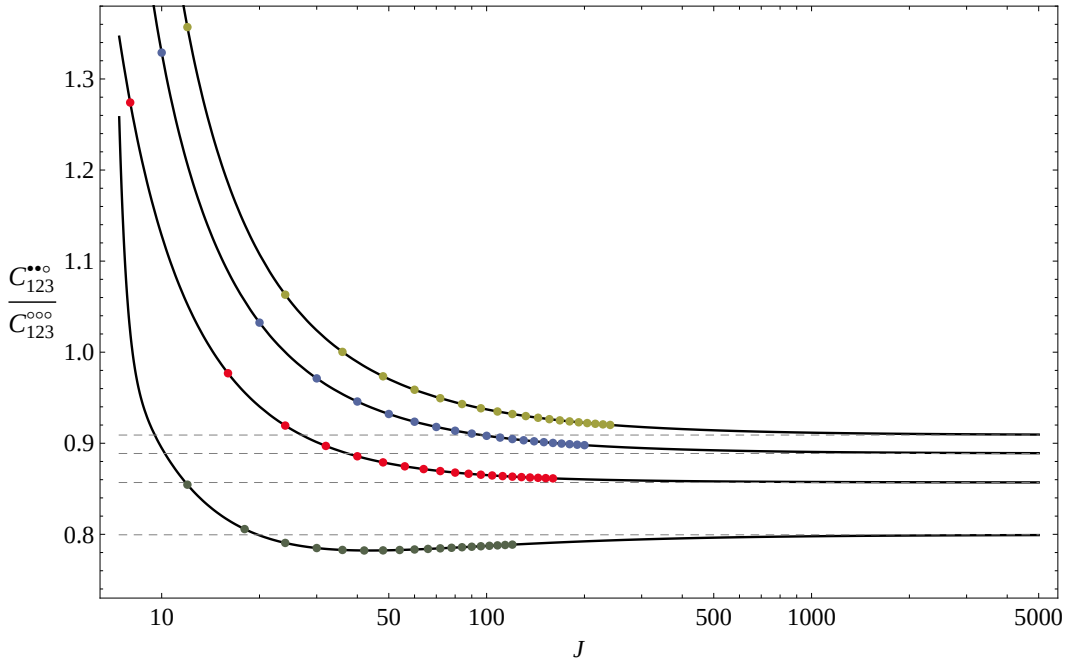

Figure 8.1: Weak/strong coupling match for three-point functions with $\mathcal{O}_3 = \mathrm{Tr}(Z^2\bar{X}^2)$. We show the fits (black curves) of the numerical data obtained with the weak coupling formula (5.21) compared to the strong coupling analytical prediction (8.3) (dashed gray lines) for different values of the filling fraction of operator $\mathcal{O}_1$: $\alpha = 1/3, 1/4, 1/5, 1/6$, from bottom to top.

```
{24,0.91941521886855988534},{32,0.89706072035365968294},
{40,0.88569795406191305813},{48,0.87899943199038460803},
{56,0.87465545336933938691},{64,0.87164398739740457834},
{72,0.86945065481644172743},{80,0.86779134596155748215},
{88,0.86649765483029201512},{96,0.86546405295652998721},
{104,0.86462137259917919779},{112,0.86392256341563745682},
{120,0.86333460580355643768},{128,0.86283370237463974408},
{136,0.86240230431904557575},{144,0.86202720944827868998},
{152,0.86169830953422218836},{160,0.86140774381062637301}};
```

where the first entry is the length of operator $\mathcal{O}_1$ and the second entry is $r_{123} = |C^{\bullet\bullet\circ}_{123}/C^{\circ\circ\circ}_{123}|$, which can be computed using the code in appendix E. Since we want to know the result of r_{123} in the classical limit, we need to extrapolate our data to $J \to \infty$. How do we do this? We perform a numerical fit as follows: given a set of data $\{J, r_{123}(J)\}$ with n points, we fit it with $n-1$ coefficients, e.g. something like $r_{123} = a_0 + a_1/J + \cdots + a_{n-1}/J^{n-1}$. This can be easily done in Mathematica as follows:

```
Fit[data,J/J^Range[Length[data]],J] ,
```

which fixes the constants a_k. In particular, a_0 is precisely what we were looking for: the

α	Analytical Prediction	Numerical Extrapolation	Error
1/3	**0.799491232730**18398082	**0.799491232730**17749944	8×10^{-15}
1/4	**0.856897622377039396**648	**0.856897622377039396**585	7×10^{-20}
1/5	**0.88875954179383961634**82477	**0.88875954179383961634**81959	6×10^{-23}
1/6	**0.90901548205573305781608**467	**0.90901548205573305781608**404	7×10^{-25}

Table 8.1: Weak/strong coupling match for three-point functions with $\mathcal{O}_3 = \mathrm{Tr}(Z^2\bar{X}^2)$. We show the strong coupling analytical prediction (8.3) compared with the extrapolated weak coupling data for different values of the filling fraction α of operator $\mathcal{O}_1$, see figure 8.1. Clearly, this is conclusive numerical evidence for the weak/strong coupling match for three-point functions in the Frolov-Tseytlin limit.

leading large-length asymptotics of r_{123}! For the case shown above, we obtain

$$r_{123}^{\text{num}} \simeq 0.85689762237703939659\,, \tag{8.5}$$

which agrees perfectly with the strong coupling result (8.4) within the numerical error. In figure 8.1 we plotted several other sets of data and their corresponding fits for different filling fractions, up to very large values of J. We see that, very non-trivially, the weak coupling results approach all the predictions from strong coupling in the Frolov-Tsetytlin limit! The numerical results for the analytical strong coupling prediction and the extrapolated weak coupling results shown in figure 8.1 are summarized in table 8.1.

Let us emphasize that the only assumption we need to make to perform the fits is on the form of the expansion of $r(J)$. Otherwise *there is no fine-tuning whatsoever* involved. For example, the $\alpha = 1/3$ curve in figure 8.1 has quite a nice non-trivial behavior with a minimum and an inflection point nicely converging from below to the predicted analytical result. This is the honest outcome of a fit like the one we described above, no fine-tuning is involved.

8.1.2 $\mathcal{O}_3 = \mathrm{Tr}(Z^j)$ and (ignoring) mixing with double traces

In the previous section we considered three-point functions in which all operators are Wick contracted to each other, see figure 5.1 and equation (7.20). When this is the case, a simple large N counting shows that we can ignore mixing of the single trace operators with double traces.

Let us provide another simple example, still using the folded string as our toy model but using a different BPS operator. Namely, we will consider

$$\mathcal{O}_3 = \mathrm{Tr}(Z^j)\,,$$

with $j_1 = j_2 = 0$ and $j = j_3$ in the setup (7.20). In this case, the length of operator $\mathcal{O}_2$ is the sum of the lengths of the other two operators. In other words, there are now no tree-level

Wick contractions between $\mathcal{O}_1$ and $\mathcal{O}_3$. In this case to compute the structure constants we must also consider the mixing of operator $\mathcal{O}_2$ with double traces [74].[51] The setup we have been using so far, the one of figure 5.1, was chosen to avoid this complication.

On the other hand, the case $\mathcal{O}_3 = \mathrm{Tr}(Z^j)$ was the case that was first extensively studied in the literature at strong coupling [62, 63, 68, 64, 65, 67, 69, 114, 70]. In all these computations, the mixing with multi-string states was not taken into account. Let us ignore the mixing with double trace effect and see what we get in the classical limit at weak coupling. Basically, the hope is that the same effect is being forgotten at weak and strong coupling and hence "cancels out" leaving a remainder quantity behind which can still be matched. Another plausible option is that this effect is negligible in the classical large L limit.

On the strong coupling side, we can use (8.2) to obtain an analytical prediction for the ratio r_{123}. For concreteness, we will consider $j = 3$ for our numerical checks below. Then, when $\mathcal{O}_1$ has filling fraction $\alpha = 1/3$ we obtain

$$r_{123} \simeq 1.037472608487046260 63\,. \tag{8.6}$$

The dashed gray lines in figure 8.2 represent the results obtained in this way for $\alpha = 1/3, 1/4, 1/5, 1/6$.

At weak coupling, we need again to be precise and face the kind of question which we already encountered in the previous section. Namely, given a classical operator $\mathcal{O}_2$, what is the operator $\mathcal{O}_1 \simeq \bar{\mathcal{O}}_2$? In this case operator $\mathcal{O}_1$ has J_1 scalars X and total length J. Operator $\mathcal{O}_2$ has J_1 scalars $\bar{X}$ (remember that now $\mathcal{O}_3$ does not have $\bar{X}$ scalars) but a slightly larger length equal to $J + j$. Operator $\mathcal{O}_2$ is parametrized by some configuration of Bethe roots like the one in figure 7.1. The position of the roots is uniquely fixed by a choice of mode numbers and by the length of the operator. Hence, a most natural choice for $\mathcal{O}_1$ is to take it to be the (conjugate of the) operator whose Bethe roots have the same mode numbers as $\mathcal{O}_2$ but slightly smaller length.

To be more concrete, consider $\mathcal{O}_2$ to be the operator dual to the folded string with unit mode number introduced in section 7.2. Then $\mathcal{O}_1$ would be the same folded string with slightly smaller length. From the string point of view this would be a folded string with the same angular momentum in the plane identified by the scalar X and with j less units of angular momentum in the plane identified by the scalar Z.

Using again the determinant form of three-point functions (5.21), we can generate weak-coupling data. For example, for $j = 3$ and $\mathcal{O}_1$ with filling fraction $\alpha = 1/3$ we get

```
data={{6,0.56476713115448865113},{12,0.65044781232074351246},
     {24,0.71729413712004076475},{24,0.76586835778725794630},
     {30,0.80209501401708243219},{36,0.82997659018657844687},
     {42,0.85203755412391650224},{48,0.86990274602484745026},
     {54,0.88465316709536216148},{60,0.89703188014875518365},
```

[51] At the same time, we should mention that there is however considerable evidence in the literature that extremal correlators can be considered as an analytic continuation of non-extremal ones [90], see also [113].

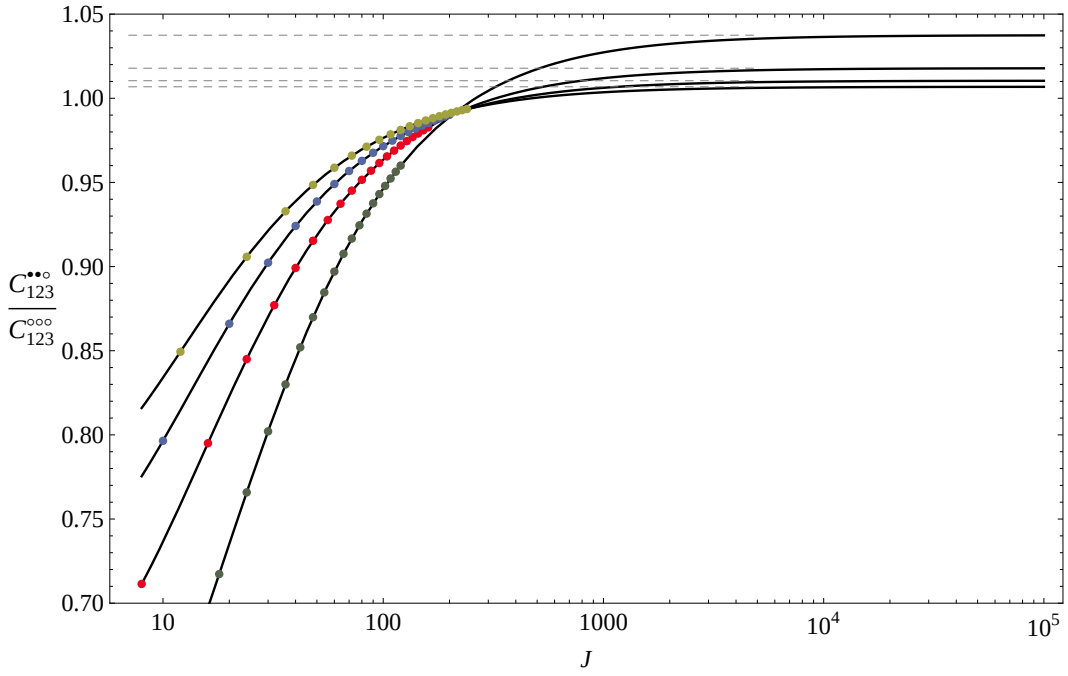

Figure 8.2: Weak/strong coupling match for three-point functions with $\mathcal{O}_3 = \mathrm{Tr}(Z^3)$. We show the fits (black curves) of the numerical data obtained with the weak coupling formula (5.21) compared to the strong coupling analytical prediction (8.3) (dashed gray lines) for different values of the filling fraction of operator $\mathcal{O}_1$: $\alpha = 1/3, 1/4, 1/5, 1/6$. As we mentioned in the main text, in this particular case we ignore mixing with double-trace operators.

```
{66,0.90756491257853738152},{72,0.91663441648012045280},
{78,0.92452438417860108286},{84,0.93145009779967499358},
{90,0.93757763528167808202},{96,0.94303711803547138097},
{102,0.94793191293945535188},{108,0.95234515472668300765},
{114,0.95634445405047852161},{120,0.95998535233451530559}};
```

where, just like before, the first entry is the length of operator $\mathcal{O}_1$ and the second entry is $r_{123} = |C_{123}^{\bullet\bullet\circ}/C_{123}^{\circ\circ\circ}|$. Fitting this data in exactly the same manner as in the previous section, we obtain the leading large-length asymptotics value:

$$r_{123}^{\mathrm{num}} \simeq 1.03747260848704329327\,, \tag{8.7}$$

which agrees perfectly with the strong coupling result (8.6) within the numerical error. Figure 8.2 shows different sets of data for $\alpha = 1/3, 1/4, 1/5, 1/6$ and their corresponding fits. Again, it is clear that the extrapolated weak coupling result approaches neatly the strong coupling results represented by the dashed grey lines. Table 8.2 shows the numerical values corresponding to this case, which again provide conclusive evidence for the weak/strong coupling match for three-point functions in the classical limit.

α	Analytical Prediction	Numerical Extrapolation	Error
1/3	**1.037472608487046**26063	**1.037472608487043**29328	3×10^{-15}
1/4	**1.017860598621845370**8901	**1.017860598621845370**97509	1×10^{-20}
1/5	**1.010419624141099846503**4010	**1.010419624141099846503**3995	1×10^{-23}
1/6	**1.006819928937576846354417**605	**1.006819928937576846354417**509	1×10^{-25}

Table 8.2: Weak/strong coupling match for three-point functions with $\mathcal{O}_3 = \mathrm{Tr}(Z^3)$. We show the strong coupling analytical prediction (8.3) compared with the extrapolated weak coupling data for different values of the filling fraction α of operator $\mathcal{O}_1$, see figure 8.2. Clearly, this constitutes yet again more conclusive numerical evidence for the weak/strong coupling match for three-point functions in the Frolov-Tseytlin limit. As we mentioned in the main text, in this particular case we ignore mixing with double-trace operators.

8.2 Four-point functions

Having performed the numerical weak/strong coupling match for three-point functions, let us move on to consider the same match for four-point functions. Let us describe the operators that we will consider. Operators $\mathcal{O}_3$ and $\mathcal{O}_4$ are taken to be the small BPS operator:

$$\mathcal{O}_3 = \mathcal{O}_4 = 2\,\mathrm{Tr}(ZZ\bar{X}\bar{X}) + \mathrm{Tr}(Z\bar{X}Z\bar{X})\,, \tag{8.8}$$

i.e. $j_1 = k_1 = 2$, $j_3 = k_3 = 2$ and $j_2, k_2 = 0$ in the setup (7.27). Just like before, operators $\mathcal{O}_1$ and $\mathcal{O}_2$ are taken to be large non-BPS operators dual to the folded string with unit mode number with two angular momenta (J_1, J_3). In short, we are considering the four-point function of $SU(2)$ operators. Given that we are interested in computing the ratio r_{1234}, see (7.31), we can directly borrow the results for three-point functions (8.3) to compute r_{123} and r_{124}, which are of course equal given our choice of light operators. Thus, at strong coupling we obtain

$$r_{1234} = \frac{\left[\alpha + q\,(1-2\alpha)\right]^2}{9\,\alpha^2\,(1-\alpha)^2}\,, \tag{8.9}$$

where α is the filling fraction of $\mathcal{O}_1$. Again, given a filling fraction we can find the corresponding value of q from (7.17) and plug everything into (8.9) to obtain a number, which will be the analytical prediction from strong coupling. The first column in table 8.3 has three different such predictions for $\alpha = 1/3, 1/4, 1/5$. The goal of this section is to show numerically that these results match the weak coupling results in the classical limit.

The setup we are considering is the holographic realization of the weak coupling setup of figure (6.1), because due to R-charge conservation, we are not allowing for contractions between operators $\mathcal{O}_3$ and $\mathcal{O}_4$. Hence, to generate weak coupling data, we have to evaluate our weak coupling formula (6.5) keeping α fixed and increasing the length of this operator. All we need to do so are the Bethe roots of the two large operators, dual to the folded string with unit number. Operator $\mathcal{O}_2$ has $J_1 - 4$ Bethe roots, while $\mathcal{O}_1$ has J_1 of them. Just like

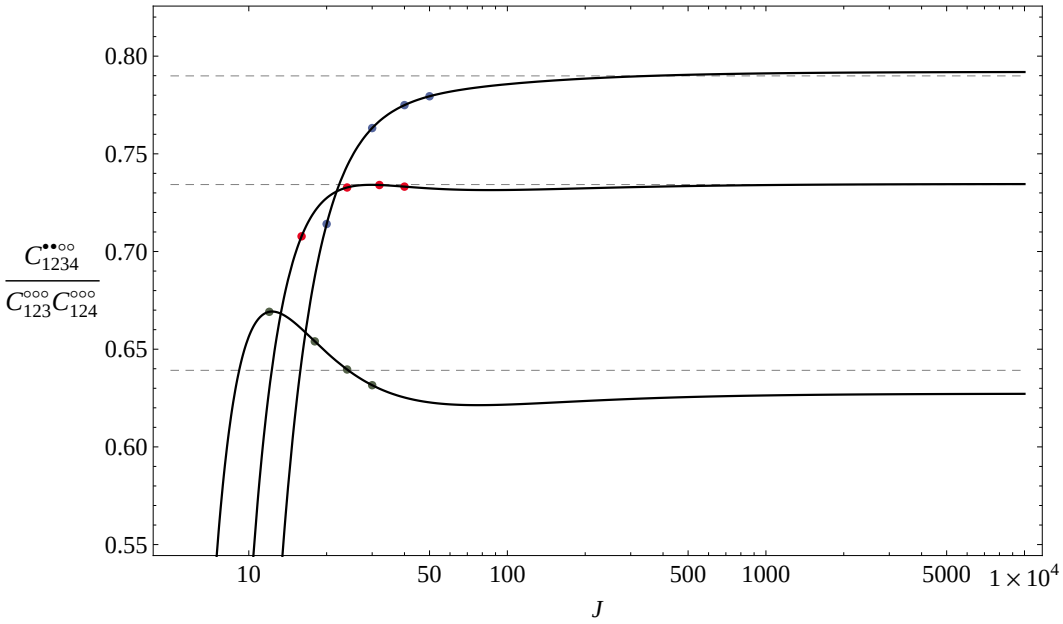

Figure 8.3: Weak/strong coupling match for four-point functions in the classical limit with $\mathcal{O}_3 = \mathcal{O}_4 = \mathrm{Tr}(Z^2\bar{X}^2)$. The bullets correspond to the numerical data obtained by evaluating the weak coupling formula (6.5) with the roots of $\mathcal{O}_1$ and $\mathcal{O}_2$ lying on the same classical cuts, for different values of $\alpha = 1/3, 1/4, 1/5$, from bottom to top. In this case the fits (solid black curves) nicely match the analytical prediction from strong coupling (dashed gray lines) obtained from (8.9).

in the case of three-point functions, we choose the extra roots of $\mathcal{O}_1$ to lie on the already existing two symmetric cuts defined by the Bethe roots of $\mathcal{O}_2$. Given our setup, this means that we add two roots to each of the cuts. This is the weak coupling choice that corresponds to $\mathcal{O}_1 \simeq \bar{\mathcal{O}}_2$ and thus reproduces the strong coupling computation.

Note that due to the sum over l, the many sums over partitions and the scalar products appearing in it, equation (6.5) is quite non-trivial to evaluate numerically if we consider a large number of excitations. Moreover, as opposed to the case of three-point functions, there is no known determinant form of this equation. This means that in practice we were only able to evaluate (6.5) for configurations with $4, 6, 8$ and 10 Bethe roots in operator $\mathcal{O}_1$ using the Mathematica codes presented in appendix E. We collected this data in the following form $\{J, r_{1234}\}$, where r_{1234} is the ratio on the l.h.s of (7.31). For example, for filling fraction $\alpha = 1/3$, we obtained

```
data={{12,0.669138111344},{18,0.654008855014},{24,0.639613251186},
                          {30,0.631580997967}};
```

We then fit this data in order to find the large J asymptotics of r_{1234}, exactly in the same way that we did for three-point functions. For the data shown above, we obtain

$$r^{\mathrm{num}}_{1234} = 0.627249\,. \tag{8.10}$$

In the second column of table 8.3 we present the values of such numerical extrapolations for three different filling fractions. We see that, with very small relative error, the numerical weak coupling results approach the analytical strong coupling predictions in the Frolov-Tseytlin limit. Figure 8.3 shows our list of data points, their fits and the analytical predictions.

α	Analytical prediction	Numerical extrapolation	Relative error
1/3	0.639186	0.627249	1.868%
1/4	0.734274	0.734578	0.042%
1/5	0.789894	0.791947	0.259%

Table 8.3: Weak/strong coupling match for four-point functions in the classical limit with $\mathcal{O}_3 = \mathcal{O}_4 = \mathrm{Tr}(Z^2\bar{X}^2)$. We compare the strong coupling analytic prediction (8.9) compared with the numerical extrapolation of the weak coupling data obtained with (6.5) for different values of the filling fraction of operator $\mathcal{O}_1$.

Before closing this chapter, let us make some comments regarding the accuracy of our numerical results for four-point functions. By looking at table 8.3 and figure 8.3, the skeptical reader might think that the results presented in this section are not conclusive enough to claim a weak/strong coupling match for four-point functions obeying the setup of figure 6.1. However, we should note again that we only used four points of data to perform each fit, compared to the 20 points used for the numerical weak/strong coupling match of three-point functions presented in the previous section. In that case, the accuracy in the numerical match was indeed much higher. However, had we only considered the first four points of data to perform the fit for the three-point functions match, the relative error between the analytical and numerical results for $\alpha = 1/3, 1/4, 1/5$ would have been $2.122\%, 0.612\%, 0.381\%$, respectively. Hence, we see that the relative errors for the weak/strong coupling match of four-point functions shown in table 8.3 are in fact smaller than the relative errors in the match of three-point functions. We can be confident that adding more points of data to our fits would simply increase the accuracy of the numerical results even further, confirming that the weak/strong coupling match presented here is indeed exact. For example, once a determinant form of equation (6.5) is derived, one could quickly check this statement. Furthermore, we will present an analytical proof of the match for four-point functions in the next chapter.

Chapter 9

Analytical Match

In the previous chapter, we provided conclusive numerical evidence for the weak/strong coupling match for tree-level three- and four-point functions of $SU(2)$ operators in the Frolov-Tseytlin limit. In this chapter we will provide an analytical proof of this match by representing the two large, classical operators as Landau-Lifshitz coherent states at weak coupling. In fact, our analytical proof is for correlation functions of $SU(3)$ operators, thus generalizing the $SU(2)$ case considered for the numerical match.

9.1 Landau-Lifshitz coherent states

Just like in the previous chapter, we will be interested in three- and four-point functions of two large non-BPS operators with one or two small BPS operators. For convenience, we focus the discussion in this section to the three-point function case, with the extension to four-point functions being very clear.

Let us take operators $\mathcal{O}_1$ and $\mathcal{O}_2$ to be very large $SU(3)$ operators with a lot of excitations such that their density is kept fixed in the large length limit. Hence, using the notation shown in (7.20) or (7.27), we consider

$$J_1, J_2, J_3 \to \infty\,, \qquad \alpha = \frac{J_1 + J_2}{J} \text{ fixed}\,,$$

where $J = J_1 + J_2 + J_3$. Moreover, we only consider low lying excitations around the ferromagnetic vacuum. These are excitations with long wavelength. That is, the momenta of the individual excitations of operators $\mathcal{O}_1$ and $\mathcal{O}_2$ are of order $1/J$. The energy of the individual excitations is of order $1/J^2$ so that the total energy is of order $1/J$. In short, we will consider the Sutherland classical limit [115, 116], rediscovered in the context of the AdS/CFT correspondence in [102].

The operators $\mathcal{O}_1$ and $\mathcal{O}_2$ are taken to be *roughly* the complex conjugate of each other in a sense that will be made precise later. The physical picture is that the large operator $\mathcal{O}_2$ interacts with the small operator $\mathcal{O}_3$ to become the slightly modified final large operator

$\mathcal{O}_1$. Note that we can not take $\mathcal{O}_1$ to be *exactly* the conjugate of $\mathcal{O}_2$: this would lead to a vanishing three-point function by R-charge conservation.

Now, in the classical limit the excitations have long wavelength and can be depicted as changing the spin configuration slowly as one goes around the spin chain. In this limit, magnon dynamics are well approximated by the Landau-Lifshitz field theory [117, 96]. More explicitly, we can use coherent states to approximate the exact $SU(3)$ states, see figure 9.1.[52] The coherent states mimic the exact Bethe states in the following precise sense: when computing with them an average of a classical quantity $\mathcal{Q}_{\text{classical}}$ such as the total spin or energy, they yield the same result up to finite size corrections. In the spin chain language,

$$\frac{\langle\Psi|\mathcal{Q}_{\text{classical}}|\Psi\rangle}{\langle\Psi|\Psi\rangle} = \frac{\langle\varphi|\mathcal{Q}_{\text{classical}}|\varphi\rangle}{\langle\varphi|\varphi\rangle}\left(1+O\left(\frac{1}{J}\right)\right), \tag{9.1}$$

where $|\Psi\rangle$ denotes the exact Bethe state while $|\varphi\rangle$ denotes the coherent state. Let us see how to describe the latter.

Since we are studying $SU(3)$ spin chains in the classical limit, see e.g. [97], at each site we have three possible degrees of freedom which we denote as $|X\rangle, |Y\rangle$ and $|Z\rangle$. Therefore, at a given site n in the spin chain we have a complex vector of the form

$$|\mathbf{u}^{(n)}\rangle = u_1^{(n)}|X\rangle + u_2^{(n)}|Y\rangle + u_3^{(n)}|Z\rangle\,,$$

which denotes a linear superposition of the three degrees of freedom. We normalize $\mathbf{u}^{(n)}$ to be a unitary vector so that automatically

$$\langle\mathbf{u}^{(n)}|\mathbf{u}^{(n)}\rangle = \bar{\mathbf{u}}^{(n)}\cdot\mathbf{u}^{(n)} = 1 \tag{9.2}$$

and, since the spin configuration is slowly varying along the chain, we must have that $\mathbf{u}^{(n+1)} - \mathbf{u}^{(n)} = O(1/J)$. Therefore, in the large J classical limit that we are considering, the very entangled and complex exact $SU(3)$ quantum states $|\Psi\rangle$, which have order (number of X's and Y's)! terms, can be approximated by coherent classical states which simply read [117]

$$|\varphi\rangle = |\mathbf{u}^{(1)}\rangle\otimes\cdots\otimes|\mathbf{u}^{(J)}\rangle\,. \tag{9.3}$$

The norm of such states is automatically equal to 1. Note that we have purposely used the letter $\mathbf{u}$ to represent the coherent states, as this will be identified with the classical string solution $\mathbf{u}$ introduced at strong coupling in chapter 7, see (7.5).

The physical picture is that of a spin wave pointing in direction $\mathbf{u}$ which changes slowly as we go from one site to the next. It is then convenient to package all the information about the classical state in a continuous field

$$\mathbf{u}^{(n)} \to \mathbf{u}(\sigma)\,, \qquad \text{with} \qquad \sigma = 2\pi\,\frac{n}{J}\,.$$

[52] See section 11.1 to learn how to construct exact $SU(3)$ eigenstates.

To get some experience with these classical states let us review the computation of the energy of such low wavelength states using the Hamiltonian (3.2), which is also the one corresponding to $SU(3)$ spin chains. We have

$$\begin{aligned}\langle\varphi|H|\varphi\rangle &= \frac{\lambda}{8\pi^2}\sum_{n=1}^{J}\langle\mathbf{u}^{(n)}|\otimes\langle\mathbf{u}^{(n+1)}|\left(\mathbb{I}_{n,n+1}-\mathbb{P}_{n,n+1}\right)|\mathbf{u}^{(n)}\rangle\otimes|\mathbf{u}^{(n+1)}\rangle \\ &= \frac{\lambda}{8\pi^2}\sum_{n=1}^{J}\Big[1-\left(\bar{\mathbf{u}}^{(n)}\cdot\mathbf{u}^{(n+1)}\right)\left(\bar{\mathbf{u}}^{(n+1)}\cdot\mathbf{u}^{(n)}\right)\Big].\end{aligned}$$

Expanding $\mathbf{u}$ as

$$\mathbf{u}^{(n+k)}=\mathbf{u}^{(n)}+\frac{2\pi k}{J}\partial_\sigma\mathbf{u}+\frac{1}{2}\left(\frac{2\pi k}{J}\right)^2\partial_\sigma^2\mathbf{u}+\dots$$

and using the equations of motion (7.7) and Virasoro constraints (7.8), we obtain

$$\langle\varphi|H|\varphi\rangle\simeq\frac{\lambda}{2J}\int_0^{2\pi}\frac{d\sigma}{2\pi}\,\partial_\sigma\bar{\mathbf{u}}\cdot\partial_\sigma\mathbf{u}\,. \tag{9.4}$$

This expression precisely agrees with the strong coupling result in the Frolov-Tseytlin limit (7.10)! Thus, we see that by using coherent states to represent large, classical operators at weak coupling, one is able to analytically prove the weak/strong coupling match for the spectrum presented in chapter 7. Finally, we should mention that the coherent states evolve in time as follows from the Schrödinger equation. That evolution is equivalent to the equation of motion (7.7) [117].

The Hamiltonian is just one of the many conserved charges of the integrable spin chain, which is a classical operator in the classical limit. The (trace of the) transfer matrix encodes all of them. Hence, a nice way of identifying whether a coherent state mimics an exact state is by measuring the expectation value of the transfer matrix and imposing that it matches the classical limit of the quantum transfer matrix [104].

A related but more technical comment is the following. The exact Bethe eigenstates are highest weights: $S^+|\Psi\rangle=0$. The coherent states which we use to mimic them are only highest weights at the level of averages, that is $\langle\varphi|S^+|\varphi\rangle=0$. Similarly, the exact states are cyclic, $e^{iP}|\Psi\rangle=|\Psi\rangle$ while $\langle\varphi|e^{iP}|\varphi\rangle=1$. Cyclicity of the exact states means that we do not need to care about where we break them when computing expectation values or correlation functions. On the other hand, to mimic these computations with coherent states we should align the operators as done in the following section.

9.2 Three-point functions

In this section we present the analytical weak/strong coupling match for three-point functions using the coherent state machinery reviewed in the previous section. Again, we will consider

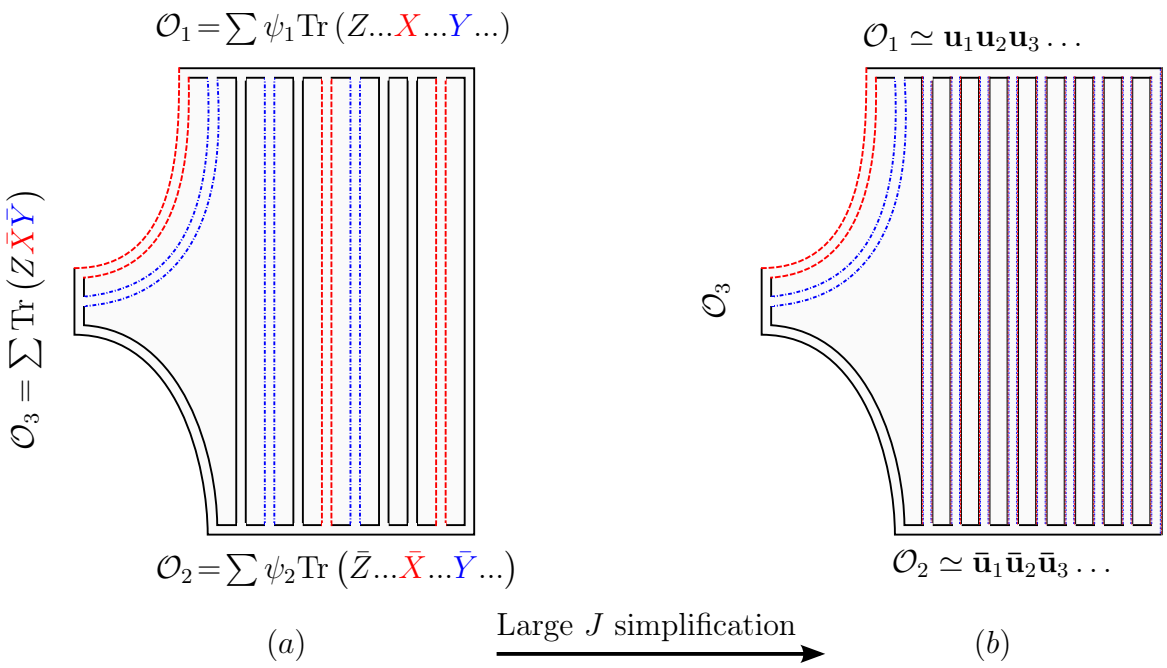

Figure 9.1: Three-point function of $SU(3)$ operators, which is a generalization of the $SU(2)$ setup of figure 5.1. $\mathcal{O}_1$ and $\mathcal{O}_2$ are large and roughly conjugate to each other while $\mathcal{O}_3$ is small. (a) Exact setup. The tree-level contraction of three pure eigenstates (see section 11.1 for an explicit expression of $SU(3)$ eigenstates). These are very entangled states with order (number of X's and Y's)! terms. All contractions are such that R-charge is preserved. (b) Classical limit. $\mathcal{O}_1$ and $\mathcal{O}_2$, represented by coherent states, are not entangled at all, so their contraction is trivial. The non-trivial contribution to the three-point function comes from tree-level contraction of the small operator $\mathcal{O}_3$ with the two large coherent states.

the computation of three-point functions where two of the operators, $\mathcal{O}_1$ and $\mathcal{O}_2$, are classical operators and are thus well approximated by coherent states. The third operator $\mathcal{O}_3$ is taken to be a small operator, see figure 9.1. In this section and the next, we will use the notation

$$\mathcal{L}_i \equiv \frac{L_i}{2\pi}\,,$$

where L_i is the length of operator $\mathcal{O}_i$. This will simplify our expressions a great deal. For now, we take $\mathcal{O}_3$ to be a BPS operator:

$$\mathcal{O}_3 = \mathcal{M}\left(\mathrm{Tr}\left[\bar{X}^{j_1}\bar{Y}^{j_2}Z^{j_3}\right] + \text{permutations}\right), \tag{9.5}$$

where we only distinguish permutations up to a cyclic permutation due to the cyclicity of the trace. The normalization coefficient

$$\mathcal{M} = \sqrt{\frac{j_1!j_2!j_3!}{j!\,j}} \tag{9.6}$$

is included so that $\mathcal{O}_3$ has norm 1, just like the coherent states (9.3). To accomplish our businesses with combinatorics let us notice that among all the terms in $\mathcal{O}_3$ only the ones of the form $\mathrm{Tr}[Z^{j_3}$ anything$]$ can give a nonzero contribution to the Wick contractions with $\mathcal{O}_1$ and $\mathcal{O}_2$, see figure 9.1b. The number of such terms is equal to $j\binom{j_1+j_2}{j_1}$.

The operators $\mathcal{O}_1$ and $\mathcal{O}_2$ are described by coherent states as introduced in the previous section:

$$\begin{aligned} |\mathcal{O}_1\rangle &= \cdots \otimes \left|\mathbf{u}(\tfrac{n}{\mathcal{L}_1})\right\rangle \otimes \left|\mathbf{u}(\tfrac{n+1}{\mathcal{L}_1})\right\rangle \otimes \dots \\ \langle\mathcal{O}_2| &= \cdots \otimes \left\langle\bar{\mathbf{u}}(\tfrac{n}{\mathcal{L}_2})\right| \otimes \left\langle\bar{\mathbf{u}}(\tfrac{n+1}{\mathcal{L}_2})\right| \otimes \dots \end{aligned} \tag{9.7}$$

The three-point function is now obtained by Wick contracting the three operators as depicted in figure 9.1b. Since there is no entanglement in operators $\mathcal{O}_1$ and $\mathcal{O}_2$ the contractions are trivial. The operator $\mathcal{O}_3$ is glued, i.e. Wick contracted, with the other states at sites $k, k-1, \dots$. We should then sum over the insertion starting point k. The Wick contractions between $\mathcal{O}_1$ and $\mathcal{O}_2$ give

$$\mathcal{I}_k = \prod_{i=k+1}^{l_{12}+k} \bar{\mathbf{u}}(i/\mathcal{L}_2)\cdot\mathbf{u}(i/\mathcal{L}_1)\,. \tag{9.8}$$

where l_{12} is the number of contractions between $\mathcal{O}_1$ and $\mathcal{O}_2$. What is left is to consider the Wick contractions between $\mathcal{O}_3$ and $\mathcal{O}_1$, $\mathcal{O}_2$. Consider one of the terms in $\mathcal{O}_3$ which gives a nonzero contribution $\mathrm{Tr}[Z^{j_3}\bar{X}\bar{X}\bar{Y}\dots]$. The Wick contraction of this operator with the coherent states $\mathcal{O}_1$, $\mathcal{O}_2$ at position $k, k-1, \dots$ gives

$$\bar{u}_3(\tfrac{k}{\mathcal{L}_2})\bar{u}_3(\tfrac{k-1}{\mathcal{L}_2})\dots\bar{u}_3(\tfrac{k-j_3+1}{\mathcal{L}_2})u_1(\tfrac{k}{\mathcal{L}_1})u_1(\tfrac{k-1}{\mathcal{L}_1})u_2(\tfrac{k-2}{\mathcal{L}_1})\dots\ .$$

Since the field changes slowly over those sites, we can approximate this contribution by

$$u_1^{j_1}(k/\mathcal{L}_1)\,u_2^{j_2}(k/\mathcal{L}_1)\,\bar{u}_3^{j_3}(k/\mathcal{L}_2)\ .$$

Thus, all nonzero Wick contractions between $\mathcal{O}_3$ and $\mathcal{O}_1$, $\mathcal{O}_2$ give approximately the same contribution and, as mentioned above, there are $j\binom{j_1+j_2}{j_1}$ of them. Hence, the result of these contractions is

$$\mathcal{J}_k = \mathcal{M}\,j\binom{j_1+j_2}{j_1}\,u_1^{j_1}(k/\mathcal{L}_1)\,u_2^{j_2}(k/\mathcal{L}_1)\,\bar{u}_3^{j_3}(k/\mathcal{L}_2)\,. \tag{9.9}$$

All together, we get

$$C_{123}^{\bullet\bullet\circ} \simeq \sum_{k=0}^{J} \mathcal{I}_k\,\mathcal{J}_k\,, \tag{9.10}$$

where we recall that J is the length of operator $\mathcal{O}_1$, see (7.20).

Note that we have a $U(1)$ gauge invariance when representing the coherent states as tensor products of single site states. That is, we can multiply the state associated with any site of

the chain by an independent phase factor

$$\mathbf{u}(j/\mathcal{L}) \to e^{i\Lambda(j)}\,\mathbf{u}(j/\mathcal{L})\ , \qquad \bar{\mathbf{u}}(j/\mathcal{L}) \to e^{-i\Lambda(j)}\,\bar{\mathbf{u}}(j/\mathcal{L})\ . \tag{9.11}$$

All observables, including the structure constant (9.10) are of course invariant under the gauge transformation. However $\mathcal{I}_k$ and $\mathcal{J}_k$ in (9.10) do transform nontrivially (for $j_3 \neq j_1 + j_2$). We can profit from this fact to choose the most convenient gauge. Namely we can fix a conformal-like gauge by demanding that $\mathcal{I}_k$ does not depend on k. That is

$$1 = \frac{\mathcal{I}_k}{\mathcal{I}_{k-1}} = \frac{\bar{\mathbf{u}}(k/\mathcal{L}_2 + l_{12}/\mathcal{L}_2)\cdot\mathbf{u}(k/\mathcal{L}_1 + l_{12}/\mathcal{L}_1)}{\bar{\mathbf{u}}(k/\mathcal{L}_2)\cdot\mathbf{u}(k/\mathcal{L}_1)}\ .$$

We have

$$\begin{aligned}
\mathbf{u}(k/\mathcal{L}_1 + l_{12}/\mathcal{L}_1) &\simeq \mathbf{u}(k/\mathcal{L}_1) - \frac{j_1+j_2}{\mathcal{L}_1}\partial_\sigma\mathbf{u}(k/\mathcal{L}_1) + O(1/\mathcal{L}_1^2)\,,\\
\bar{\mathbf{u}}(k/\mathcal{L}_2 + l_{12}/\mathcal{L}_2) &\simeq \bar{\mathbf{u}}(k/\mathcal{L}_2) - \frac{j_3}{\mathcal{L}_2}\partial_\sigma\bar{\mathbf{u}}(k/\mathcal{L}_2) + O(1/\mathcal{L}_2^2)\,,
\end{aligned}$$

where we used the fact that $l_{12} = L_1 - (j_1 + j_2) = L_2 - j_3$, $\mathbf{u}(\sigma + 2\pi) = \mathbf{u}(\sigma)$ and similarly for $\bar{\mathbf{u}}$. Thus we have to require that

$$(j_1 + j_2 - j_3)\ \bar{\mathbf{u}}\cdot\partial_\sigma\mathbf{u} = 0\ , \tag{9.12}$$

which matches nicely the Virasoro constraint (7.8). In the conformal-like gauge (9.12), we further have that

$$\mathcal{I}_0 = \prod_{i=1}^{l_{12}} \bar{\mathbf{u}}(i/\mathcal{L}_2)\cdot\mathbf{u}(i/\mathcal{L}_1) \simeq \exp\int_0^{2\pi-\frac{j_3}{\mathcal{L}_2}} J\frac{d\sigma}{2\pi}\,\log\left(\bar{\mathbf{u}}\cdot\left[1 - \frac{j_1+j_2-j_3}{\mathcal{L}}\sigma\partial_\sigma\right]\mathbf{u}\right) = 1 + O(1/\mathcal{L})\,.$$

We conclude that in this gauge:

$$C_{123}^{\bullet\bullet\circ} \simeq \frac{(j_1+j_2)!}{j_1!j_2!}\sqrt{j\frac{j_1!j_2!j_3!}{j!}}\int_0^{2\pi} J\frac{d\sigma}{2\pi}\,u_1^{j_1}\,u_2^{j_2}\,\bar{u}_3^{j_3}\ , \tag{9.13}$$

which is precisely the strong coupling result (7.25)! This is the main result of this section. Notice also that if we substitute v_a from (7.4) instead of u_a we get

$$C_{123}^{\circ\circ\circ} = J\frac{(j_1+j_2)!}{j_1!j_2!}\sqrt{j\frac{j_1!j_2!j_3!}{j!}}\left(\frac{J_1}{J}\right)^{j_1/2}\left(\frac{J_2}{J}\right)^{j_2/2}\left(\frac{J_3}{J}\right)^{j_3/2} \tag{9.14}$$

which is indeed the limit $J_a \gg j_a$ of the known BPS formula (7.21), see (7.22). Of course, upon dividing the two equations above and taking the absolute value, we obtain the ratio

r_{123}, which matches exactly with the strong coupling result (7.26). Moreover, in some sense this result justifies that fact that we represented the large operators by coherent states, as it matches the numerical extrapolation of our formulas of chapter 5 (see figure 8.1). This concludes our analytical proof of the weak/strong coupling match for three-point functions in the classical limit.

9.2.1 Non-BPS operator $\mathcal{O}_3$

The tree-level computation of the previous section did not rely on the small operator being protected.[53] We can therefore trivially generalize it to any small $SU(3)$ operator $\mathcal{O}_3$ as we will now explain. All the manipulations of the previous subsection involving the large operators were not sensitive to the precise form of the small operator and only depended on its global charges. The only difference when considering non-protected small operators is in the combinatorial factor outside the integral in (9.13). That is, the more general weak coupling result is

$$C_{123}^{\bullet\bullet\bullet} = \mathcal{D} \int_0^{2\pi} J \frac{d\sigma}{2\pi}\, u_1^{j_1}\, u_2^{j_2}\, \bar{u}_3^{j_3}\ , \tag{9.15}$$

where $\mathcal{D}$ is the sum of the coefficients of the traces in $\mathcal{O}_3$ in which all the Z fields are next to each other.

To illustrate this point let us consider a simple example where $\mathcal{O}_3$ is the Konishi operator

$$\mathcal{O}_3 = \frac{1}{\sqrt{3}}\Big[\mathrm{Tr}\left(Z^2\bar{X}^2\right) - \mathrm{Tr}\left(Z\bar{X}Z\bar{X}\right)\Big] \quad \Rightarrow \quad \mathcal{D} = \frac{1}{\sqrt{3}} \quad \Rightarrow \quad \frac{C_{123}^{\bullet\bullet\bullet}}{C_{123}^{\bullet\bullet\circ}} = \frac{1}{\sqrt{3}}\sqrt{\frac{3}{2}}\,. \tag{9.16}$$

This ratio is exact and does not rely on the classical limit. Note that although in this example $\mathcal{O}_3$ is in the $SU(2)$ subsector, the operators $\mathcal{O}_1$ and $\mathcal{O}_2$ can be generic $SU(3)$ operators. Another simple example is

$$\mathcal{O}_3 = \frac{1}{\sqrt{2}}\Big[\mathrm{Tr}(Z\bar{X}\bar{Y}) - \mathrm{Tr}(Z\bar{Y}\bar{X})\Big] \qquad \Rightarrow \qquad \mathcal{D} = 0\,. \tag{9.17}$$

If we restrict to the $SU(2)$ sector considered in chapter 5, see figure 5.1, we have

$$\frac{C_{123}^{\bullet\bullet\bullet}}{C_{123}^{\bullet\bullet\circ}} = \frac{C_{123}^{\circ\circ\bullet}}{C_{123}^{\circ\circ\circ}} = \sqrt{\frac{1}{j}\binom{j}{j_3}}\frac{\mathscr{A}(j_1|\{w\})}{\mathscr{B}(\{w\})}\,, \tag{9.18}$$

where we used the results from table 5.1. In particular, note that the dependence on $\mathcal{O}_1$ and $\mathcal{O}_2$ has canceled out. Recall that we are now considering non-BPS operators $\mathcal{O}_3$ which can be parametrized by its Bethe roots: those are the w_j. Again, this formula is exact and does not rely on any classical limit.

[53] Three-point functions of two heavy operators and certain light non-BPS operators were discussed in [64].

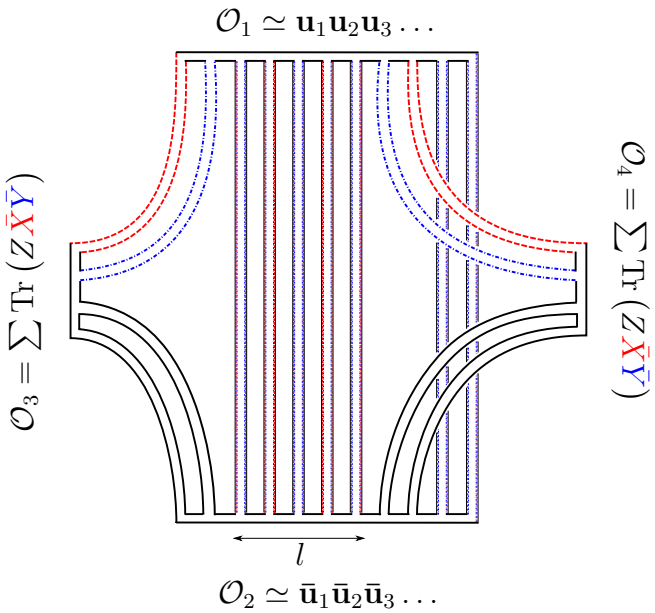

Figure 9.2: Four-point function of $SU(3)$ operators with no contractions between $\mathcal{O}_3$ and $\mathcal{O}_4$. This is the $SU(3)$ generalization of the $SU(2)$ setup considered in figure 6.1. $\mathcal{O}_1$ and $\mathcal{O}_2$ are large and roughly conjugate to each other. They are represented by coherent states, so their contraction is trivial. The non-trivial contribution to the four-point function comes from tree-level contraction of the small operators $\mathcal{O}_3$ and $\mathcal{O}_4$ with the two large coherent states.

For non-protected operators however, we do not expect a match with strong coupling in the classical limit considered so far. That can be seen already at one loop. A main ingredient for the match between strong and weak coupling in the Frolov-Tseytlin limit is that the perturbative expansion organized itself in powers of λ/J^2. At one loop, there are two types of corrections [38]. One is the insertion of one-loop Hamiltonians right where we cut a given operator. The other is the two-loop correction to the Bethe wave functions. In contradistinction to the case where the small operator is BPS, these two types of corrections are not suppressed by $1/J^2$ and therefore, do not follow the Frolov-Tseytlin scaling.

9.3 Four-point functions

We now consider the $SU(3)$ generalization of the four-point function setup for $SU(2)$ operators of figure 6.1. In particular, two of the operators are classical, while the other two are small and are not Wick contracted between themselves, see figure 9.2. The operators $\mathcal{O}_1$ and $\mathcal{O}_2$ are taken to be large operators with their charges and lengths being much larger than the corresponding charges and lengths of $\mathcal{O}_3$ and $\mathcal{O}_4$. Thus, the exact Bethe states that correspond to $\mathcal{O}_1$ and $\mathcal{O}_2$ are again well approximated by the coherent states (9.7). The

operators $\mathcal{O}_3$ and $\mathcal{O}_4$ are the small BPS operators:

$$\begin{aligned}\mathcal{O}_3 &= \mathcal{M}_3\big(\mathrm{Tr}[\bar{X}^{j_1}\bar{Y}^{j_2}Z^{j_3}] + \text{permutations}\big),\\ \mathcal{O}_4 &= \mathcal{M}_4\big(\mathrm{Tr}[\bar{X}^{k_1}\bar{Y}^{k_2}Z^{k_3}] + \text{permutations}\big),\end{aligned} \tag{9.19}$$

where the normalization constants are

$$\mathcal{M}_3 = \sqrt{\frac{j_1!j_2!j_3!}{j!\,j}}\,, \qquad\qquad \mathcal{M}_4 = \sqrt{\frac{k_1!k_2!k_3!}{k!\,k}}\,. \tag{9.20}$$

The operator $\mathcal{O}_3$ is Wick contracted with $\mathcal{O}_1$ and $\mathcal{O}_2$ at sites $q, q-1, \ldots$. For a given q and l (see figure 9.2), the Wick contractions between the large operators $\mathcal{O}_1$ and $\mathcal{O}_2$ are given by

$$\mathcal{I}_{q,l} = \prod_{i=q+1}^{l+q} \bar{\mathbf{u}}(i/\mathcal{L}_2)\cdot\mathbf{u}(i/\mathcal{L}_1) \prod_{j=q+l+k_1+1}^{l_{12}+q+k_1} \bar{\mathbf{u}}(j/\mathcal{L}_2)\cdot\mathbf{u}(j/\mathcal{L}_1)\,. \tag{9.21}$$

Let us consider the contractions between $\mathcal{O}_3$ or $\mathcal{O}_4$ with the classical operators. Given the present configuration, the only terms of $\mathcal{O}_3$ which give a nonzero contribution are $\mathrm{Tr}[Z^{j_3}\bar{X}^{j_1}\bar{Y}^{j_2}]$, i.e. those in which all Z fields are together. Similary, the only terms in $\mathcal{O}_4$ that contribute are $\mathrm{Tr}[Z^{k_3}\bar{X}^{k_1}\bar{Y}^{k_2}]$. For a fixed q and l, we denote the Wick contractions of $\mathcal{O}_3$ and $\mathcal{O}_4$ with the classical operators by $\mathcal{J}^{(3)}_{q,l}$ and $\mathcal{J}^{(4)}_{q,l}$, respectively. Following the same logic that led to (9.9), we get

$$\mathcal{J}^{(3)}_{q,l} \simeq \mathcal{M}_3\, j \binom{j_1+j_2}{j_1} u_1^{j_1}\!\left(\frac{q}{\mathcal{L}_1}\right) u_2^{j_2}\!\left(\frac{q}{\mathcal{L}_1}\right) \bar{u}_3^{j_3}\!\left(\frac{q}{\mathcal{L}_2}\right),$$

$$\mathcal{J}^{(4)}_{q,l} \simeq \mathcal{M}_4\, k \binom{k_1+k_2}{k_1} u_1^{k_1}\!\left(\frac{q+l+1}{\mathcal{L}_1}\right) u_2^{k_2}\!\left(\frac{q+l+1}{\mathcal{L}_1}\right) \bar{u}_3^{k_3}\!\left(\frac{q+l+1}{\mathcal{L}_2}\right).$$

Finally, we get[54]

$$C^{\bullet\bullet\circ\circ}_{1234} \simeq \sum_{l=0}^{J}\sum_{q=0}^{J} \mathcal{I}_{q,l}\,\mathcal{J}^{(3)}_{q,l}\,\mathcal{J}^{(4)}_{q,l}\,, \tag{9.22}$$

where we recall that J is the length of operator $\mathcal{O}_1$, see (7.27).

Just like in the case of three-point functions, we will now argue that to leading order, the contractions between the large operators is simply 1, i.e. $\mathcal{I}_{q,l} \simeq 1$. For that, we may use the fact that $|C^{\bullet\bullet\circ\circ}_{1234}|$ must be invariant under multiplying each single site state by a phase, see (9.11). We fix this gauge by choosing the conformal-like gauge (9.12). Then, with this gauge and using

$$\mathcal{L}_2 = \mathcal{L}_1 + \frac{k_1+k_2+j_1+j_2-k_3-j_3}{2\pi}\,, \tag{9.23}$$

[54]The upper limit in the sum over l should be $J-j_1-j_2-k_1-k_2$. We replaced it by J, since $J \gg j_a, k_a$.

(9.21) can be rewritten as

$$\begin{aligned}\mathcal{I}_{q,l} &\simeq \exp\int_0^{2\pi l}\frac{d\sigma}{2\pi}\,\log\left(\bar{\mathbf{u}}\cdot\left[\mathbf{u}-\frac{j_3+k_3-j_1-j_2-k_1-k_2}{2\pi\mathcal{L}_2}\sigma\partial_\sigma\mathbf{u}\right]\right)\\ &\quad\times\exp\int_0^{2\pi(l_{12}-l)}\frac{d\sigma'}{2\pi}\,\log\left(\bar{\mathbf{u}}\cdot\left[\mathbf{u}-\frac{j_3+k_3-j_1-j_2-k_1-k_2}{2\pi\mathcal{L}_2}\sigma'\partial_{\sigma'}\mathbf{u}\right]\right)\\ &\simeq 1+O\left(1/\mathcal{L}_2\right).\end{aligned}$$

With this simplification, the remaining part of the formula becomes

$$\begin{aligned}C^{\bullet\bullet\circ\circ}_{1234} \simeq\ & \mathcal{M}_3\,\mathcal{M}_4\,j\,k\binom{j_1+j_2}{j_1}\binom{k_1+k_2}{k_1}\times\\ & \sum_{l=0}^{J}\sum_{q=0}^{J}u_1^{j_1}\!\left(\frac{q}{\mathcal{L}_1}\right)u_2^{j_2}\!\left(\frac{q}{\mathcal{L}_1}\right)\bar{u}_3^{j_3}\!\left(\frac{q}{\mathcal{L}_2}\right)u_1^{k_1}\!\left(\frac{q+l+1}{\mathcal{L}_1}\right)u_2^{k_2}\!\left(\frac{q+l+1}{\mathcal{L}_1}\right)\bar{u}_3^{k_3}\!\left(\frac{q+l+1}{\mathcal{L}_2}\right)\\ \simeq\ & \left[\frac{(j_1+j_2)!}{j_1!j_2!}\sqrt{j\frac{j_1!j_2!j_3!}{j!}}\int_0^{2\pi}J\frac{d\sigma}{2\pi}u_1^{j_1}(\sigma)u_2^{j_2}(\sigma)\bar{u}_3^{j_3}(\sigma)\right]\times\\ & \left[\frac{(k_1+k_2)!}{k_1!k_2!}\sqrt{k\frac{k_1!k_2!k_3!}{k!}}\int_0^{2\pi}J\frac{d\sigma}{2\pi}u_1^{k_1}(\sigma)u_2^{k_2}(\sigma)\bar{u}_3^{k_3}(\sigma)\right]\end{aligned}$$

where in the last step we have used (9.23) and the periodicity of the chain, which allowed us to factorize the double sum in the first line. We immediately recognize that the first term in brackets is $C^{\bullet\bullet\circ}_{123}$, while the second one is $C^{\bullet\bullet\circ}_{124}$, see (7.25). This constitutes an analytical proof of the factorization formula (7.29). Of course, upon dividing the expression above by $C^{\circ\circ\circ}_{123}C^{\circ\circ\circ}_{124}$, which can be read from (7.22), and taking the absolute value we exactly obtain the strong coupling result for r_{1234}, see (7.31)!

9.3.1 More general four-point functions and $1/J$ supression

Let us now consider the more general setup for four-point functions that we first introduced in figure 6.2, which in the classical limit looks like the one in figure 9.3. Using exactly the same methods as before, we again impose the conformal-like gauge such that the contractions between heavy operators are approximately one. The contributions from the contractions between the light operators $\mathcal{O}_3$ and $\mathcal{O}_4$ with the heavy operators are respectively given by

$$\mathcal{J}^{(3)}_{q,l,\{m_j\}} \simeq \binom{m_1+m_2}{m_1}\mathcal{M}_3\,j\,\bar{u}_1^{j_1-m_1}\left(\frac{q}{\mathcal{L}_2}\right)\bar{u}_2^{j_2-m_2}\left(\frac{q}{\mathcal{L}_2}\right)u_3^{j_3-m_3}\left(\frac{q}{\mathcal{L}_1}\right),$$

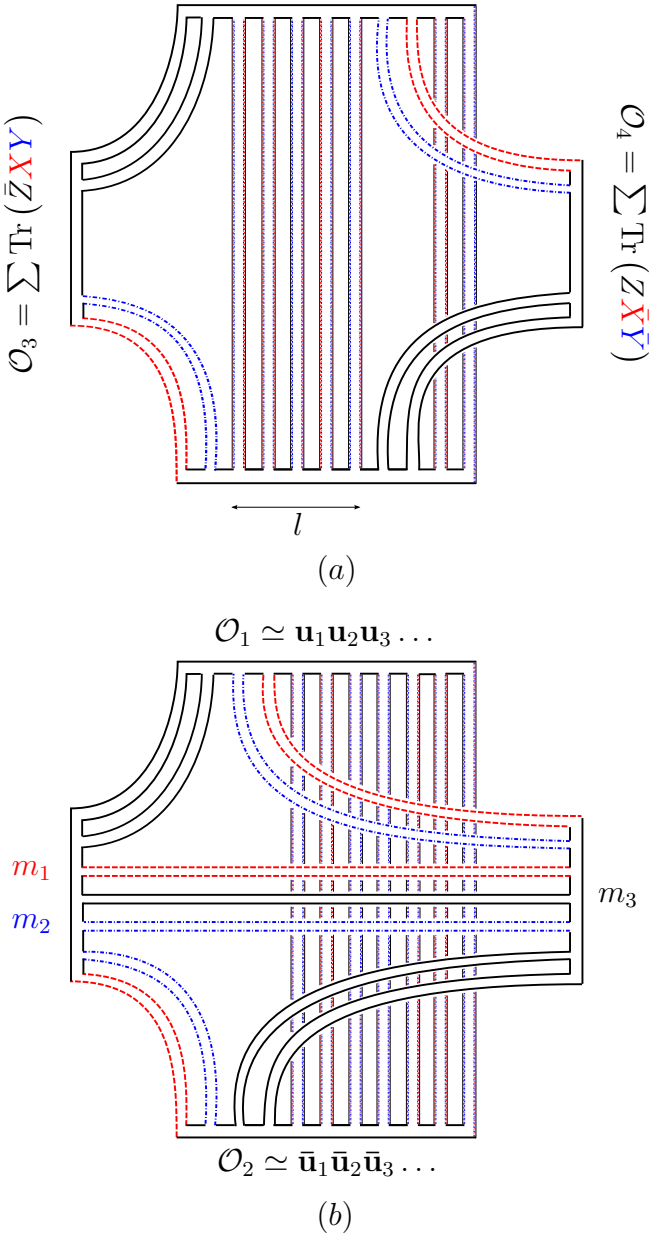

Figure 9.3: More general four-point function of $SU(3)$ operators, which allow contractions between $\mathcal{O}_3$ and $\mathcal{O}_4$. This is the $SU(3)$ generalization of the $SU(2)$ setup considered in figure 6.2. Again, the contraction between the large operators $\mathcal{O}_1$ and $\mathcal{O}_2$ is trivial. Thus, the only contribution comes from the Wick contractions between the light operators and the large operators and between the light operators themselves. (a) When there are no contractions between the light operators, the diagrams are planar for any l. (b) If there are contractions between $\mathcal{O}_3$ and $\mathcal{O}_4$, the diagrams are planar only for $l = 0$. We denote by m_1, m_2 and m_3 the number of fields X, Y and Z (and their conjugates) contracted between the light operators.

$$\mathcal{J}^{(4)}_{q,l,\{m_j\}} \simeq \binom{m_1+m_2}{m_1}\mathcal{M}_4\, k\, u_1^{k_1-m_1}\left(\frac{q+l+1}{\mathcal{L}_1}\right) u_2^{k_2-m_2}\left(\frac{q+l+1}{\mathcal{L}_1}\right)\bar{u}_3^{k_3-m_3}\left(\frac{q+l+1}{\mathcal{L}_2}\right),$$

where q is the site of the heavy operators where $\mathcal{O}_3$

For $l \neq 0$ and $m_1+m_2+m_3 \neq 0$ the diagrams are non-planar, and hence $1/N$ suppressed. Hence, in the planar limit, the four-point function is given by

$$\begin{aligned} G_4(x_1,x_2,x_3,x_4) \;\simeq\; & \frac{1}{N^2}\sum_{l=0}^{J}\sum_{q=0}^{J}\mathcal{G}_{\{0\}}(x_1,x_2,x_3,x_4)\,\mathcal{J}^{(3)}_{q,l,\{0\}}\,\mathcal{J}^{(4)}_{q,l,\{0\}} + \\ & + \frac{1}{N^2}\sum_{m_1=0}^{\min\{j_1,k_1\}}\sum_{m_2=0}^{\min\{j_2,k_2\}}\sum_{m_3=0}^{\min\{j_3,k_3\}}\sum_{q=0}^{J}\delta_{m_1+m_2+m_3\neq 0}\,\mathcal{G}_{\{m_j\}}(x_1,x_2,x_3,x_4)\,\mathcal{J}^{(3)}_{q,0,\{m_j\}}\mathcal{J}^{(4)}_{q,0,\{m_j\}} \end{aligned} \tag{9.24}$$

where

$$\begin{aligned} \mathcal{G}_{\{m_j\}}(x_1,x_2,x_3,x_4) = & \frac{1}{|x_{12}|^{2(J-k_1-k_2-j_3+m)}|x_{13}|^{2(j_3-m_3)}|x_{14}|^{2(k_1+k_2-m_1-m_2)}}\times \\ & \times\frac{1}{|x_{23}|^{2(j_1+j_2-m_1-m_2)}|x_{24}|^{2(k_3-m_3)}|x_{34}|^{2m}}\,. \end{aligned} \tag{9.25}$$

The first term takes into account the contribution of the diagrams for which $\{m_1,m_2,m_3\} = \{0,0,0\}$ and any l. The second term corresponds to the diagrams with $l=0$ and $m_1+m_2+m_3 \neq 0$. Taking the continuum limit of this expression in a similar way as was done before, we obtain

$$\begin{aligned} & G_4(x_1,x_2,x_3,x_4) \simeq \\ & \frac{1}{N^2}\,\mathcal{G}_{\{0\}}(x_1,x_2,x_3,x_4)\,\mathcal{M}_3\mathcal{M}_4\int_0^{2\pi}J\frac{d\sigma}{2\pi}\bar{u}_1^{j_1}(\sigma)\bar{u}_2^{j_2}(\sigma)u_3^{j_3}(\sigma)\int_0^{2\pi}J\frac{d\sigma'}{2\pi}u_1^{k_1}(\sigma')u_2^{k_2}(\sigma')\bar{u}_3^{k_3}(\sigma') + \\ & + \frac{1}{N^2}\sum_{m_1=0}^{\min\{j_1,k_1\}}\sum_{m_2=0}^{\min\{j_2,k_2\}}\sum_{m_3=0}^{\min\{j_3,k_3\}}\delta_{m_1+m_2+m_3\neq 0}\,\mathcal{G}_{\{m_j\}}(x_1,x_2,x_3,x_4)\binom{m_1+m_2}{m_1}^2\mathcal{M}_3\mathcal{M}_4\times \\ & \qquad\times\int_0^{2\pi}J\frac{d\sigma}{2\pi}\bar{u}_1^{j_1-m_1}(\sigma)\,\bar{u}_2^{j_2-m_2}(\sigma)\,u_3^{j_3-m_3}(\sigma)\,u_1^{k_1-m_1}(\sigma)\,u_2^{k_2-m_2}(\sigma)\,\bar{u}_3^{k_3-m_3}(\sigma)\,. \end{aligned} \tag{9.26}$$

The first term corresponds to the case of figure 6.2a and is again the strong coupling result (7.31), see also (9.24). The second term corresponds to figure 6.2b and is suppressed by $1/J$ compared to the first one. The holographic description of the process described by this second term is clear. In this case there is only a single light BPS operator being integrated over the worldsheet defined by the large classical states, see figure 9.4. This is why this process is supressed by $1/J$ with respect to the one shown in (7.4), where there are two

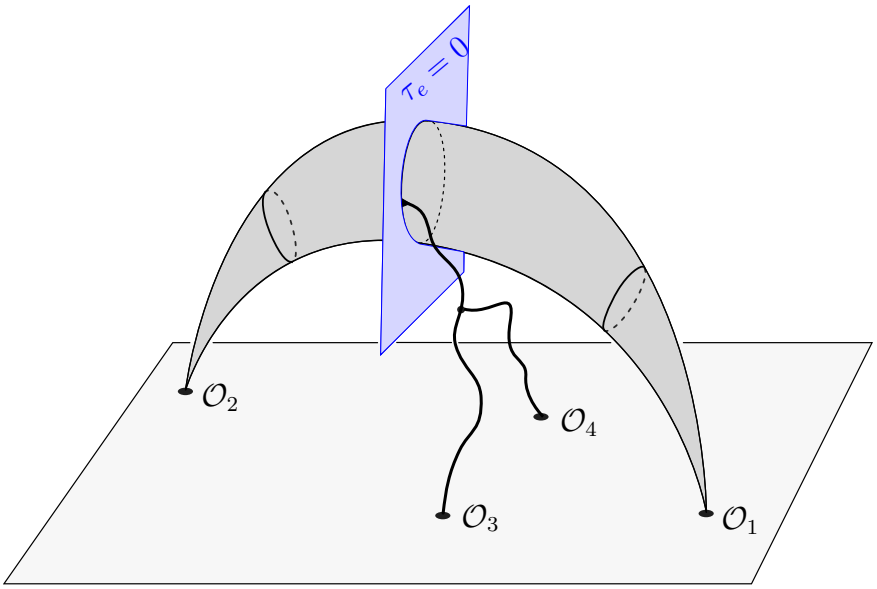

Figure 9.4: Although this is a tree-level diagram, it is suppressed by $1/J$ with respect to the case of figure 7.4 since in this case only one integration over the worldsheet is performed. This is analogous to the weak coupling configuration of figures 6.2b or 9.3b.

integrations over the worldsheet. This light operator then decays into the two the final light BPS operators $\mathcal{O}_3$ and $\mathcal{O}_4$. It would be very interesting to compare the second term in (9.26) with the result of a strong coupling computation of the tree-level four-point function of figure 9.4 and see if a match occurs for them.

Chapter 10

The Issue of Back-reaction

In the previous two chapters, we performed the weak/strong coupling match for correlation functions in the classical limit by noticing that, at weak coupling, $\mathcal{O}_1 \simeq \bar{\mathcal{O}}_2$ corresponds to putting the extra roots of $\mathcal{O}_1$ on the already existing cuts of $\mathcal{O}_2$. We will now examine other options for the positions of the extra roots and see that they indeed give different results when comparing weak and strong coupling results.

10.1 Deforming a classical state

As explained in previous chapters, eigenstates of the one-loop Hamiltonian are labeled by a set of Bethe roots u_j. States that describe a classical solution correspond to configurations of Bethe roots like the one shown in figure 7.1, where the roots are forming some dense cuts in the complex plane. Recall that in our general setups for three- and four-point functions, see figures 5.1 and 6.1, the state $\mathcal{O}_2$ had in general a smaller number of Bethe roots than the state $\mathcal{O}_1$. When performing the numerical weak/strong coupling match for $C_{123}^{\bullet\bullet\circ}$ and $C_{1234}^{\bullet\bullet\circ\circ}$ in chapter 8, we had to decide where to put the extra roots of $\mathcal{O}_1$ with respect to those of $\mathcal{O}_2$. We chose to put them on the already existing classical cuts formed by the latter. As anticipated then, it turns out that this is not the unique possibility to deform a classical state. Indeed, there are in fact three natural options when it comes to adding extra roots to a classical configuration (these are depicted in figure 10.1).

(A) One option is to put the extra roots at infinity (i.e. with zero momenta). This corresponds to acting with a global symmetry generator on the classical configuration, see e.g. [112, 81]. In order to put n extra roots at infinity, we simply consider the $\mathcal{O}_1$ spin chain state to be obtained by acting on the $\bar{\mathcal{O}}_2$ state n times with the lowering operator S^-. This is the global symmetry operator which converts a Z field into an X field.

(B) Another option is to add roots at finite values outside the existing classical cuts. Putting roots outside the cuts at finite values can be interpreted as considering quantum fluctuations around the classical solution [118, 119, 120].

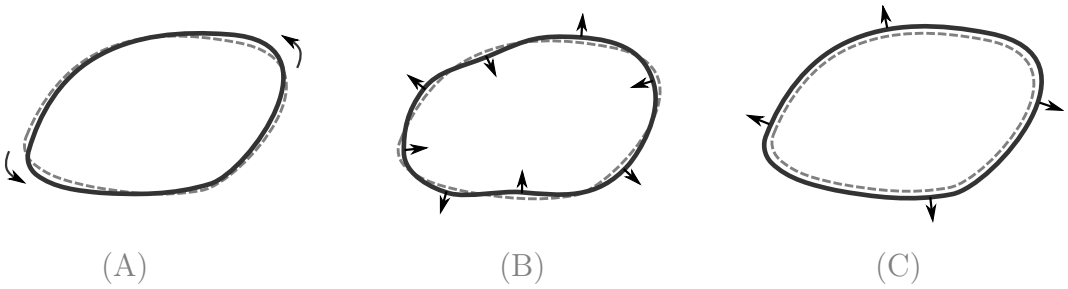

Figure 10.1: Three different types of deformations of a classical state: (A) A global symmetry transformation. (B) A quantum fluctuation. (C) A fluctuation in an already existing cut (i.e. adding a "zero mode").

(C) The last option is to add more roots to the classical cuts which already exist. The number of roots on each of these classical cuts corresponds to the action variables of the classical solution [121]. Hence adding roots to already open cuts leads to a new classical state with slightly larger magnitude for the same excited action variables.

Naively, it might seem like it does not matter where we add the extra roots and all of these options should correspond to $\mathcal{O}_1 \simeq \bar{\mathcal{O}}_2$. As we saw explicitly in chapter 8, this is *not* the case. There is a sense in which only option (C) corresponds to $\mathcal{O}_1 \simeq \bar{\mathcal{O}}_2$. In the present chapter, we discuss numerical and analytical results concerning the other options (A) and (B). We refer to the study of these other possibilities as the issue of *back-reaction*. While we will focus our discussion on the three-point functions $C^{\bullet\bullet\circ}_{123}$, the arguments presented in this chapter should also be valid for four-point functions of the type $C^{\bullet\bullet\circ\circ}_{1234}$.[55]

10.2 Back-reaction numerically

In this section we begin our study of back-reaction. We will start by a simple analytical example and then provide some numerics to gain intuition about the more general picture. We will again use the folded string introduced in chapter 7 as our toy model to obtain numerical data. A general analytical discussion is presented in the next section.

Let us consider a specific example where $C^{\bullet\bullet\circ}_{123}$ can be computed exactly, which we will use to draw some general conclusions about back-reaction. The case in mind is

$$\mathcal{O}_3 = \mathrm{Tr}\left(Z\bar{X}\right)$$

and for simplicity, we take $\mathcal{O}_1$ and $\mathcal{O}_2$ to be in the $SU(2)$ sector. The point is that the Wick contraction of $\mathcal{O}_3$ with $\mathcal{O}_1$ flips one of the X fields into a Z field and therefore effectively acts as S^+. Now suppose we take $\mathcal{O}_1$ to be a Bethe eigenstate. Since Bethe eigenstates are highest weight states, they are annihilated by S^+, so $C^{\bullet\bullet\circ}_{123} = 0$.

[55] In fact, numerical evidence to support this claim was given in [41], but we chose not to include it in this thesis for presentation purposes.

Now suppose that, instead, we take

$$\mathcal{O}_1 = \frac{1}{\sqrt{J_3 - J_1 + 2}} \left[S^-, \bar{\mathcal{O}}_2\right]$$

where $\mathcal{O}_2$ is represented by an exact Bethe eigenstate $|\Psi_2\rangle$ and we are again using the notation of (7.20), but restricted to the $SU(2)$ sector (i.e. only Z and X fields). Here S^- flips one Z field into an X and is normalized such that it preserves the *unit* norm of $|\Psi_2\rangle$. We get that[56]

$$C_{123}^{\bullet\bullet\circ} = \sqrt{J_3 - J_1 + 2}\,.$$

On the other hand, the result for three BPS operators (7.21) reduces in this case to

$$C_{123}^{\circ\circ\circ} = \sqrt{J_1(J_3 + 1)}\,.$$

Therefore, we find that in the classical limit:

$$r_{123}^{(\mathrm{A})} = \frac{C_{123}^{\bullet\bullet\circ}}{C_{123}^{\circ\circ\circ}} = \frac{1}{\sqrt{J}} \sqrt{\frac{1 - 2\alpha + 2/J}{\alpha(1 - \alpha + 1/J)}}\,, \tag{10.1}$$

where the superscript (A) indicates that this ratio was obtained when considering the option of placing the extra root of $\mathcal{O}_1$ at infinity. Even in this simple example, we see that the result for the ratio r_{123} is very sensitive to the position of the extra roots. As we saw in chapter 8, in the classical limit, the leading term of the ratio $r_{123}^{(\mathrm{C})}$ was of order one, while here we see that the one for $r_{123}^{(\mathrm{A})}$ is of order $1/\sqrt{J}$.

10.2.1 Numerical results for roots at infinity

Here we study the option (A) from the list above. We consider $\mathcal{O}_3$ to be a BPS operator with $j/2$ scalars $\bar{X}$ and $j/2$ scalars Z for even j. In this case the final operator $\mathcal{O}_1$ and $\mathcal{O}_2$ have the same length, but $\mathcal{O}_1$ has $n \equiv j/2$ more Bethe roots than the operator $\mathcal{O}_2$. We consider the situation when the extra n roots are sent to infinity, which means that $\mathcal{O}_1$ is a descendant of $\bar{\mathcal{O}}_2$.

For the simplest case $n = 1$ we computed the result exactly above, see (10.1). This suggests that for general n, the ratio $r_{123}^{(\mathrm{A})}$ should go as

$$r_{123}^{(\mathrm{A})} = \frac{C_{123}^{\bullet\bullet\circ}}{C_{123}^{\circ\circ\circ}} \sim \frac{1}{J^{n/2}}\,. \tag{10.2}$$

[56] $\sqrt{J_3 - J_1 + 2}\, C_{123}^{\bullet\bullet\circ} = \langle\Psi_2|S^+S^-|\Psi_2\rangle = \langle\Psi_2|\,[S^+, S^-]\,|\Psi_2\rangle = \langle\Psi_2|S_z|\Psi_2\rangle = (J_3 - J_1 + 2)$.

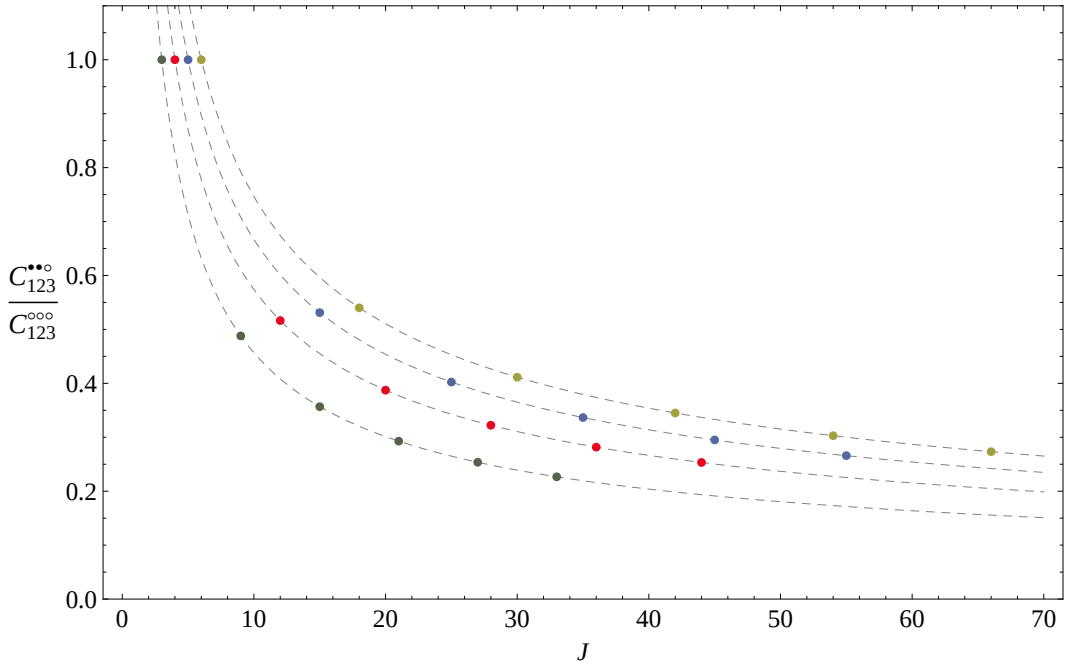

Figure 10.2: The bullets correspond to the numerical data for the ratio $r^{(\mathrm{A})}_{123} = C^{\bullet\bullet\circ}_{123}/C^{\circ\circ\circ}_{123}$ computed for the case (A), i.e. by adding extra roots at infinity, against the analytical prediction (10.1) (dashed gray lines) for different values of the filling fraction of operator $\mathcal{O}_1$: $\alpha = 1/3, 1/4, 1/5, 1/6$, from bottom to top.

Indeed the numerics for the case $n = 2$ and $\alpha = 1/5$ give

J	10	20	30	40	50	60
$r^{(\mathrm{A})}_{123}$	1	0.27036118	0.14195150	0.092991262	0.068076848	0.053258866

Fitting this data as $J^a \sum_{i=0}^{4} \frac{b_i}{J^i}$ we obtain $a = -1.01$, which is indeed consistent with eq.(10.2).[57] Notice that for exactly the same $\mathcal{O}_2$ and $\mathcal{O}_3$, but in the situation when all roots of $\mathcal{O}_1$ belong to the big classical cuts of the roots of $\mathcal{O}_2$, we obtained a finite value $r^{(\mathrm{C})}_{123} = 0.8887595$ by fitting the numerical data to infinite length (see table 8.1). Thus we see that back-reaction is very important in this case and that adding roots at infinity gives a completely different result compared to the option (C) studied in chapter 8.

In the next section we give a simple reason for this behavior and draw a general criteria for back-reaction.

10.2.2 Numerical results for finite roots

We now want to study numerically option (B) with $n = 2$. To keep the zero momentum condition in $\mathcal{O}_1$, the two extra finite roots that we add should have opposite mode numbers

[57] We also considered cases with more Bethe roots at infinity and found again evidence for (10.2) although the precision decreases substantially as we increase the number n of Bethe roots sent to infinity.

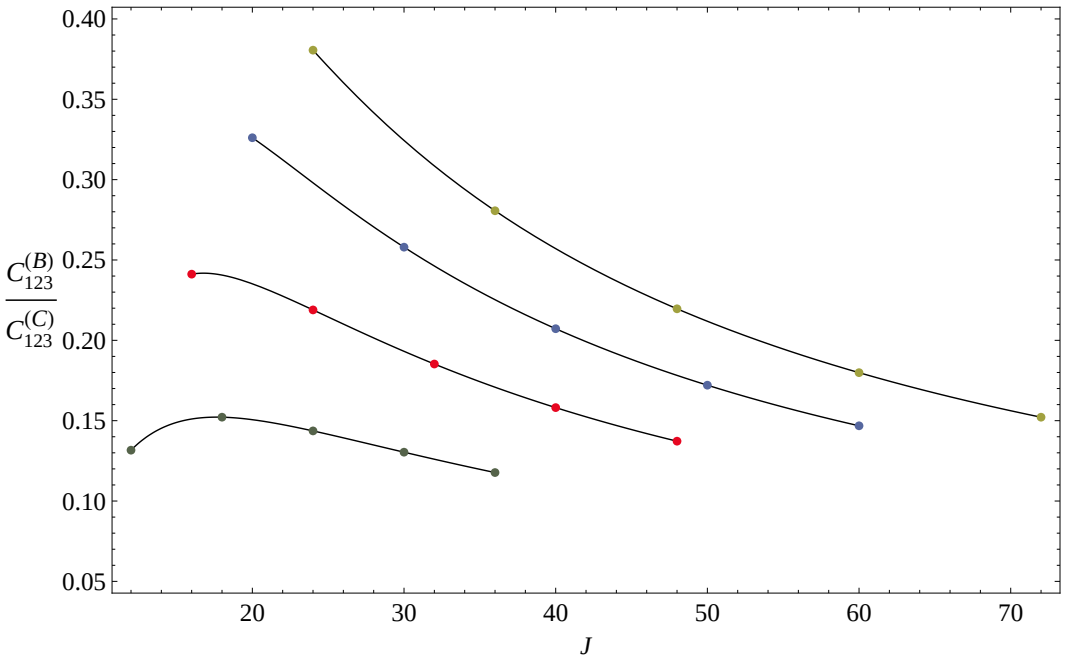

Figure 10.3: Numerical data for the three-point $C_{123}^{\bullet\bullet\circ}$ function with operator $\mathcal{O}_1$ deformed by adding two finite roots with mode numbers $k = \pm 3$ (option (B)) divided by the same three-point function with operator $\mathcal{O}_1$ deformed by adding two roots to the already existing cuts with mode numbers $k = \pm 1$ (option (C)) for different filling fractions of operator $\mathcal{O}_1$: $\alpha = 1/3, 1/4, 1/5, 1/6$ (from bottom to top). We see that the ratio does not go to one. In other words, back-reaction is relevant.

k and $-k$. The case $k = 1$ is the one that we considered in chapter 8: it amounts to adding more roots to the already open classical cuts. The cases $k = 2, 3, \ldots$ correspond to option (B) from the list above.

The main question is whether we get the same result for $C_{123}^{\bullet\bullet\circ}$ when adding the two extra roots with mode number $k \neq 1$ compared to the case $k = 1$ considered previously. To answer this question we use again the analytic results of chapter 5 and evaluate these expressions numerically for both cases. The results are shown in figure 10.3. We conclude that again the answer is no and that the result differ considerably. In other words, back-reaction is also relevant when adding extra roots at finite values outside the classical cuts of $\mathcal{O}_2$.

10.3 General criteria for back-reaction

In this section we will give a qualitative explanation for the dependence of the result on the type of modification of the state $\mathcal{O}_1$ with respect to the state $\bar{\mathcal{O}}_2$, which is necessary for R-charge conservation. As we discussed above there are three options (see figure 10.1). One can think about the case (A) as a limit of (B) when the mode number k of the extra roots goes to zero. In this section we focus therefore on cases (B) versus case (C).

To understand better the difference between these two cases, we first consider the example

of a free massless scalar field $\phi(\sigma,\tau)$ on the cylinder. A general classical solution is of the form:[58]

$$\phi(\sigma,\tau)=\sum_n A_n\cos\left(n(\sigma+\tau)+\phi_n\right)\ .$$

The analog of the finite gap solution would be the situation when the sum has only finitely many terms. The amplitude A_n is related to the number of excitations inside a cut through a Bohr-Sommerfeld quantization condition, which in the present case coincides of course with the oscillator $nA_n^2=cN_n$ where $c\sim\hbar$ is a small constant and N_n is the number of excitations at mode number n called *filling number*. We see that

$$A_n\simeq\sqrt{\frac{N_n}{n}}\ . \tag{10.3}$$

Suppose we start with an unperturbed solution consisting of a single large cut

$$\phi_0(\sigma,0)=A\cos(n\sigma)\ .$$

There are two different types of perturbations we can introduce. One is by adding a small number of excitations, l, to the existing large cut

$$\phi^{(\mathrm{C})}(\sigma,0)=\left[A+\delta A^{(\mathrm{C})}\right]\cos(n\sigma)\ .$$

The other, is by adding the small number of excitations l at a different mode number $k\neq n$

$$\phi^{(\mathrm{B})}(\sigma,0)=A\cos(n\sigma)+\delta A^{(\mathrm{B})}\cos(k\sigma)\ .$$

These perturbations obviously correspond to the options (C) and (B) introduced in the previous section. Since the amplitude is proportional to the square root of the filling number (10.3), for the case $N\gg l$ we get

$$\delta A^{(\mathrm{C})}\simeq A\frac{l}{2N}\ \ ,\qquad \delta A^{(\mathrm{B})}\simeq\sqrt{\frac{l}{k}}\simeq A\sqrt{\frac{nl}{Nk}}\,. \tag{10.4}$$

We see that in these cases the scaling of the correction to the wave function is very different.

Having understood this let us turn back to our calculation of the three-point function at weak coupling and see how the difference between the two behaviors in (10.4) really matters. The only difference between the quasi-classical approximation for the Bethe eigenstates and the free field example is that now the specific form of the solutions are more complicated and when we add new roots, the old roots get a small correction. These differences are irrelevant for the behavior (10.4).

In the large J limit, the quasi-classical approximation is valid and we can repeat our previous calculation of the three-point function as prescribed in chapter 9. For simplicity we

[58] For simplicity, we only consider the left-moving solutions.

consider the case $j_3 = j_1 + j_2$ in the setup (7.20) so that the lengths $\mathcal{L}_1 = \mathcal{L}_2$ are equal and we do not have to worry about the $U(1)$ gauge transformations (9.11). This time however, let us be a bit more careful about back-reaction. Namely we assume that the coherent states for $\mathcal{O}_1$ and $\mathcal{O}_2$ are a bit different and are parametrized by two different functions $\mathbf{u}_2(\sigma) \equiv \bar{\mathbf{u}}(\sigma)$ and $\mathbf{u}_1(\sigma) \equiv \mathbf{u}(\sigma) + \delta\mathbf{u}(\sigma)$. Since $\mathbf{u}_1$ is a unit vector, we have

$$\bar{\mathbf{u}} \cdot \delta\mathbf{u} + \delta\bar{\mathbf{u}} \cdot \mathbf{u} = -\delta\bar{\mathbf{u}} \cdot \delta\mathbf{u} \,. \tag{10.5}$$

An important step in the previous calculation of chapter 9 was the proof that the direct Wick contractions between $\mathcal{O}_1$ and $\mathcal{O}_2$ (9.8) are trivial. The overlap of the two coherent wave functions is equal to

$$\mathcal{I} \equiv \exp\left(\frac{J}{2\pi}\int d\sigma \log(1 + \bar{\mathbf{u}} \cdot \delta\mathbf{u})\right) \simeq \exp\left(\frac{J}{2\pi}\int d\sigma \left[\bar{\mathbf{u}} \cdot \delta\mathbf{u} - \frac{1}{2}(\bar{\mathbf{u}} \cdot \delta\mathbf{u})^2\right]\right) . \tag{10.6}$$

As we are only interested in the absolute value of the three-point function, we only need to consider the real part of the integrand. The real part of the first term in the integrand is precisely the left-hand side of (10.5). Thus we see that the real part of the integrand is of order $\sim J\|\delta\mathbf{u}\|^2$.

For the type of correction (C) where the roots are added to the big open cuts, we found that $\delta\mathbf{u}^{(C)} \sim l/J$. In that case, the integrand goes as l^2/J and the overlap $\mathcal{I}$ is indeed 1. That lead us to the main result (9.13). For the second type of corrections where the roots are not added to the big cuts, we found that $\delta\mathbf{u}^{(B)} \sim \sqrt{l/J}$. In that case we then get

$$|\mathcal{I}| \simeq e^{-cl} \tag{10.7}$$

and thus for this case we have an additional exponential suppression for large l (the coefficient must be negative since the overlap cannot exceed 1). Furthermore, in this case, (10.7) is not even the only correction. This is indeed the case according to what we found from our numerics. That is, for small l's we found an order 1 correction compared to case (C) studied in chapter 8.

Note that if we try to pass to the limit $k \to 0$ corresponding to the case (A), the wave function correction goes to infinity as one can easily see from eq.(10.4). This indicates that when adding roots at infinity, the suppression should be even stronger in agreement with our finding (10.2).

We end this section by noting that at strong coupling, the classical operators are described by the same coherent states. Our findings indicate that also at strong coupling, the three-point function of two large and one small operators is dominated by the overlap of the wave functions. As such, we expect the above criteria for back-reaction to apply.

Part V

Beyond the $SU(2)$ sector and Conclusions

Chapter 11

Beyond the $SU(2)$ sector

In order to compute correlation functions of general single-trace operators in $\mathcal{N}=4$ SYM using integrability, we need to generalize some of the techniques presented in part II of this thesis. In this chapter we provide some tools that will be useful to go beyond the $SU(2)$ sector of the theory. The contents of this chapter slightly deviate from the logical flow of the previous ones. Hence, the reader can first read to the conclusions and then come back to this chapter.

11.1 Coordinate nested Bethe ansatz for $SU(K)$ and $SU(K-J|J)$ spin chains

First, let us explain the procedure to construct the Bethe states of a spin chain with a general Lie (super) group in the coordinate basis. In particular, we will give a detailed account on how to construct $SU(K)$ and $SU(K-J|J)$ spin chains states. These cases will allow us to introduce the concept of *nested wave function*. The simplest example, namely the $SU(2)$ spin chain, was already considered in chapter 3. For convenience, let us recall that in the coordinate basis, a generic N-magnon $SU(2)$ Bethe state is given by

$$|\Psi\rangle_{\text{co}} = \sum_{1\leq n_1<n_2<\cdots<n_N\leq L} \psi\left(n_1,\ldots,n_N\right)|n_1,\ldots,n_N\rangle\,, \tag{11.1}$$

with Bethe wave function

$$\psi\left(n_1,\ldots,n_N\right) = \sum_P A(P)\prod_{j=1}^{N}\left(\frac{u_{P_j}+\frac{i}{2}}{u_{P_j}-\frac{i}{2}}\right)^{n_j}, \tag{11.2}$$

where the sum runs over all $N!$ permutations P of $(1,2,\ldots,N)$. The plane wave coefficients are such that they obey the following relation $\frac{A(\ldots,j,i,\ldots)}{A(\ldots,i,j,\ldots)} = S(u_j,u_i)$, where $S(u_j,u_i)$ is the $SU(2)$ S-matrix introduced in (3.15). The states Ψ_{co} diagonalize the $SU(2)$ Hamiltonian (3.2). The goal of this chapter is to generalize this construction to higher rank groups. As

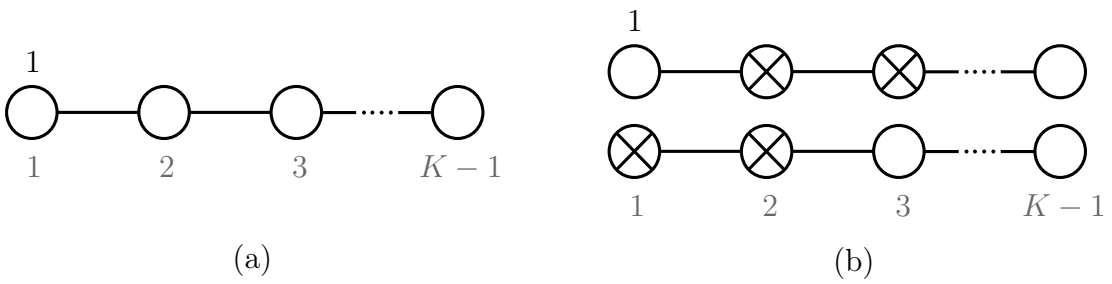

Figure 11.1: Excitations at a spin chain site are created by exciting nodes in the corresponding Dynkin diagram. (a) $SU(K)$ Dynkin diagram. There are $K-1$ nodes, labeled by the lower (gray) numbers, while the upper number 1 is the Dynkin label, indicating the massive, momentum-carrying node. (b) Two possible choices of Dynkin diagram for a given $SU(K-J|J)$ spin chain. Both are related by a fermionic duality, which in this case was applied to the second node (see [122] for details). In this case there are also $K-1$ nodes.

usual, we choose to write our formulas in terms of the rapidities u introduced in (3.14) instead of the momenta.

Let us consider an $SU(K)$ or $SU(K-J|J)$ spin chain of length L. In this case, the Hamiltonian that we have to diagonalize is

$$\hat{H} = \frac{\lambda}{8\pi^2} \sum_{n=1}^{L} \left(\mathbb{I}_{n,n+1} - \mathbb{SP}_{n,n+1} \right) , \tag{11.3}$$

where $\mathbb{SP}_{n,n+1}$ is the super permutation operator. The action of this operator is analogous to the normal permutation operator $\mathbb{P}_{n,n+1}$, except that it picks a minus sign when exchanging two fermions at positions n and $n+1$. Before explaining how to diagonalize this Hamiltonian, let us recall what is the Hilbert space of the spin chains that we are considering.

At each site in the chain there is a spin with one of K different polarizations. The Dynkin diagrams of the corresponding algebras provide a convenient way to see what type of excitations can be created at a given spin chain site. In the fundamental representation of the group, the $SU(K)$ Dynkin diagram is the one shown in figure 11.1a. In the case of super groups, there is no unique Dynkin diagram and all possible choices are related by so-called *fermionic dualities* [122] (we review these in appendix D). Figure 11.1b shows two possible choices for a given $SU(K-J|J)$ spin chain. In all these cases, there are a total of r nodes in the diagram, with $r = K-1$ being the rank of the group. The construction that we are about to present is valid for both types of chains.[59]

The eigenstates of the Hamiltonian (11.3) are

$$|\Psi\rangle_{\text{co}} = \sum_{\text{positions}} \psi \, |\{n_{1,j}\}, \{n_{2,j}\}, \ldots, \{n_{r,j}\}\rangle \, , \tag{11.4}$$

where ψ is the spin chain wave function and the sum runs over the different allowed positions

[59] In fact, it can also be used for $SL(2)$ spin chains, which we will brielfy review in section 11.3.

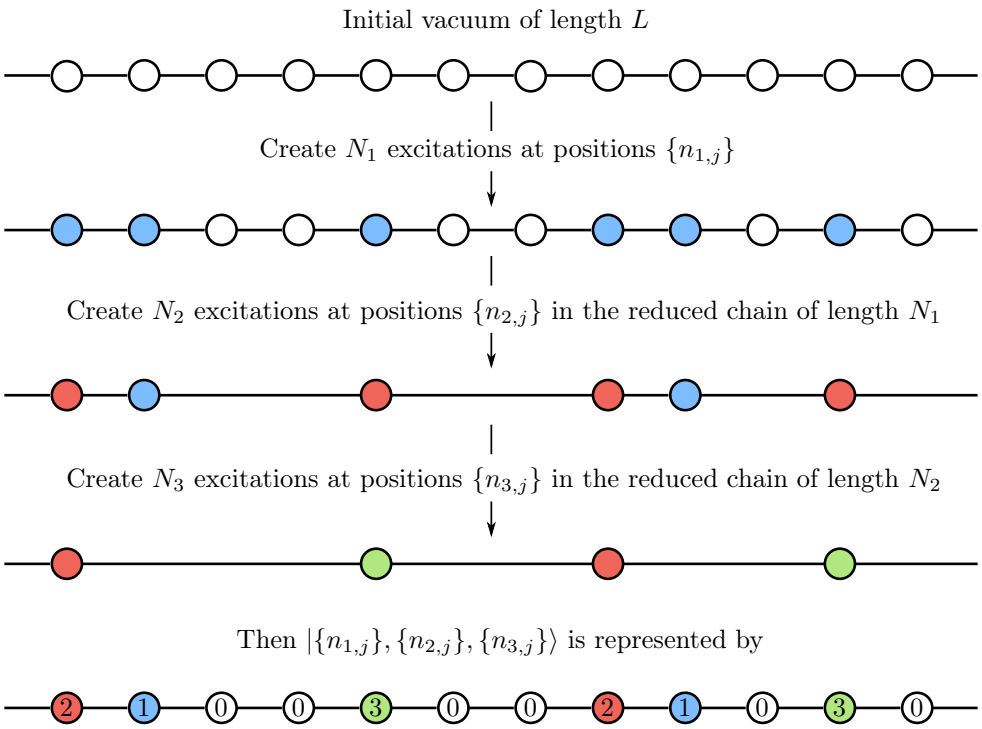

Figure 11.2: Nesting procedure for the case of $SU(4)$ or $SU(K-J|J)$ with $K=4$, $L=12$, $\{n_{1,j}\}=\{1,2,5,8,9,11\}$, $\{n_{2,j}\}=\{1,3,4,6\}$ and $\{n_{3,j}\}=\{2,4\}$. For $a=2,3$, we have N_a excitations at positions $\{n_{a,j}\}$ in a reduced spin chain of length N_{a-1}.

of the excitations described above. We will now proceed to explain how to construct each of the terms appearing in (11.4). First, let us explain how to construct the ket on the r.h.s. and give explicitly the limits of summation in this formula.

11.1.1 Nested ket

The ket $|\{n_{1,j}\},\{n_{2,j}\},\ldots,\{n_{r,j}\}\rangle$ is obtained by exciting N_a times node a in one of the Dynkin diagrams of figure 11.1 and putting the corresponding excitations at the following positions:

$$\begin{aligned} &1\leq n_{1,1}<\cdots<n_{1,N_1}\leq L\,,\\ &1\leq n_{a,1}<\cdots<n_{a,N_a}\leq N_{a-1},\quad \text{for } 2\leq a\leq r\,. \end{aligned} \tag{11.5}$$

These are the limits of the sum appearing in (11.4). This procedure is called *nesting* and is illustrated in figure 11.2 for the case of $SU(4)$ or $SU(K-J|J)$ with $K=4$, $L=12$, $\{n_{1,j}\}=\{1,2,5,8,9,11\}$, $\{n_{2,j}\}=\{1,3,4,6\}$ and $\{n_{3,j}\}=\{2,4\}$. In this case the resulting ket is

$$|\{n_{1,j}\},\{n_{2,j}\},\ldots,\{n_{r,j}\}\rangle=|2\,1\,0\,0\,3\,0\,0\,2\,1\,0\,3\,0\rangle,$$

where the numbers a on the right-hand side denote an excitation of node a in the Dynkin diagram, with 0 being an original vacuum site. It is then clear that for generic $SU(K)$ or $SU(K-J|J)$ spin chains, we have N_1 excitations at positions $\{n_{1,j}\}$ in the original spin chain of length L, while for $2 \leq a \leq r$, we have N_a excitations at positions $\{n_{a,j}\}$ in a reduced spin chain of length N_{a-1}. This is precisely what the limits (11.5) tell us. Moreover, we will denote by $\{u_{a,j}\}$ the rapidities of the excitations of node a, with $j = 1, \ldots, N_a$.

11.1.2 Nested wave function

It should be clear from the nesting procedure explained above that the wave function ψ appearing in (11.4) will not only depend on the first-node rapidities and positions, $\{u_{1,j}\}$ and $\{n_{1,j}\}$, but must also contain information about the rapidities and positions of the excitations of the other nodes. This can be made precise using the *nested Bethe ansatz* [123], which introduces the concept of *nested wave function*: the spin chain wave function ψ is written in terms of wave functions ψ_a, for $2 \leq a \leq r$, associated with the different nodes in the Dynkin diagram. The dependence of these wave functions on the positions and rapidities is such that

$$\psi_a\left(\{n_{a,j}\}, \{n_{a+1,j}\}, \ldots, \{n_{r,j}\}; \{u_{a-1,j}\}, \{u_{a,j}\}, \{u_{a+1,j}\}, \ldots, \{u_{r,j}\}\right) .$$

However, for notational convenience, we will *not* write these arguments explicitly. Instead, we will only write the dependence of the wave functions on the permutation of the rapidities of the previous node. More explicitly, the wave function appearing in (11.4) is

$$\psi = \sum_{P_1} A_1(P_1) \prod_{j=1}^{N_1} \left(\frac{u_{1,P_{1,j}} + \frac{i}{2}}{u_{1,P_{1,j}} - \frac{i}{2}} \right)^{n_{1,j}} \psi_2(P_1) \,, \tag{11.6}$$

while for $2 \leq a \leq r$, the nested wave functions are given by

$$\psi_a(P_{a-1}) = \sum_{P_a} A_a(P_a) \prod_{j=1}^{N_a} \prod_{k=1}^{n_{a,j}} \frac{\left(u_{a,P_{a,j}} - u_{a-1,P_{a-1,k}} - M_{a-1,a}\,\frac{i}{2}\right)^{\delta_{k \neq n_{a,j}}}}{u_{a,P_{a,j}} - u_{a-1,P_{a-1,k}} + M_{a-1,a}\,\frac{i}{2}} \; \psi_{a+1}(P_a) \,, \tag{11.7}$$

with $\psi_{r+1}(P_r) = 1$ and $M_{a,b}$ being the Cartan matrix of the Lie (super) group.[60] In these formulas, P_a denotes the set of all permutations of $(1, \ldots, N_a)$. Thus, $P_{a,j}$ simply denotes the jth element of P_a. Spin chain states of the form (11.4), whose wave functions are given by (11.6), are referred to as *Bethe states*.

The terms in the product over k in (11.7) might seem strange at first, so, let us explain the

[60] For example, in the case of $SU(K)$, the Cartan matrix corresponding to the Dynkin diagram of figure 11.1a is a matrix of size $(K-1) \times (K-1)$:

$$M_{a,b} = 2\delta_{a,b} - \delta_{a-1,b} - \delta_{a+1,b} \,. \tag{11.8}$$

For super groups, the choice of Dynkin diagram, and hence of Cartan matrix, is not unique. See appendix D to learn how to write the Cartan matrices for the the Dynkin diagrams of figure 11.1b.

physical picture behind them. Recall that the excitations with rapidities $\{u_{a,j}\}$ are placed at positions $\{n_{a,j}\}$ in a reduced spin chain formed by the excitations $\{u_{a-1,j}\}$. Thus, the product over $k = 1, \dots, n_{a,j} - 1$ is interpreted as the cost of moving a u_a excitation in the new vacuum formed by the u_{a-1} excitations. The last term $k = n_{a,j}$ (for which the numerator in (11.7) is simply one) corresponds to the cost of placing the u_a excitation at its final position in the reduced chain.

Our choice of normalization is such that at each level the plane wave coefficient for which no rapidities have been exchanged is set to one, i.e. $A_a(1, \dots, N_a) = 1$. Moreover, all other plane wave coefficients A_a can be uniquely determined as they obey the following relation

$$\frac{A_a(\dots, k, j, \dots)}{A_a(\dots, j, k, \dots)} = S_a(u_{a,k}, u_{a,j}) \,, \tag{11.9}$$

where $S_a(u_{a,k}, u_{a,j})$ is the S-matrix at node a, which is explicitly given by

$$S_a(u_{a,k}, u_{a,j}) = (-1)^{\delta_{M_{a,a},0}} \, \frac{u_{a,k} - u_{a,j} + M_{a,a} \, \frac{i}{2}}{u_{a,k} - u_{a,j} - M_{a,a} \, \frac{i}{2}} \,. \tag{11.10}$$

Having described the exact form of the nested ket and wave function appearing in the state (11.4), we can check in Mathematica that the latter is indeed an eigenstate of the Hamiltonian (11.3), such that $\hat{H} \, |\Psi\rangle_{\text{co}} = E |\Psi\rangle_{\text{co}}$, with eigenvalue

$$E = \frac{\lambda}{8\pi^2} \sum_{j=1}^{N_1} \frac{1}{u_{1,j}^2 + \frac{1}{4}} \,. \tag{11.11}$$

Here $u_{1,j}$ are the rapidities of the momentum-carrying node. We performed this check for several $SU(K)$ and $SU(K-J|J)$ spin chains.

Finally, by imposing periodicity of the wave function ψ, we obtain the nested Bethe equations, which can be written in the following compact form [124]

$$\left(\frac{u_{a,j} + V_a \, \frac{i}{2}}{u_{a,j} - V_a \, \frac{i}{2}} \right)^L = \prod_{b=1}^{r} \prod_{\substack{k=1 \\ (a,j) \neq (b,k)}}^{N_b} \frac{u_{a,j} - u_{b,k} + M_{a,b} \, \frac{i}{2}}{u_{a,j} - u_{b,k} - M_{a,b} \, \frac{i}{2}} \,, \tag{11.12}$$

where V_a are the Dynkin labels (for all the cases in this section, we have $V_a = \delta_{a,1}$). If all rapidities satisfy these equations, then the state (11.4) is a *Bethe eigenstate*.

An example: the $SU(3)$ spin chain

In order to be as pedagogical as possible, let us show how to construct the nested wave function for the $SU(3)$ spin chain using the procedure outlined above. Since the rank of the group is $r = 2$ with the Cartan matrix given by (11.8), the Bethe wave function in this case

reads

$$\psi = \sum_{P_1} A_1(P_1) \prod_{j=1}^{N_1} \left(\frac{u_{1,P_{1,j}} + \frac{i}{2}}{u_{1,P_{1,j}} - \frac{i}{2}} \right)^{n_{1,j}} \psi_2(P_1)\,,$$

where

$$\psi_2(P_1) = \sum_{P_2} A_2(P_2) \prod_{j=1}^{N_2} \prod_{k=1}^{n_{2,j}} \frac{\left(u_{2,P_{2,j}} - u_{1,P_{1,k}} + \frac{i}{2}\right)^{\delta_{b\neq n_{2,j}}}}{u_{2,P_{2,j}} - u_{1,P_{1,k}} - \frac{i}{2}}$$

and the coefficients $A_1(P_1)$ and $A_2(P_2)$ obey (11.10). Let us explicitly write out the first terms in both expressions above. We have

$$\begin{aligned}\psi = &\left(\frac{u_{1,1} + \frac{i}{2}}{u_{1,1} - \frac{i}{2}} \right)^{n_{1,1}} \left(\frac{u_{1,2} + \frac{i}{2}}{u_{1,2} - \frac{i}{2}} \right)^{n_{1,2}} \dots \left(\frac{u_{1,N_1} + \frac{i}{2}}{u_{1,N_1} - \frac{i}{2}} \right)^{n_{1,N_1}} \psi_2(1,2,\dots,N_1)\,, \\ &+ \frac{u_{1,2} - u_{1,1} + i}{u_{1,2} - u_{1,1} - i} \left(\frac{u_{1,2} + \frac{i}{2}}{u_{1,2} - \frac{i}{2}} \right)^{n_{1,1}} \left(\frac{u_{1,1} + \frac{i}{2}}{u_{1,1} - \frac{i}{2}} \right)^{n_{1,2}} \dots \left(\frac{u_{1,N_1} + \frac{i}{2}}{u_{1,N_1} - \frac{i}{2}} \right)^{n_{1,N_1}} \psi_2(2,1,\dots,N_1) + \dots\end{aligned}$$

$$\begin{aligned}\psi_2(P_1) = &\prod_{k=1}^{n_{2,1}} \frac{\left(u_{2,1} - u_{1,P_{1,k}} + \frac{i}{2}\right)^{\delta_{k\neq n_{2,1}}}}{u_{2,1} - u_{1,P_{1,k}} - \frac{i}{2}} \prod_{k=1}^{n_{2,2}} \frac{\left(u_{2,2} - u_{1,P_{1,k}} + \frac{i}{2}\right)^{\delta_{k\neq n_{2,2}}}}{u_{2,2} - u_{1,P_{1,k}} - \frac{i}{2}} \dots \\ &+ \frac{u_{2,2} - u_{2,1} + i}{u_{2,2} - u_{2,1} - i} \prod_{k=1}^{n_{2,1}} \frac{\left(u_{2,2} - u_{1,P_{1,k}} + \frac{i}{2}\right)^{\delta_{k\neq n_{2,1}}}}{u_{2,2} - u_{1,P_{1,k}} - \frac{i}{2}} \prod_{k=1}^{n_{2,2}} \frac{\left(u_{2,1} - u_{1,P_{1,k}} + \frac{i}{2}\right)^{\delta_{k\neq n_{2,2}}}}{u_{2,1} - u_{1,P_{1,k}} - \frac{i}{2}} \dots + \dots\end{aligned}$$

Writing out explicitly the dependence of the wave function on the positions of the excitations, we can impose the periodicity conditions at each level of the nesting as

$$\begin{aligned}\psi(\{n_{1,1}, n_{1,2}, \dots, n_{1,N_1}\}, \{n_{2,j} + 1\}) &= \psi(\{n_{1,2}, n_{1,3}, \dots, n_{1,1} + L\}, \{n_{2,j}\})\,, \\ \psi_2(\{n_{2,1}, n_{2,2}, \dots, n_{2,N_2}\}) &= \psi_2(\{n_{2,2}, n_{2,3}, \dots, n_{2,1} + N_1\})\,.\end{aligned}$$

These two conditions lead to the $SU(3)$ Bethe equations

$$\begin{aligned}\left(\frac{u_{1,j} + \frac{i}{2}}{u_{1,j} - \frac{i}{2}} \right)^L &= \prod_{k\neq j}^{N_1} \frac{u_{1,j} - u_{1,k} + i}{u_{1,j} - u_{1,k} - i} \prod_{k=1}^{N_2} \frac{u_{1,j} - u_{2,k} - \frac{i}{2}}{u_{1,j} - u_{2,k} + \frac{i}{2}} \\ 1 &= \prod_{k=1}^{N_1} \frac{u_{2,j} - u_{1,k} - \frac{i}{2}}{u_{2,j} - u_{1,k} + \frac{i}{2}} \prod_{k\neq j}^{N_2} \frac{u_{2,j} - u_{2,k} + i}{u_{2,j} - u_{2,k} - i}\,,\end{aligned} \tag{11.13}$$

which indeed agree with what we obtain using the formula for nested Bethe equations (11.12).

11.2 Norm of Bethe eigenstates

To generalize the results of this thesis to any type of operator in $\mathcal{N} = 4$ SYM, one of the first ingredients that we need is the norm of such operators. In this chapter, we present a formula

to compute the norm of Bethe eigenstates of spin chains with general Lie (super) group.

11.2.1 Norm of Bethe eigenstates for general Lie groups

Let us consider a spin chain of length L with Lie (super) group of rank r with Cartan matrix $M_{a,b}$. The physical space at each site can be either the space where the fundamental representation acts or some other space where a representation with Dynkin label V_a lives. Then, just like in the previous section, each quantum state is parametrized by a set of Bethe roots $\{u_{a,j}\}$, where $a = 1, \dots, r$ refers to the Dynkin node and $j = 1, \dots, N_a$, with N_a being the number of magnons of type a. We will find it useful to introduce some useful notation, which we will use throughout this chapter to write equations in a more compact form. In particular, let us introduce the Baxter polynomials

$$Q_a(u) \equiv \prod_{j=1}^{N_a} (u - u_{a,j})\,. \tag{11.14}$$

With them, the general Bethe equations (11.12) can be written as

$$\left(\frac{u_{a,j} + V_a \frac{i}{2}}{u_{a,j} - V_a \frac{i}{2}}\right)^L = s_a \prod_{b=1}^{r} \frac{Q_b\big(u_{a,j} + M_{a,b}\frac{i}{2}\big)}{Q_b\big(u_{a,j} - M_{a,b}\frac{i}{2}\big)}, \tag{11.15}$$

where $s_a = -1, 1$ if node a is bosonic or fermionic respectively. We can take the logarithm of the Bethe equations and define the following phases

$$\phi_{a,j} \equiv \frac{1}{i} \log \left[s_a \left(\frac{u_{a,j} + V_a \frac{i}{2}}{u_{a,j} - V_a \frac{i}{2}}\right)^L \prod_{b=1}^{r} \frac{Q_b\big(u_{a,j} - M_{a,b}\frac{i}{2}\big)}{Q_b\big(u_{a,j} + M_{a,b}\frac{i}{2}\big)} \right]. \tag{11.16}$$

In the case of $SU(2)$ spin chains, this equation simply reduces to the one introduced in (3.16).

In the coordinate base, the norm of a Bethe eigenstate of the spin chain described above reads:

$$\mathcal{N}_{\text{co}} = \prod_{j=1}^{N_m} \left(u_{m,j}^2 + \frac{1}{4}\right) \left|\det_{I,J} \partial_I \phi_J\right|, \tag{11.17}$$

where m denotes the massive node in the Dynkin diagram and we combined the indices a and j into single indices $I, J = 1, 2, \dots, (N_1 + \cdots + N_r)$.

We checked numerically the validity of formula (11.17) by comparing it to the value obtained from the brute force computation of the norm as

$$\mathcal{N}_{\text{co}} = {}_{\text{co}}\langle \Psi | \Psi \rangle_{\text{co}}\,, \tag{11.18}$$

where $|\Psi\rangle_{\text{co}}$ is constructed using the procedure explained in the previous section. Needless to say, formula (11.17) is far more efficient than (11.18) from a computational point of view.

The former involves the calculation of a determinant of size $(N_1 + \cdots + N_r)$, while the latter involves a sum over $(N_1! \dots N_r!)^2$ plane wave terms for *each* possible configuration of positions $\{n_{1,j}\}$,$\{n_{2,j}\}$,...,$\{n_{r,j}\}$ in (11.18), see (11.5). We performed this check for several types of spin chains, considering different configurations of Bethe roots in each case, always making sure that these probed the interactions at all levels of the nesting. More specifically, we considered the following cases: $SU(2)$, $SU(3)$, $SU(4)$, $SU(1|1)$, $SU(1|2)$, $SU(2|1)$, $SU(1|3)$, $SU(2|2)$ and $SU(3|1)$. The agreement between the two formulas for the norm (11.17) and (11.18) was perfect in all cases. We should note that for each super group we considered two different choices of Dynkin diagram related by a fermionic duality, see figure 11.1.

We now want to show that it is possible to write the non-trivial part of (11.17), i.e. the determinant, in terms of an object related to the transfter matrix $T(u)$. To make our expressions more compact, let us introduce some further notation. Given a function $f(u)$, we will use

$$f^{\pm}(u) \equiv f(u \pm i/2)\,, \qquad f^{[n]}(u) \equiv f(u + i\,n/2)\,. \tag{11.19}$$

For a Lie (super) group of rank r, the transfer matrix $T(u)$ takes the schematic form

$$T(u) = T_1(u) + T_2(u) + \cdots + T_r(u) + T_{r+1}(u)\,, \tag{11.20}$$

where the T_a's are ratios of Baxter polynomials. Also, the T_a corresponding to the massive node in the Dynkin diagram will have the usual term $(u+i/2)^L/(u-i/2)^L$. Our convention when writing the transfer matrix is that the Bethe equations for node a are recovered from the residues of T_a and T_{a+1} at the shifted Bethe roots $u = u_{a,j} + i(1-a)/2$. Now, we can define $\mathcal{T}(u)$ by multiplying $T(u)$ by the product of all Baxter polynomials appearing in the denominators of the building blocks $T_a(u)$. Thus, schematically:

$$\mathcal{T}(u) = \mathcal{T}_1(u) + \mathcal{T}_2(u) + \cdots + \mathcal{T}_r(u) + \mathcal{T}_{r+1}(u)\,. \tag{11.21}$$

The Bethe equations for node a are recovered from

$$e^{i\phi_{a,j}^{[1-a]}} \equiv -\frac{\mathcal{T}_a^{[1-a]}(u_{a,j})}{\mathcal{T}_{a+1}^{[1-a]}(u_{a,j})} = 1\,, \tag{11.22}$$

where the phases $\phi_{a,j}$ are precisely the ones introduced in (11.16).

Moreover, consider two consecutive terms in (11.21) $\mathcal{T}_a(u) + \mathcal{T}_{a+1}(u)$ and let us take the derivative of this with respect to the roots $u_{b,k}$. Using (11.22), we arrive at

$$\partial_{u_{b,k}}\big[\mathcal{T}_a(u) + \mathcal{T}_{a+1}(u)\big] = \big(1 - e^{i\phi_a(u)}\big)\partial_{u_{b,k}}\mathcal{T}_{a+1}(u) - ie^{i\phi_a(u)}\mathcal{T}_{a+1}(u)\partial_{u_{b,k}}\phi_a(u)\,.$$

If we evaluate this expression at the shifted Bethe roots $u = u_{a,j} + i(1-a)/2$, the term in brackets on the r.h.s. vanishes and we obtain:

$$\partial_{u_{b,k}}\Big[\mathcal{T}_a^{[1-a]}(u_{a,j}) + \mathcal{T}_{a+1}^{[1-a]}(u_{a,j})\Big] = i\mathcal{T}_a^{[1-a]}(u_{a,j})\partial_{u_{b,k}}\phi_{a,j}\,. \tag{11.23}$$

We readily identify the non-trivial part of (11.17). Therefore, we arrive at the conclusion that the norm of a coordinate Bethe eigenstate can be obtained by making the following replacement in (11.17):

$$\det \partial_{u_{b,k}} \phi_{a,j} = \left(\prod_{a=1}^{r} \prod_{j=1}^{N_a} \frac{1}{i\, \mathcal{T}_a^{[1-a]}(u_{a,j})} \right) \det \partial_{u_{b,k}} \left[\mathcal{T}_a^{[1-a]}(u_{a,j}) + \mathcal{T}_{a+1}^{[1-a]}(u_{a,j}) \right] . \tag{11.24}$$

Let us show how the fundamental objects (11.20) and (11.21) look for the $SU(3)$ spin chain. In this case, and in our conventions, the transfer matrix reads

$$T(u) = \left(\frac{u+\frac{i}{2}}{u-\frac{i}{2}} \right)^L \frac{Q_1^{--}(u)}{Q_1(u)} + \frac{Q_1^{++}(u) Q_2^{-}(u)}{Q_1(u) Q_2^{+}(u)} + \frac{Q_2^{+++}(u)}{Q_2^{+}(u)} ,$$

where we are using the notation introduced in (11.14) and (11.19). One can readily check that the residues of the first two terms at $u_{1,j}$ give the first set of equations in (11.13). Likewise, the residues of the last two terms at $u_{2,j} - i/2$ give the second set of equations in (11.13). Following the procedure outlined above, we can introduce $\mathcal{T}(u)$ by multiplying the transfer matrix by $Q_1(u) Q_2^{+}(u)$:

$$\mathcal{T}(u) = \left(\frac{u+\frac{i}{2}}{u-\frac{i}{2}} \right)^L Q_1^{--}(u) Q_2^{+}(u) + Q_1^{++}(u) Q_2^{-}(u) + Q_2^{+++}(u) Q_1(u) .$$

It is now clear what are the building blocks $\mathcal{T}_a$ that we need to use in (11.24) in the case of $SU(3)$. Again, we obtain a perfect numerical match when comparing (11.17) in its original form versus the same formula, but with the replacement (11.24).

11.2.2 Norm of Bethe eigenstates and dualities

The general nested Bethe equations (11.15) obey some important dualities called *fermionic* [122, 110] and *bosonic* [125] dualities. We refer the reader to appendix D, where we review both types of dualities in detail. Here we will simply sketch the idea behind them to set the stage. Moreover, the discussion in this subsection pertains to the $SU(K)$ and $SU(K|J)$ spin chains reviewed in section 11.1.

Let us suppose that we solve the Bethe equations (11.15) corresponding to a spin chain whose symmetry group has rank r. Doing so, we find a set of Bethe roots $\{u_{1,j}, \ldots, u_{d,j}, \ldots, u_{r,j}\}$. By applying either a fermionic or bosonic duality to a non-massive node in the Dynkin diagram, say node d, we obtain a new system of nested Bethe equations, whose solutions are $\{u_{1,j}, \ldots, \tilde{u}_{d,j}, \ldots, u_{r,j}\}$. As reviewed in appendix D, the new set of $\tilde{N}_d$ dual roots $\{\tilde{u}_{d,j}\}$ is completely determined by the set of roots $\{u_{d-1,j}\}$ and $\{u_{d+1,j}\}$. From now on, we will use a tilde to denote quantities obtained after a duality.

The norms of the corresponding spin chain eigenstates before and after the duality can of course be computed from (11.17). However, we find that the ratio of these norms takes the

very simple form:

$$\frac{\tilde{\mathcal{N}}_{\rm co}}{\mathcal{N}_{\rm co}} = \frac{\left|\det_{j,k} \partial_{\tilde{u}_{d,k}} \tilde{\phi}_{d,j}\right|}{\left|\det_{j,k} \partial_{u_{d,k}} \phi_{d,j}\right|}\,, \tag{11.25}$$

where

$$\tilde{\phi}_{d,j} = \tilde{\phi}_{d,j}\left(\{u_{d-1,j}, \tilde{u}_{d,j}, u_{d+1,j}\}\right)\,, \qquad \phi_{d,j} = \phi_{d,j}\left(\{u_{d-1,j}, u_{d,j}, u_{d+1,j}\}\right)\,.$$

Formula (11.25) involves only the phases $\tilde{\phi}_d, \phi_d$ corresponding to the node on which we apply the duality, see (11.16). Thus, the determinants on the r.hs. of (11.25) are of size $\tilde{N}_d$ (numerator) and N_d (denominator). This is a big simplification, since in principle the ratio on the l.h.s. of (11.25) involves two determinants of size $(N_1 + \cdots + \tilde{N}_d + \cdots + N_r)$ and $(N_1 + \cdots + N_d + \cdots + N_r)$, see (11.17).

Let us now use formula (11.25) to obtain explicit expressions for a couple of examples. First, consider an $SU(2|1)$ spin chain. The corresponding Bethe equations can be obtained from the more general $SU(3|1)$ spin chain that we review in appendix D. They read:[61]

$$e^{i\phi_{1,j}} \equiv -e^{i\tau_1}\left(\frac{u+i/2}{u-i/2}\right)^L \frac{Q_1^{--}Q_2^{+}}{Q_1^{++}Q_2^{-}}\bigg|_{u=u_{1,j}} = 1\,, \qquad e^{i\phi_{2,j}} \equiv e^{i\tau_2}\frac{Q_1^{+}}{Q_1^{-}}\bigg|_{u=u_{2,j}}\,,$$

where we have defined the phases corresponding to each node. After applying a fermionic duality to the second node, we obtain the following new system of equations:

$$e^{i\tilde{\phi}_{1,j}} \equiv e^{i(\tau_1+\tau_2)}\left(\frac{u+i/2}{u-i/2}\right)^L \frac{\tilde{Q}_2^{-}}{\tilde{Q}_2^{+}}\bigg|_{u=u_{1,j}} = 1\,, \qquad e^{i\tilde{\phi}_{2,j}} \equiv e^{-i\tau_2}\frac{Q_1^{-}}{Q_1^{+}}\bigg|_{u=\tilde{u}_{2,j}}\,,$$

where the new Baxter polynomials $\tilde{Q}_2(u)$ are defined in a similar way as in (11.14):

$$\tilde{Q}_2(u) \equiv \prod_{j=1}^{\tilde{N}_2}(u - \tilde{u}_{2,j})\,.$$

One can readily check that the matrices entering (11.25) are diagonal in this case. Explicitly, we get:

$$\frac{\tilde{\mathcal{N}}_{\rm co}}{\mathcal{N}_{\rm co}} = \frac{\prod_{k=1}^{\tilde{N}_2}\sum_{j=1}^{N_1}\frac{-1}{(\tilde{u}_{2,k}-u_{1,j})^2+1/4}}{\prod_{k=1}^{N_2}\sum_{j=1}^{N_1}\frac{1}{(u_{2,k}-u_{1,j})^2+1/4}}. \tag{11.26}$$

Let us now consider an $SU(3)$ spin chain, whose Bethe equations can be obtained from

[61] We are introducing twists τ_a in the Bethe equations to keep the discussion more general, see appendix D.

the more general $SU(4)$ spin chain reviewed in appendix D. They are:

$$e^{i\phi_{1,j}} \equiv -e^{i\tau_1}\left(\frac{u+\frac{i}{2}}{u-\frac{i}{2}}\right)^L \frac{Q_1^{--}Q_2^{+}}{Q_1^{++}Q_2^{-}}\bigg|_{u=u_{1,j}}, \qquad e^{i\phi_{2,j}} \equiv -e^{i\tau_2}\frac{Q_1^{+}Q_2^{--}}{Q_1^{-}Q_2^{++}}\bigg|_{u=u_{2,j}}.$$

After applying a bosonic duality to the second node in the Dynkin diagram, we obtain the following system:

$$e^{i\tilde{\phi}_{1,j}} \equiv -e^{i(\tau_1+\tau_2)}\left(\frac{u+\frac{i}{2}}{u-\frac{i}{2}}\right)^L \frac{Q_1^{--}\tilde{Q}_2^{+}}{Q_1^{++}\tilde{Q}_2^{-}}\bigg|_{u=u_{1,j}}, e^{i\tilde{\phi}_{2,j}} \equiv -e^{-i\tau_2}\frac{Q_1^{+}\tilde{Q}_2^{--}}{Q_1^{-}\tilde{Q}_2^{++}}\bigg|_{u=\tilde{u}_{2,j}}.$$

In this case the matrices entering (11.25) are not diagonal and we obtain:

$$\frac{\tilde{\mathcal{N}}_{\rm co}}{\mathcal{N}_{\rm co}} = \frac{\det\limits_{j,k}\left[\delta_{jk}\left(\sum\limits_{l=1}^{N_1}\frac{1}{(\tilde{u}_{2,j}-u_{1,l})^2+1/4}-\sum\limits_{l=1}^{\tilde{N}_2}\frac{2}{(\tilde{u}_{2,j}-\tilde{u}_{2,l})^2+1}\right)+\frac{2}{(\tilde{u}_{2,j}-\tilde{u}_{2,k})^2+1}\right]}{\det\limits_{j,k}\left[\delta_{jk}\left(\sum\limits_{l=1}^{N_1}\frac{1}{(u_{2,j}-u_{1,l})^2+1/4}-\sum\limits_{l=1}^{N_2}\frac{2}{(u_{2,j}-u_{2,l})^2+1}\right)+\frac{2}{(u_{2,j}-u_{2,k})^2+1}\right]}. \tag{11.27}$$

11.3 $SL(2)$ and $SU(1|1)$ scalar products

In this section we give several formulas for the scalar products of $SL(2)$ and $SU(1|1)$ spin chains, which are dual to single-trace operators in the other two rank-1 subsectors of $\mathcal{N}=4$ SYM. These formulas were obtained from the ones for $SU(2)$ spin chains presented in chapter 4 and appendix A by making educated guesses. We checked their validity by comparing them to the result obtained from the brute force computation of the scalar product using the $SL(2)$ and $SU(1|1)$ wave functions, which we brielfy review below.

11.3.1 $SL(2)$ scalar products

Single-trace operators in the $SL(2)$ sector of $\mathcal{N}=4$ SYM are made out of L fields Z and N covariant derivatives D. This type of operators are dual to strings rotating in AdS_3 [73] and play an important role in the computation of gluon scattering amplitudes and expectation values of Wilson loops in the theory [126].

In the spin chain picture, the N covariant derivatives D are regarded as excitations on a vacuum of L scalar fields Z, i.e. the number of fields Z determines the length of the spin chain. The covariant derivatives do not really occupy spin chain sites, but simply act on the corresponding vacuum fields. As opposed to the $SU(2)$ case, the $SL(2)$ spin chain is non-compact, which physically means that there is no bound on the number of excitations

that we can have at a given site. Hence, a generic $SL(2)$ state is of the form

$$|\Psi\rangle_{SL(2)} = \sum_{1\leq n_1\leq n_2\leq\cdots\leq n_N\leq L} \psi_{SL(2)}(n_1,\ldots,n_N)|n_1,\ldots,n_N\rangle\,.$$

It is important to take into account these new limits of summation when computing scalar products by brute force. The wave function $\psi_{SL(2)}$ can be constructed using the procedure explained in section 11.1 with Cartan matrix $M=-2$. That is, in this case the wave function is given by

$$\psi_{SL(2)}\left(n_1,\ldots,n_N\right) = \sum_P A(P)\prod_{a=1}^{N}\left(\frac{u_{P_a}+\frac{i}{2}}{u_{P_a}-\frac{i}{2}}\right)^{n_a}\,, \tag{11.28}$$

where the plane wave coefficients obey

$$\frac{A(\ldots,b,a,\ldots)}{A(\ldots,a,b,\ldots)} = S_{SL(2)}(u_b,u_a) = \frac{u_b-u_a-i}{u_b-u_a+i}\,.$$

States constructed in this way diagonalize the $SL(2)$ Hamiltonian, whose density $\mathcal{H}_{SL(2)}$ acts on two adjacent sites with k and $n-k$ covariant derivatives D in the following way [127]

$$\mathcal{H}_{SL(2)}|k,n-k\rangle = \frac{\lambda}{8\pi^2}\sum_{k'=0}^{n}\left[\delta_{k=k'}\Big(h(k)+h(n-k)\Big) - \frac{\delta_{k\neq k'}}{|k-k'|}\right]|k',n-k'\rangle\,,$$

where $h(j)$ are the harmonic numbers: $h(j)=\sum_{k=1}^{j}\frac{1}{k}$ and the energy eigenvalues are again given by (11.11). Finally, by imposing periodicity of the wave function we obtain the corresponding Bethe equations:

$$\left(\frac{u_j+\frac{i}{2}}{u_j-\frac{i}{2}}\right)^L = \prod_{k\neq j}^{N}\frac{u_j-u_k-i}{u_j-u_k+i}\,.$$

Having quickly reviewed the main facts about $SL(2)$ operators in $\mathcal{N}=4$ SYM and their corresponding spin chain description, let us now give explicit formulas to compute $SL(2)$ scalars products in the latter picture.

General scalar product

Our claim is that the scalar product in the algebraic basis $S_N^{\rm al}(\{v^*\},\{u\})$ between two generic $SL(2)$ spin chains with rapidities $\{u\}$ and $\{v\}$ can be computed using the new recursion

relation (4.25) or formula (A.2), but with the following expressions for the building blocks:[62]

$$a(u) = \left(u + \frac{i}{2}\right)^L, \quad d(u) = \left(u - \frac{i}{2}\right)^L,$$

$$f(u) = \frac{u-i}{u}, \quad g(u) = -\frac{i}{u}, \quad h(u) = \frac{u-i}{-i}, \quad t(u) = \frac{-1}{u(u-i)}.$$

In order to make sure that this proposal is correct, we need the scalar product in the coordinate basis. In this way, we will be able to compare it against the result obtained from the brute force computation using the wave functions (11.28). The conversion factor that relates the scalar product in the coordinate and algebraic basis is obtained from that for $SU(2)$ spin chains, see (A.3), but with a minor modification:

$$^{\rm co}\langle\{v\}|\{u\}\rangle^{\rm co} \;=\; \frac{(-1)^N}{d^{\{u\}}a^{\{v^*\}}g^{\{u+\frac{i}{2}\}}g^{\{v^*-\frac{i}{2}\}}f_<^{\{u\}\{u\}}\,f_>^{\{v^*\}\{v^*\}}}\,S_N^{\rm al}(\{v^*\},\{u\}) \qquad (11.29)$$

Scalar product with a Bethe eigenstate

If the set of rapidities $\{u\}$ satisfy the $SL(2)$ Bethe equations, the general scalar product in the algebraic basis simplifies to

$$S_N^{\rm al}(\{v\},\{u\}) = g_>^{\{u\}\{u\}}\,g_<^{\{v\}\{v\}}\,d^{\{u\}}\det_{j,k}\Omega(u_j,v_k)\;, \qquad (11.30)$$

where the matrix Ω is

$$\Omega(u_j,v_k) = a(v_k)t(u_j-v_k)h^{\{u-v_k\}} - (-1)^N d(v_k)t(v_k-u_j)h^{\{v_k-u\}}.$$

Norm of a Bethe eigenstate

Finally, the norm in the coordinate basis is given by our conjectured formula (11.17)

$$\mathcal{N}_{\rm co} = \prod_{j=1}^N \left(u_j^2 + \frac{1}{4}\right)\left|\det_{j,k}\partial_j\phi_k\right|,$$

where the phases ϕ_j are defined as

$$e^{i\phi_j} \equiv \left(\frac{u_j+i/2}{u_j-i/2}\right)^L \prod_{k\neq j}^N \frac{u_j-u_k+i}{u_j-u_k-i} = 1\,.$$

[62] Just like in the spectrum problem, $SL(2)$ equations can be obtained from those for $SU(2)$ by changing $i \to -i$.

11.3.2 $SU(1|1)$ scalar products

Single-trace operators in the $SU(1|1)$ sector of $\mathcal{N}=4$ SYM are made out of $L-N$ fields Z and N fermions Ψ. In the spin chain picture, the N fermions are regarded as excitations on a vacuum of scalar fields Z. A generic $SU(1|1)$ state is of the form

$$|\Psi\rangle_{SU(1|1)} = \sum_{1\leq n_1<n_2<\cdots<n_N\leq L} \psi_{SU(1|1)}(n_1,\ldots,n_N)|n_1,\ldots,n_N\rangle\,,$$

where the wave function $\psi_{SU(1|1)}$ can be constructed using the procedure explained in section 11.1 with Cartan matrix $M=0$. That is, in this case the wave function is again of the form (11.28), but the plane wave coefficients obey

$$\frac{A(\ldots,b,a,\ldots)}{A(\ldots,a,b,\ldots)} = S_{SU(1|1)}(u_b,u_a) = -1\,.$$

Thus, in this case the scattering is trivial: the excitations behave as free fermions! States constructed in this way diagonalize the $SU(1|1)$ Hamiltonian given in (11.3), with corresponding energy eigenvalues given by (11.11). Finally, we have to take Fermi statistics into account when imposing periodicity of the wave function. For example, from $\psi_{SU(1|1)}(n_1,n_2,\ldots,n_N) = (-1)^{N-1}\psi(n_2,n_3,\ldots,n_N,n_1+L)$ we obtain the Bethe equations

$$\left(\frac{u_j+\frac{i}{2}}{u_j-\frac{i}{2}}\right)^L = 1\,,$$

which are of course trivially solved by $u_j = \frac{1}{2}\cot\frac{\pi n_j}{L}$. Let us now give explicit formulas to compute scalar products of $SU(1|1)$ spin chains.

General scalar product

Just like before, the scalar product $S_N^{\rm al}(\{v^*\},\{u\})$ of two generic $SU(1|1)$ spin chains with rapidities $\{u\}$ and $\{v\}$ can be computed using the new recursion relation (4.25) or the sum over partitions formula of (A.2), but with the following expressions for the building blocks

$$a(u) = \left(u+\frac{i}{2}\right)^L\,,\quad d(u) = \left(u-\frac{i}{2}\right)^L\,,$$

$$f(u) = \frac{i}{u},\quad g(u) = \frac{i}{u},\quad h(u)=1,\quad t(u) = \frac{i}{u}$$

In this case, the relation between the scalar product in the algebraic and coordinate bases is exactly the same as that for $SU(2)$, see (A.3).

Scalar product with a Bethe eigenstate

Then, if the set of rapidities $\{u\}$ satisfy the $SU(1|1)$ Bethe equations, the scalar product simplifies to

$$S_N^{\rm al}(\{v\},\{u\}) = g_>^{\{u\}\{u\}}\, g_<^{\{v\}\{v\}}\, d^{\{u\}} \det \Omega(u_j, v_k)\,, \tag{11.31}$$

where the matrix Ω is now given by

$$\Omega(u_j, v_k) = (-i)^N \left[a(v_k)t(u_j - v_k) + d(v_k)t(v_k - u_j)\right].$$

Norm of a Bethe eigenstate

Again, the norm in the coordinate basis is given by formula (11.17) with ϕ_j defined as

$$e^{i\phi_j} = 1 \qquad \text{where} \qquad e^{i\phi_j} \equiv \left(\frac{u_j + i/2}{u_j - i/2}\right)^L .$$

Chapter 12

Conclusions and Future Directions

In this thesis, we have shown that integrability techniques, so useful in the spectrum problem, can also be used to tackle the computation of correlation functions at weak coupling in $\mathcal{N} = 4$ SYM. In particular, we explained in great detail how to efficiently compute all tree-level three- and four-point functions of single-trace gauge-invariant operators in the $SU(2)$ sector of the theory. The method we used involves thinking of the operators as spin chain states that are cut, flipped and sewed into the corresponding correlation functions.

Using the classical limit of our weak coupling results for three- and four-point functions, we performed a weak/strong coupling match by comparing them to the results obtained for the corresponding holographic correlation functions in the Frolov-Tseytlin limit. In order to do this, we precisely identified what $\mathcal{O}_1 \simeq \bar{\mathcal{O}}_2$ means at weak coupling. Since this type of match was instrumental in guessing all-loop results in the spectrum problem [112, 111], we hope the same will be the case for three-point functions. That is, one should not view this weak/strong coupling match as fundamental, but rather as a guiding principle in the pursuit of higher-loop results. In this spirit, it was recently shown that the match persists at one loop for three-point functions of two heavy operators and a light BPS operator in the $SU(2)$ sector [46].

We should also emphasize the important role that numerics played in our work. The Mathematica implementation of our weak coupling formulas of chapter 5 and 6 (see appendix E) allows us to obtain *exact* numerical results for operators with small or large charges. Using our code, we were able to show numerically the weak/strong coupling match for three- and four-point functions. In turn, this result justified the use of coherent states to represent the large operators in the correlation functions. Recently, the numerical weak/strong coupling match for three-point functions was extended to one loop [46]. The analytical coherent state computation of this match is yet to be performed (see [128] for an interesting effort). Finally, let us recall that we were able to identify the issue of back-reaction in chapter 10 precisely because of our numerical work. In short, the use of numerical results was a powerful guiding tool in our research.

As first pointed out in [40], the building blocks of the weak coupling results of part III of this thesis are the same that appear in the spectrum problem. To promote tree-level results

up to four-loops in the spectrum problem, one has to modify the expression for the energy and the momenta of excitations. For example:

$$e^{ip} = \frac{u+\frac{i}{2}}{u-\frac{i}{2}} \quad \to \quad \frac{x(u+\frac{i}{2})}{x(u-\frac{i}{2})}\,,$$

where

$$\frac{\sqrt{\lambda}}{2\pi}\,x(u) = u + \sqrt{u^2 - \frac{\lambda}{4\pi^2}}$$

is the so-called Zhukovsky variable introduced in [129]. We expect that such replacements in our tree-level expressions for correlation functions capture most of the correct higher-loop result for asymptotic operators, i.e. those for which there are no wrapping corrections. Recent results for one-loop three-point functions seem to confirm this claim [46]. This is expected because for asymptotic operators, the dominant contribution to their correlation functions comes from the overlap of their wave functions, which is precisely what we studied in this thesis.

From a broader perspective, computing three-point functions in $\mathcal{N}=4$ SYM is an ambitious goal with far reaching consequences. The main motivation to develop efficient methods to compute these observables is that, together with the two-point functions, the three-point functions are enough to reconstruct any higher-point function in this conformal field theory. The material presented in this thesis constitutes the first step toward finding a systematic procedure that will allow us to compute all three-point functions in the theory, just like the Y-system does for the spectrum of anomalous dimensions. Of course, in order to accomplish this longer-term goal, we need to extend the techniques presented in this thesis. Thus, let us comment on some future directions of research.

Other sectors of $\mathcal{N}=4$ SYM

An obvious first step is to generalize our results to compute tree-level correlation functions of operators in other sectors of the theory. After all, to glue three-point functions together into higher-point correlation functions we will need the most general cases. Recall that for the spectrum problem, we needed to know the spectrum of eigenvalues of integrable Hamiltonians. As we showed in the main text, for correlation functions the basic ingredient is the precise form of the eigenstates, i.e. the precise structure of the spin chain wave functions. The nested coordinate Bethe ansatz for $SU(K)$ and $SU(K|J)$ spin chains that we presented in section 11.1 allows us to construct the eigenstates corresponding to a large class of operators in $\mathcal{N}=4$ SYM. A feature shared by these types of spin chain is that the massive node in their Dynkin diagrams is the first one, see figure 11.1. What remains to be done is to understand how to construct the wave functions of spin chains whose Dynkin diagrams have two wings, i.e. in these cases the massive node is the middle one. This is important because the Dynkin diagram corresponding to the spin chain of $\mathcal{N}=4$ SYM is precisely of this type [112].

The best starting point to address this issue is to study the $SO(6)$ spin chain corresponding

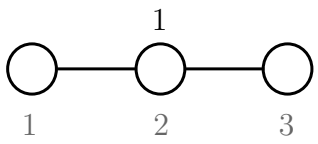

Figure 12.1: $SO(6)$ Dynkin diagram, where the upper number 1 indicates the momentum-carrying node. Note that the lower (gray) numbers label the nodes and the middle node is common to both wings.

to operators made out of all complex scalars in the theory. The Hamiltonian in this case is known [14] and the Dynkin diagram is the same as that of $SU(4)$, but with the massive node being the middle one (see figure 12.1). Thus, each of the two wings looks like an $SU(3)$ Dynkin diagram. This naturally leads to conjecture that we can write the $SO(6)$ wave function as a product of two $SU(3)$ wave functions constructed using the procedure from section 11.1. We have numerical evidence that this is indeed the case (one has to take into account some subtelties related to the fact that the two $SU(3)$ wings share the middle node).

Once the wave functions are known, we need to develop new technology for computing scalar products of Bethe states for higher-rank groups. That is, we need to generalize the $SU(2)$ formulas presented in chapter 4.[63] As a first step we generalized the formula for the normalization of Bethe states to generic Lie (super) algebras, see (11.17). As explained in section 11.2, we tested the validity of our conjectured formula by comparing it against the brute force computation of the norm of a Bethe state constructed using the wave functions of section 11.1. The numerical match was perfect in all cases. Moreover, taking into account the subtelties mentioned in the previous paragraph, we also checked that the formula is valid for $SO(6)$ spin chains.

For the other rank-one sectors of $\mathcal{N} = 4$ SYM, i.e. for the $SL(2)$ and the $SU(1|1)$ sectors, we went a bit further. For these cases we generalized all possible scalar products (and not only the norm) in section 11.3. Hence, we can trivially convert the results of the main text to their analogue in the other rank-one sectors.

The next step in complexity is to understand how to generalize the formulas of chapter 4 to compute general scalar products of $SU(3)$ spin chains.

Loops

Another natural direction is to develop integrability techniques to compute correlation functions at loop order. There are two type of loop corrections that one needs to take into account, which we explain below for the case of three-point functions.

[63] To our knowledge the only previous results for scalar products of Bethe states in nested Bethe ansatz systems are [130] for the norm of $SU(3)$ Bethe eigenstates and [131] for the norm of eigenstates in the Hubbard model. See also [132] for recent progress in computing particular limits of $SU(3)$ scalar products.

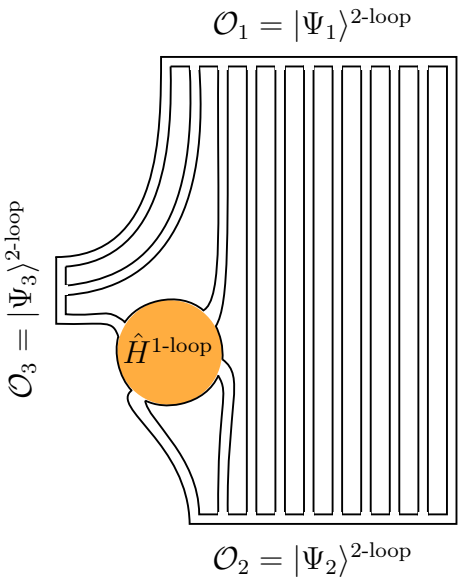

Figure 12.2: At one loop, the three-point function gets two types of corrections. One type is the two-loop correction to the external wave functions eigenstates. The other correction shown in this figure comes from the one-loop Hamiltonian insertion $\hat{H}$ between legs that originate from one of the operators and goes to two different operators. As opposed to the overlap of the wave functions, that contribution is very local and therefore it is somehow simpler. It can be thought of as measuring the energy cost of splitting the string [38]. Outside the scalar sector the picture seems to be more involved [39].

- The first are loop corrections to the wave functions of the three operators. These comprise nonlocal corrections – due to the dependence of the scattering matrices (3.5) on the coupling – and also local corrections due to the insertion of the so-called contact terms [133]. Due to the degeneracy of the spectrum at tree level, the computation of these corrections to the three-point functions at l loops involves the $(l+1)$-loop wave functions.

- The second are loop corrections to the contraction of the three operators. At low loop orders, these are local corrections which dress the nonlocal overlap of the three wave functions. At one loop, and in the scalar sector, these corrections are captured by Hamiltonian density insertions at the spin chain breaking points [38, 39], see figure 12.2. One can think of these Hamiltonian insertions as measuring the energy cost of splitting the three operators [38]. Outside the scalar sector the picture seems to be more involved [39].

It was recently shown in [46] that one can indeed use integrability techniques to compute three-point functions at one loop in the $SU(2)$ sector. The idea is to introduce rapidities θ_j at all sites of a spin chain of length L, just like we did in chapter 5 when deriving the determinant form of three-point functions. It was realized in [46] that *all* the corrections listed above can be accounted for by introducing a novel differential operator called Θ-derivative, which acts

on a function as

$$\Big(\!\Big(f\Big)\!\Big)_\theta \equiv f + \frac{\lambda}{32\pi^2}\sum_{i=1}^{L}\left(\partial_{\theta_i}-\partial_{\theta_{i+1}}\right)^2 f\,\Big|_{\theta_j\to 0} + O(\lambda^2)\,. \tag{12.1}$$

Quite remarkably, by acting with this operator on eigenstates of the one-loop Hamiltonian (3.2), we obtain, up to some factor, eigenstates of the two-loop $SU(2)$ Hamiltonian [134]

$$\hat{H} = \left(\frac{\lambda}{8\pi^2}-\frac{\lambda^2}{32\pi^4}\right)\sum_{n=1}^{L}\mathcal{H}_{n,n+1} + \frac{\lambda^2}{128\pi^4}\sum_{n=1}^{L}\mathcal{H}_{n,n+2}\,, \tag{12.2}$$

where $\mathcal{H}_{a,b}\equiv\mathbb{I}_{a,b}-\mathbb{P}_{a,b}$. Namely, if we consider an operator with rapidities $\{u\}$:

$$|\{u\}\rangle^{\text{2-loop}} = \left(1-\frac{\lambda}{16\pi^2}\Gamma_u\,\mathcal{H}_{L,1}\right)\Big(\!\Big(|\{u\}\rangle^{\text{1-loop}}\Big)\!\Big)_\theta\,, \tag{12.3}$$

where Γ_u is the sum part of the one-loop energy (3.17). This is precisely the first type of correction mentioned above. What is even more suprising is that the Θ-derivative also takes care of considering the Hamiltonian insertions between the three operators. Namely, the one-loop three-point functions in the $SU(2)$ sector are simply given by

$$C_{123}^{\text{1-loop}} = \sqrt{L_1L_2L_3}\,\frac{\Big(\!\Big(C_{123}^{\text{tree-level}}/\tilde{\Omega}_{123}\Big)\!\Big)_{\theta^1}}{\Big(\!\Big(\sqrt{\mathcal{N}}_1\Big)\!\Big)_{\theta^1}\Big(\!\Big(\sqrt{\mathcal{N}}_2\Big)\!\Big)_{\theta^2}\Big(\!\Big(\sqrt{\mathcal{N}}_3\Big)\!\Big)_{\theta^3}}\,, \tag{12.4}$$

where $\mathcal{N}_1 = {}^{\text{1-loop}}\langle\{u\}|\{u\}\rangle^{\text{1-loop}}$, and similarly for $\mathcal{N}_2$ and $\mathcal{N}_3$, while θ^i are the rapidities introduced for each operator. In this equation, $C_{123}^{\text{tree-level}}$ should be understood as the expression appearing on the r.h.s. of (5.21). This is remarkable: the Θ-derivative basically acts as a "loop generator" on three-point functions. As an example, all one-loop three-point functions shown in table C.1 (which were computed by brute force) are reproduced by (12.4) [135].

It is natural to expect that by considering higher-order terms in λ in the Θ-derivative (12.1), one should be able to obtain higher-loop three-point functions in the $SU(2)$ sector in a similar fashion. Unfortunately, there are no explicit Feynman diagram computations of three-point functions in $\mathcal{N}=4$ SYM beyond one loop. Thus, it would be important to initiate a systematic perturbative study of three-point functions at loop order to compare those results with the ones obtained from the integrability approach.

Classical limit

An important direction of research is the classical limit of the general tree-level results that we obtained in chapters 5 and 6. This limit proves to be very useful for comparison with string theory computations through the Frolov-Tseytlin limit. In the case of three-point functions, this limit has already been worked out in [45, 46]. Let us flash one of these results.

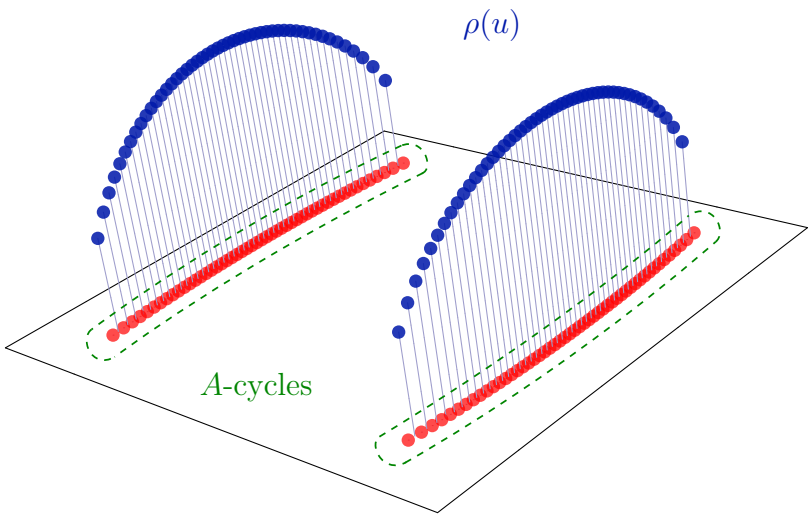

Figure 12.3: In the classical limit, the Bethe roots distribute themselves alongs some cuts (red bullets) described by some density $\rho(u)$ (blue bullets). In this limit, the three-point function $C_{123}^{\circ\bullet\circ}$ can be expressed as an integral over the A-cycles that encircle the cuts (green curves) and an integral over the cuts themselves, see (12.7). In this particular example, we show the Bethe roots for a two-cut solution with $L = 1000, N = 100$.

Recall that classical scaling limit that we considered is the Sutherland limit [115], which was rediscovered in [102] in the context of the AdS/CFT correspondence. In this limit, the length L, the number of Bethe roots N and the roots themselves are very large:

$$N \sim L \sim v \to \infty \tag{12.5}$$

and are of the same order. Moreover, the roots distribute themselves in contours $\mathcal{C}_k$ described by some density $\rho(v)$, see figure 12.3. These contours are also called *cuts*. A systematic description of the spectrum in the classical limit is achieved through the finite gap method of KMMZ [104]. In this method one introduces a resolvent

$$G(u) = \sum_{k=1}^{N} \frac{1}{u - v_k} = \int\limits_{\cup \mathcal{C}_k} dv \, \frac{\rho(v)}{u - v} \tag{12.6}$$

where the integral is over all the contours $\mathcal{C}_k$ where the roots lie in the continuum limit. In this language, the classical limit of the ratio $C_{123}^{\circ\bullet\circ}/C_{123}^{\circ\circ\circ}$ is given by [44]

$$\frac{C_{123}^{\circ\bullet\circ}}{C_{123}^{\circ\circ\circ}} \propto \frac{\mathscr{A}(l|\{v\})}{\mathscr{B}(\{v\})} = \exp \int_0^1 dt \left[\oint\limits_{\cup \mathcal{C}_k} \frac{dv}{2\pi i} \, q \log\left(1 - e^{iqt}\right) - \int\limits_{\cup \mathcal{C}_k} dv \, \rho \, \log\big(2 \sinh(\pi t \rho)\big) \right] \tag{12.7}$$

where

$$q(u) = \frac{l}{u} - G(u) \tag{12.8}$$

is a sort of trimmed quasi-momenta. In this expression all the roots are taken to be finite. The integral involving the quasi-momenta $q(v)$ is over the A-cycles that encircles the cuts, while the integral involving the density $\rho(u)$ is taken over the cuts, see figure 12.3. Note from table 5.1 that the ratio $\mathscr{A}/\mathscr{B}$ is also the essential building block of $C_{123}^{\bullet\circ\circ}$ and $C_{123}^{\circ\circ\bullet}$. Hence (12.7) is also the answer for those cases.

The scaling limit of the more general $SU(2)$ cases in table 5.1 can be also analyzed. Indeed, the result for the most general three-point function $C_{123}^{\bullet\bullet\bullet}$ of three heavy, non-BPS operators was recently derived in [45]. In that case, the result is also neatly expressed in terms of integrals of the quasi-momenta around the cuts formed by the roots of each operator. Finally, as first proposed in [40], the all-loop answer in the classical limit might be obtained from the tree-level result of [45] by using the exact expression for the quasi-momenta to higher-loop order, including the dressing phase [136]. It would be very interesting to explore this possibility.

Strong coupling

There are also interesting directions to pursue on the strong coupling side. An important open problem is to compute the full holographic correlation function of three heavy operators. So far, only the AdS_5 contribution to the answer has been computed [71], while the S^5 part remains to be found. Once the full result is known, one could compare its Frolov-Tseytlin limit with the classical limit of the weak coupling result, which was obtained in [45], to see if a match occurs. One would also like to extend the integrability techniques for three-point functions developed in [71] and [72] to compute higher-point correlation functions at strong coupling. When such techniques are available, it would be interesting to make a comparison of the strong coupling results and our weak coupling results of chapter 6 when more than two operators in the four-point function are heavy and see if a weak/strong coupling match occurs.

Another interesting avenue is the study of back-reaction at strong coupling. Recall that for the holographic three-point function of two heavy non-BPS operators and a light BPS operator, we showed in chapter 10 that $\mathcal{O}_1 \simeq \bar{\mathcal{O}}_2$ corresponds to option (C) at weak coupling. This means adding the extra roots of $\mathcal{O}_1$ to the existing classical cuts formed by the roots of $\mathcal{O}_2$. It would be interesting to identify what strong coupling computations correspond to the options (A) and (B) at weak coupling, in which we add the extra roots of $\mathcal{O}_1$ outside of the cuts of $\mathcal{O}_2$ at infinity or finite values, respectively. Recall that these options correspond to acting with global symmetry generators on the classical solution or considering quantum fluctuations around it, see figure 10.1. In both of these cases we still have that the classical state $\mathcal{O}_1$ seems similar to $\bar{\mathcal{O}}_2$.

Of course, one would also like to be able to compute the holographic correlation function

of one heavy non-BPS operator and two light BPS operators, for which we know the result at weak coupling, see (12.7).

Finally, it would be interesting to compute the $1/J$ correction to the holographic four-point function of figure 9.4 and see it a match occurs with our weak coupling prediction (9.26) in the Frolov-Tseytlin limit.

Appendices

Appendix A

$SU(2)$ Scalar Products

In this appendix, we write several useful formulas for $SU(2)$ scalar product in both the algebraic and coordinate bases. These complement the formulas in chapter 4. We also give explicit expressions for the scalar products for $SL(2)$ and $SU(1|1)$ spin chains. In order to simplify the expressions, it is convenient to introduce the following functions

$$h(u) = \frac{f(u)}{g(u)} = \frac{u+i}{i}\,, \qquad t(u) = \frac{g^2(u)}{f(u)} = \frac{-1}{u(u+i)}\,, \tag{A.1}$$

and make use of the shorthand notation introduced in (3.43).

General scalar product as a sum over partitions

If all rapidities involved in the scalar product are arbitrary complex numbers, the scalar product can be written as a sum over all possible partitions of the two sets of rapidities. Explicitly [85, 83]

$$S_N^{\rm al}(\{v\},\{u\}) = g_<^{\{u\}\{u\}}\, g_>^{\{v\}\{v\}} \sum_{\substack{\alpha\cup\bar\alpha=\{u\}\\ \gamma\cup\bar\gamma=\{v\}}} (-1)^{P_\alpha+P_\gamma} d^\alpha a^{\bar\alpha} a^\gamma d^{\bar\gamma} h^{\alpha\gamma} h^{\bar\gamma\bar\alpha} h^{\alpha\bar\alpha} h^{\bar\gamma\gamma} \det t^{\alpha\gamma} \det t^{\bar\gamma\bar\alpha}\,, \tag{A.2}$$

where we are using the notation introduced in (4.3) and $(-1)^{P_\alpha}$ is defined as a sign of the permutation of the ordered set $\{v\}$ which gives $\alpha\cup\bar\alpha$. Note that the sum runs over all partitions $\alpha\cup\bar\alpha=\{u\}$ and $\gamma\cup\bar\gamma=\{v\}$, such that the number of elements in α and the number of elements in γ are equal. We can use the conversion factor in (3.42) to obtain the corresponding expression in the coordinate basis as:

$${}^{\rm co}\langle\{v\}|\{u\}\rangle^{\rm co} \;=\; \frac{1}{d^{\{u\}} a^{\{v^*\}} g^{\{u+\frac{i}{2}\}} g^{\{v^*-\frac{i}{2}\}} f_<^{\{u\}\{u\}}\, f_>^{\{v^*\}\{v^*\}}}\, S_N^{\rm al}(\{v^*\},\{u\}) \tag{A.3}$$

where $S_N^{\rm al}$ is defined in (4.16). Recall that $\mathcal{C}(u^*) = -\left[\mathcal{B}(u)\right]^\dagger$ so that

$$S_N^{\rm al}(\{v^*\},\{u\}) = (-1)^{N\,{\rm al}}\langle\{v\}|\{u\}\rangle^{\rm al}\,. \tag{A.4}$$

New recursion relation in the coordinate basis

Alternatively, we can define the general scalar product recursively, as in (4.25). Using the conversion factor (3.42), the new recursion relation in the coordinate basis reads

$$\begin{aligned} S_N^{\rm co}\left(\{v_1,\ldots,v_N\},\{u_1,\ldots,u_N\}\right) &= \sum_n b_n^{\rm co}\, S_{N-1}^{\rm co}(\{v_1,\ldots,\hat{v}_n,\ldots,v_N\},\{\hat{u}_1,u_2,\ldots,u_N\}) \\ -\sum_{n<m} c_{n,m}^{\rm co}\, S_{N-1}^{\rm co}(\{u_1,v_1,\ldots\hat{v}_n,\ldots,\hat{v}_m,\ldots v_N\},\{\hat{u}_1,u_2,\ldots,u_N\})\,, \end{aligned} \tag{A.5}$$

with the coefficients being in this case

$$b_n^{\rm co} = \frac{\displaystyle\prod_{j\neq n}^{N} f(u_1-v_j)\prod_{j<n}^{N} S(v_j,v_n) - \frac{a(u_1)d(v_n)}{d(u_1)a(v_n)}\prod_{j\neq n}^{N} f(v_j-u_1)\prod_{j>n}^{N} S(v_n,v_j)}{\dfrac{g(u_1+\frac{i}{2})\,g(v_n-\frac{i}{2})}{g(u_1-v_n)}\displaystyle\prod_{j\neq 1}^{N} f(u_1-u_j)}$$

$$c_{n,m}^{\rm co} = \frac{S(v_m,v_n)\dfrac{d(v_n)}{a(v_n)}\displaystyle\prod_{j>n} S(v_n,v_j)\prod_{j<m} S(v_j,v_m) + \dfrac{d(v_m)}{a(v_n)}\displaystyle\prod_{j>m} S(v_m,v_j)\prod_{j<n} S(v_j,v_n)}{\left[\dfrac{d(u_1)\,g(u_1+\frac{i}{2})\;g(v_n-\frac{i}{2})\,g(v_m-\frac{i}{2})\displaystyle\prod_{j\neq 1} f(u_1-u_j)}{a(u_1)\,g(u_1-\frac{i}{2})\,g(u_1-v_n)\,g(u_1-v_m)\displaystyle\prod_{n\neq n,m} f(v_j-u_1)}\right]}$$

where we used the usual $SU(2)$ S-matrix $S(u,v) = f(u-v)/f(v-u)$.

Usual recursion relation

Finally, for completeness, we write the recursion relation for the general scalar product known in the literature [85]

$$\begin{aligned} S_N^{\rm al}\left[a(x),d(x)\right] = \sum_{n=1}^{N} g(u_1-v_n)\prod_{j\neq 1}^{N} g(u_1-u_j)\prod_{k\neq n}^{N} g(v_k-v_n)_{k\neq n} \\ \times\left\{a(v_n)d(u_1)S_{N-1}^{\rm al}\left[a(x)h(u_1-x),d(x)h(x-v_n)\right]\right. \\ \left. -\,a(u_1)d(v_n)S_{N-1}^{\rm al}\left[a(x)h(v_n-x),d(x)h(x-u_1)\right]\right\}\,, \end{aligned} \tag{A.6}$$

where the sets of magnons entering $S_{N-1}^{\rm al}$ are obtained from the set entering $S_N^{\rm al}$ by omitting u_1 and v_n. The difference between both sides of (A.6) lies in the action of the operators $\mathcal{A}(u)$

and $\mathcal{D}(u)$ on the vacuum. For $S_N^{\rm al}$, this action is simply given by $a(u)$ and $d(u)$, see (3.31). For the first $S_{N-1}^{\rm al}$ in (A.6), this action is given by $a(u)h(u_1-u)$ and $d(u)h(u-v_n)$, while for the second $S_{N-1}^{\rm al}$ it is $a(u)h(v_n-u)$ and $d(u)h(u-u_1)$. That is, this recursion relation uses somehow generalized objects at each recursion stage, see also discussion at the end of section 4.3.1.

Scalar product with a Bethe eigenstate

If the set of rapidities $\{u\}$ satisfies the Bethe equations (3.13), while $\{v\}$ are arbitrary complex numbers, the scalar product simplifies to [83]

$$S_N^{\rm al}(\{v\},\{u\}) = g_>^{\{u\}\{u\}}\, g_<^{\{v\}\{v\}}\, d^{\{u\}} \det_{j,k} \Omega(u_j,v_k)\ , \tag{A.7}$$

where

$$\Omega(u_j,v_k) = a(v_k)t(u_j-v_k)h^{\{u-v_k\}} - (-1)^N d(v_k)t(v_k-u_j)h^{\{v_k-u\}}\ ,$$

where we are using our short-hand notation, such that $h^{\{u-v_k\}} = \prod_{j=1}^N h(u_j-v_k)$. In order to derive (A.7), one starts with (A.2) and makes use of the fact that the Bethe equations (3.13) for $\{u\}$ can be written as

$$\frac{a(u_j)}{d(u_j)} = (-1)^{N-1}\frac{h^{\{u_j-u\}}}{h^{\{u-u_j\}}}.$$

We refer the reader to [83] for the details of the derivation.

Appendix B

Three-Point Functions of BMN Operators

In this appendix we consider a simple limit of the three-point functions of chapter 5, when the lengths of operators L_a scale to infinity whereas the numbers of magnons M_a are fixed. We also assume that the momenta of the magnons are small (or equivalantly the Bethe roots are large). That is, similarly to the thermodynamical limit we have $u_a \simeq L_a$. These states describe small quasi-classical fluctuations about the BMN point-like string. For related papers, see [74, 137, 138, 113].

In this limit, one can replace the S-matrix factor by 1 in the Bethe ansatz equations, which leads to the trivial quantization condition:

$$u_k \simeq \frac{L}{2\pi n_k} \tag{B.1}$$

where n_k is an integer. In general one should assume that all n_k's are different. Otherwise there is a degeneracy which is lifted at the next order only.[64]

As it was shown in the main text, in order to construct all the structure constants one needs only tree key structures denoted by $\mathscr{A}, \mathscr{B}, \mathscr{C}$. They can be easily expanded in the near

[64] Namely, for the M_n roots with $n_k = n$ to the next order in $1/\sqrt{L}$ are [116]

$$u_l \simeq \frac{1}{2\pi n}\left(L + iz_l\sqrt{2L}\right) \quad , \quad l = 1, \ldots, M_n \tag{B.2}$$

where z_l are the zeros of the Hermite polynomial, $\mathrm{H}_{M_n}(z_k) = 0$. In what follows we assume that the roots are large and well separated between each other.

BMN limit[65]

$$\mathscr{A}(l|\{u\}) \simeq \prod_k \left(1 - e^{\frac{l}{iu_k}}\right) \tag{B.3}$$

$$\mathscr{B}(\{u\}) \simeq \sqrt{\begin{pmatrix} L-2M \\ N-M \end{pmatrix} \frac{1}{L}} \prod_{k=1}^{M} \frac{i\sqrt{L}}{u_k} \tag{B.4}$$

$$\mathscr{C}(l|\{u\},\{v\}) \simeq \sum_\sigma \prod_k \frac{e^{\frac{il}{u_k}} - e^{\frac{il}{v_{\sigma_k}}}}{i(u_k - v_{\sigma_k})} \,. \tag{B.5}$$

Having these quantities at hand we simply combine them into structure constants using the expressions in table 5.1. For example,

$$C_{123}^{\bullet\bullet\circ} \simeq \frac{\prod_{k=1}^{M_1} \frac{v_k}{i\sqrt{L_1}} \prod_{k=1}^{M_2} \frac{u_k}{i\sqrt{L_2}}}{\sqrt{\frac{\binom{L_1-2M_1}{N_1-M_1}\binom{L_2-2M_2}{N_2-M_2}\binom{L_3}{N_3}}{L_1 L_2 L_3}}} \sum_{\substack{\alpha \cup \bar{\alpha} = \{u\} \\ |\bar{\alpha}| = l_{13}}} \sum_\sigma \left[\prod_{k=1}^{|\alpha|} \frac{e^{\frac{il_{12}}{\alpha_k}} - e^{\frac{il_{12}}{v_{\sigma_k}}}}{i(\alpha_k - v_{\sigma_k})}\right] \left[\prod_{k=1}^{|\bar{\alpha}|} e^{\frac{iL_1}{\bar{\alpha}_k}} - e^{\frac{il_{12}}{\bar{\alpha}_k}}\right] . \tag{B.6}$$

[65] It is also very simple to derive them directly from their definition and the form of the wave function (3.10). Recall that up to trivial factors $\mathscr{B}, \mathscr{A}, \mathscr{C}$ are related to the norm of eigenstates, inner product with vacuum descendants and general inner product respectively. When the S-matrix is replaced by 1 all these quantities are very simple to compute directly without any fancy integrability machinery.

Appendix C

Data: Three-Point Functions at One-Loop

In this appendix we present numerical data for one-loop structure constants. As mentioned in the conclusions, two things need to be done: we need to contract the external wave functions of the three operators using Hamiltonian insertions [38, 37, 39] and we need to take into account the $O(\lambda)$ correction to the wave function, which is a two-loop effect. The latter effect was not taken into account in previous works [38, 37, 39] but its importance was mentioned in the conclusions of [38].

For simplicity we shall consider two kind of operators only: BPS operators and non-BPS operators with two impurities with opposite momentum. We can write any BPS state with N excitations and length L, which we denote by $[N, L]$, as

$$[N,L] = \sum_{1\le n_1<n_2<\cdots<n_N\le L} \mathrm{Tr}(Z\ldots\underset{\downarrow}{X}_{n_1}\ldots\underset{\downarrow}{X}_{n_2}\cdots\ldots\underset{\downarrow}{X}_{n_N}\ldots Z)$$

For example:

$$\begin{aligned}
[2,5] &= 5\,\mathrm{Tr}\left(Z^3X^2\right) + 5\,\mathrm{Tr}\left(Z^2XZX\right)\,,\\
[3,6] &= 6\,\mathrm{Tr}\left(Z^3X^3\right) + 6\,\mathrm{Tr}\left(Z^2XZX^2\right) + 6\,\mathrm{Tr}\left(Z^2X^2ZX\right) + 2\,\mathrm{Tr}\left(ZXZXZX\right)\,.
\end{aligned}$$

The non-BPS operators that we will consider diagonalize the two-loop Hamiltonian (12.2). Their rapidities are given by

$$u = \pm\left(\frac{1}{2}\cot\frac{\pi n}{L-1} + \frac{\lambda}{8\pi^2}\frac{L}{L-1}\sin\frac{2\pi n}{L-1} + O(\lambda^2)\right) \tag{C.1}$$

and their energy is

$$\Delta = \frac{\lambda}{\pi^2}\sin^2\frac{n\pi}{L-1} - \frac{\lambda^2}{4\pi^4}\frac{1}{L-1}\left(1+L+2\cos\frac{2\pi n}{L-1}\right)\sin^4\frac{\pi n}{L-1} + O(\lambda^3)\,. \tag{C.2}$$

The integer $n = 1, \ldots, L/2-1$ is called the mode number. Thus, we will denote these operators by (n, L). We take $(g^2 = \lambda/16\pi^2)$

$$
\begin{aligned}
(1,4) &= \mathrm{Tr}\,[Z,X]^2\ , \\
(1,5) &= \mathrm{Tr}\left(Z^3X^2\right) - \mathrm{Tr}\left(Z^2XZX\right)\ , \\
(1,6) &= \mathrm{Tr}\left(Z^4X^2\right) - \frac{3-\sqrt{5}}{2}(1+g^2)\,\mathrm{Tr}\left(Z^3XZX\right) + \frac{1-\sqrt{5}+(3-\sqrt{5})g^2}{2}\,\mathrm{Tr}\left(Z^2XZ^2X\right)\ , \\
(2,6) &= \mathrm{Tr}\left(Z^4X^2\right) - \frac{3+\sqrt{5}}{2}(1+g^2)\,\mathrm{Tr}\left(Z^3XZX\right) + \frac{1+\sqrt{5}+(3+\sqrt{5})g^2}{2}\,\mathrm{Tr}\left(Z^2XZ^2X\right) \\
(1,7) &= \mathrm{Tr}\left(Z^5X^2\right) - \frac{g^2}{2}\,\mathrm{Tr}\left(Z^4XZX\right) - \frac{1}{2}(2-g^2)\,\mathrm{Tr}\left(Z^3XZ^2X\right)\ , \\
(2,7) &= \mathrm{Tr}\left(Z^5X^2\right) - \left(2+\frac{3g^2}{2}\right)\,\mathrm{Tr}\left(Z^4XZX\right) + \left(1+\frac{3g^2}{2}\right)\,\mathrm{Tr}\left(Z^3XZ^2X\right)\ , \\
(1,8) &= \mathrm{Tr}\left(Z^6X^2\right) + \left[\sec\left(\frac{\pi}{7}\right)\sin\left(\frac{\pi}{14}\right) - 0.489997\,g^2\right]\,\mathrm{Tr}\left(Z^5XZX\right) \\
&\quad - \left[\sec\left(\frac{\pi}{7}\right)\sin\left(\frac{3\pi}{14}\right) - 0.206966\,g^2\right]\,\mathrm{Tr}\left(Z^4XZ^2X\right) \\
&\quad - \left[\frac{1}{2}\sec\left(\frac{\pi}{7}\right) - 0.283031\,g^2\right]\,\mathrm{Tr}\left(Z^3XZ^3X\right)\ , \\
(2,8) &= \mathrm{Tr}\left(Z^6X^2\right) - \left[\cos\left(\frac{\pi}{7}\right)\csc\left(\frac{3\pi}{14}\right) + 1.117057\,g^2\right]\,\mathrm{Tr}\left(Z^5XZX\right) \\
&\quad - \left[\sin\left(\frac{\pi}{14}\right)\csc\left(\frac{3\pi}{14}\right) - 1.023185\,g^2\right]\,\mathrm{Tr}\left(Z^4XZ^2X\right) \\
&\quad + \left[\frac{1}{2}\csc\left(\frac{3\pi}{14}\right) + 0.093872\,g^2\right]\,\mathrm{Tr}\left(Z^3XZ^3X\right)\ , \\
(3,8) &= \mathrm{Tr}\left(Z^6X^2\right) - \left[\csc\left(\frac{\pi}{14}\right)\sin\left(\frac{3\pi}{14}\right) + 3.392947\,g^2\right]\,\mathrm{Tr}\left(Z^5XZX\right) \\
&\quad + \left[\csc\left(\frac{\pi}{14}\right)\cos\left(\frac{\pi}{7}\right) + 8.769849\,g^2\right]\,\mathrm{Tr}\left(Z^4XZ^2X\right) \\
&\quad - \left[\frac{1}{2}\csc\left(\frac{\pi}{14}\right) + 5.376903\,g^2\right]\,\mathrm{Tr}\left(Z^3XZ^3X\right)\ .
\end{aligned}
$$

Note that for convenience, we gave the numerical values of exact expressions in the states shown above. For example, in the last term of $\mathcal{O}_{3,8}$, we have

$$
5.376903 = \sqrt{\frac{9 - 8\cos\left(\frac{\pi}{7}\right) + 8\sin\left(\frac{3\pi}{14}\right)}{44 - 54\cos\left(\frac{\pi}{7}\right) + 78\sin\left(\frac{\pi}{14}\right) - 20\sin\left(\frac{3\pi}{14}\right)}}\ .
$$

All the states written in this appendix consider the vacuum as being Z fields and the excitations as being the X fields. In other words, they are good states for the operator $\mathcal{O}_1$. For the operators $\mathcal{O}_2$ and $\mathcal{O}_3$ we use the same states but with different scalars playing the role of vacuum and excitations, see (5.2).

Having computed the two-loop eigenstates (n, L) and knowing how to write any BPS operator $[N, L]$ with a given length and number of excitations, we provide a list of ratios of one-loop structure constants to tree-level structure constants in table C.1 involving these two kind of operators. These were computed by directly Wick contracting the constituent fields of the operators and inserting the one-loop Hamiltonian (3.2) at the point where we break each operator to be contracted with the other two, see figure 12.2.

$\mathcal{O}_1$	$\mathcal{O}_2$	$\mathcal{O}_3$	r	$\mathcal{O}_1$	$\mathcal{O}_2$	$\mathcal{O}_3$	r
(1,4)	BPS	BPS	-6	(3,8)	BPS	BPS	-9.561263
BPS	BPS	(1,4)	-6	[2, 4]	(3,8)	[0, 4]	-23.396074
(1,5)	BPS	BPS	-4	[4, 4]	(3,8)	[2, 8]	-9.561263
BPS	BPS	(1,5)	-4	[4, 8]	(3,8)	[2, 4]	-9.561263
(1,6)	BPS	BPS	$-11/2+13\sqrt{5}/10$	[3, 5]	(3,8)	[1, 5]	-8.188323
[3, 4]	(1,6)	[1, 4]	$3\sqrt{5}/10-7/2$	[4, 6]	(3,8)	[2, 6]	-8.188323
[4, 5]	(1,6)	[2, 5]	$3\sqrt{5}/10-7/2$	[3, 6]	(3,8)	[1, 4]	-5.330327
BPS	BPS	(1,6)	$-11/2+13\sqrt{5}/10$	[4, 7]	(3,8)	[2, 5]	-5.330327
(2,6)	BPS	BPS	$-11/2-13\sqrt{5}/10$	[4, 5]	(3,8)	[2, 7]	-5.330327
[3, 4]	(2,6)	[1, 4]	$-3\sqrt{5}/10-7/2$	[3, 4]	(3,8)	[1, 6]	-5.330327
[4, 5]	(2,6)	[2, 5]	$-3\sqrt{5}/10-7/2$	BPS	BPS	(3,8)	-9.561263
BPS	BPS	(2,6)	$-11/2-13\sqrt{5}/10$	BPS	(1,4)	(1,4)	-12
(1,7)	BPS	BPS	$-7/4$	[4, 5]	(1,5)	(1,4)	-10
[3, 4]	(1,7)	[1, 5]	-2	(1,4)	[0, 5]	(1,5)	-10
[3, 5]	(1,7)	[1, 4]	-2	[4, 6]	(1,6)	(1,4)	$13\sqrt{5}/10-23/2$
[4, 5]	(1,7)	[2, 6]	-2	(1,4)	[0, 6]	(1,6)	$13\sqrt{5}/10-23/2$
[4, 6]	(1,7)	[2, 5]	-2	[4, 7]	(1,7)	(1,4)	$-31/4$
BPS	BPS	(1,7)	$-7/4$	(1,4)	[0, 7]	(1,7)	$-31/4$
(2,7)	BPS	BPS	$-27/4$	[4, 8]	(1,8)	(1,4)	-7.237755
BPS	BPS	(2,7)	$-27/4$	(1,4)	[0, 8]	(1,8)	-7.237755
(1,8)	[0, 8]	[2, 4]	-1.237755	(1,4)	(1,8)	[0, 4]	5.123727
[2, 4]	(1,8)	[0, 4]	-4.525727	[4, 6]	(2,6)	(1,4)	$-13\sqrt{5}/10-23/2$
[4, 6]	(1,8)	[2, 6]	-1.513645	(1,4)	[0, 6]	(2,6)	$-13\sqrt{5}/10-23/2$
[3, 5]	(1,8)	[1, 5]	-1.513645	[4, 7]	(2,7)	(1,4)	$-51/4$
[3, 4]	(1,8)	[1, 6]	-1.455824	(1,4)	[0, 7]	(2,7)	$-51/4$
[3, 6]	(1,8)	[1, 4]	-1.455824	[4, 8]	(2,8)	(1,4)	-11.200983
[4, 5]	(1,8)	[2, 7]	-1.455824	(1,4)	[0, 8]	(2,8)	-11.200983
[4, 7]	(1,8)	[2, 5]	-1.455824	(1,4)	(2,8)	[0, 4]	-1.554117
[4, 4]	(1,8)	[2, 8]	-1.237755	[4, 8]	(3,8)	(1,4)	-15.561263
[4, 8]	(1,8)	[2, 4]	-1.237755	(1,4)	[0, 8]	(3,8)	-15.561263
BPS	BPS	(1,8)	-1.237755	(1,4)	(3,8)	[0, 4]	-9.293748
(2,8)	[0, 8]	[2, 4]	-5.200983	[4, 4]	(1,5)	(1,5)	-8
[2, 4]	(2,8)	[0, 4]	-10.078199	(1,5)	[0, 6]	(1,5)	-8
[4, 7]	(2,8)	[2, 5]	-7.213849	[4, 5]	(1,6)	(1,5)	$3\sqrt{5}/10-15/2$
[4, 5]	(2,8)	[2, 7]	-7.213849	(1,5)	[0, 7]	(1,6)	$13\sqrt{5}/10-19/2$
[3, 6]	(2,8)	[1, 4]	-7.213849	[4, 6]	(1,7)	(1,5)	-6
[3, 4]	(2,8)	[1, 6]	-7.213849	(1,5)	[0, 8]	(1,7)	$-23/4$
[4, 8]	(2,8)	[2, 4]	-5.200983	[4, 7]	(1,8)	(1,5)	-5.455824
[4, 4]	(2,8)	[2, 8]	-5.200983	[4, 5]	(2,6)	(1,5)	$-3\sqrt{5}/10-15/2$
[3, 5]	(2,8)	[1, 5]	-0.298032	(1,5)	[0, 7]	(2,6)	$-13\sqrt{5}/10-19/2$
[4, 6]	(2,8)	[2, 6]	-0.298032	(1,5)	[0, 8]	(2,7)	$-43/3$
BPS	BPS	(2,8)	-5.200983	[4, 7]	(2,8)	(1,5)	-11.213849

Table C.1: Data for the absolute value of the ratio between the one-loop and tree-level structure constants parametrized by r in $C_{123} = C_{123}^{(0)}\left(1+g^2 r+\mathcal{O}(g^4)\right)$. The notation (n, L) indicates a two-magnon operator with mode number n and length L. The notation $[N, L]$ indicates a BPS operator with N spin flips and total length L. The vacuum and excitation choice for each of the three operators is given in (5.2). When we write BPS we can replace it by any $[N, L]$ with $N \leq 4$ and $L \leq 8$ (such that the three-point function exists); in this case the result is independent of N and L. To make the table easier to read we colored the BPS operators in red and the non-BPS operators in blue. We also colored in green the ratios for configurations with $l_{13} = 0$. For these cases (and only for these cases) the mixing of $\mathcal{O}_2$ with double trace operators should in principle be included [74, 76] (we did not take this effect into account).

Appendix D

Fermionic and Bosonic Dualities

In this appendix we briefly review the fermionic and bosonic dualities that related different sets of the nested Bethe equations. We used the results obtained here in section 11.2. To keep the discussion as general as possible, let us introduce twists into the Bethe equations. Namely:

$$e^{i\tau_a}\left(\frac{u_{a,j}+V_a\frac{i}{2}}{u_{a,j}-V_a\frac{i}{2}}\right)^L = s_a\prod_{b=1}^{r}\frac{Q_b\big(u_{a,j}+M_{a,b}\frac{i}{2}\big)}{Q_b\big(u_{a,j}-M_{a,b}\frac{i}{2}\big)}\,, \tag{D.1}$$

where the Baxter polynomials $Q_a(u)$ were introduced in (11.14). These are the nested equations that we will consider in this appendix. The effect of the twists is to modify the periodic boundary conditions of the chain. Of course, the usual Bethe equations (11.15) are recovered from $\tau_a = 0$.

D.1 Fermionic dualities

Contrary to what happens for usual Lie algebras, the Dynkin diagram and Cartan matrix of a super algebra are not unique. Consider for example the super algebra $su(K|J)$. The different Dynkin diagrams can be identified as the different paths that one can draw on a rectangular lattice of size $K\times J$, starting from the upper-right corner and ending on the lower-left corner. Depending on the type of node that it passes, the path either continues in the same direction (bosonic nodes) or makes a ninety degree turn (fermionic nodes), always approaching the end point of the path. All the different paths are related by fermionic dualities [122, 110]. An important feature regarding these dualities is that when applied to a given node in the Dynkin diagram, the adjacent nodes change from bosonic to fermionic, or viceversa. This is illustrated in figure D.1. The Cartan matrix associated with a specific diagram is given by

$$M_{a,b} = (p_a + p_{a+1})\delta_{a,b} - p_{a+1}\delta_{a+1,b} - p_a\delta_{a,b+1}\,, \tag{D.2}$$

where p_a corresponds to the link between node a and node $a+1$ (see the grey numbers in figure D.1) and is equal to $+1$ (-1) for a vertical (horizontal) link.

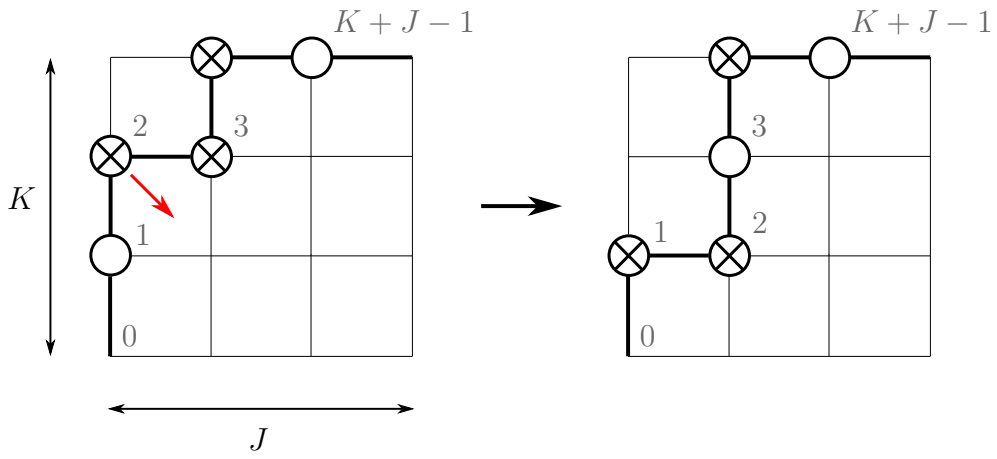

Figure D.1: The Dynkin diagram for $su(K|J)$ is not unique. A given diagram can be drawn in a rectangular lattice of size $K \times J$, starting at (J, K) and ending at $(0, 0)$, always approaching the latter. When passing through a bosonic node, the path continues in the same direction, while a fermionic node makes the path turn 90 degrees. All the different diagrams are related by fermionic dualities [122, 110]. Graphically, the action of a fermionic duality changes a left-down turn into a down-left turn, and viceversa. In our example, a duality was applied to node 2, and as a consequence, the adjacent nodes 1 and 3 changed their nature.

Let us show explicitly how the fermionic dualities work with a specific example: the $SU(3|1)$ spin chain with Dynkin labels $V_a = \delta_{a,1}$. This example is general enough to illustrate all the features of this duality. Suppose we start with the choice of Dynkin diagram shown in figure D.2a. The corresponding Bethe equations are given by (D.1):

$$e^{i\tau_1}\left(\frac{u+i/2}{u-i/2}\right)^L = -\frac{Q_1^{++}Q_2^-}{Q_1^{--}Q_2^+}\bigg|_{u=u_{1,j}},$$

$$e^{i\tau_2} = \frac{Q_1^-Q_3^+}{Q_1^+Q_3^-}\bigg|_{u=u_{2,j}}, \qquad e^{i\tau_3} = \frac{Q_2^+}{Q_2^-}\bigg|_{u=u_{3,j}}, \tag{D.3}$$

where we are omitting the argument of the Baxter polynomials, so that $Q_a^\pm$ should be understood as $Q_a(u \pm i/2)$, see (11.19). We will apply a fermionic duality to the second node in the diagram.[66] To do so, notice that the second set of equations (D.3) are equivalent to the following polynomial equation:

$$e^{-i\tau_2/2}Q_1^-Q_3^+ - e^{i\tau_2/2}Q_1^+Q_3^-\Big|_{u=u_{2,j}} = 0\,. \tag{D.4}$$

By definition, some of the zeros of this equation are the roots $u_{2,j}$, which are neatly packaged

[66]For simplicity, throughout this appendix we will only apply fermionic and bosonic dualities to non-momentum-carrying nodes. Taking into account some subtelties, they can also be applied to massive nodes, see [122, 125].

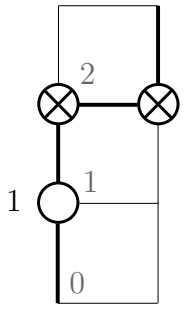

$$M_{a,b} = \begin{pmatrix} 2 & -1 & 0 \\ -1 & 0 & 1 \\ 0 & 1 & 0 \end{pmatrix}$$

(a)

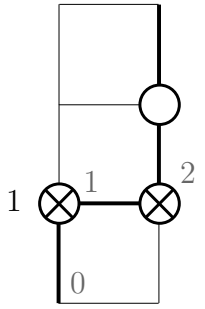

$$M_{a,b} = \begin{pmatrix} 0 & 1 & 0 \\ 1 & 0 & -1 \\ 0 & -1 & 2 \end{pmatrix}$$

(b)

Figure D.2: Two possible choice of Dynkin diagram for an $SU(3|1)$ spin chain. The black label 1 denotes the non-zero Dynkin label. The Cartan matrices are given by (D.2). The diagram in (b) is obtained from the first one after applying a fermionic duality on the second node.

in the Baxter function Q_2. Therefore, we can write:

$$e^{i\tau_2/2}Q_1^+Q_3^- - e^{-i\tau_2/2}Q_1^-Q_3^+ = 2i\sin\left(\frac{\tau_2}{2}\right)Q_2\tilde{Q}_2\,. \tag{D.5}$$

The polynomial on the l.h.s. has degree $N_1 + N_3$, such that

$$\tilde{Q}_2(u) \equiv \prod_{j=1}^{\tilde{N}_2}(u - \tilde{u}_{2,j})\,,$$

with $\tilde{N}_2 = N_1 + N_3 - N_2$. This Baxter function defines the position of a new set of dual Bethe roots $\tilde{u}_{2,j}$. From now on, we will use a tilde to denote objects obtained after applying a duality.

It is now straightforward to shift the argument of (D.5) by $\pm i/2$ to obtain the following equations:

$$-e^{i\tau_2}\frac{Q_1^{++}}{Q_1^{--}} = \frac{Q_2^+\tilde{Q}_2^+}{Q_2^-\tilde{Q}_2^-}\Big|_{u=u_{1,j}}, \qquad -e^{-i\tau_2}\frac{Q_3^{++}}{Q_3^{--}} = \frac{Q_2^+\tilde{Q}_2^+}{Q_2^-\tilde{Q}_2^-}\Big|_{u=u_{3,j}}.$$

We can use these expressions and plug them into the original Bethe equations (D.3) to obtain a new nested system:

$$e^{i(\tau_1+\tau_2)}\left(\frac{u+i/2}{u-i/2}\right)^L = \frac{\tilde{Q}_2^+}{\tilde{Q}_2^-}\Big|_{u=u_{1,j}},$$

$$e^{-i\tau_2} = \frac{Q_1^+Q_3^-}{Q_1^-Q_3^+}\Big|_{u=\tilde{u}_{2,j}}, \qquad e^{i(\tau_3+\tau_2)} = -\frac{\tilde{Q}_2^-Q_3^{++}}{\tilde{Q}_2^+Q_3^{--}}\Big|_{u=u_{3,j}}, \tag{D.6}$$

One can readily check that these are precisely the Bethe equations corresponding to the choice of Cartan matrix shown in figure D.2b. As we anticipated, by applying a fermionic duality to the second node, the first node is now fermionic, while the third one turned into a bosonic node.

The procedure we just explained is quite general and can be applied to any non-massive fermionic node a in a given Dynkin diagram. The starting point is always to write the equivalent to equation (D.5):

$$e^{i\tau_a/2}Q^+_{a-1}Q^-_{a+1} - e^{-i\tau_a/2}Q^-_{a-1}Q^+_{a+1} = 2i\sin\left(\frac{\tau_a}{2}\right)Q_a\tilde{Q}_a$$

and manipulate it just as we did above. Of course, $Q_{a\pm1}$ may be absent from this equation, depending on the position of node a in the Dynkin diagram. For example, if we apply the duality to the third node in figure D.2a, the above equation would read $e^{i\tau_3/2}Q^+_2 - e^{-i\tau_3/2}Q^-_2 = 2i\sin\left(\frac{\tau_3}{2}\right)Q_3\tilde{Q}_3$.

D.2 Bosonic dualities

The other important duality obeyed by the nested Bethe equations are the so-called bosonic dualities, first introduced in [125]. As their name suggests, these are applied to bosonic nodes in the Dynkin diagram. In this case, there is no nice diagrammatic interpretation like there was for fermionic dualities, see figure D.1. Therefore, let us go straight to the equations. We will consider an $SU(4)$ spin chain with $V_a = \delta_{a,1}$. Again, this example is general enough to illustrate all the features of this duality. The Cartan matrix is

$$M_{a,b} = \begin{pmatrix} 2 & -1 & 0 \\ -1 & 2 & -1 \\ 0 & -1 & 2 \end{pmatrix},$$

so that the corresponding Bethe equations are

$$e^{i\tau_1}\left(\frac{u+\frac{i}{2}}{u-\frac{i}{2}}\right)^L = -\left.\frac{Q_1^{++}Q_2^-}{Q_1^{--}Q_2^+}\right|_{u=u_{1,j}},$$

$$e^{i\tau_2} = -\left.\frac{Q_1^-Q_2^{++}Q_3^-}{Q_1^+Q_2^{--}Q_3^+}\right|_{u=u_{2,j}}, \tag{D.7}$$

$$e^{i\tau_3} = -\left.\frac{Q_2^-Q_3^{++}}{Q_2^+Q_3^{--}}\right|_{u=u_{3,j}}. \tag{D.8}$$

We want to apply a bosonic duality to the second node. In order to do so, we consider the following equation [125]:

$$2i\sin\left(\frac{\tau_2}{2}\right)Q_1Q_3 = e^{i\tau_2/2}Q_2^-\tilde{Q}_2^+ - e^{-i\tau_2/2}Q_2^+\tilde{Q}_2^- \,, \tag{D.9}$$

which defines a new set of Bethe roots $\tilde{u}_{2,j}$:

$$\tilde{Q}_2(u) \equiv \prod_{j=1}^{\tilde{N}_2}(u-\tilde{u}_{2,j})\,,$$

with $\tilde{N}_2 = N_1 + N_3 - N_2$. We can now do a couple of things. First, we shift the argument of (D.9) by $\pm i/2$ and evaluate the resulting equations at $u = \tilde{u}_{2,j}$. Second, we can directly evaluate (D.9) at $u = u_{1,j}, u_{3,j}$. The equations we obtain are

$$e^{-i\tau_2} = -\frac{Q_1^-\tilde{Q}_2^{++}Q_3^-}{Q_1^+\tilde{Q}_2^{--}Q_3^+}\Big|_{u=\tilde{u}_{2,j}}\,, \qquad e^{-i\tau_2}\frac{\tilde{Q}_2^-}{\tilde{Q}_2^+} = \frac{Q_2^-}{Q_2^+}\Big|_{u=u_{1,j},u_{3,j}}\,.$$

Combining the above equations with the original $SU(4)$ Bethe equations (D.7), we obtain the following new nested system:

$$\begin{aligned} e^{i(\tau_1+\tau_2)}\left(\frac{u+\frac{i}{2}}{u-\frac{i}{2}}\right)^L &= -\frac{Q_1^{++}\tilde{Q}_2^-}{Q_1^{--}\tilde{Q}_2^+}\Big|_{u=u_{1,j}}\,, \\ e^{-i\tau_2} &= -\frac{Q_1^-\tilde{Q}_2^{++}Q_3^-}{Q_1^+\tilde{Q}_2^{--}Q_3^+}\Big|_{u=\tilde{u}_{2,j}}\,, \qquad \text{(D.10)} \\ e^{i(\tau_3+\tau_2)} &= -\frac{\tilde{Q}_2^-Q_3^{++}}{\tilde{Q}_2^+Q_3^{--}}\Big|_{u=u_{3,j}}\,. \qquad \text{(D.11)} \end{aligned}$$

We see that, as opposed to the fermionic ones, a bosonic duality applied to a node a does not change the nature of the adjacent nodes $a-1$ and $a+1$ in the Dynkin diagram.

Again, the procedure we just explained is quite general and can be applied to any non-massive bosonic node a in a given Dynkin diagram. The starting point is always to write the equivalent to equation (D.9) and manipulate it just like we did above. Of course, $Q_{a\pm1}$ may be absent from this equation, depending on the position of node a in the Dynkin diagram.

Appendix E

Mathematica Codes

In this appendix we provide the Mathematica codes for computing the three- and four-point functions described in the main text. In both cases we implement the brute force and integrability-based formulas, giving some explicit examples on how to use the codes. With some slight modifications of the code presented below, equation (6.8) can be implemented in a similar manner, but we leave that to the interested reader. Also, we refer to section 7 of [107] to see how to find the positions of a very large number of Bethe roots.

E.1 General formulas

Useful functions

```
Le=Length;
n[0]=0; m[0]=0;
f[u_]=1+I/u; g[u_]=I/u; h[u_]=f[u]/g[u]; t[u_]=g[u]^2/f[u];
f[l1_List,l2_List]:=Product[f[l1[[j1]]-l2[[j2]]],{j1,Le[l1]},{j2,Le[l2]}]
h[l1_List,l2_List]:=Product[h[l1[[j1]]-l2[[j2]]],{j1,Le[l1]},{j2,Le[l2]}]
fs[l1_List]:=Product[f[l1[[j1]]-l1[[j2]]],{j1,Le[l1]},{j2,j1+1,Le[l1]}]
gs[l1_List]:=Product[g[l1[[j1]]-l1[[j2]]],{j1,Le[l1]},{j2,j1+1,Le[l1]}]
fb[l1_List]:=Product[f[l1[[j1]]-l1[[j2]]],{j1,Le[l1]},{j2,j1-1}]
gb[l1_List]:=Product[g[l1[[j1]]-l1[[j2]]],{j1,Le[l1]},{j2,j1-1}]
gp[l_List]:=Times@@g[l+I/2]; gm[l_List]:=Times@@g[l-I/2]
e[l_List]:=Times@@((l+I/2)/(l-I/2))
Dvd[ls_List]:=({Complement[ls,#],#}&)/@Subsets[ls,{0,Le[ls]}];
BPS[N_]:=Table[10^(10+j),{j,N}];
Prn[a_]:=(NotebookDelete[prntmp];prntmp=PrintTemporary[a];);
BPlot[l_]:=ListPlot[{Re[#],Im[#]}&/@l];
```

Two-cut $SU(2)$ Bethe equations (3.16)

```
BAE[N_,L_]:=Block[{j,k},Table[((u[j]+I/2)/(u[j]-I/2))^L
```

```
==-Product[(u[j]-u[k]+I)/(u[j]-u[k]-I),{k,1,N}],{j,N}]];
BetheRoots[M_,N_,Lf_,Li_,m_,n_]:=Block[{u,u0,L=Li},
u0=Join[Li/(2*Pi*m)+(I*Sqrt[2*Li]*zk)/(2*Pi*m)/.NSolve[HermiteH[M,zk]==0,zk],
Li/(2*Pi*n)+(I*Sqrt[2*Li]*zk)/(2*Pi*n)/.NSolve[HermiteH[N,zk]==0,zk]];
Do[u0=Table[u[k],{k,M+N}]/.FindRoot[BAE[M+N,L],Table[{u[k],u0[[k]]},
{k,M+N}],WorkingPrecision->100,AccuracyGoal->10];Prn[L],{L,Li,Lf,-1/2}];u0];
```

Let us show how to use this code to find the Bethe roots of an operator dual to the folded string with unit mode number considered in chapters 7 and 8. For example, to obtain the roots represented by the big blue bullets in figure 7.1, we would simply run

```
M=14; L=42;
roots=BetheRoots[M/2,M/2,L,L+10,1,-1];
BPlot@(roots/L)
```

$SU(2)$ wave functions

```
Off[Det::matsq];
S[x_,y_]:=(x-y+I)/(x-y-I)
Wave[l_List]:=Block[{p=Permutations[Range[Le[l]]],i,j},Sum[A[p[[i]]]
Product[((l[[p[[i,j]]]]+I/2)/(l[[p[[i,j]]]]-I/2))^n[j],{j,1,Le[l]}],{i,1,Le[p]}]
//.{A[{a___,b_,c_,d___}]:>S[l[[b]],l[[c]]]A[{a,c,b,d}]/;b>c}
/.{A[a___]:>1/;a==Range[Le[a]]}];
```

Norm of Bethe eigenstates (4.19)

```
dphi[L_,l_List]:=Det@Table[-If[i==j,L/(l[[i]]^2+1/4)-Sum[2/((l[[i]]-l[[k]])^2+1),
{k,Le[l]}],0]-2/(1+(l[[i]]-l[[j]])^2),{i,Le[l]},{j,Le[l]}]/.Det[{}]->1
normdet[L_,l_List]:=Block[{inf,fin,onlyfin},inf=Select[l,Abs[#]>10^8&];
If[inf=={},fin=l,fin=Select[l,MemberQ[inf,#]==False&]];
onlyfin=(fb[fin]dphi[L,fin])/(fb[Conjugate[fin]]gp[fin]gm[fin]);
If[inf=={},onlyfin,(((L-2Le[fin])!Le[inf]!)onlyfin)/(L-2Le[fin]-Le[inf])!]]
```

Norm of Bethe states by brute force (5.5)

```
normbf[L_,l_List]:=Sum[(Wave[l]/.Complex[a_,b_]->a-b I)Wave[l],
Evaluate[Sequence@@Table[{n[j],n[j-1]+1,L},{j,Le[l]}]]]
```

Note that the norm of Bethe eigenstates can be computed by brute force using `normbf`, as in (5.5), or using `normdet`, which is just the implementation of (4.19). In practice, we choose to use the latter as it is computationally much more efficient to compute a determinant than performing the sums involved in (5.5).

New recursion relation for $SU(2)$ scalar products (4.25)

```
AtoC[u_List,v_List,L_]:=Block[{a,d,f,g,z},a[z_]=(z+I/2)^L;d[z_]=(z-I/2)^L;
f[z_]=(z+I)/z;g[z_]=I/z;(1/(Times@@g[u+I/2]Times@@g[v-I/2]
Times@@a[v] Times@@d[u]))(1/(Product[f[u[[j1]]-u[[j2]]],{j1,Le[u]},
{j2,j1+1,Le[u]}]Product[f[v[[j1]]-v[[j2]]],{j1,Le[u]},{j2,j1-1}]))]

NewrecAl[u_,v_,L_]:=NewrecAl[u,v,L]=Module[{N=Le[u],n,i,j,a,d,z,f,g,n1,n2},
a[z_]=(z+I/2)^L; d[z_]=(z-I/2)^L; f[z_]=(z+I)/z; g[z_]=I/z;
Sum[g[u[[1]]-v[[n]]](Product[If[j!=n,f[u[[1]]-v[[j]]],1],{j,1,N}]
Product[If[j!=n,f[v[[j]]-v[[n]]],1],{j,1,N}]a[v[[n]]]d[u[[1]]]-
Product[If[j!=n,f[v[[j]]-u[[1]]],1],{j,1,N}]
Product[If[j!=n,f[v[[n]]-v[[j]]],1],{j,1,N}]a[u[[1]]]d[v[[n]]])
NewrecAl[Drop[u,1],Drop[v,{n}],L],{n,1,N}]-
If[Le[v]==1,0,Sum[(g[u[[1]]-v[[n1]]]g[u[[1]]-v[[n2]]])
(Product[f[v[[n1]]-j]f[j-v[[n2]]],{j,Join[Take[v,n1-1],
Take[v,{n1+1,n2-1}],Take[v,{n2+1,Le[v]}]]}]f[v[[n1]] - v[[n2]]]
a[v[[n2]]]d[v[[n1]]]+Product[f[j-v[[n1]]]f[v[[n2]]-j],
{j,Join[Take[v,n1-1],Take[v,{n1+1,n2-1}],
Take[v,{n2+1,Le[v]}]]}]f[v[[n2]]-v[[n1]]]a[v[[n1]]]d[v[[n2]]])
NewrecAl[Drop[u,1],Join[{u[[1]]},Join[Take[v,n1-1],Take[v,{n1+1,n2-1}],
Take[v,{n2+1,Le[v]}]]],L],{n2,2,N},{n1,1,n2-1}]]]
NewrecAl[{},{},L_]=1;
SProduct[u_List,v_List,L_]:=AtoC[u,v,L]NewrecAl[u,v,L]
```

Note that `NewrecAl` is the implementation of the new recursion relation in the algebraic basis, while `AtoC` is the scalar product conversion factor between the algebraic and coordinate bases shown in (A.3).

$\mathscr{A}(l|\{u\})$, $\mathscr{B}_j$ and $\mathscr{C}(l|\{u\},\{v\})$ from section 5.5

```
sign[a_List,ab_List,v_List]:=Signature[Join[a,ab]]Signature[v]
dett[l1_List,l2_List]:=Det@Table[t[l1[[i]]-l2[[j]]],{i,Le[l1]},
{j,Le[l2]}]/.Det[{}]->1
A[L_,ls_List]:=Block[{dv=Dvd[ls],al,alb},Sum[al=dv[[i,1]];
alb=dv[[i,2]];(-1)^Le[al]f[al,alb]/e[al]^L,{i,Le[dv]}]];
B[L_,N_,l_List]:=gm[l]fs[l]Sqrt[fb[l]dphi[L,l]Binomial[L-2Le[l],N-Le[l]]
/(fb[Conjugate[l]]L)]/Sqrt[gp[l]gm[l]]
T[n_,u_List,v_List]:=Block[{dv=Dvd[v],du=Dvd[u],al,alb,be,beb},gs[u]gb[v]Sum[
al=dv[[i,1]];alb=dv[[i,2]];be=du[[j,1]];beb=du[[j,2]];If[Le[al]==Le[be]&&
Le[alb]==Le[beb],sign[al,alb,v]sign[be,beb,u]dett[be,al]dett[alb,beb]e[beb]^n
e[al]^n h[be,al]h[alb,beb]h[be,beb]h[alb,al],0],{i,Le[dv]},{j,Le[du]}]]
```

E.2 Three-point functions

Brute force formula (5.3)

```
C123[L1_,N1_,L2_,N2_,L3_,N3_,l1_List,l2_List,l3_List]:=
Block[{i,j,psis,norms,limits},
psis=(Wave[l1]/.n[j_]:>L1-N3+j-N2/;j>N2)
(Wave[l2]/.n[j_]->L2+1-n[N2-j+1])(Wave[l3]/.n[j_]->j);
norms=normdet[L1,l1]normdet[L2,l2]normdet[L3,l3];
limits=Sequence@@Table[{n[j],n[j-1]+1,L1-N3},{j,N2}];
Sqrt[L1 L2 L3/norms]If[limits===Sequence[],psis,Sum[psis,limits]]]
```

Integrability-based formulas from table 5.1

```
Cooo[L1_,N1_,L2_,N2_,L3_,N3_]:=(Binomial[L1-N1+N2,N2]/
(B[L1,N1,{}]B[L2,N2,{}]B[L3,N3,{}]))
Cxoo[L1_,N1_,L2_,N2_,L3_,N3_,l1_List]:=(Binomial[L1-N1+N2-Le[l1],N2]
A[N1-N2,l1]/(B[L1,N1,l1]B[L2,N2,{}]B[L3,N3,{}]))
Coxo[L1_,N1_,L2_,N2_,L3_,N3_,l2_List]:=(Binomial[L1-N1+N2-Le[l2],N2-Le[l2]]
A[L1-N1+N2,l2]/(B[L1,N1,{}]B[L2,N2,l2]B[L3,N3,{}]))
Coox[L1_,N1_,L2_,N2_,L3_,N3_,l3_List]:=(Binomial[L1-N1+N2,N2]
A[N1-N2,l3]/(B[L1,N1,{}]B[L2,N2,{}]B[L3,N3,l3]))
Coxx[L1_,N1_,L2_,N2_,L3_,N3_,l2_List,l3_List]:=(Binomial[L1-N1+N2-Le[l2],N2-Le[l2]]
A[L1-N1+N2,l2]A[N1-N2,l3]/(B[L1,N1,{}]B[L2,N2,l2]B[L3,N3,l3]))
Cxox[L1_,N1_,L2_,N2_,L3_,N3_,l1_List,l3_List]:=(Binomial[L1-N1+N2-Le[l1],N2]
A[N1-N2,l1]A[N1-N2,l3]/(B[L1,N1,l1]B[L2,N2,{}]B[L3,N3,l3]))
Cxxo[L1_,N1_,L2_,N2_,L3_,N3_,l1_List,l2_List]:=(dv=Dvd[l1];
Sum[al=dv[[i,1]];alb=dv[[i,2]];If[Le[al]==N1-N2,e[al]^L1 f[alb,al]A[N1-N2,al]
T[L1-N1+N2,alb,l2],0],{i,Le[dv]}]/(B[L1,N1,l1]B[L2,N2,l2]B[L3,N3,{}]))
Cxxx[L1_,N1_,L2_,N2_,L3_,N3_,l1_List,l2_List,l3_List]:=(A[N1-N2,l3]B[L3,N3,{}]
Cxxo[L1,N1,L2,N2,L3,N3,l1,l2]/B[L3,N3,l3])
```

As determinants 5.21

```
normdet2[L_,u_List]:=Product[If[i==j,1,f[u[[i]]-u[[j]]]],{i,1,Le[u]},
{j,1,Le[u]}]dphi[L,u];
F[u_List,v_List,w_List,N3_]:=(Times@@((u+I/2)^N3)Times@@((w+I/2)^N3))/
(Product[u[[j]]-u[[i]],{i,1,Le[u]},{j,i+1,Le[u]}]
Product[v[[i]]-v[[j]],{i,1,Le[v]},{j,i+1,Le[v]}]
Product[w[[i]]-w[[j]],{i,1,Le[w]},{j,i+1,Le[w]}]);
Z[w_List]:=Table[(1/(j-1)!)D[I/((w[[i]]-theta+I/2)
(w[[i]]-theta-I/2)),{theta,j-1}]/.theta->0,{i,Le[w]},{j,Le[w]}];
RS[L1_,u_List,v_List]:=Block[{N1=Le[u],N2=Le[v]},
Table[If[j<=N2,(I/(u[[i]]-v[[j]]))(((v[[j]]+I/2)/(v[[j]]-I/2))^L1
```

```
Product[If[k==i,1,u[[k]]-v[[j]]+I],{k,1,N1}]-
Product[If[k==i,1,u[[k]]-v[[j]]-I],{k,1,N1}]),
(1/(j-N2-1)!)D[(I/((u[[i]]-theta+I/2)(u[[i]]-theta-I/2)))
Product[1/(v[[k]]-theta-I/2),{k,1,N2}],{theta,j-N2-1}]
/.theta->0],{i,N1},{j,N1}]];
C123det[L1_,L2_,L3_,u_List,v_List,w_List]:=(Sqrt[L1 L2 L3]/Sqrt[normdet2[L1,u]
normdet2[L2,v]normdet2[L3,w]])F[u,v,w,Le[w]]Det[Z[w]]Det[RS[L1,u,v]];
```

Ratio r_{123} for the numerical match of chapter 8

```
r123[L1_,N1_,L2_,N2_,L3_,N3_,u_List,v_List]:=(Sqrt[Binomial[L1,N1]Binomial[L2,N2]]
F[u,v,{},N3]Det[RS[L1,u,v]])/(Sqrt[normdet2[L1,u]normdet2[L2,v]]Binomial[L1-N3,N2]);
```

Examples

Let us show how to use the code above to compute the most general case $C_{123}^{\bullet\bullet\bullet}$ in table 5.1 for some three-point function configuration. In this example, the sets of rapidities `us`, `vs`, `ws` satisfy the Bethe equations of operators $\mathcal{O}_1$, $\mathcal{O}_2$ and $\mathcal{O}_3$, respectively, with the lengths and number of excitations indicated in each case. Evaluating

```
L1=9;N1=4;L2=9;N2=2;L3=4;N3=2;
us={0.414080361016-0.993048580811 I,0.409292874229,
    0.414080361016+0.993048580811 I,-0.131911999475};
vs={-0.207106781187,0.207106781187};
ws={-0.288675134595,0.288675134595};
Abs@C123[L1,N1,L2,N2,L3,N3,us,vs,ws]
Abs@Cxxx[L1,N1,L2,N2,L3,N3,us,vs,ws]
Abs@C123det[L1,L2,L3,us,vs,ws]
```

we obtain a perfect match between the brute force computation (5.3), the analytic prediction of table 5.1 and the determinant formula for three-point functions (5.21). For these values of the Bethe roots we find

$$|C_{123}^{\bullet\bullet\bullet}| = 0.480198\,.$$

We can also use the codes above to get analytic results. For example, to reproduce $C_{123}^{\circ\bullet\circ}$ for the case of two magnons $N_2 = 2$, see equation (5.11), we would simply run

```
ClearAll[L1,N1,L2,N2,L3,N3]
fsi=FullSimplify[#,{0<p<\[Pi]/2}]&;
fsi2=#//.{Exp[a_]-Exp[b_]:>Exp[(a+b)/2]2Sinh[(a-b)/2//fsi],
Exp[a_]-1:>Exp[a/2]2Sinh[a/2//fsi],Exp[a_]:>Exp[a//fsi]}&;
fsi@Coxo[L1,N3+2,L2,2,L3,N3,{u,-u}]/.u->Cot[p/2]/2//TrigToExp//Factor//fsi//fsi2
```

Finally, we can compute the ratio $r_{123} = C_{123}^{\bullet\bullet\circ}/C_{123}^{\circ\circ\circ}$ considered in chapter 8. For simplicity, the discussion in this appendix refers to the case when all roots in the heavy operators are

finite. After some slight modifications, the codes given in this appendix can (and were) used to compute the cases when some roots are at infinity. For example, if we wanted to reproduce the third point for $\alpha = 1/4$ in figure 8.1, we would simply run

```
us={-2.8928215931306757460+1.2863414912352617840 I,-3.0063106400693221845,
    -2.8928215931306757460-1.2863414912352617840 I,2.8928215931306757460-
    1.2863414912352617840 I,3.0063106400693221845,2.8928215931306757460+
    1.2863414912352617840 I};
vs={-3.2898499173796199229+0.7760278937943849641 I,-3.2898499173796199229-
    0.7760278937943849641 I,3.2898499173796199229-0.7760278937943849641 I,
    3.2898499173796199229+0.7760278937943849641 I};
Abs@r123[24,6,24,4,4,2,us,vs]
```

to obtain

$$r_{123} = 0.919415219\,.$$

The roots `us` and `vs` were found using the function `BetheRoots` that we introduced above, which finds the Bethe roots with 100 digits of precision. However, here we are only showing their first 20 decimal places, which is why the result for r_{123} shown here has only a few digits compared to the one in section 8.1.1. As we mentioned in the main text, the determinant form of the three-point function is very efficient from a computational point of view. It allowed us to compute many more points of data for the numerical match of section 8.1.1 compared to the number of points originally considered in [40].

E.3 Four-point functions

Brute force formula (6.2)

```
C1234bf[L1_,N1_,L2_,N2_,L3_,N3_,L4_,N4_,l1_List,l2_List,l3_List,l4_List]:=
Block[{j,k,psis,norms,lim,lim2},psis[r_,s_]:=(Wave[l1]/.{n[j_]:>r+j-s/;s<j<=s+N4,
n[k_]:>N4+r+m[k-s-N4]/;s+N4<k<=N1-N3,n[q_]:>L1+q-N1/;q>N1-N3})
(Wave[l2]/.{n[k_]:>L2-(L4-N4+r+m[N1-N3-N4-s-k+1])+1/;k<=N1-(N3+N4+s),
n[j_]:>L2-n[N1-(N3+N4)-j+1]+1/;j>N1-(s+N3+N4)})(Wave[l3]/.n[j_]->j)
(Wave[l4]/.n[j_]->L4-N4+j);
norms=normdet[L1,l1]normdet[L2,l2]normdet[L3,l3]normdet[L4,l4];
lim[s_,r_]:=Sequence@@Table[{n[j],n[j-1]+1,r},{j,s}];
lim2[s_,r_]:=Sequence@@Table[{m[k],m[k-1]+1,L1-N3-N4-r},{k,N1-N3-N4-s}];
Sqrt[L1 L2 If[L3==0,1,L3]If[L4==0,1,L4]/norms]
Sum[Sum[If[L3==0 || L4==0,1/(L1-N3-N4+1),1]psis[r,s],lim2[s,r],lim[s,r]],
{r,0,L1-N3-N4},{s,0,Min[r,N1-N3-N4]}]]
```

Integrability-based formula (6.5)

```
C1234int[le_,L1_,N1_,L2_,N2_,L3_,N3_,L4_,N4_,l1_List,l2_List,l3_List,l4_List]:=
```

```
Block[{a1,a1b,a2,a2b,a3,a3b,b1,b1b,b2,b2b,b3,b3b,dv1,dv2,dv3,dv4,norms},
dv1=Dvd[l1]; dv2=Dvd[l2];
norms=normdet[L1, l1]normdet[L2, l2]normdet[L3,l3]normdet[L4,l4];
Sqrt[(L1 L2 If[L3==0,1,L3]If[L4==0,1,L4])/norms]
Sum[If[L4==0||L3==0,1/(L1-N3-N4+1),1](a1=dv1[[i,1]];a1b=dv1[[i,2]];
b2=dv2[[j,1]];b2b=dv2[[j,2]];If[Le[a1]==Le[b2b],dv3=Dvd[a1b];
Sum[a2=dv3[[k,1]];a2b=dv3[[k,2]];If[Le[a2]==N4,dv4=Dvd[a2b];Sum[a3=dv4[[l,1]];
a3b=dv4[[l,2]];If[Le[a3b]==N3&&Le[a3]==Le[b2],(1/(fs[l1]fs[l2]))
e[a1b]^(L1-N3-N4-le)e[a2b]^N4 e[a3b]^(N3+le+1)e[l2]^(L3-N3+le+1)
e[b2b]^(L2-L3+N3-le)e[l4]^(L4+1)f[a1,a1b]fs[a1]f[a2,a2b]fs[a2]f[a3,a3b]fb[a3b]
fs[a3]f[b2,b2b]fb[b2]fb[b2b](fb[l4]/fs[l4])SProduct[a3,b2,le]
SProduct[a1,b2b,L1-N3-N4-le]SProduct[a2,l4,N4]SProduct[l3,a3b,N3],0],
{l,1,Le[dv4]}],0],{k,1,Le[dv3]}],0]),{i,1,Le[dv1]},{j,1,Le[dv2]}]];
C1234int[L1_,N1_,L2_,N2_,L3_,N3_,L4_,N4_,l1_List,l2_List,l3_List,l4_List]:=
(temp[le_]=C1234int[le,L1,N1,L2,N2,L3,N3,L4,N4,l1,l2,l3,l4];Sum[temp[le],
{le,0,L1-N3-N4}])
```

Examples

Let us now show how to use the code to compute four-point functions. Note that the functions `C1234bf` and `C1234int` can be used to compute any four-point function obeying the setup of figure 6.1. In the examples below, `us`, `vs`, `ws` and `zs` are the Bethe roots of operators $\mathcal{O}_1$, $\mathcal{O}_2$, $\mathcal{O}_3$ and $\mathcal{O}_4$, respectively, for the charges indicated in each case. Let us consider first an example in which all four operators are non-BPS. Running the following code

```
L1=12;N1=6;L2=12;N2=2;L3=4;N3=2;L4=4;N4=2;
us={0.676245041405-0.993633391204 I,0.678017442247,0.676245041405+0.993633391204 I,
-0.676245041405+0.993633391204 I,-0.678017442247,-0.676245041405-0.993633391204 I};
vs={1.702843619444,-1.702843619444};
ws={0.288675134594,-0.288675134594};
zs={0.288675134594,-0.288675134594};
C1234bf[L1,N1,L2,N2,L3,N3,L4,N4,us,vs,ws,zs]
C1234int[L1,N1,L2,N2,L3,N3,L4,N4,us,vs,ws,zs]
```

we obtain a perfect agreement between the brute force computation and the integrability-based formula, giving

$$C_{1234}^{\bullet\bullet\bullet\bullet} = 1.28031 - 0.66373\, i\,.$$

As we mentioned in the main text of the paper, the integrability-based formula is computationally much faster than the brute force formula. This can be checked in Mathematica for the example above by simply using the function `AbsoluteTiming` when executing `C1234bf` and `C1234int`. The result is that the former takes 18 seconds to compute, while the latter only takes 1 second! Of course, the gain in efficiency is even more notorious as we increase the length and number of excitations of each operator in the four-point function.

Now, let us consider a case in which $\mathcal{O}_3$ and $\mathcal{O}_4$ are BPS operators and compute the ratio $r_{1234} = C^{\bullet\bullet\circ\circ}_{1234}/(C^{\circ\circ\circ}_{123}C^{\circ\circ\circ}_{124})$. The following configuration corresponds to the second point of data for $\alpha = 1/3$ used in section 8.2. Running

```
L1=18;N1=6;L2=18;N2=2;L3=4;N3=2;L4=4;N4=2;
us={1.892118528217-1.114121041954 I,1.976939483361,1.892118528217+1.114121041954 I,
-1.892118528217+1.114121041954 I,-1.976939483361,-1.892118528217-1.114121041954 I};
vs={2.674763752754,-2.674763752754};
ws={10^10,10^15};
zs={10^11,10^16};
r=Abs@C1234int[L1,N1,L2,N2,L3,N3,L4,N4,us,vs,ws,zs]/
  (Cooo[L1,N1,L2,N2+N4,L3,N3]Cooo[L1,N1,L2,N2+N3,L4,N4])//FullForm
```

we obtain

$$r_{1234} = 0.6540088550\,,$$

which is exactly the second blue bullet plotted in figure 8.3.

Note that when some of the operators in the four-point function are BPS, it is computationally more efficient to replace the appropriate general scalar products `SProduct` (which compute formula (A.5)) appearing in `C1234int` by a function that implements the scalar product between a Bethe state and a BPS state (4.20).

Appendix F

Copyright Agreements

Jorge Escobedo <jescob@gmail.com>

Permission request for my PhD Thesis

Jorge Escobedo <jescob@gmail.com> Sat, Mar 24, 2012 at 11:28 PM
To: Pedro Vieira <pedrogvieira@gmail.com>, Nikolay Gromov <nikgromov@gmail.com>, Amit Sever <amit.sever@gmail.com>, Joao Caetano <joao.caetanus@gmail.com>

Hi all,

I'm writing to you to request permission to use the following papers that we co-authored in my PhD thesis:

Authors: J. Escobedo, N. Gromov, A. Sever and P. Vieira
Title: Tailoring three-point functions and integrability
Published in JHEP 1109 (2011) 028
arXiv: 1012.2475

Authors: J. Escobedo, N. Gromov, A. Sever and P. Vieira
Title: Tailoring three-point functions and integrability II
Published in JHEP 1109 (2011) 029
arXiv: 1104.5501

Authors: J. Escobedo and J. Caetano
Title: On four-point functions and integrability in N=4 SYM: from weak to strong coupling
Published in JHEP 1109 (2011) 080
arXiv: 1107.5580

Best,
Jorge

Jorge Escobedo <jescob@gmail.com>

Permission request for my PhD Thesis

Pedro Vieira <pedrogvieira@gmail.com> Sun, Mar 25, 2012 at 10:42 AM
To: Jorge Escobedo <jescob@gmail.com>

Sure
p

Jorge Escobedo <jescob@gmail.com>

Permission request for my PhD Thesis

Nikolay Gromov <nikgromov@gmail.com> Sun, Mar 25, 2012 at 10:31 AM
To: Jorge Escobedo <jescob@gmail.com>
Cc: Pedro Vieira <pedrogvieira@gmail.com>, Amit Sever <amit.sever@gmail.com>, Joao Caetano <joao.caetanus@gmail.com>

Dear Mr. Jorge Escobedo,

By this letter I would like to let you know
that I would be the most happy if these
fruitful results would become a part of your
forthcoming fascinating thesis.

Sincerely yours,
Dr. Nikolay Gromov
Telephone: +44 020 7848 2149
Email: nikolay.gromov@kcl.ac.uk
Office: S5.27, Strand Building, Strand Campus
Research Group: Theoretical Physics

Jorge Escobedo <jescob@gmail.com>

Permission request for my PhD Thesis

Amit Sever <amit.sever@gmail.com> Sun, Mar 25, 2012 at 10:25 AM
To: Jorge Escobedo <jescob@gmail.com>

Dear Jorge,

Yes, you have my permission to use the papers we co-authored in your PhD thesis.

Best,

Amit

Jorge Escobedo <jescob@gmail.com>

Permission request for my PhD Thesis

João Caetano <joao.caetanus@gmail.com> Sun, Mar 25, 2012 at 5:23 PM
To: Jorge Escobedo <jescob@gmail.com>

Dear Jorge Escobedo,

I'm glad to give you the permission to use the paper that we co-authored in you PhD thesis.

Best regards,
João Caetano
[Quoted text hidden]

Jorge Escobedo <jescob@gmail.com>

Permission request for my PhD Thesis

JHEP Editorial Office <jhep-eo@jhep.sissa.it> Wed, Mar 28, 2012 at 4:33 AM
Reply-To: jhep-eo@jhep.sissa.it
To: Jorge Escobedo <jescob@gmail.com>
Cc: JHEP Editorial Office <jhep-eo@jhep.sissa.it>

Dear Jorge,

Thank you for your message.

According to JHEP policy authors are granted a personal license to use all or part of their work in personal compilations, or other publications of the author's own works, provided that this is for non-commercial use.

Should you need any further information please do not hesitate to contact us.

Kind regards,

Gabriella

--
Gabriella Furlan - JHEP Editorial Office
http://jhep.sissa.it
SISSA Medialab S.r.l.
via Bonomea 265, 34136 Trieste (Italy)
Tel +39-040-3787 646
Fax +39-040-3787 640
e-mail: jhep-eo@jhep.sissa.it

On 03/27/2012 06:09 PM, Jorge Escobedo wrote:

> Dear Publisher,
>
> I'm writing to you to request permission to include in my PhD Thesis the following papers that I co-authored and were published in JHEP:
>
> Authors: J. Escobedo, N. Gromov, A. Sever and P. Vieira
> Title: Tailoring three-point functions and integrability
> Published in JHEP 1109 (2011) 028
> arXiv: 1012.2475
>
> Authors: J. Escobedo, N. Gromov, A. Sever and P. Vieira
> Title: Tailoring three-point functions and integrability II
> Published in JHEP 1109 (2011) 029
> arXiv: 1104.5501
>
> Authors: J. Escobedo and J. Caetano
> Title: On four-point functions and integrability in N=4 SYM: from weak to strong coupling
> Published in JHEP 1109 (2011) 080
> arXiv: 1107.5580
>
> Thank you in advance for your reply.
>
> Best,
> Jorge

Bibliography

[1] L. Brink, J. H. Schwarz, and J. Scherk, "Supersymmetric Yang-Mills Theories," *Nucl.Phys.* **B121** (1977) 77.

[2] P. Di Francesco, P. Mathieu, and D. Senechal, "Conformal field theory,".

[3] P. H. Ginsparg, "Applied Conformal Field Theory," `arXiv:hep-th/9108028 [hep-th]`.

[4] F. Dolan and H. Osborn, "Conformal four point functions and the operator product expansion," *Nucl.Phys.* **B599** (2001) 459–496, `arXiv:hep-th/0011040 [hep-th]`.

[5] F. Dolan and H. Osborn, "Conformal Partial Waves: Further Mathematical Results," `arXiv:1108.6194 [hep-th]`. 49 pages, v2 section on recursion relations rewritten, other additions and corrections.

[6] L. Mason and D. Skinner, "The Complete Planar S-matrix of N=4 SYM as a Wilson Loop in Twistor Space," *JHEP* **1012** (2010) 018, `arXiv:1009.2225 [hep-th]`.

[7] S. Caron-Huot, "Notes on the scattering amplitude / Wilson loop duality," *JHEP* **1107** (2011) 058, `arXiv:1010.1167 [hep-th]`.

[8] N. Arkani-Hamed, J. L. Bourjaily, F. Cachazo, S. Caron-Huot, and J. Trnka, "The All-Loop Integrand For Scattering Amplitudes in Planar N=4 SYM," *JHEP* **1101** (2011) 041, `arXiv:1008.2958 [hep-th]`.

[9] L. F. Alday, J. Maldacena, A. Sever, and P. Vieira, "Y-system for Scattering Amplitudes," *J.Phys.A* **A43** (2010) 485401, `arXiv:1002.2459 [hep-th]`.

[10] L. F. Alday, D. Gaiotto, J. Maldacena, A. Sever, and P. Vieira, "An Operator Product Expansion for Polygonal null Wilson Loops," *JHEP* **1104** (2011) 088, `arXiv:1006.2788 [hep-th]`.

[11] L. F. Alday, B. Eden, G. P. Korchemsky, J. Maldacena, and E. Sokatchev, "From correlation functions to Wilson loops," *JHEP* **1109** (2011) 123, `arXiv:1007.3243 [hep-th]`.

[12] B. Eden, G. P. Korchemsky, and E. Sokatchev, "From correlation functions to scattering amplitudes," *JHEP* **1112** (2011) 002, arXiv:1007.3246 [hep-th].

[13] N. Beisert, C. Ahn, L. F. Alday, Z. Bajnok, J. M. Drummond, *et al.*, "Review of AdS/CFT Integrability: An Overview," *Lett.Math.Phys.* **99** (2012) 3–32, arXiv:1012.3982 [hep-th].

[14] J. Minahan and K. Zarembo, "The Bethe ansatz for N=4 superYang-Mills," *JHEP* **0303** (2003) 013, arXiv:hep-th/0212208 [hep-th].

[15] J. A. Minahan, "Review of AdS/CFT Integrability, Chapter I.1: Spin Chains in N=4 Super Yang-Mills," *Lett.Math.Phys.* **99** (2012) 33–58, arXiv:1012.3983 [hep-th].

[16] H. Bethe, "Zur Theorie der Metalle. 1. Eigenwerte und Eigenfunktionen der linearen Atomkette (On the theory of metals. 1. Eigenvalues and eigenfunctions for the linear atomic chain)," *Z.Phys.* **71** (1931) 205–226.

[17] N. Gromov, V. Kazakov, and P. Vieira, "Exact Spectrum of Anomalous Dimensions of Planar N=4 Supersymmetric Yang-Mills Theory," *Phys.Rev.Lett.* **103** (2009) 131601, arXiv:0901.3753 [hep-th].

[18] N. Gromov, V. Kazakov, A. Kozak, and P. Vieira, "Exact Spectrum of Anomalous Dimensions of Planar N = 4 Supersymmetric Yang-Mills Theory: TBA and excited states," *Lett.Math.Phys.* **91** (2010) 265–287, arXiv:0902.4458 [hep-th].

[19] N. Gromov, V. Kazakov, S. Leurent, and D. Volin, "Solving the AdS/CFT Y-system," arXiv:1110.0562 [hep-th].

[20] N. Gromov, V. Kazakov, and P. Vieira, "Exact Spectrum of Planar $\mathcal{N} = 4$ Supersymmetric Yang-Mills Theory: Konishi Dimension at Any Coupling," *Phys.Rev.Lett.* **104** (2010) 211601, arXiv:0906.4240 [hep-th].

[21] J. M. Maldacena, "The Large N limit of superconformal field theories and supergravity," *Adv.Theor.Math.Phys.* **2** (1998) 231–252, arXiv:hep-th/9711200 [hep-th].

[22] S. Gubser, I. R. Klebanov, and A. M. Polyakov, "Gauge theory correlators from noncritical string theory," *Phys.Lett.* **B428** (1998) 105–114, arXiv:hep-th/9802109 [hep-th].

[23] E. Witten, "Anti-de Sitter space and holography," *Adv.Theor.Math.Phys.* **2** (1998) 253–291, arXiv:hep-th/9802150 [hep-th].

[24] O. Aharony, O. Bergman, D. L. Jafferis, and J. Maldacena, "N=6 superconformal Chern-Simons-matter theories, M2-branes and their gravity duals," *JHEP* **0810** (2008) 091, arXiv:0806.1218 [hep-th].

[25] O. Aharony, O. Bergman, and D. L. Jafferis, "Fractional M2-branes," *JHEP* **0811** (2008) 043, arXiv:0807.4924 [hep-th].

[26] G. 't Hooft, "Dimensional reduction in quantum gravity," arXiv:gr-qc/9310026 [gr-qc]. Essay dedicated to Abdus Salam.

[27] O. Aharony, S. S. Gubser, J. M. Maldacena, H. Ooguri, and Y. Oz, "Large N field theories, string theory and gravity," *Phys.Rept.* **323** (2000) 183–386, arXiv:hep-th/9905111 [hep-th].

[28] E. D'Hoker and D. Z. Freedman, "Supersymmetric gauge theories and the AdS / CFT correspondence," arXiv:hep-th/0201253 [hep-th].

[29] A. Tseytlin, "Review of AdS/CFT Integrability, Chapter II.1: Classical AdS5xS5 string solutions," *Lett.Math.Phys.* **99** (2012) 103–125, arXiv:1012.3986 [hep-th].

[30] T. McLoughlin, "Review of AdS/CFT Integrability, Chapter II.2: Quantum Strings in AdS5xS5," *Lett.Math.Phys.* **99** (2012) 127–148, arXiv:1012.3987 [hep-th].

[31] M. Beccaria and G. Macorini, "Quantum folded string in S^5 and the Konishi multiplet at strong coupling," *JHEP* **1110** (2011) 040, arXiv:1108.3480 [hep-th].

[32] N. Gromov, D. Serban, I. Shenderovich, and D. Volin, "Quantum folded string and integrability: From finite size effects to Konishi dimension," *JHEP* **1108** (2011) 046, arXiv:1102.1040 [hep-th].

[33] R. Roiban and A. Tseytlin, "Semiclassical string computation of strong-coupling corrections to dimensions of operators in Konishi multiplet," *Nucl.Phys.* **B848** (2011) 251–267, arXiv:1102.1209 [hep-th].

[34] B. C. Vallilo and L. Mazzucato, "The Konishi multiplet at strong coupling," *JHEP* **1112** (2011) 029, arXiv:1102.1219 [hep-th]. 4 pages/ v2: corrections and improvements, conclusions unchanged.

[35] R. Roiban and A. A. Tseytlin, "Quantum strings in AdS(5) x S**5: Strong-coupling corrections to dimension of Konishi operator," *JHEP* **0911** (2009) 013, arXiv:0906.4294 [hep-th]. 33 pages, Latex v2: minor comments added, misprints corrected v3: misprint corrected v4: misprints corrected.

[36] S. Lee, S. Minwalla, M. Rangamani, and N. Seiberg, "Three point functions of chiral operators in D = 4, N=4 SYM at large N," *Adv.Theor.Math.Phys.* **2** (1998) 697–718, arXiv:hep-th/9806074 [hep-th].

[37] R. Roiban and A. Volovich, "Yang-Mills correlation functions from integrable spin chains," *JHEP* **0409** (2004) 032, arXiv:hep-th/0407140 [hep-th].

[38] K. Okuyama and L.-S. Tseng, "Three-point functions in N = 4 SYM theory at one-loop," *JHEP* **0408** (2004) 055, arXiv:hep-th/0404190 [hep-th].

[39] L. F. Alday, J. R. David, E. Gava, and K. Narain, "Structure constants of planar N = 4 Yang Mills at one loop," *JHEP* **0509** (2005) 070, arXiv:hep-th/0502186 [hep-th].

[40] J. Escobedo, N. Gromov, A. Sever, and P. Vieira, "Tailoring Three-Point Functions and Integrability," *JHEP* **1109** (2011) 028, arXiv:1012.2475 [hep-th].

[41] J. Caetano and J. Escobedo, "On four-point functions and integrability in N=4 SYM: from weak to strong coupling," *JHEP* **1109** (2011) 080, arXiv:1107.5580 [hep-th].

[42] J. Escobedo, N. Gromov, A. Sever, and P. Vieira, "Tailoring Three-Point Functions and Integrability II. Weak/strong coupling match," *JHEP* **1109** (2011) 029, arXiv:1104.5501 [hep-th].

[43] G. Georgiou, "SL(2) sector: weak/strong coupling agreement of three-point correlators," *JHEP* **1109** (2011) 132, arXiv:1107.1850 [hep-th].

[44] N. Gromov, A. Sever, and P. Vieira, "Tailoring Three-Point Functions and Integrability III. Classical Tunneling," arXiv:1111.2349 [hep-th].

[45] I. Kostov, "Classical Limit of the Three-Point Function from Integrability," arXiv:1203.6180 [hep-th].

[46] N. Gromov and P. Vieira, "Quantum Integrability for Three-Point Functions," arXiv:1202.4103 [hep-th].

[47] D. Z. Freedman, S. D. Mathur, A. Matusis, and L. Rastelli, "Correlation functions in the CFT(d) / AdS(d+1) correspondence," *Nucl.Phys.* **B546** (1999) 96–118, arXiv:hep-th/9804058 [hep-th].

[48] G. Arutyunov and S. Frolov, "Some cubic couplings in type IIB supergravity on AdS(5) x S**5 and three point functions in SYM(4) at large N," *Phys.Rev.* **D61** (2000) 064009, arXiv:hep-th/9907085 [hep-th].

[49] M. Bianchi, S. Kovacs, G. Rossi, and Y. S. Stanev, "Properties of the Konishi multiplet in N=4 SYM theory," *JHEP* **0105** (2001) 042, arXiv:hep-th/0104016 [hep-th].

[50] S. Lee, "AdS(5) / CFT(4) four point functions of chiral primary operators: Cubic vertices," *Nucl.Phys.* **B563** (1999) 349–360, arXiv:hep-th/9907108 [hep-th].

[51] E. D'Hoker, D. Z. Freedman, S. D. Mathur, A. Matusis, and L. Rastelli, "Graviton exchange and complete four point functions in the AdS / CFT correspondence," *Nucl.Phys.* **B562** (1999) 353–394, arXiv:hep-th/9903196 [hep-th].

[52] E. D'Hoker, D. Z. Freedman, and L. Rastelli, "AdS / CFT four point functions: How to succeed at z integrals without really trying," *Nucl.Phys.* **B562** (1999) 395–411, arXiv:hep-th/9905049 [hep-th].

[53] G. Arutyunov and S. Frolov, "Four point functions of lowest weight CPOs in N=4 SYM(4) in supergravity approximation," *Phys.Rev.* **D62** (2000) 064016, arXiv:hep-th/0002170 [hep-th].

[54] F. Dolan, M. Nirschl, and H. Osborn, "Conjectures for large N superconformal N=4 chiral primary four point functions," *Nucl.Phys.* **B749** (2006) 109–152, arXiv:hep-th/0601148 [hep-th].

[55] L. Berdichevsky and P. Naaijkens, "Four-point functions of different-weight operators in the AdS/CFT correspondence," *JHEP* **0801** (2008) 071, arXiv:0709.1365 [hep-th].

[56] L. I. Uruchurtu, "Four-point correlators with higher weight superconformal primaries in the AdS/CFT Correspondence," *JHEP* **0903** (2009) 133, arXiv:0811.2320 [hep-th].

[57] R. A. Janik, P. Surowka, and A. Wereszczynski, "On correlation functions of operators dual to classical spinning string states," *JHEP* **1005** (2010) 030, arXiv:1002.4613 [hep-th].

[58] A. Tsuji, "Holography of Wilson loop correlator and spinning strings," *Prog.Theor.Phys.* **117** (2007) 557–568, arXiv:hep-th/0606030 [hep-th].

[59] E. Buchbinder and A. Tseytlin, "On semiclassical approximation for correlators of closed string vertex operators in AdS/CFT," *JHEP* **1008** (2010) 057, arXiv:1005.4516 [hep-th].

[60] A. A. Tseytlin, "On semiclassical approximation and spinning string vertex operators in AdS(5) x S**5," *Nucl.Phys.* **B664** (2003) 247–275, arXiv:hep-th/0304139 [hep-th].

[61] E. I. Buchbinder, "Energy-Spin Trajectories in $AdS_5 \times S^5$ from Semiclassical Vertex Operators," *JHEP* **1004** (2010) 107, arXiv:1002.1716 [hep-th].

[62] K. Zarembo, "Holographic three-point functions of semiclassical states," *JHEP* **1009** (2010) 030, arXiv:1008.1059 [hep-th].

[63] M. S. Costa, R. Monteiro, J. E. Santos, and D. Zoakos, "On three-point correlation functions in the gauge/gravity duality," *JHEP* **1011** (2010) 141, arXiv:1008.1070 [hep-th].

[64] R. Roiban and A. Tseytlin, "On semiclassical computation of 3-point functions of closed string vertex operators in AdS_5xS^5," *Phys.Rev.* **D82** (2010) 106011, arXiv:1008.4921 [hep-th].

[65] R. Hernandez, "Three-point correlation functions from semiclassical circular strings," *J.Phys.A* **A44** (2011) 085403, arXiv:1011.0408 [hep-th].

[66] S. Ryang, "Correlators of Vertex Operators for Circular Strings with Winding Numbers in AdS5xS5," *JHEP* **1101** (2011) 092, arXiv:1011.3573 [hep-th].

[67] G. Georgiou, "Two and three-point correlators of operators dual to folded string solutions at strong coupling," *JHEP* **1102** (2011) 046, arXiv:1011.5181 [hep-th].

[68] J. Russo and A. Tseytlin, "Large spin expansion of semiclassical 3-point correlators in AdS_5xS^5," *JHEP* **1102** (2011) 029, arXiv:1012.2760 [hep-th].

[69] D. Arnaudov, R. Rashkov, and T. Vetsov, "Three and four-point correlators of operators dual to folded string solutions in AdS_5xS^5," *Int.J.Mod.Phys.* **A26** (2011) 3403–3420, arXiv:1103.6145 [hep-th].

[70] E. Buchbinder and A. Tseytlin, "Semiclassical four-point functions in $AdS_5 \times S^5$," *JHEP* **1102** (2011) 072, arXiv:1012.3740 [hep-th].

[71] R. A. Janik and A. Wereszczynski, "Correlation functions of three heavy operators: The AdS contribution," *JHEP* **1112** (2011) 095, arXiv:1109.6262 [hep-th].

[72] Y. Kazama and S. Komatsu, "On holographic three point functions for GKP strings from integrability," *JHEP* **1201** (2012) 110, arXiv:1110.3949 [hep-th].

[73] S. Gubser, I. Klebanov, and A. M. Polyakov, "A Semiclassical limit of the gauge / string correspondence," *Nucl.Phys.* **B636** (2002) 99–114, arXiv:hep-th/0204051 [hep-th].

[74] N. Beisert, C. Kristjansen, J. Plefka, G. Semenoff, and M. Staudacher, "BMN correlators and operator mixing in N=4 superYang-Mills theory," *Nucl.Phys.* **B650** (2003) 125–161, arXiv:hep-th/0208178 [hep-th].

[75] N. R. Constable, D. Z. Freedman, M. Headrick, and S. Minwalla, "Operator mixing and the BMN correspondence," *JHEP* **0210** (2002) 068, arXiv:hep-th/0209002 [hep-th].

[76] C. Kristjansen, "Review of AdS/CFT Integrability, Chapter IV.1: Aspects of Non-Planarity," *Lett.Math.Phys.* **99** (2012) 349–374, arXiv:1012.3997 [hep-th].

[77] D. E. Berenstein, J. M. Maldacena, and H. S. Nastase, "Strings in flat space and pp waves from N=4 superYang-Mills," *JHEP* **0204** (2002) 013, arXiv:hep-th/0202021 [hep-th].

[78] V. Korepin, N. Bogoliubov, and A. Izergin, "Quantum inverse scattering method and correlation functions,".

[79] M. Gaudin, "La fonction d'onde de Bethe,".

[80] M. Karbach and G. Muller, "Introduction to the Bethe ansatz I," *Computers in Physics* **11** (1997) 36–43, arXiv:cond-mat/9809162 [cond-mat].

[81] L. Faddeev, "How algebraic Bethe ansatz works for integrable model," arXiv:hep-th/9605187 [hep-th].

[82] N. Slavnov, "The algebraic Bethe ansatz and quantum integrable systems," *Russian Mathematical Surveys* **62** no. 4, 727–766.

[83] N. Slavnov, "Calculation of scalar products of wave functions and form factors in the framework of the algebraic Bethe ansatz," *Theoretical and Mathematical Physics* **79** no. 2, 502–508.

[84] A. Izergin and V. Korepin, "The quantum inverse scattering method approach to correlation functions," *Commun.Math.Phys.* **94** (1984) 67–92.

[85] V. Korepin, "Calculation of norms of Bethe wave functions," *Commun.Math.Phys.* **86** (1982) 391–418.

[86] M. Gaudin *Journal de Physique* **37** (1976) 1087.

[87] B. McCoy, T. Wu, and M. Gaudin *Phys. Rev. D* **23** (1981) 417.

[88] F. Cachazo, P. Svrcek, and E. Witten, "MHV vertices and tree amplitudes in gauge theory," *JHEP* **0409** (2004) 006, arXiv:hep-th/0403047 [hep-th].

[89] R. Britto, F. Cachazo, B. Feng, and E. Witten, "Direct proof of tree-level recursion relation in Yang-Mills theory," *Phys.Rev.Lett.* **94** (2005) 181602, arXiv:hep-th/0501052 [hep-th].

[90] E. D'Hoker, D. Z. Freedman, S. D. Mathur, A. Matusis, and L. Rastelli, "Extremal correlators in the AdS / CFT correspondence," arXiv:hep-th/9908160 [hep-th].

[91] H. Liu and A. A. Tseytlin, "Dilaton - fixed scalar correlators and AdS(5) x S**5 - SYM correspondence," *JHEP* **9910** (1999) 003, arXiv:hep-th/9906151 [hep-th].

[92] O. Foda, "N=4 SYM structure constants as determinants," arXiv:1111.4663 [math-ph].

[93] A. Izergin, "Partition function of the six-vertex model in a finite volume," *Sov. Phys. Dokl.* **32** (1987) 878–879.

[94] N. Kitanine, J. M. Maillet, and V. Terras, "Form factors of the XXZ Heisenberg spin-1/2 finite chain," *Nuclear Physics B* 647–678, arXiv:math-ph/9807020.

[95] M. Wheeler, "An Izergin-Korepin procedure for calculating scalar products in six-vertex models," *Nucl.Phys.* **B852** (2011) 468–507, arXiv:1104.2113 [math-ph].

[96] M. Kruczenski, "Spin chains and string theory," *Phys.Rev.Lett.* **93** (2004) 161602, arXiv:hep-th/0311203 [hep-th].

[97] J. Stefanski, B. and A. A. Tseytlin, "Large spin limits of AdS/CFT and generalized Landau-Lifshitz equations," *JHEP* **0405** (2004) 042, arXiv:hep-th/0404133 [hep-th].

[98] S. Frolov and A. A. Tseytlin, "Semiclassical quantization of rotating superstring in AdS(5) x S**5," *JHEP* **0206** (2002) 007, arXiv:hep-th/0204226 [hep-th].

[99] S. Frolov and A. A. Tseytlin, "Multispin string solutions in AdS(5) x S**5," *Nucl.Phys.* **B668** (2003) 77–110, arXiv:hep-th/0304255 [hep-th].

[100] S. Frolov and A. A. Tseytlin, "Rotating string solutions: AdS / CFT duality in nonsupersymmetric sectors," *Phys.Lett.* **B570** (2003) 96–104, arXiv:hep-th/0306143 [hep-th].

[101] A. A. Tseytlin, "Spinning strings and AdS / CFT duality," arXiv:hep-th/0311139 [hep-th].

[102] N. Beisert, J. Minahan, M. Staudacher, and K. Zarembo, "Stringing spins and spinning strings," *JHEP* **0309** (2003) 010, arXiv:hep-th/0306139 [hep-th].

[103] N. Beisert, S. Frolov, M. Staudacher, and A. A. Tseytlin, "Precision spectroscopy of AdS / CFT," *JHEP* **0310** (2003) 037, arXiv:hep-th/0308117 [hep-th].

[104] V. Kazakov, A. Marshakov, J. Minahan, and K. Zarembo, "Classical/quantum integrability in AdS/CFT," *JHEP* **0405** (2004) 024, arXiv:hep-th/0402207 [hep-th].

[105] G. Arutyunov, S. Frolov, J. Russo, and A. A. Tseytlin, "Spinning strings in AdS(5) x S**5 and integrable systems," *Nucl.Phys.* **B671** (2003) 3–50, arXiv:hep-th/0307191 [hep-th].

[106] J. Engquist, J. Minahan, and K. Zarembo, "Yang-Mills duals for semiclassical strings on AdS(5) x S(5)," *JHEP* **0311** (2003) 063, arXiv:hep-th/0310188 [hep-th].

[107] T. Bargheer, N. Beisert, and N. Gromov, "Quantum Stability for the Heisenberg Ferromagnet," *New J.Phys.* **10** (2008) 103023, arXiv:0804.0324 [hep-th].

[108] J. Minahan, A. Tirziu, and A. A. Tseytlin, "1/J**2 corrections to BMN energies from the quantum long range Landau-Lifshitz model," *JHEP* **0511** (2005) 031, arXiv:hep-th/0510080 [hep-th].

[109] N. Beisert, V. Kazakov, K. Sakai, and K. Zarembo, "The Algebraic curve of classical superstrings on AdS(5) x S**5," *Commun.Math.Phys.* **263** (2006) 659–710, arXiv:hep-th/0502226 [hep-th].

[110] N. Beisert, V. Kazakov, K. Sakai, and K. Zarembo, "Complete spectrum of long operators in N=4 SYM at one loop," *JHEP* **0507** (2005) 030, arXiv:hep-th/0503200 [hep-th]. Dedicated to the memory of Hans Bethe.

[111] G. Arutyunov, S. Frolov, and M. Staudacher, "Bethe ansatz for quantum strings," *JHEP* **0410** (2004) 016, arXiv:hep-th/0406256 [hep-th].

[112] N. Beisert and M. Staudacher, "Long-range psu(2,2|4) Bethe Ansatze for gauge theory and strings," *Nucl.Phys.* **B727** (2005) 1–62, arXiv:hep-th/0504190 [hep-th]. In honor of Hans Bethe.

[113] G. Georgiou, V. L. Gili, and R. Russo, "Operator mixing and three-point functions in N=4 SYM," *JHEP* **0910** (2009) 009, arXiv:0907.1567 [hep-th].

[114] R. Hernandez, "Three-point correlators for giant magnons," *JHEP* **1105** (2011) 123, arXiv:1104.1160 [hep-th].

[115] B. Sutherland, "Low-Lying Eigenstates of the One-Dimensional Heisenberg Ferromagnet for any Magnetization and Momentum," *Phys.Rev.Lett.* **74** (1995) 816–819.

[116] A. Dhar and B. Sriram Shastry, "Bloch Walls and Macroscopic String States in Bethe's Solution of the Heisenberg Ferromagnetic Linear Chain," *Phys.Rev.Lett.* **85** (2000) 2813–2816.

[117] E. H. Fradkin, "Field theories of condensed matter systems,".

[118] N. Beisert and L. Freyhult, "Fluctuations and energy shifts in the Bethe ansatz," *Phys.Lett.* **B622** (2005) 343–348, arXiv:hep-th/0506243 [hep-th].

[119] N. Gromov and P. Vieira, "The AdS(5) x S**5 superstring quantum spectrum from the algebraic curve," *Nucl.Phys.* **B789** (2008) 175–208, arXiv:hep-th/0703191 [HEP-TH].

[120] N. Gromov, S. Schafer-Nameki, and P. Vieira, "Efficient precision quantization in AdS/CFT," *JHEP* **0812** (2008) 013, arXiv:0807.4752 [hep-th].

[121] N. Dorey and B. Vicedo, "On the dynamics of finite-gap solutions in classical string theory," *JHEP* **0607** (2006) 014, arXiv:hep-th/0601194 [hep-th].

[122] V. Kazakov, A. S. Sorin, and A. Zabrodin, "Supersymmetric Bethe ansatz and Baxter equations from discrete Hirota dynamics," *Nucl.Phys.* **B790** (2008) 345–413, arXiv:hep-th/0703147 [HEP-TH].

[123] C.-N. Yang, "Some exact results for the many body problems in one dimension with repulsive delta function interaction," *Phys.Rev.Lett.* **19** (1967) 1312–1314.

[124] N. Beisert and M. Staudacher, "The N=4 SYM integrable super spin chain," *Nucl.Phys.* **B670** (2003) 439–463, arXiv:hep-th/0307042 [hep-th].

[125] N. Gromov and P. Vieira, "Complete 1-loop test of AdS/CFT," *JHEP* **0804** (2008) 046, arXiv:0709.3487 [hep-th].

[126] M. Kruczenski, "A Note on twist two operators in N=4 SYM and Wilson loops in Minkowski signature," *JHEP* **0212** (2002) 024, arXiv:hep-th/0210115 [hep-th].

[127] N. Beisert, "The complete one loop dilatation operator of N=4 superYang-Mills theory," *Nucl.Phys.* **B676** (2004) 3–42, arXiv:hep-th/0307015 [hep-th].

[128] A. Bissi, T. Harmark, and M. Orselli, "Holographic 3-Point Function at One Loop," *JHEP* **1202** (2012) 133, arXiv:1112.5075 [hep-th].

[129] N. Beisert, V. Dippel, and M. Staudacher, "A Novel long range spin chain and planar N=4 super Yang-Mills," *JHEP* **0407** (2004) 075, arXiv:hep-th/0405001 [hep-th].

[130] N. Y. Reshetikhin, "Calculation of the norm of bethe vectors in models with su(3)-symmetry," *Journal of Mathematical Sciences* **46** (1989) 1694–1706. http://dx.doi.org/10.1007/BF01099200.

[131] F. Gohmann and V. Korepin, "The Hubbard chain: Lieb-Wu equations and norm of the eigenfunctions," *Phys.Lett.* **A263** (1999) 293–298, arXiv:cond-mat/9908114 [cond-mat].

[132] M. Wheeler, "Scalar products in generalized models with SU(3)-symmetry," arXiv:1204.2089 [math-ph].

[133] M. Staudacher, "The Factorized S-matrix of CFT/AdS," *JHEP* **0505** (2005) 054, arXiv:hep-th/0412188 [hep-th].

[134] N. Beisert, C. Kristjansen, and M. Staudacher, "The Dilatation operator of conformal N=4 superYang-Mills theory," *Nucl.Phys.* **B664** (2003) 131–184, arXiv:hep-th/0303060 [hep-th].

[135] N. Gromov and P. Vieira. Private communication.

[136] N. Beisert, B. Eden, and M. Staudacher, "Transcendentality and Crossing," *J.Stat.Mech.* **0701** (2007) P01021, arXiv:hep-th/0610251 [hep-th].

[137] S. Dobashi and T. Yoneya, "Impurity non-preserving 3-point correlators of BMN operators from PP-wave holography. I. Bosonic excitations," *Nucl.Phys.* **B711** (2005) 54–82, arXiv:hep-th/0409058 [hep-th].

[138] S. Dobashi and T. Yoneya, "Resolving the holography in the plane-wave limit of AdS/CFT correspondence," *Nucl.Phys.* **B711** (2005) 3–53, arXiv:hep-th/0406225 [hep-th].